University of São Paulo
"Luiz de Queiroz" College of Agriculture

Long and short-term pedogenetic processes in ferralsols from magmatic province of Paraná, Brazil

Mariane Chiapini

Thesis presented to obtain de degree of Doctor in Science. Area: Soil and Plant Nutrition

Piracicaba
2021

Mariane Chiapini
Agronomist

Long and short-term pedogenetic processes in ferralsols from magmatic province of Paraná, Brazil

versão revisada de acordo com a resolução CoPGr 6018 de 2011

Advisor:
Prof. Dr. **PABLO VIDAL TORRADO**

Thesis presented to obtain the degree of Doctor in Science. Area: Soil and Plant Nutrition

Piracicaba
2021

Dados Internacionais de Catalogação na Publicação

DIVISÃO DE BIBLIOTECA – DIBD/ESALQ/USP

Chiapini, Mariane

Long and short-term pedogenetic processes in ferralsols from magmatic province of Paraná, Brazil / Mariane Chiapini. - - versão revisada de acordo com a resolução CoPGr 6018 de 2011. - - Piracicaba, 2021.

189 p.

Tese (Doutorado) - - USP / Escola Superior de Agricultura "Luiz de Queiroz".

1. Ferralitização 2. Bioturbação 3. Brunificação 4. Hematita 5. Reconstituição paleoambiental 6. Matéria orgânica do solo I. Título

ACKNOWLEDGMENTS

My sincere gratitude to Prof. Dr. Pablo Vidal Torrado, my advisor, for the incentive, support, trust, knowledge transmitted, friendship and above all, for his patience during these eleven years.

I would like to thank the Graduate Program in Soils and Plant Nutrition and the Soil Science Department of ESALQ/USP for the opportunity of taking the course and for the availability of the facilities, resources and materials for the development of my research.

I thank the São Paulo Research Foundation (FAPESP; Process 2017/22608-1) and CAPES for the regular doctorate scholarship.

I thank the owners/fundations of the studied sites for authorizing access in order to perform this research, in particular, the Mineradora Drisner (Palotina/Maripá), Parque Natural Municipal das Araucárias (Guarapuava), Universidade Estadual do Centro-Oeste do Paraná (Unicentro, Campus Cedeteg, Guarapuava, in special, Prof ª Dr. Aline Marques Genu), Fundação para o Desenvolvimento Científico e Tecnológico (FUNDETEC, Cascavel), Escola tecnológica Agropecuária (AGROTEC, Cascavel), Western Paraná State University (Campus Marechal Cândido Rondon), Parque Estadual Reserva São Camilo (Palotina) and Instituto Agronômico do Paraná (Iapar-Palotina).

I am very grateful also to Drª Judith Schellekens her teachings and knowledge transmitted, great collaboration, suggestions, trust, friendship and patience.

Thanks Dr. Luiz Carlos Forti, Dr. Nadia Caldato, Dr. Jairo Calderari de Oliveira Junior, Dr. Gabriel Ramatis Pugliese Andrade, Dr. Márcia Regina Calegari, Dr. Plínio Barbosa de Camargo, Fabiana Cristina Fracassi Adorno, Dr. Maria Diva Landgraf, Dr. Maria Olímpia de Oliveira Rezende, Patrick Lavelle, George Brown, Luiz Carlos Forti, Og F.F. de Souza and Tiago F. Carrijo for teachings and laboratory analysis.

I thank Andrews Nataniel Raber, Bruno Aparecido da Silva, Geovane Ricardo Calixto and Patrícia Antonio de Oliveira for their help with the fieldwork.

Thanks to my friends of the graduate program Taís, Daniela, Sara, Paulo, Júlio, Karina and André for their collaboration, fellowship, laughter and incentives. Special thanks to Matheus Coletti Cantero for his help with analytical activities.

Thanks to my friend's house (Virginetes) for their friendship, knowledge, parties and incentive.

Thanks to the teachers of the Soil Science Department - ESALQ/USP for the knowledge they transmitted and their contribution to my education.

I thank Luiz Silva, Sônia, Chiquinho, Leandro, Rossi and Marina, the technicians of the Soil Science Department - ESALQ/USP for their attention and support in the laboratory analyses. In special to Nivanda Maria de Moura Ruiz (Ni) for her friendship, incentive and support in the laboratory analyses.

Thanks to employees of the Soil Science Department - ESALQ/USP, Dorival Grisotto, Sueli and Paulo.

Special thanks to my family, Carlos, Marinalva, and my brother Frederico for the unconditional love and encouraging the pursuit of my goals.

Special thanks to Bruno H. M. Ventura, for inconditional love, care and for always being in my side during these years.

To all the people who contributed directly or indirectly to this research.

Thank you!

CONTENTS

RESUMO

Processos pedogenéticos de longo e curto prazo em latossolos da província magmática do Paraná, Brasil

Apesar de amplamente estudados, diversas perguntas ainda estão sem respostas consistentes sobre a gênese e morfologia dos latossolos. O foco excessivo das investigações pedológicas dentro da seção de controle (200 cm) tem deixado sistematicamente de lado registros que podem existir de diferentes momentos da pedogênese e que estão a maiores profundidades. Este trabalho tem por objetivo compreender os principais processos pedogenéticos que atuam ao longo de perfis completos de latossolos da Província Magmática do Paraná (PMP), e como as mudanças climáticas do Quaternário os podem ter influenciado, uma vez que os processos tem atuação temporal distinta, de longo e curto prazo. Foram descritos e coletados dez pedons em uma topoclimosequência na PMP (Guarapuava: G1–G4; Cascavel: C1–C3 e Palotina: P1–P3) sob basalto e riodacito. Para este fim, análises físicas, químicas, mineralógicas, geoquímicas e micromorfológicas de solos em combinação com a caracterização qualitativa da matéria orgânica do solo (MOS) e análises isotópicas de C e N para reconstituição paleoambiental foram realizadas. Os latossolos da PMP são formados *in situ*, respondendo às mudanças climáticas e da paisagem de acordo com um processo morfoclimático e de intenso intemperismo geoquímico. Nesse contexto se deu um processo parcial de ferralitização resultando num predomínio de caulinita (37–68%) com conteúdos variáveis de gibbsita (3–28%), hematita (7–28%), goethita (1–13%) e traços de minerais 2:1 com hydroxy-Al entre camadas. As condições ambientais do passado e atuais afetam a formação e a estabilidade dos óxidos de Fe dando lugar a diferentes momentos e posições nos perfis dos processos de rubeificação e brunificação, caracterizando a coloração brunada e avermelhada. Feições pedorreliquiais como nódulos de ferro e nódulos densos de argila foram descritos e interpretados numa relação hierárquica como desenvolvidos *in situ*. Os nódulos de ferro são originados em condições redoximórficas na frente de intemperismo em períodos mais úmidos e depois decompostos. O caráter ácrico apareceu nestes solos cauliníticos com teores de gibbsita inferiores a 28%. O caráter eutrófico foi identificado nos perfis de Palotina e foi hipotetizado que se deva à ferralitização parcial seguida da ciclagem de Ca e Mg realizada por maior concentração de raízes de plantas C_4 sob um clima mais seco e prolongado, aliado à proteção pelos microagregados. Há diferentes zonas de bioturbação intensa, mesmo abaixo do biomanto, influenciadas pelas condições climáticas do Quaternário. Diferentes biofeições específicas permitiram identificar os principais agentes bioturbadores, alguns deles pouco ou não registrados na literatura em grandes profundidades. A gênese dos microagregados é complexa, no saprolito ocorrem microagregados de origem geoquímica, zoogenética e física, os quais são retrabalhados pela fauna em diferentes profundidades do solo. Microagregados complexos oriundos da agregação de outros menores e da atividade de formigas também estão presentes nos latossolos da PMP. A MOS e sua composição isotópica foram influenciadas pelas condições climáticas do Quaternário, registrando os períodos mais secos com predomínio de plantas C_4 e maiores contribuições (%) de compostos afetados pelo fogo, permitindo que os latossolos possam ser utilizados como registros paleoambientais até os horizontes mais profundos.

Palavras-chave: Ferralitização, Bioturbação, Brunificação, Hematita, Reconstituição paleoambiental, Matéria orgânica do solo

ABSTRACT

Long and short-term pedogenetic processes in ferralsols from magmatic province of Paraná, Brazil

Despite being widely studied, several questions are still without consistent answers, with respect to the genesis and morphology of ferralsols. The excessive focus of pedological investigations within the control section (200 cm) has systematically left aside the records that may exist of different moments in the pedogenesis of these soils and that are registered at greater depths. The objective of this work is to understand the main pedogenetic processes that act in complete profiles of ferralsols of the Paraná Magmatic Province (PMP), and how the Quaternary climatic changes may have influenced them, since the processes have different temporal scale, long and short-term. Ten soil profiles were described and collected in a topo-climate-sequence in PMP (Guarapuava: G1–G4; Cascavel: C1–C3 e Palotina: P1–P3) under basaltic and rhyo-dacitic rocks. To this end, a combination of physical, chemical, mineralogical, geochemical and micromorphological analyses of soils in combination with the qualitative characterization of soil organic matter (SOM) and isotopic analyses of C and N for paleoenvironmental reconstruction was carried out. The ferralsols of PMP have developed *in situ*, responding to climatic and landscape changes according to a morphoclimatic process and intense geochemical weathering. In this context, a partial ferralitization process took place resulting in a predominance of kaolinite (37–68%), with variable contents of gibbsite (3–28%), hematite (7–28%), goethite (1–13%) and traces of hydroxy-interlayered 2:1 minerals. Paleo and current environmental conditions affect the formation and stability of Fe oxides, giving rise to different moments and positions in the profiles of the rubification and brunification processes, characterizing the brownish and reddish colours. Pedorelict features such as iron nodules and dense clayey nodules were described and interpreted in a hierarchical relationship as developed *in situ*. Iron nodules originate in redoximorphic conditions in the weathering front in wetter periods and then decompose. The geric property appeared in these kaolinitic soils with gibbsite contents below 28%. The eutric property was identified in the Palotina profiles and it was hypothesized to be due to partial ferralitization followed by cycling of Ca and Mg carried out by a higher concentration of C_4 plant roots under a drier and prolonged climate, combined with protection of microaggregates. There are different zones of intense bioturbation, even below the biomantle, influenced by the Quaternary climatic conditions. Different specific biofeatures allowed to identify the main bioturbation agents, some of them little or not registered in the literature in great depths. The genesis of microaggregates is complex, in saprolite there are microaggregates of geochemical, zoogenetic and physical origin, which are reworked by soil fauna to different soil depths. Complex microaggregates from the aggregation of smaller microaggregates and ant activity are also present in PMP ferralsols. The SOM and its isotopic composition were influenced by the Quaternary climatic conditions, recording the driest periods with a predominance of C_4 plants, and higher contributions (%) of compounds affected by fire, allowing ferralsols to be used as paleoenvironmental records up to the most deep horizons.

Keywords: Ferralitization, Bioturbation, Brunification, Hematite, Paleoenvironmental reconstruction, Soil organic matter

1. INTRODUCTION

Ferralsols are common soils in Brazil, occupying 32% of the national territory. They are usually associated with the highest and most stable geomorphic surfaces of Pleistocene (2.58 M. y.) age or older (Muggler, 1998; Driessen et al., 2001; Anjos et al., 2012; Paisani et al., 2013; 2014; Zhou et al., 2015). These soils occur in the Brazilian tropical zone (southeast and central-west) in planed surfaces proposed by Lester Charles King (1956): *Pós-Gondwana*, *Sul Americana*, *Velhas* and *Paraguaçú*, while in the subtropical zone (southern Brazil) are mainly related to the planation surfaces proposed by Bigarella and Andrade (1965): Pd_3 (pediplane 3), Pd_2, Pd_1 and Pd_0. Discussions related to the uniformity of parent material of ferralsols (allochthony *vs.* autochthony) are commonly observed in the literature, due to, its location in stable and old surfaces of Pleistocene age. Stoops (1989, 1997), Santos et al. (1989), Muggler (1998) and Vidal-Torrado and Lepsch (1999), consider ferralsols, as the probable result of a polycyclic and polygenetic processes from nearby previously weathered rocks and sediments (allochthonous materials or *ex situ* formation). On the other hand, ferralsols can develop by the homogeneous alteration of underlying materials with the contribution of strong pedoturbation (bioturbation), such as *in situ* formation (autochthonous material) (Millot, 1977; Miklós, 1992; Eschenbrenner, 1996). Therefore, investigation of the uniformity of parent material (allochthony *vs.* autochthony) is a prerequisite to assess the long and short-term pedogenetic processes of ferralsols in a time continuum from the surface to deep soil horizons (Wang and Arnold, 1973; Anda et al., 2009).

The main pedogenetic processes involved in the formation of ferralsols are ferralitization and bioturbation (van Wambeke et al., 1983; Johnson, 1990; Buol and Eswaran, 1999; Vidal-Torrado and Cooper, 2008). The term ferralitization was defined by French pedologists and applied to describe the main biogeochemical process in the formation of ferralitic soils (Aubert, 1962). The ferralitization process involves hydrolysis and the loss of basic cations (Ca^{2+}, Mg^{2+}, $K^{+,}$ Na^{+}) and silica with the relative accumulation of iron (Fe-) and/or aluminum (Al-) oxyhydroxides under intense chemical weathering (Aubert and Segalen, 1966; Segalen, 1966; Pedro et al., 1975; van Wambeke et al., 1983; Duchaufour, 1988; Buol and Eswaran, 1999; Driessen et al, 2001). With this, kaolinite, gibbsite, iron oxides and the occasional presence of hydroxy-interlayered minerals dominate the clay fraction of most ferralsols. The concept of ferralitization occurring in different degrees was accepted internationally and today it is used to define the genesis of corresponding soils such

as Oxisols (Soil Survey Staff, 1999), *Latossolos* (Santos et al., 2018) and Ferralsols (IUSS Working Group WRB, 2015).

Bioturbation is largely attributed to the activities of animals (fauna) and roots (flora) on reworking the soil material (Darwin, 1838, 1881; Soil Survey Staff, 1975; Johnson, 1990; Humphreys, 1993; Paton et al., 1995; Johnson et al., 2005a; 2005b). Ants, termites and earthworms are the main agents of the soil macrofauna and are recognized as the principal bioturbating agents of soils, currently being denominated as ecosystem engineers (Johnson, 1990; Stork and Eggleton, 1992; Jones et al., 1994; Paton et al., 1995; Humphreys, 2003; Wright and Jones, 2006; Wilkinson et al., 2009). The soil macrofauna can be divided into three functional groups according to their location in the soil profile, and include epigeic, anecic and endogeic species (Lavelle, 1988; Lavelle et al., 1992; Tonneijck and. Jongmans, 2008). The epigeic species live in the litter and their main effect is the fragmentation and partial digestion of litter. Endogeic species live in the soil and are active diggers whithin short vertical distances that may greatly enhance soil aggregation. Anecic species live in the soil in subterranean nests and galleries affecting the exportation of litter to the subsoil and soil physical characteristics at deeper layers (Lavelle et al., 1992).

The activities of soil fauna promotes soil displacement through mixing, mounding and burial actions reaching down to 70 m by termites (Yakushev, 1968; Wood 1988), 10 m by ants (Gallo et al., 1988; Garcia et al., 2003; Moreira et al., 2004; Miklós, 2012; Swanson et al., 2019) and 6 m by earthworms (Bachelier, 1978). The action of mounding, mixing and burial by the ecosystem engineers are able to create porous and homogenize layers in soils, which is known as biomantle. According to Johnson (1990) and Johnson et al. (2005a; 2005b), the biomantle is defined as a homogeneous layer reaching the saprolite zone with biofeatures (BFs) content of at least 50%. In general, the biofeatures that make up the biomantle are known as biopores, biological (micro) aggregates, excrements, several infillings of biopores (krotovinas) and roots. The soil (micro) aggregates of the biomantle in ferralic horizons from ferralsols are an important characteristic element exhibiting several morphologies such as oval granular, rounded and polyhedral types. The shape of the (micro) aggregates are related to their formation process and can be of biological origin (Stoops, 1983; Eschenbrenner, 1986; Miklós, 1992; Vidal-Torrado, 1994; Schaefer, 2001; Cooper et al., 2005a), geochemical origin (Chauvel et al., 1978; Cambier, 1986; Santos et al., 1989), physical origin (Muller, 1977; Trapnell and Webster, 1986) or complex origin (Muller, 1977; Vidal-Torrado, 1994). In addition, the soil engineers play an important role in nutrient

cycling, decomposition of soil organic matter (SOM) and vertical distribution and maintenance of physical properties of soil (Barros et al., 2001; Jouquet et al., 2005).

Thus, the main morphological attributes of ferralsols such as homogeneity in color and the distribution of clay with depth, strong microaggregation and weak development of the macrostructure reflect both intense ferralitization and bioturbation processes (Schaetzel and Anderson 2005; Buol et al., 2011). Furthermore, the abundance of strong and stable (micro) aggregates in these soils is related to high iron and aluminum oxides content, bound to kaolinite particles, and intense activity of the soil fauna (van Wambeke et al., 1983; Barthès et al., 2008; Rabbi et al., 2015; Jouquet et al., 2016).

Although less common, deeply weathered ferralsols with high carbon content are also reported in many tropical and subtropical areas, thereby providing potential paleoenvironmental records (Calegari et al., 2015; 2017; Luz et al., 2019). It is known that the soil organic matter (SOM) contains about three times more carbon than the atmosphere and terrestrial vegetation (Lal, 2004; Schmidt et al., 2011) and is an important source carbon potentially released into atmosphere. Therefore, it is important to understand the paleoenvironmental conditions during the short-term formation of ferralsols and the stability of organic matter in these soils. Furthermore, the organic fraction of ferralsols is still poorly understood and studied, because of the diversity and complexity of the composition and structure of SOM in relation to the mineral soil fraction (Magdoff and Weil, 2004). Therefore, techniques such as nuclear magnetic resonance (NMR) and pyrolysis coupled with gas chromatography and mass spectroscopy (pyrolysis-GC/MS), associated with chemical and physical fractionations have been applied to study these compounds. The use of pyrolysis-GC/MS allows the identification of the molecular structure of these compounds, resulting in detailed molecular information for all chemical groups in a single analysis, and is, therefore, a very powerful method for analyzing complex and unknown mixtures of organic matter, such as SOM.

Tropical and subtropical pedologists have studied ferralsols, but the answer to some questions about the genesis of these soils still remain unclear or unanswered. Some pedofeatures are often poorly described or not interpreted, such as clay nodules in the middle of a microaggregate matrix. What would they represent? Quaternary climate changes are well known and ferralsols are often related as old aged soils: could those changes affect the crystallographic parameters of clay particles in ferralsols? What is the hierarchy and pedogenetic relationship between the different types of microaggregates? What is the deep

record and fingerprint of ferralsols organic matter like? What depth in ferralsols can be used as effective environmental records? Is there a record of the biological activity (macrofauna and roots) with depth? Is bioturbation in ferralsols similar under different climatic conditions?

These are some questions that have not been consistently answered by pedologists. In addition, there is a historical predominance of studies with focus on the first two meters in depth of ferralsols, since 200 cm is the control section within soil classification systems, such as SiBCS (Santos et al., 2018), Soil Taxonomy (Soil Survey Staff, 1999) and WRB-FAO (IUSS Working Group WRB, 2015). How can we interpret and reconstruct the history of soils that are several meters deep, if we only care about their first two meters or less? It seems that by systematically maintaining these protocols a lot of information can be lost or misinterpreted in the description and hierarchy of features and attributes that result from formation processes of these soils. On the other hand, multiproxy studies have been carried out in order to improve the knowledge obtained in classical studies of the genesis and paleoenvironmental reconstruction of ferralsols.

Considering these gaps and the pedogenetic process that occurred in ferralsols, the current research has hypothesized that: a) quantitative and crystallographic differences in the clay fraction of subtropical ferralsols are related to geochemical composition of the parent material (basalt and rhyo-dacite) and pedoenvironmental conditions across a time gradient; b) bioturbation depends on the fauna ecology and can reach the weathering front being influenced by variations in climatic conditions (precipitation and temperature); c) the formation of (micro) aggregates varies with depth and has a geochemical origin in the weathering front after which is reworked by the soil fauna until the soil surface result in a homogeneous soil matrix with depth. Thus, the objectives of research were: a) verifying the pedogenetic processes involved in the genesis of subtropical ferralsols; b) reconstructing paleoenvironmental changes and relate them to the genesis of ferralsols; c) identifying and quantifying the dominant minerals of the clay fraction, as well as, studying their crystallographic parameters; d) quantifying bioturbation by the occurrence of biofeatures; e) verifying the existence of preferential zones of bioturbation in the studied soils; f) identifying the major bioturbating agents; and g) understanding the role of bioturbation in the formation of (micro) aggregates from the soil surface to deep soil horizons.

So, in order to understand the principal long and short-term pedogenetic processes that occurred in subtropical ferralsols in Paraná Magmatic Province Brazil, in association with climatic changes, classical soil analysis (morphology, micromorphology, chemical, physical,

mineralogy and geochemical) were carried out in combination to a qualitative characterization of SOM by pyrolysis-GC/MS to study its molecular composition and specific analysis for paleoenvironmental reconstruction ($\delta^{13}C$ isotopic composition and ^{14}C datings), in a continuum from the soil surface to weathering front.

2. MATERIALS AND METHODS

2.1. Study area

2.1.1. Paraná Magmatic Province (PMP): geology

The Paraná Magmatic Province (PMP) is one of the most important Mesozoic (250–66 M.y.) continental igneous provinces observed on the Earth's surface, characterized by the lava flows of the Serra Geral formation (SGF) (Nardy et al., 2014) (Figure 1).

The SGF are mainly composed of flood basalts, with less common occurrence of intermediate and acid rocks. The acid rocks in the SGF are classified as *Palmas*-type (ATP) and *Chapecó*-type (ATC) (Nardy et al., 2008). The ATP rocks are characterized by a light gray to yellowish gray colour, hypohialins, with a granophylic matrix, presenting intense growth of quartz and alkaline feldspar grains (orthoclase). Microcrystals of plagioclase, pyroxene, magnetite and ilmenite occur (Besser et al., 2015). The ATC rocks are characterized by a greenish gray to reddish brown colour, porphyritic texture, presenting phenocrystals of plagioclase, augite, pigeonite and Ti-magnetite. The rock matrix present intergrowth of quartz and alkaline feldspar, plagioclase, pyroxenes, Ti-magnetite, ilmenite and apatite (Ghidin, 2003; Nardy et al., 2008; Besser et al., 2015). The basaltic and intermediate rocks are represented by basalt and andesites. According to Nardy (1988; 1995) the basaltic and intermediate rocks presents a fine-grained texture with dark gray to black colour. Plagioclase, pigeonite, augite, magnetite, ilmenite and olivine compose the matrix, but it may also contain alkaline feldspar, quartz, apatite and vitreous material as accessories minerals. The stratigraphy of the basaltic rocks is well defined with tabular units (trapp) with an average thickness of 30 m. Thin vitreous layers with small vesicles are present at the base of the basaltic flood. Veins of calcite are common in the horizontal diaclases. The central part shows a microcrystalline texture, usually very dark when not altered, and vertical diaclasing (pseudo-columnar structure). The upper part has a vesicular and rugged appearance, with reddish colour (Nardy et al., 2002; Ferreira et al., 2014).

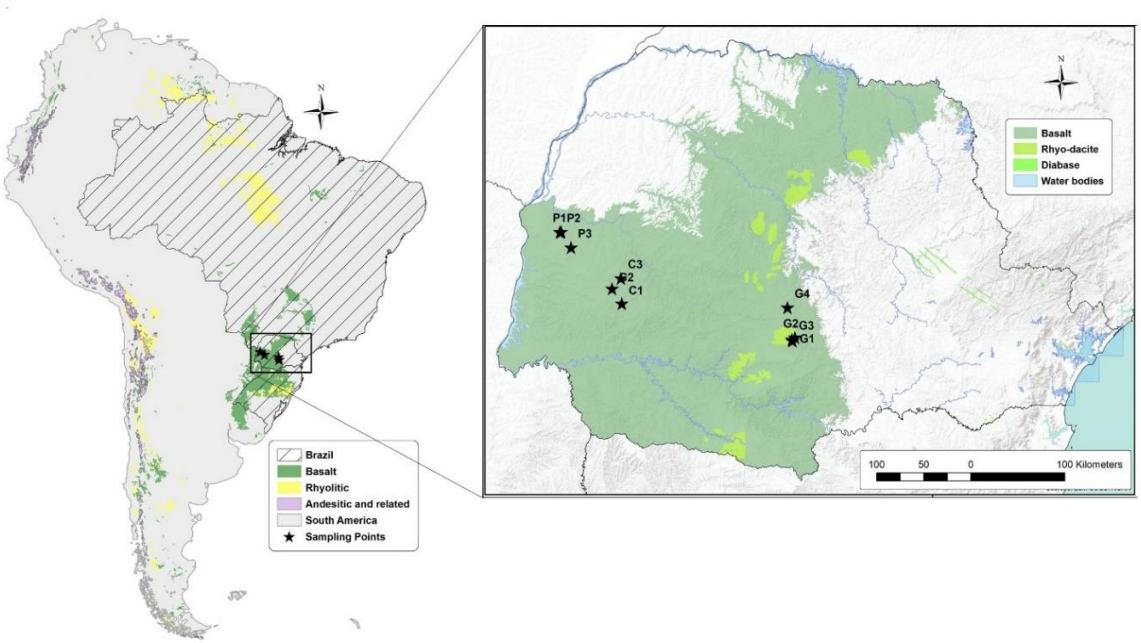

Figure 1. Geology of the Serra Geral formation in Paraná State-Brazil. Location of the ten studied soil profiles (Guarapuava: G1–G4; Cascavel: C1–C3; Palotina: P1–P3).

Geographical variation in the chemical composition of the basic rocks has been reported (Guimarães, 1933; Gutmans, 1943; Leinz, 1949; Rüegg, 1969; Rüegg and Amaral, 1976; Ferreira et al., 2014; Gomes et al., 2018). Gutmans (1943), investigating the parent material of "*Terra Roxa* soils" (ferralsols and nitisols) in Brazil, observed two main groups of the basic rocks according to mineral components and petrographic characteristics, the *Meláfiros* basalts and Diabases/Porphyritic-Diabases. Generally, the *Meláfiros* basalts are the black basalts with vesicles usually filled with calcite, quartz, smectite and celadonite, which may correspond to the top/base vesicular level of the basaltic floods (Ferreira et al., 2014). The diabases/porphyritic-diabases are green rocks and are characterized by the presence of amphibole, chlorite and feldspar. In addition, two major groups of basalts are recognized: tholeiitic basalts and alkali olivine basalts. In the SGF there is a predominance of basalts of tholeiitic affinity and are composed by plagioclase feldspar, clinopyroxene, little or no olivine (Poldervaart, 1964; Melfi et al., 1988). Recently, many geochemical classification criteria for the Paraná magmatic province rocks have been proposed. Bellieni et al. (1984), Mantovani et al. (1985), Marques et al. (1989), Peate et al. (1992) and Gomes et al. (2018) suggested a classification based on the variation of TiO_2 content and ratios of oxides and trace elements.

According to these authors, two groups are considered, a) rocks with TiO_2 < 2% (low Ti) and b) rocks with TiO_2 > 2% (high Ti).

2.1.2. Paraná Magmatic Province: geomorphology

The geomorphological units in the State of Paraná, in particular the *Terceiro Planalto Paranaense*, resulted of the climatic variations, sometimes controlled by the geological structures (Maack, 1947). The magmatic extrusion on the Cretaceous (145 M.y.), originating the rocks of SGF evolved in a complex way controlled by climatic and tectonic factors, which defined the characteristics of the tropical and subtropical landscapes of the *Terceiro Planalto Paranaense* (Justus et al., 1986; Paisani et al., 2019; Silva et al., 2021).

Maack (1947), Ab' Saber (1969), Bigarella and Andrade (1965), Bigarella (2003) and collaborators, Santos et al. (2006) and Paisani et al. (2008; 2013; 2014; 2019), have studied the geomorphology of the Paraná Magmatic Province. The *Terceiro Planalto Paranaense* geomorphological unit has an inclination towards the west in the direction of the Paraná River and the highest elevations occur at the limit between the *Terceiro* and the *Segundo Planalto* (Bigarella and Andrade, 1965; Riffel at al., 2016). According to Bigarella and Andrade (1965), and Bigarella (2003) four major erosional/planned surfaces exists characterizing a cyclical landscape: *pediplano* Pd_3 or *superfície de Cimeira*, *pediplano* Pd_2, *pediplano* Pd_1 and *superfície interplanáltica* Pd_0. However, as reported by Paisani et al. (2013; 2014; 2019) and Silva et al. (2021), the planed surfaces of Paraná Magmatic Province were understood as erosion surfaces from the polycyclic evolution with the occurrence of etchplanation process and interaction of tectonic reactivations and basaltic lithostructure control, suggesting the occurrence of soils with *in situ* formation (autochthonous material) coexisting with *ex situ* ones (allochthonous material).

The studies of Santos et al. (2006) and collaborators, showed that the geomorphology of the *Paraná* state was divided into geomorphological subunits (morphostructural). The ferralsols located in the geomorphological subunits of *Palmas/Guarapuava* and *Pitanga/Ivaiporã* Plateaus, *Cascavel* Plateau and *Campo Mourão* Plateau were chosen for our studies. The *Palmas/Guarapuava* and *Pitanga/Ivaiporã* Plateaus were characterized with high elevations varying between 1000 and 1100 meters above sea level (m a.s.l.) showing a landscape with medium level of dissection and declivity between 6% and < 12% (Santos et al., 2006). These Plateaus represents the *superfície de Cimeira* considered as one of the oldest

and most dissected of the region of the studied areas, with frequent erosion cycles and age of at least 6.5 M.y. (Bigarella, 2003; Paisani et al., 2008; 2013; Riffel et al., 2016). Riffel et al. (2016) reported that the formation and maintenance of deep weathering profiles in the *Palmas/Guarapuava* plateau, indicates an equilibrium between weathering and erosion phases, while the absence of deep weathering profiles suggests conditions of erosive phase, inhibiting the development and preservation of the lateritic weathering crust. *Cascavel* Plateau is characterized by altitudes varying between 700 and 800 m a.s.l., a landscape with medium level of dissection and declivity < 12% (Santos et al., 2006). *Campo Mourão* Plateau is a landscape with altitudes less than 600 m a.s.l. with low level of dissection and declivity < 6%. Soils formed on this last plateau (*Campo Mourão* Plateau) are considered relatively young in the environmental and topographic gradient studied here (Santos et al., 2006; Paisani et al., 2008).

2.1.3. Study sites and sampling

The soil profiles are all situated at the summit of the four chosen Plateaus (*Palmas/Guarapuava*, *Pitanga/Ivaiporã*, *Cascavel* and *Campo Mourão*) in three areas that differ in altitude, climate and native/current vegetation. Four profiles were sampled in the city of Guarapuava (G1–G4), three in the city of Cascavel (C1–C3) and three in the city of Palotina (P1–P3) (Figure 1; Table 1). The soil profiles were digged and cleaned until the saprolite zone. In the three studied areas, deep trenches (G1, C1, C2, P1, P2 and P3 profiles) were digged using a mechanical digger. The soil profiles (G2, G3, G4 and C3) were cleaned at ~100 cm into the soil profile. In addtion, the soil profile C3 was collected from a recent road duplication. Photographs of studied soil profiles can be observed in Figure 2 and Appendix A–C. The parent material is basaltic rock, with exception of three soil profiles from Guarapuava (G1, G2 and G3) that were derived from acidic volcanic rocks from Chapecó-type (porphyritic rhyo-dacite) (Nardy et al., 2011).

The climate is temperate and humid subtropical (Cfb, Köppen classification) with a mean annual precipitation of 2000 mm/yr and a mean annual temperature of 18°C in Guarapuava. The climate in Cascavel and Palotina is classified as subtropical and humid (Cfa, Köppen classification), with a mean annual precipitation of 2000 mm/yr and 1800 mm/yr, respectively; the mean annual temperature is 22°C in Cascavel and 23°C in Palotina (Nitsche et al., 2019). The native vegetation in Guarapuava is a mosaic of ombrophilous forest (with

Araucaria spp. trees) and grassland. In Cascavel and Palotina, the native vegetation is semideciduous forest, with presence of *Araucaria spp*. trees in Cascavel (Appendix D–F).

Table 1. Location, current vegetation, land use, altitude, parent material and local and regional relief of the studied soil profiles.

Location	Study sites	Coordinates	Current vegetation	Land use	Altitude (m a.s.l)[1]	Parent material	Local and regional relief
Guarapuava, Brazil	G1	25°23’ 11,11” S, 51°29’29,6” W	Grasses and shrubs	Abandoned agriculture	1033	Rhyo-dacite	SU; SU –U
	G2	25°21’ 10,37” S, 51°28’1,89” W	Araucaria forest	Preservation area	1076	Rhyo-dacite	SU; SU–U
	G3	25°22’ 22,5” S, 51°29’54,1” W	Araucaria forest	Preservation area	971	Rhyo-dacite	U–SU; SU–U
	G4	25°04’ 03,1” S, 51°32’32” W	Araucaria forest	Preservation area	1113	Basalt	SU–U; U–STU
Cascavel, Brazil	C1	25°00’ 45,1” S, 53°17’19,0” W	Sweet potato	Agriculture	790	Basalt	SU; SU
	C2	24°52’ 16,3” S, 53°23’12,5” W	Semideciduous forest with Araucaria trees and ferns	Preservation area	674	Basalt	SU; SU
	C3	24°46’ 21,3” S, 53°17’34,2” W	Soybean/Maize	Agriculture	669	Basalt	SU; SU
Palotina, Brazil	P1	24°19’ 14,27” S, 53°54’29,23” W	Semideciduous forest	Preservation area	332	Basalt	SU; SU
	P2	24°19’ 19,2” S e 53°55’25,5” W	Soybean/Maize	Agriculture	343	Basalt	SU; SU
	P3	24°28’14,5” S e 53°48’39,63” W	Soybean/Maize	Agriculture	438	Basalt	SU; SU

[1] m a.s.l. = meters above sea level. [2] SU = slightly undulating; U = undulating; STU = Strong undulating.

The ten soil profiles were described and sampled according to pedogenic horizons determined in the field from the surface to the contact with the saprolite (Schoeneberger et al., 2002; Santos et al., 2013). The most of the analysis were performed using these samples. In addition, the soil profiles were sampled at regular depths (10 cm intervals) for $\delta^{13}C$ isotopic composition and pyrolysis-GC/MS (ten studied soils) and sand fraction content (representative ones: G1, G4, C3 and P3). The samples were air-dried, ground and sieved through 2 mm mesh for laboratory analyses. Representative soil profiles were chosen according with soil depth (deep soils) and the presence of BCr horizon (G1, G4, C3 and P3).

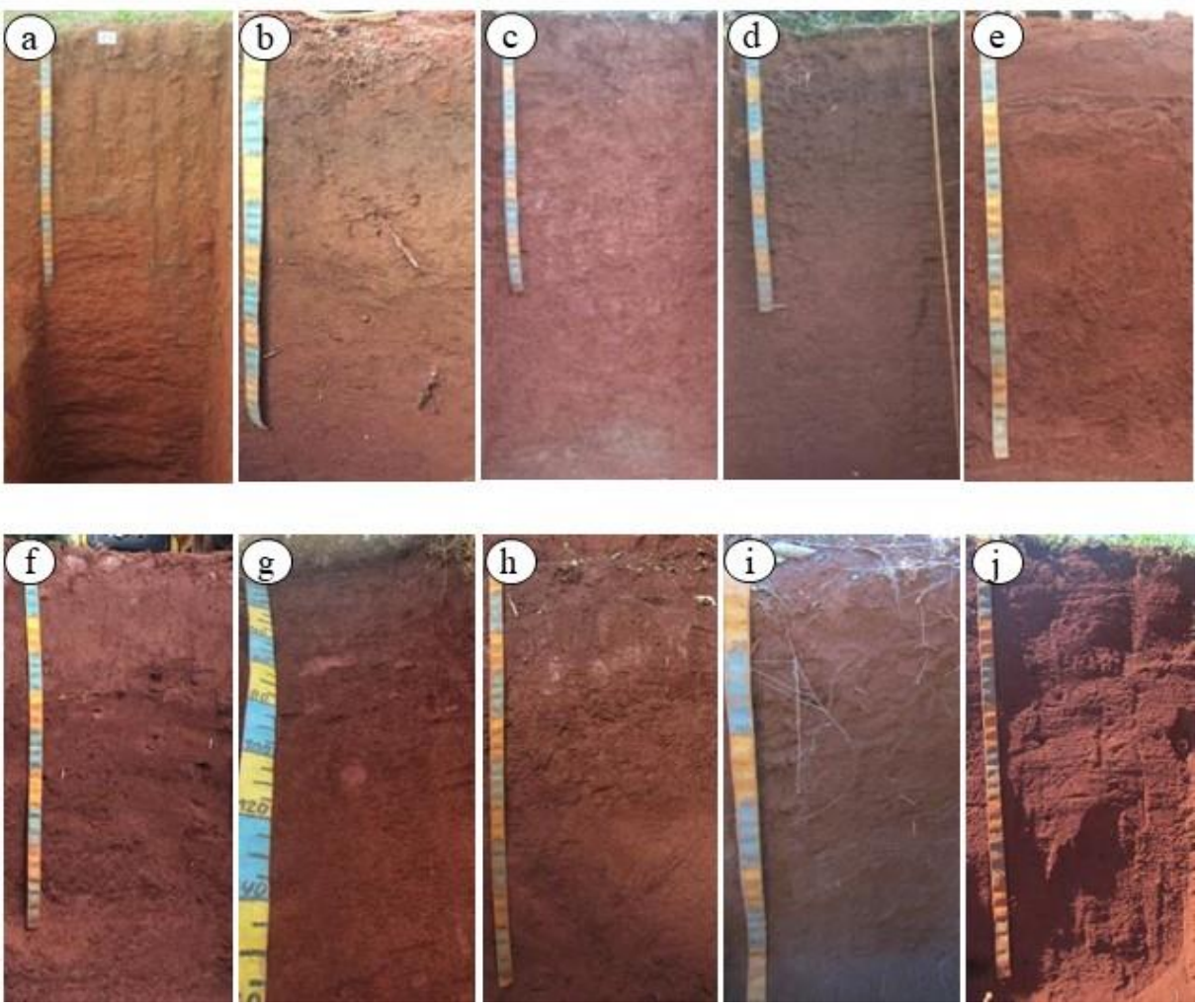

Figure 2. Photographs of the ten studied soil profiles. a)–d) Guarapuava soil profiles: G1–G4; e)–g) Cascavel soil profiles: C –C3; h)–j) Palotina profiles: P1–P3; the photographs show the first two meters for all profiles, but scales may slightly differ).

2.2. Analytical

2.2.1. Physical and chemical analysis and soil classification

Physical and chemical analyses were carried out in soil samples of pedogenetic horizons. The clay and sand fraction (% wt.) were determined by the hydrometer method after removing OM with hydrogen peroxide and dispersion with 1 mol L^{-1} NaOH (Teixeira et al., 2017). The silt fraction was calculated by subtraction of the clay+sand fraction contents minus the initial soil mass. In addition, the sand fraction was sieved into five size fractions of the representative soil profiles (G1, G4, C3 and P3): very coarse (VC: 2–1 mm), coarse (C: 1–0.5 mm), medium (M: 0.5–0.25 mm), fine (F: 0.25–0.10 mm) and very fine (VF: 0.10–0.05 mm) sand (Appendix G–J).

Chemical analysis included the determination of pH (H_2O and KCl), exchangeable Ca^{2+}, Mg^{2+} and Al^{3+} after extraction by KCl 1 mol L^{-1}, exchangeable H+Al using extraction calcium acetate (0.5 mol^{-1}) at pH 7, and P, K^+ and Na^+ by mild acidic Mehlich solution. Ca^{2+} and Mg^{2+} were determined by atomic absorption spectrometry, Na^+ and K^+ by flame atomic emission photometry and P by colorimetry using a UV-VIS spectrophotometer. Al^{3+} and H+Al were determined by titration. Cation exchange capacity (CEC) was calculated by the sum of the exchangeable cations at pH 7 (Ca^{2+}, Mg^{2+}, K^+, H^+, Al). In addition, contents of Fe (Fe_2O_3), Al (Al_2O_3), Ti (TiO_2) and Si (SiO_2) of the sulphuric extract of the samples from the Bfl horizons of the representative soil profiles (G1, G4, C3 and P3) were carried out. The soil profiles were classified using the Brazilian Soil Classification System–SiBCS (Santos et al., 2018), and WRB–FAO system (IUSS Working Group WRB, 2015).

2.2.2. Bulk chemical analysis

We analyzed the soil bulk chemical composition using a Shimadzu EDX–720 x-ray fluorescence spectrophotometer (XRF) (Shimadzu Corp. Kyoto, Japan). The K, Ca, Mg, Mn, Fe, Ti, Al, Zr, and Si contents were determined for all pedogenetic soil samples from the representative soil profiles (G1, G4, C3 and P3). The calibration curves were obtained using nine internal standards developed at the Nuclear Instrumentation Lab at CENA/USP in addition to reference standard materials (USGS BCR-2; USGS DNC-1; USGS GSP-2; USGS QLO-1a; USGS SDC-1; USGS W-2a; USGS COQ-1; NIST 2710; NIST 2711; NIST 2704;

NIST 2586; EMBRAPA Sand soil; GBW 07411 Soil; BCR 142R; BCR-143R; RTC CRM025-050; RTC CRM030-050). The recovery were performed to check the accuracy of the calibration curves and presented a % recovery = 81%. All pulverized samples and standards were analysed for 200 seconds at 40 kV. The same samples were heated in an oven at 1050 ℃ for 2 h and the mass loss was determined by gravimetric means and assigned as loss on ignition (LOI). Yttrium (Y) was determined in a reduced number of samples (38 horizons) of the studied soil profiles after digestion in lithium metaborate and tetraborate at 1050 °C during 30 min. The resultant pellet was dissolved in 10% hydrochloric acid and were determined by ICP-OES according to Nóbrega et al. (2017).

2.2.3. Dithionite, oxalate and pyrophosphate extractable Fe

The Fe contents associated with different componentes of solid fraction were determined for the selected soil samples from the pedogenetic horizons of representative profiles (G1: Ap, AB, BA, Bfl_1, BC_1 and BC_2; G4: A_1, A_3, AB, BA, Bfl_1, Bfl_2, Bfl_3, BCr; C3: Ap, BA, Bfl_1, Bfl_2, Bfl_3, BC_2, BCr; P3: Ap, Bfl_1, Bfl_2, Bfl_3, Bfl_6 and Bfl_7). Extraction with 0.1 mol L^{-1} sodium pyrophosphate was carried out at pH 10, according to USDA (1996) in bulk soil samples of the selected pedogenetic horizons of the representative profiles, providing the Fe content that is associated with OM (Fe_P). Fe contents was determined by atomic absorption spectrometry. Free Fe-oxyhydroxides were extracted using sodium citrate-bicarbonate-dithionite (Fe_{CBD}) treatment (four times at 65ºC for 30 min) (Mehra and Jackson, 1960; Jackson, 1979) from the clay fraction of the selected pedogenetic horizons of the representative profiles. Fe associated with non-crystalline Fe-oxyhydroxides (Fe_{AO}) was determined after extraction with 0.2 mol L^{-1} ammonium oxalate in the dark at pH 3.0 from the clay fraction of the representative profiles (McKeague, 1966). Fe contents was determined by colorimetry using a UV-VIS spectrophotometer.

2.2.4. Mineralogy

2.2.4.1. X-Ray diffraction

Mineralogical analysis was performed on the clay fraction of the same soil samples submitted to selective Fe extraction (*section 2.2.3*). The sand fraction was separated from the

silt + clay fractions by sieving after dispersion with 0.2 mol L^{-1} NaOH (0.053 mm sieve opening). Thereafter, the clay fraction was separated from the silt by decantation, following Stokes' law (Jackson, 1979). X-ray diffractograms (XRD) were obtained for oriented mounts, with clay samples saturated with K^+ (KCl 1 mol L^{-1}) and Mg^{2+} (MgCl 1 mol L^{-1}). The K-saturated samples were heated at 550°C for 2h before studied at the XRD. The Mg-saturated samples were studied at room temperature and after solvation with ethylene glicol. The XRD device (Panalitycal X'Pert3 Powder) was operated at 40 mA and 40 kV, at a rate of 0.02º 2θ and a speed of 1 sec/step, in the range from 4–65º 2θ. The diffractometer was equipped with a Ni filter, and the Cu (CuKα) radiation was used. In addition, the XRD of sand fraction of the same soil samples and the rock samples from G1 (rhyo-dacite porphyritic), G4 and P3 (basalts) sites were obtained using a scanning range from 3°–65° 2θ on non-oriented powdered samples on glass slides.

The crystallinity index value (CI) of kaolinite (Kt) was calculated from the random powder diffraction patterns, according to Hughes and Brown (1979). The relative values of the asymmetry index values (AI) of the d 001 Kt peak were obtained according to Melo and Wypych (2009). The mean crystallite dimension (MCD) of Kt and Gb were calculated from the width at half maximum height (WHH) of basal peaks using the Scherrer's equation (Klug and Alexander, 1954). The average number layers (ALN) of Kt in the 001 direction was calculated by dividing MCD by the d 001 values.

The Fe-oxyhydroxides in the clay fraction were concentrated using NaOH 5 mol L^{-1} solution at 80°C, which removes clay minerals and Al-hydroxides (Norrish and Taylor, 1961). Sodium metasilicate was added to reach 0.2 mol L^{-1} Si concentration in solution to avoid formation of iron oxides with high Al isomorphic substitution (Kämpf and Schwertmann, 1982). Sodalite [$Na_4Al_3Si_3O_{12}(OH)$] formed during extraction was removed by washing the samples twice with 50 mL of 0.5 mol L^{-1} HCl solution, followed by washing with 50 mL of deionized water (Norrish and Taylor, 1961; Singh and Gilkes, 1991). The mineral components of the concentrated Fe residue were identified by XRD, carried out on non-oriented powdered samples on concave glass slides, using a scanning range from 3°–60° 2θ.

The goethite/hematite ratio [Gt/(Gt + Hm)] was estimated using an adaptation of the formula presented by Torrent and Cabedo (1986) according to Melo et al. (2020). This adaptation was made replacing the ratio of Gt(111)/Hm(110) peak areas by the ratio of Gt(110)/Hm(104) peak areas, because of the absence of Gt(111) peak in the most of soil samples (Melo et al. 2020). Fe isomorphic substitution by Al (IS) in Gt was calculated

according to Schulze (1984) and in Hm according to Schwertmann et al. (1979). The Gt and Hm contents were estimated based on the crystalline Fe content (Fe_{CBD} - Fe_{AO}), considering the Gt/(Gt+Hm) ratio, the IS level, and the least mineral formulas (Melo et al., 2001).

2.2.4.2. Thermal analysis

The kaolinite (Kt) and gibbsite (Gb) contents in the clay fraction were determined in the residual material derived from CBD treatment, via simultaneous differential thermal analysis (DTA) and thermogravimetric (TG) analyses. Approximately 10 mg of clay sample free from Fe-oxyhydroxides (placed in a platinum crucible) were heated from room temperature to 950°C, at a rate of 10°C min^{-1} under N_2 flow of 50 mL min^{-1}. The exothermic dehydroxylation events for Gb (~250ºC) and Kt (~500ºC) recorded in DTA were used for quantification, by measuring their peak areas (Melo et al., 2001).

2.2.5. Micromorphology

2.2.5.1. Rocks and soils

Rocks exposed on the surface (G1, G4, C2 and P3; weathered rocks) and undisturbed and oriented soil samples from studied soil profiles were taken from the main soil horizons (A, Bfl and C), transitions between horizons (AB and BA) and the weathering front (BCr). One hundred and seven polished blocks (5 × 11 cm), 65 thin soil sections (5 × 9 cm) and 4 rock thin sections were prepared. The identification of the rock minerals was carried out according to Heinrich (1965) and Delvigne (1998). For thin soil sections the description were carried out according to Bullock et al. (1985), Castro and Cooper (2019) and Stoops (2021).

2.2.5.2. Electron microscopy analysis: SEM-EDS

Thin sections were selected to investigate the elemental distribution and composition of specific points of rock, saprolite and deep horizons using a Jeol JSM-IT300LV scanning electron microscopy coupled with an energy dispersive X-ray detector (SEM-EDS), following the recommendations of Bisdom and Ducloux (1983).

2.2.6. Parent material uniformity

In order to study the uniformity of parent material and assess pedogenetic processes and their continuity over time in the representative soil profiles (G1, G4, C3 and P3), many approaches were used: a) Zr distribution; b) Ti/Zr ratio; c) fine sand/course sand ratio (FS/CS); d) sand grain shape parameter; e) Y distribution; and f) mineralogy of sand fraction (Chittleborough et al., 1984; Karanthanasis and Macneal, 1994; Schaetzl, 1998; Tsai and Chen, 2000; Anda et al., 2009; Novais Filho et al., 2012).

The sand grain shape parameter was studied in some soil samples (G1: AB, Bfl_4 and BC_2; G4: A_3, Bfl_1 and BC_2; C3: Bfl_1, Bfl_3 and BC_1; P3: Blf_3, Bfl_5, Bfl_7), observing and photographing 50 typical quartz grains (fine sand (0.25–0.10 mm) at G1, C3 and P3 profiles; very fine sand (0.10–0.05 mm) at G4) under an optical microscopy. Image analysis was performed using the *ImageJ* software. The shape index used was Roundness (Rd) and was calculated according to Eq. 1. The roundness is a geometrical estimation of the time of residence of a particle in an abrasion process. Values of 1.0 indicates the circular shape, and values close to 0.0 indicate that the object is less circular (Teixeira et al., 2017).

$$\text{Roundness} = 4 \times \frac{[Area]}{\pi \times [major\ axis]^2} \qquad \text{Equation 1}$$

2.2.7. Weathering indices and geochemical mass balance calculations

Weathering indices and geochemical mass balance calculations were studied for the representative soil profiles (G1, G4, C3 and P3). Weathering indices were calculated using soil bulk chemical data (from XRF analysis, *section 2.2.2*) to investigate weathering trends. Three weathering indices were calculated: Ruxton Ratio (R; Ruxton, 1968), Silica/Titania Index (STI; Jayawardena and Izawa, 1994) and the A weathering index adapted from Kronberg and Nesbitt (1981) (Table 2).

Table 2. Summary of the weathering indices used in the studied soil profiles. Listing modified from Price and Velbel (2003) and Yost et al. (2019).

Index	Formula	Increase in the weathering trend
Ruxton Ratio (R)	$R = \frac{SiO_2}{Al_2O_3}$	Negative
Silica/Titanium Index (STI)	$STI = 100 \times \left[\frac{\left(\frac{SiO_2}{TiO_2}\right)}{\left(\frac{SiO_2}{TiO_2}\right)+\left(\frac{SiO_2}{Al_2O_3}\right)+\left(\frac{Al_2O_3}{TiO_2}\right)} \right]$	Negative
A Index	$A = \left[\frac{(SiO_2+CaO+K_2O}{Al_2O_3+SiO_2+CaO+K_2O}\right]$	-

Geochemical mass balance calculations were performed following the methods described by Brimhall and Dietrich (1987), Chadwick et al. (1990), Anderson et al. (2002), Caner et al. (2014) and Andrade et al. (2019), considering the development *in situ* from the soil profiles and Zr as the conservative element. Thus, the mass transfer ((τ), gain/losses) of each element with respect to the parent material, was calculated from Eq. (2) (Andrade et al., 2019):

$$\tau = \left(\frac{C_{j,w}\ C_{i,p}}{C_{i,w}\ C_{j,p}}\right) - 1 \qquad \text{Eq. 2}$$

$C_{j,w}$ is considered the concentration of the element j in soil horizon (w) or in the parent material (p), and $C_{i,p}$ and $C_{i,w}$ are the concentrations of immobile element (Zr) in the parent material and soil horizons. Positive $\tau_{j,w}$ values indicate element gains, while negative values indicate losses. In addition, the physical variations during the weathering are calculated based on strain values (ε), (Equation (3)) (Andrade et al., 2019):

$$\varepsilon_{i,w} = \left(\frac{\rho_p\ C_{i,p}}{C_{i,w}\ C_{j,p}}\right) - 1 \qquad \text{Eq. 3}$$

ρ_p and ρ_w are the density of the parent material and soil horizon, respectively. ε positive values indicate volume increase (dilation), while negative values indicate contraction after weathering. The ε values are used for mass flux calculations, in Eq. (4) (Andrade et al., 2019):

$$m_{j,flux} = \rho_p C_{j,p} \tau_w Z_w \left(\frac{1}{\varepsilon_{i,w+1}}\right) \quad \text{Eq. 4}$$

$M_{j,flux}$ represents the elemental gains and losses per unit area (kg m^{-2}), and Z_w is soil or saprolite horizon thickness.

The geochemical mass balance calculations for C3 soil profile was performed using a reference rock collected 13.5 km distant away from the soil profile, assumed as identical to basaltic rock (parent material) of the C3 profile.

2.2.8. ^{14}C dating

Because no macroscopic charcoal was present, the humin fraction was used for ^{14}C dating. This means that the ^{14}C values of humin fraction were used to reflect minimum soil ages (Gouveia et al., 1999). Humin of the soil samples was separated according to the method described by Pessenda (1996). Samples from horizons of the representative soil profiles were chosen and included: A_2, BA, Bfl_3 horizons (profile G4); BA, Bfl_3, BCr horizons (profile C3); and Bfl_1, Bfl_3, Bfl_5 horizons (profile P3).^{14}C analysis was carried out at the Radiocarbon Laboratory (Centro de Energia Nuclear na Agricultura, CENA and the AMS Laboratory at University of Georgia, USA). ^{14}C values were calibrated (2δ) and expressed in years before present (BP).

2.2.9. Total C and N, and δ^{13}C isotopic composition

The soil samples were collected at 10 cm intervals (554 samples) from the ten soil profiles and analyzed for total C and N contents (Ct and Nt), and for ^{13}C isotopic composition. δ^{13}C analysis was determined using a C/N elemental analyzer coupled to an ANCA-SL mass spectrometer 2020 Scientific Europe at Isotopic Ecology lab (CENA/USP). The results were expressed in the delta per mil notation (‰). The ^{13}C results are expressed as δ^{13}C, with respect to the VPDB standard (Gonfiantini, 1978). Total C and N were determined by dry

combustion, using a C/N elemental analyzer coupled with an ANCA-SL mass spectrometer 2020 from Scientific Europe at the Isotopic Ecology Laboratory of CENA/USP.

2.2.10. Pyrolysis-GC/MS

To study the molecular composition of SOM, a selection of samples were analyzed by pyrolysis-GC/MS. To this end, regular depth intervals of 30 cm were chosen from 0 to 250 cm depth, and intervals of 100 cm from 250 cm downwards each profile, resulting in a total of 152 samples.

2.2.10.1. SOM isolation

In order to demineralise the soil samples, five grams of air-dried soil were sieved through 0.053 mm and were shaken with 40 ml 1M HF/HCl (3:1) for 6 hours. The suspension was centrifuged (15 min, 8000 rpm) and the extract was discarded. This process was repeated seven times to remove reactive minerals (Zegouagh et al., 2004). The residue was shaken for two hours with 40 ml 1 M HCl and left standing overnight. The suspension was centrifuged (15 min, 8000 rpm), after which the supernatant was discarded and the residue washed with distilled water. The washed residue was dried at 40 °C, homogenized and analysed by pyrolysis-GC/MS.

2.2.10.2. Analytical

Py-GC/MS was performed at the Environmental Chemistry Lab of IQSC/USP (São Carlos, Brazil) using a single shot PY-3030S pyrolyser (Frontier Laboratories, Fukushima, Japan) coupled to a GCMS-QP2010 plus (Shimadzu, Kyoto, Japan). The pyrolysis temperature was set at 600 °C (± 0.1 °C); the carrier gas used was Helium at a constant flow of 34.5 ml min^{-1}. The injection temperature of the GC (split 1:20) and the GC/MS interface were set at 320 °C. The GC oven was heated from 50 to 320 °C (held 10 min) at 7 °C min^{-1}. The GC instrument was equipped with an Ultra Alloy capillary column, length 30 m, thickness 0.25 mm, diameter 0.25 μm. The MS scanned over the range of *m/z* 45–600.

2.2.10.3. Quantification

Pyrolysis products were identified using the NIST '14 mass spectral library. Due to the low Ct content of some deep samples, some of the pyrograms were not of sufficient intensity to reliably reflect its composition; these were excluded for further analysis and include samples: G1 (245 cm and 345 cm), G2 (105 cm and 165 cm); G3 (105 cm and 145 cm); G4 (145 cm, 225 cm and 245 cm); C1 (65 cm and 545 cm); C3 (145 cm, 185 cm and 745 cm); P1 (145 cm, 205 cm, 225 cm and 345 cm); P2 (125 cm, 545 cm and 645 cm); and P3 (145 cm and 345 cm).

Identified products comprised lignin phenols, phenols, (alkyl) benzenes, polycyclic aromatic hydrocarbons (PAHs), benzofurans, carbohydrates, N-containing compounds, S-containing compounds, triterpenes, and aliphatics. From these, a selection of 34 products were quantified for soil organic matter composition (Appendix K). Quantification was based on the peak area of one or more characteristic fragment ions (*m/z* values) for each pyrolysis product. For each sample, the sum of peak areas was set at 100% and expressed as total ion current (TIC), and relative proportions were calculated with respect to this sum. The resulting quantification allows a reliable comparison of the relative abundance of each pyrolysis product within a set of samples. Factor analysis was applied to pyrolysis products using Statistica software, version 6 (Statsoft), to provide an indication of the main chemical differences between soil profiles and with depth.

2.2.11. Bioturbation study

For the bioturbation study and test the hypothesis (b) and part of (c), identification and quantification of the biofeatures (BFs) were carried out in a macro and microscale. The corresponding bioturbating agents (Ba) were identified according to the existing literature in mainly three soil profiles (one representative of each study area) and specific soil horizons (G4: A_3, Bfl_1, Bfl_3 and BC_2; C3: AB, Bfl_1, Bfl_3, Bfl_4 and BC_2; P3: Bfl_1, Bfl_2, Bfl_4 and Bfl_6). In addition, we will present representative images of the other studied profiles to make generalizations between the studied areas. Furthermore, an ant experiment was realized in order to study the (micro) aggregate morphology to test the particular participation of ants in soil bioturbation and (micro) aggregate formation.

2.2.11.1. Biofeatures on the macroscale

Biofeatures are visible at different scales. In order to identify biofeatures on a macroscale (visible in the field), the ten soil profiles were described morphologically using a mesh divided into quadrants of 30 × 30 cm until the contact with saprolite (Figure 3). The BFs were described and photographed according to these quadrants. The area of biofeatures was calculated using *ImageJ* software, and bioturbation (%) according to equation 5 (adapted from Rodrigues, 2019).

$$\text{Bioturbation (\%)} = \frac{(Total\ area\ of\ BFs\ at\ determined\ soil\ depth)}{(Analyzed\ area\ at\ determined\ soil\ depth)} \times 100 \qquad \text{Eq. 5}$$

In addition, some BFs were collected and the total C content (%) determined to analyse the input of carbon by the soil fauna.

2.2.11.2. Biofeatures on the microscale

The quantification of BFs was carried out on images from polished blocks using a Nikon camera under UV-light. The area of biofeatures was delineated on the UV-images using *ImageJ software* (Humphreys, 1993) (Figure 4). The area of biofeatures and bioturbation (%) on a microscale were calculated relative to each polished block according to equation 6 (Rodrigues, 2019).

$$\text{Bioturbation}(\%) = \frac{(Total\ area\ of\ BFs\ in\ the\ polished\ block)}{(Representative\ area\ of\ polished\ block)} \times 100 \qquad \text{Eq. 6}$$

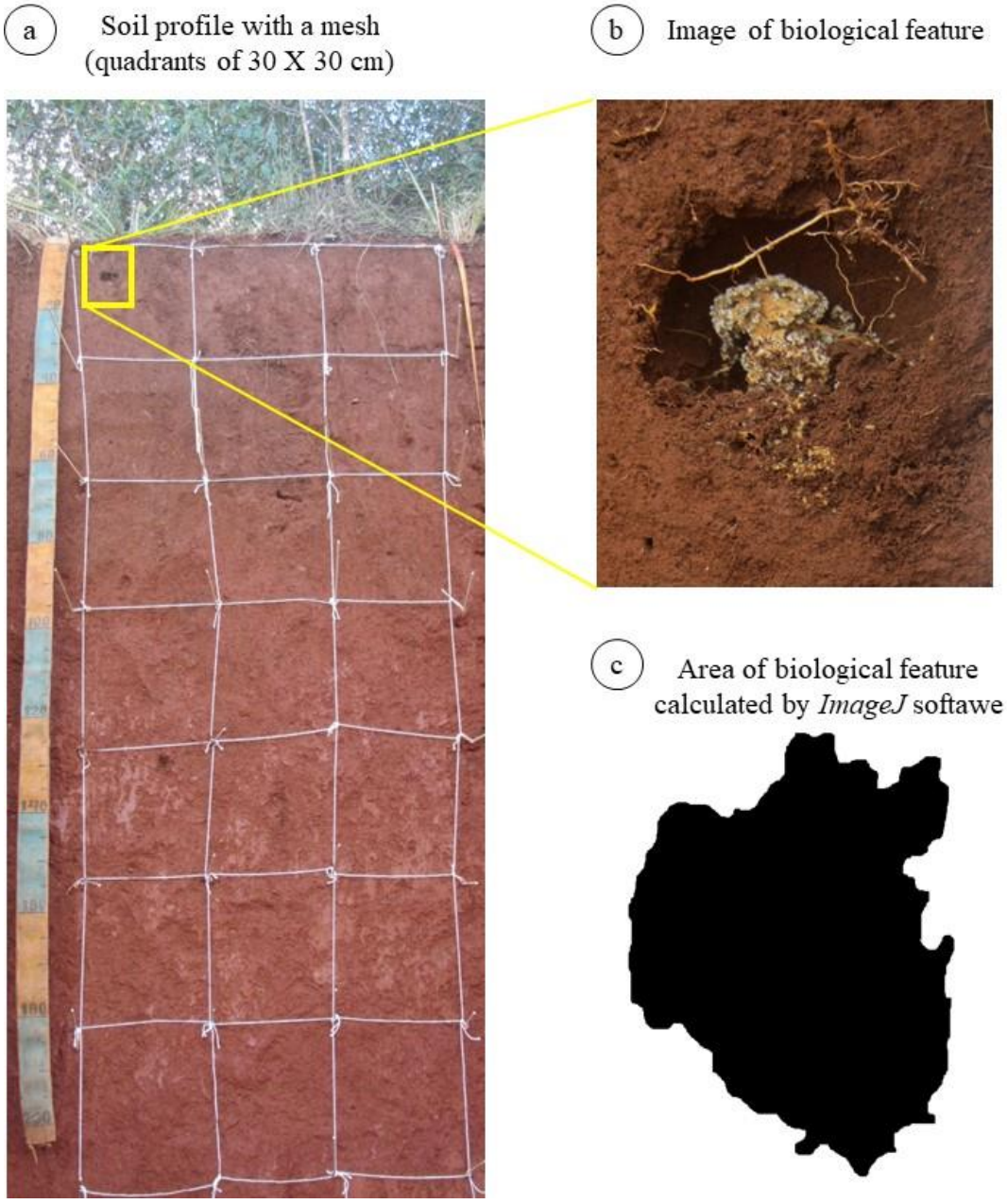

Figure 3. Methodological design of the image analysis used for the quantification of biofeatures on a macroscale; expressed as percentage (%) of analyzed area at a determined depth.

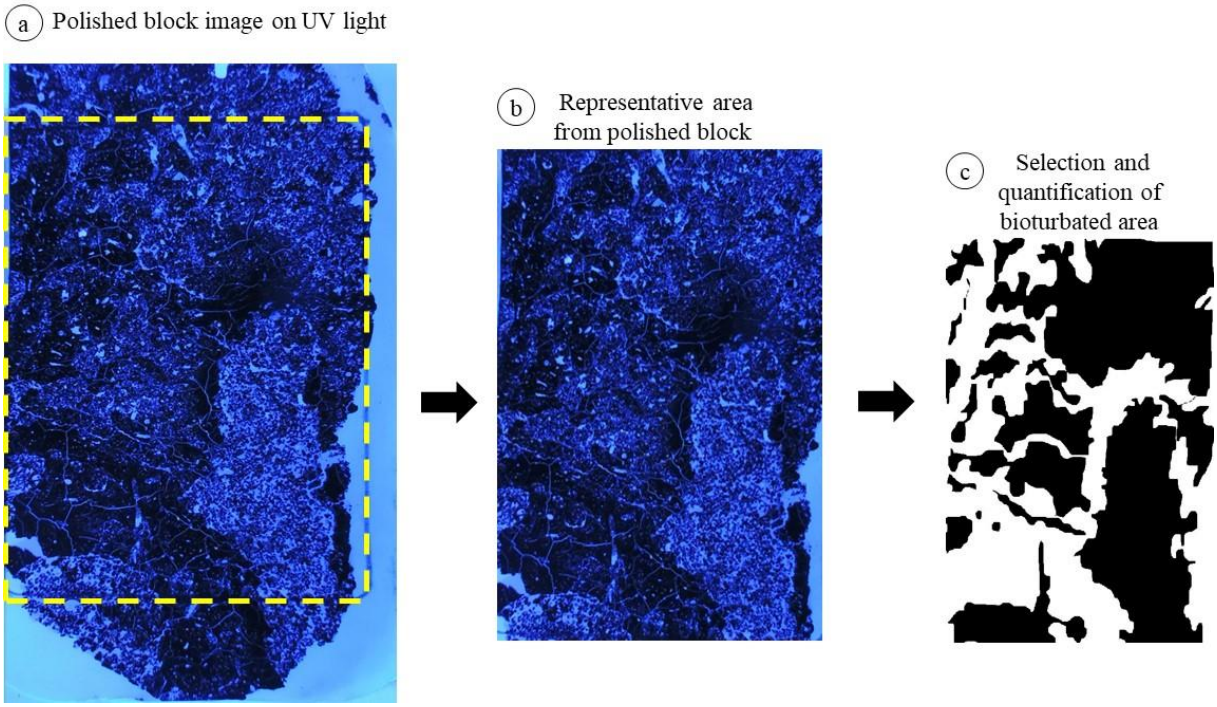

Figure 4. Example of image analysis for quantification (%) of bioturbation on a microscale from polished blocks.

2.2.11.3. Ant laboratory experiment: the production of biological (micro) aggregates

Based on their role in soil formation and broad occurrence in Brazil, a specie of leaf-cutting ant, *Atta sexdens rubropilosa* was selected (Gallo et al., 1988; Garcia et al., 2003). A laboratory experiment with ant colonies was carried out in the Social-Pest Insects laboratory at São Paulo State University (Botucatu-SP, Brazil). We used the soil samples from profile G4 from Guarapuava-PR, Brazil (25°04'3.1"S; 51°32'32"W) and profile P3 from Palotina-PR, Brazil (24°28'14.5"S; 53°48'39.63"W). For both profiles, composite samples of 1 kg from the soil horizons were prepared. The soil samples were air-dried, homogenized, and sieved through a 0.149 mm mesh. Prior to soil mandibulation by the ants (i.e. digging and (micro) aggregate formation), the soil samples (250 g) were wetted and material from the fungus chamber (1 g) was added to stimulate the digging process. The number of ants used to dig the nest and produce the (micro) aggregates was 25 to 30 workers, randomly chosen. The experiment lasted one day and was carried out in duplicate. An example of the structure used in the experiment can be observed in Figure 5.

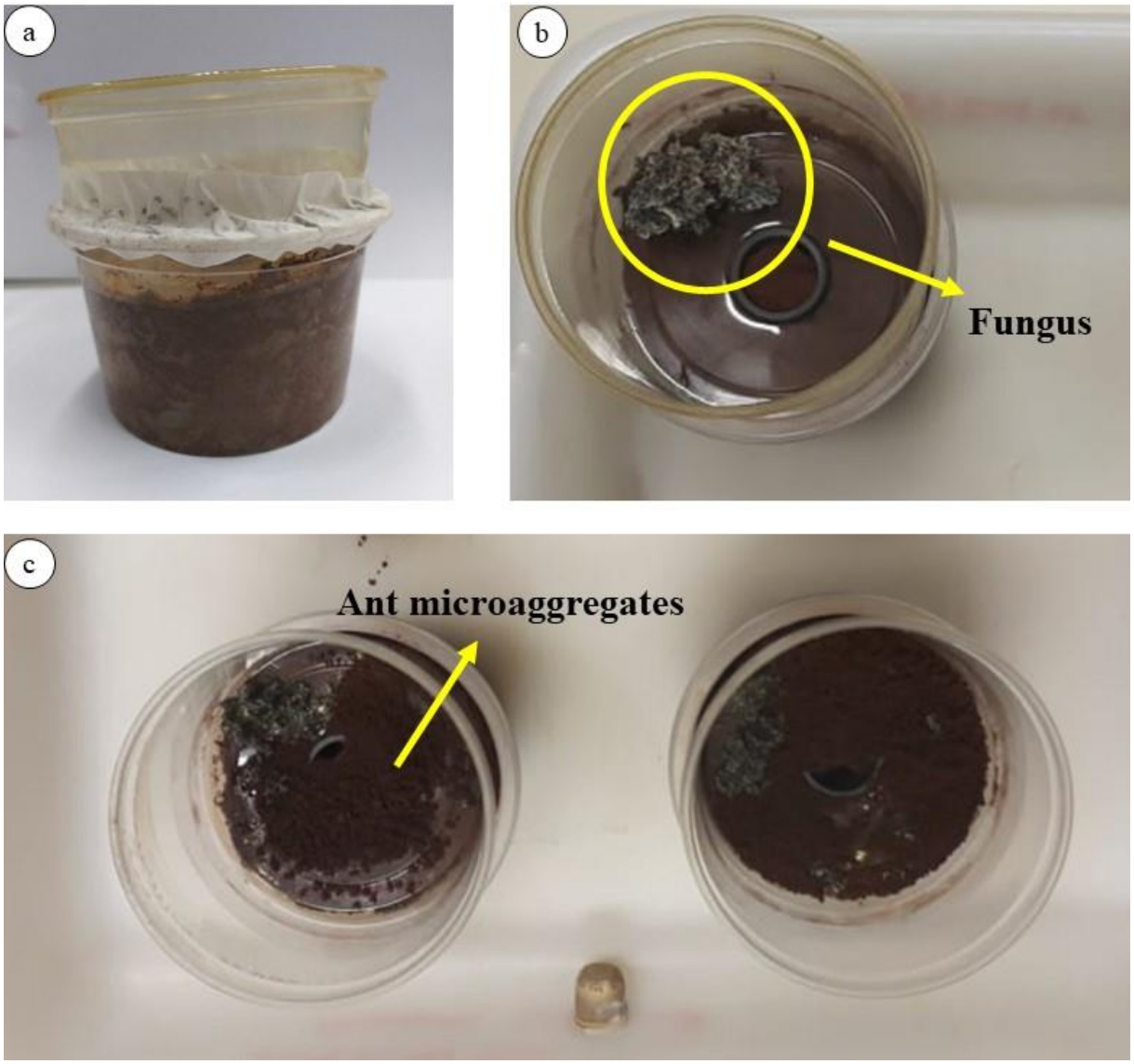

Figure 5. Ant experiment structure. a) Lateral view; b) Upper view, from where it is possible to observe the fungus; c) Superior view after the process of excavation and production of ant aggregates (biological (micro) aggregates).

3. RESULTS AND DISCUSSION

3.1. Parent material uniformity in ferralsols: an old literature question and prerequisite to assess pedogenetic processes

The distribution curves of Zr concentration, Ti/Zr ratio and Y as a function of depth for the four representative soil profiles (G1, G4, C3 and P3) are shown in Figure 6. The curves of Zr concentration showed a similar trend with a smooth shape, without inflection for G1, G4, C3 and P3 soil profiles. The highest Zr values were observed in samples from upper horizons. According to Brewer (1976), Smeck et al. (1994) and Anda et al. (2009), the absence of inflection associated with highest Zr contents in upper horizons indicate parent material uniformity. The results of Ti/Zr ratio of the studied soil profiles indicate that the parent material for each soil was initially homogeneous. All Ti/Zr ratio showed a very high degree of similarity with depth and coefficient of variation (CV), i.e. < 25% (CV: G1 = 9.8%; G4 = 9.5%; C3 = 23.9%; P3 = 21.5%) indicating the absence of lithologic discontinuity (Figure 6). In addition, the distribution curves of Y concentration showed a high degree of similarity with depth, presenting CV < 25% for G1 (CV = 23.1%) and P3 (20.5%) soil profiles. However, for profiles G4 and C3, the CVs were > 25% (41.8 % and 36.7%, respectively), which could characterize the occurrence of lithological discontinuity.

Generally, several studies addressed the CV of elemental ratios (Zr, Zr/Ti or Ti/Zr and Y), in combination with soil morphology, to detect lithologic discontinuity and parent material uniformity. Drees and Wilding (1978) considered deviations higher than 22% to assign lithologic discontinuity in soil profiles. Chapman and Horn (1968) considered differences CV > 100% or more, and Chittleborough et al. (1984) adopted a value of 25%. In this study, we adopted the value of 25% for CV to elemental distribution according to Chittleborough et al. (1984).

In addition to the elemental distributions, the FS/CS ratio of the studied soil profiles showed a very high similarity with depth, presenting a CV < 50% (CV: G1 = 33.3%; G4 = 22.3%; C3 = 16.1%; P3 = 11.4%) indicating low data dispersion (Figure 6). According to Karanthanasis and Macneal (1994) and Novais Filho et al. (2012), the occurrence of a CV < 50% for the FS/CS ratio, associated to Ti/Zr ratio and Zr distribution curves without inflection and homogeneous profile morphology, are indicative of the uniformity of the parent material.

The sand grain shape parameter (Roundness–Rd) is another feature that can be used to assess parent material uniformity (examples in Figure 7). The average values of Rd showed high degree of similarity within the soil profiles (Ave. Rd G1 = 0.72; Ave. Rd G4 = 0.72; Ave. Rd C3 = 0.69; Ave. Rd P3 = 0.73), indicating the prevalence of a subrounded shape. The CV (%) values presented a low dispersion (G1 = 7.1%; G4 = 1.58%; C3 = 4.27%; P3 = 1.0%). Therefore, the FS/CS ratio and sand grain shape parameter enhance the perception of parent material homogeneity for all soil profiles.

The XRD of sand fraction showed a mineral assemblage predominantly composed of magnetite and quartz (Appendix L). Minerals such as ilmenite (Il), rutile (Ru), anatase (An) and zircon (Zr) were also detected in these samples. There was no significant variation in the qualitative mineral composition of the sand fraction in depth for the studied soil profiles, emphasizing uniformity of the parent material.

The evidences shown above suggest that the soils do not present lithological discontinuity (LD), emphasizing homogeneity of the soil material. Thus, the studied ferralsols are developed *in situ* from basaltic (G4, C3 and P3) and rhyo-dacitic rocks (G1), without the contribution of allochthonous material.

As reported by Paisani et al. (2008; 2013; 2014; 2019), soils developed *in situ* and *ex situ* coexist in the Paraná Magmatic Province. The evidences of parent material uniformity in the studied profiles allows some statements about the landscape evolution. In fact, the areas may have evolved according with morphoclimatic processes (Bigarella and Andrade, 1965). Probably, the humid epochs favored the development of thick regoliths by the etchplanation process (Büdel, 1982). With this, the planed surfaces evolved through an exhumed washing surface and a basal leaching surface. Normally, the chemical weathering acts constantly with high intensity in wet periods and relative tectonic stability, creating a thick weathering mantle for later occurrence of laminar erosion, which could explain the occurrence of deep soils developed *in situ* in the studied areas. In addition, the dissection of the relief would have been conditioned by the morphological and structural diferences presented by the flood basalts (Silva et al., 2021) in association to recent tectonic (Riffel et al., 2016; Peyerl et al., 2018).

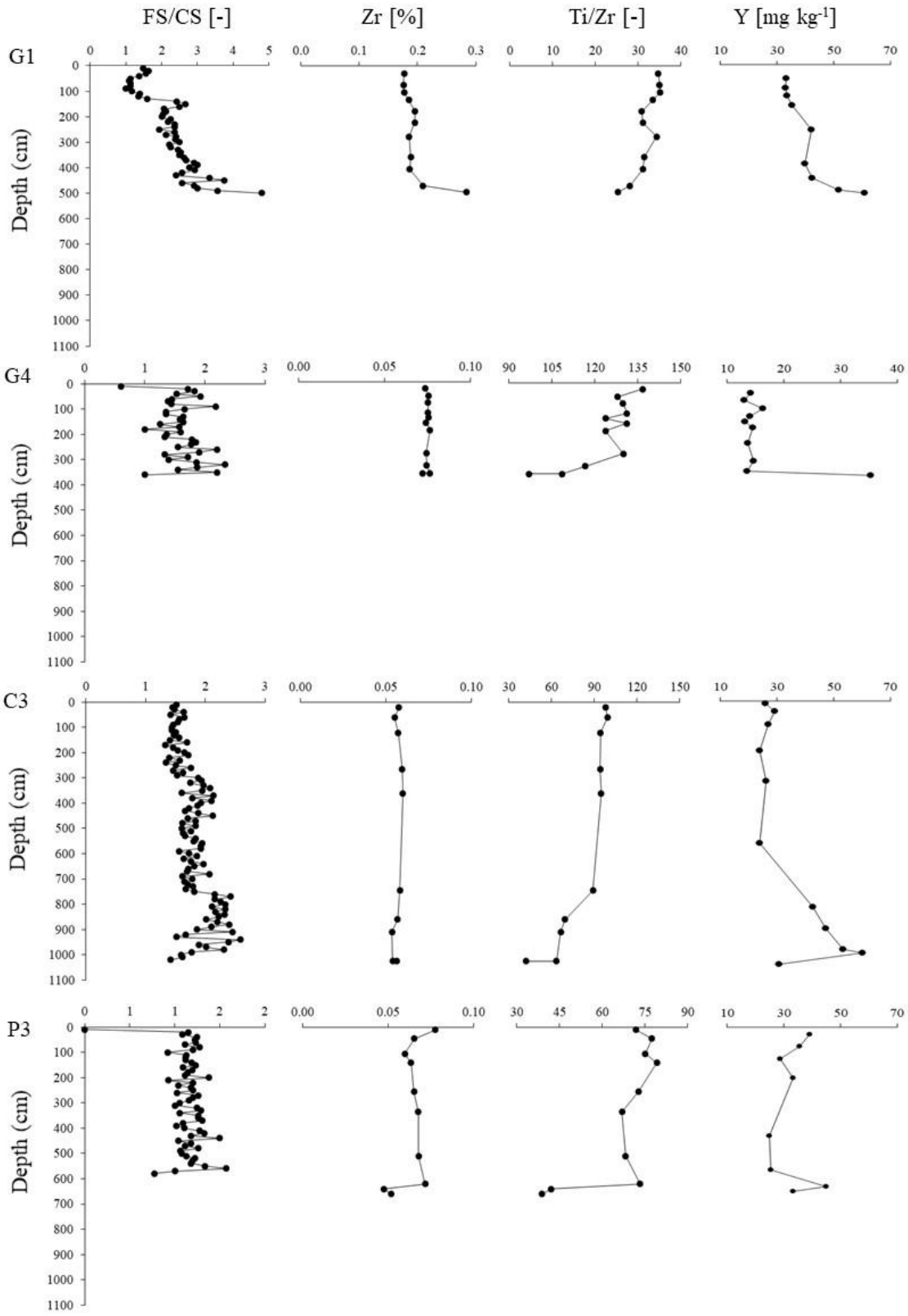

Figure 6. Depth records of parameters that reflect parent material uniformity (FS/CS ratio, Zr distribution, Ti/Zr ratio and Y distribution) of the representative soil profiles (G1, G4, C3 and P3). Note the different scale of the x-axis. Some inflections were observed in the base of the graphs of the soil profiles (G1 and P3: Zr; G4 and P3: Ti/Zr; 4 profiles: Y). These inflections occur because these samples refer to the saprolite region (BCr horizon), where we have a concentration of these elements due to the high occurrence of iron and clay nodules, which are derived from the weathering of the parent material.

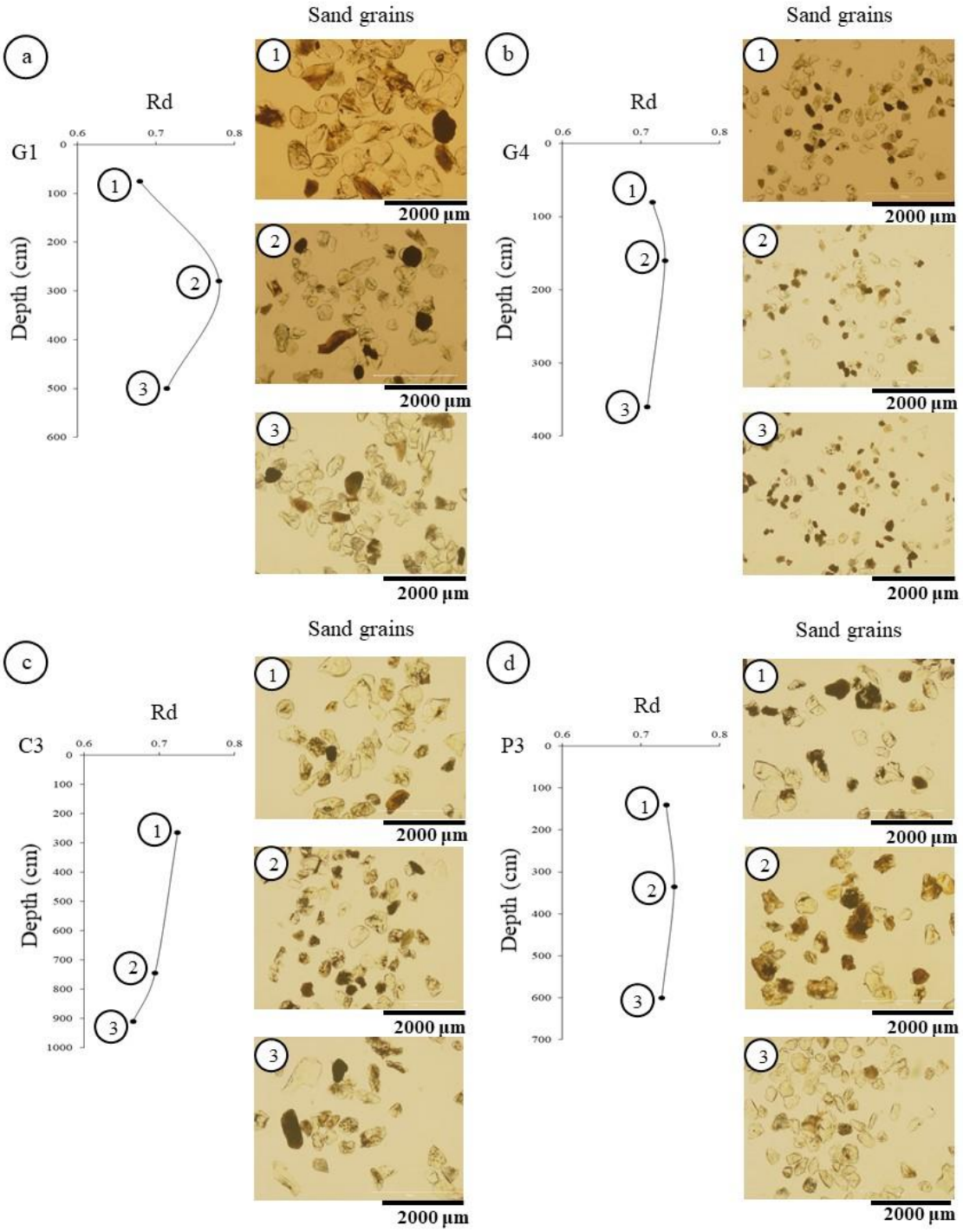

Figure 7. Roundness (Rd) and sand grains photomicrographs in the studied soil profiles. a) G1 profile; b) G4 profile; c) C3 profile and d) P3 profile. The presence of iron coated sand grains can also be noted. The differences observed in the images and in the curves, for example in G1 profile, were not relevant to characterize the occurrence of lithologic discontinuity.

3.2. Evidence of long-term pedogenetic processes in the studied ferralsols

3.2.1. Morphological, micromorphological and physicochemical evidences

The soil profiles showed a range color from dark brown to dark reddish brown (G1–G4 profiles presenting hues between 7.5YR and 2.5YR) and dark red colour (C1–C3 and P1–P3 profiles presenting hues between 5YR and 2.5YR) (Tables 3–5). The darker colour in upper horizons in the G1–G4 profiles is related to a larger contribution of the organic matter (OM or total carbon (Ct); ranging from 39.0 to 1.3 g kg^{-1}). This OM accumulation results from the lower temperature and high precipitation (2000 mm/year) that favours the formation of a profundihumic A horizon (varying from 75 to 120 cm of thickness) and the melanization process in the area (Bennema, 1974; Sanchez and Buol, 1975; Calegari et al., 2013; Macedo et al., 2017). The high organic carbon content observed in the upper horizons in the Guarapuava soil profiles associated with the presence of iron oxides contribute to the brunification of the soil profiles (Gaucher, 1977). Furthermore, in deeper horizons from Guarapuava (G1–G4) a reddish colour was observed, enhancing the rubification process, which originated from the weathering of the parent material rich in Fe-bearing primary minerals under conditions of free drainage (Gaucher, 1977; Buol et al., 2011). Soil profiles from Cascavel (C1–C3) and Palotina (P1–P3) showed a reddish and homogeneous colour from the surface to deep soil horizons (BC_r), showing the occurrence of rubification process (Gaucher, 1977). This reddish colour is a result of basalt weathering in a warm and humid climate, producing and accumulating crystalline iron oxides (mainly hematite and goethite) under conditions of free drainage (Gaucher, 1977; Schwertmann and Kämpf, 1985) (Figure 2).

The horizon with greater pedogenetic expression was identified as the Ferralic B horizon (Bfl, IUSS Working Group WRB (2015)). This horizon corresponds to the *Latossólico* B horizon (Bw) in the Brazilian Soil Classification System (Santos et al., 2018) and varied in thickness from 140–305 cm in the Guarapuava soils, from 455–740 cm in the Cascavel profiles and from 380–610 cm in the Palotina ones (Tables 3–5). The thickness of B ferralic horizons presented in the Guarapuava soils is related to the high occurrence of denudation and erosion cycles during the last 6.5 M.y. in addition to climatic changes in this old and dissected Plateaus (*Palmas/Guarapuava* and *Pitanga/Ivaiporã* plateaus = *superfície de Cimeira*) (Calegari, 2008; Paisani et al., 2008; 2013; 2014; 2019; Riffel et al., 2016).

Field and micromorphological descriptions showed that the soil structure and density of the ferralic B horizon varied with depth and between soil profiles (Tables 3–5; Appendix M–O). The small subangular blocks and granular with moderate to strong degree of pedality of the first B ferralic horizon, changes to large subangular blocks with moderate degree of pedality beyond the control section (deeper horizons), a consistent trend with the increase of kaolinite and decrease of crystalline iron oxides content in most of the studied soil profiles (Figure 8). According to Cooper et al. (2005b), this change in structure of the Bfl horizons is caused by an aggregate densification, which decreases the total porosity and the change of pore morphology (from packing voids to polyconcave and fissure voids). In addition, the weight of soil column, the increase of kaolinite content and the heritage of altered rock structure in the deeper horizons with few swell-shrinking cycles in alternating dry and humid periods, contribute to the formation of larger and denser structures, because kaolinite tends to form crystallite packaging in inter and intra-aggregates (Moniz, 1980). The lower activity of fauna and roots in these deeper soil horizons may also contribute to the development of a denser structure (Macedo et al., 2017; Chiapini et al., 2021).

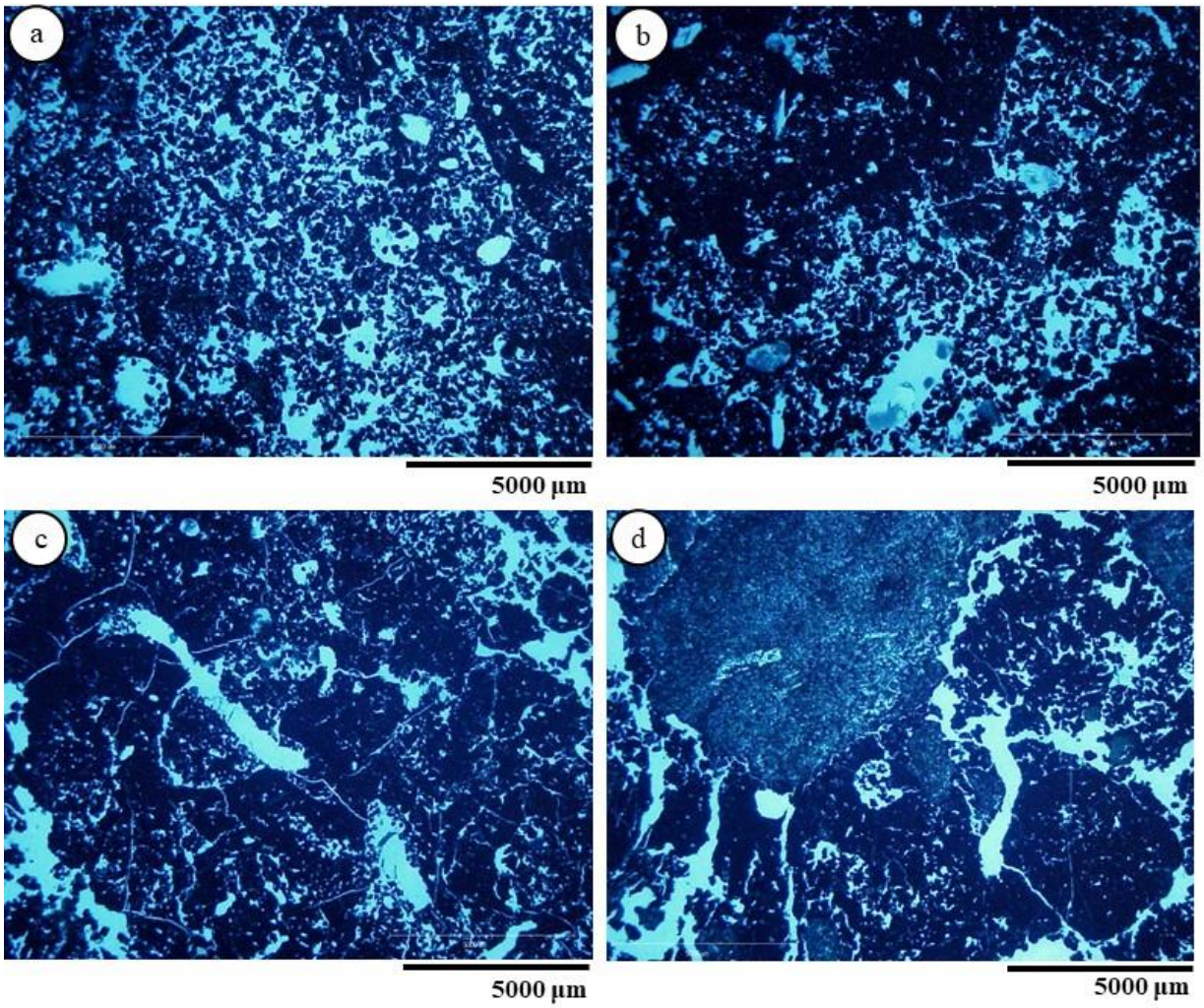

Figure 8. Increase in the structure and density with depth in soil profile G4 (Guarapuava); a) BA horizon with granular structure (127–140 cm deep), UV; b) Bfl_1 horizon with granular and subangular block structure (150–165 cm deep), UV; c) Bfl_3 horizon with block subangular structure (220–235 cm deep), UV; d) BC_2 horizon with subangular block structure (340–355cm deep), UV.

Associated with the increase in structure and density beyond the control section, waxy and shiny peds were observed in the field. In the Guarapuava (G1–G4) and Cascavel (C1–C3) profiles, the waxy and shiny peds were described as little and weak, and for Palotina soil profiles (P1–P3) as common and strong. Furthermore, in the Palotina profiles, dense clay volumes with waxy and shiny peds were observed beyond the control section characterizing a relict feature of nitic B horizon (Figure 9). The presence of relict features of nitic B horizon in the Palotina profiles shows the development of a ferralic B horizon from the ancient nitic one. According to Stoops (1968), Pedro et al. (1976) and Cooper (1999), the transition of nitic B horizon to ferralic occurs by fissuration due to the expansion and contraction of the clayed matrix, allowing the circulation of water, air and soil fauna. Subsequently, the bioturbation changes the soil structure producing the granular structure of ferralic B horizon and

homogenize the soil material. On a microscale, the studied soil profiles did not show clay coatings and infillings, which would characterize the waxy feature, but porostriated b-fabric features were observed, the result of the swell-shrinking (expansion and contraction) of clayed soil in alternating dry and humid periods.

As reported by Eswaran (1972), dense clayey red nodules were observed in soil thin sections of representative soil profiles (G1, G4, C3 and P3) decreasing the size towards soil surface, presenting a blocky morphology, groundmass and geochemical constitution very similar to that of the soil matrix (Figure 10). Weathered basaltic zones were observed in the BCr horizons from G4, C3 and P3 profiles, showing pedoplasmation, responsible for the red dense porphyric matrix formation. In profile G1 we also observed a dense porphyric soil matrix in BC_2 and BC_g horizons derived from the weathering of rhyo-dacite rock. The dense and clayey red nodules can be considered a result of *in situ* porphyric soil matrix fissuration associated with the mechanic and geochemical evolution of soil structure and also the bioturbation process (Figure 10a, 10b and 10c).

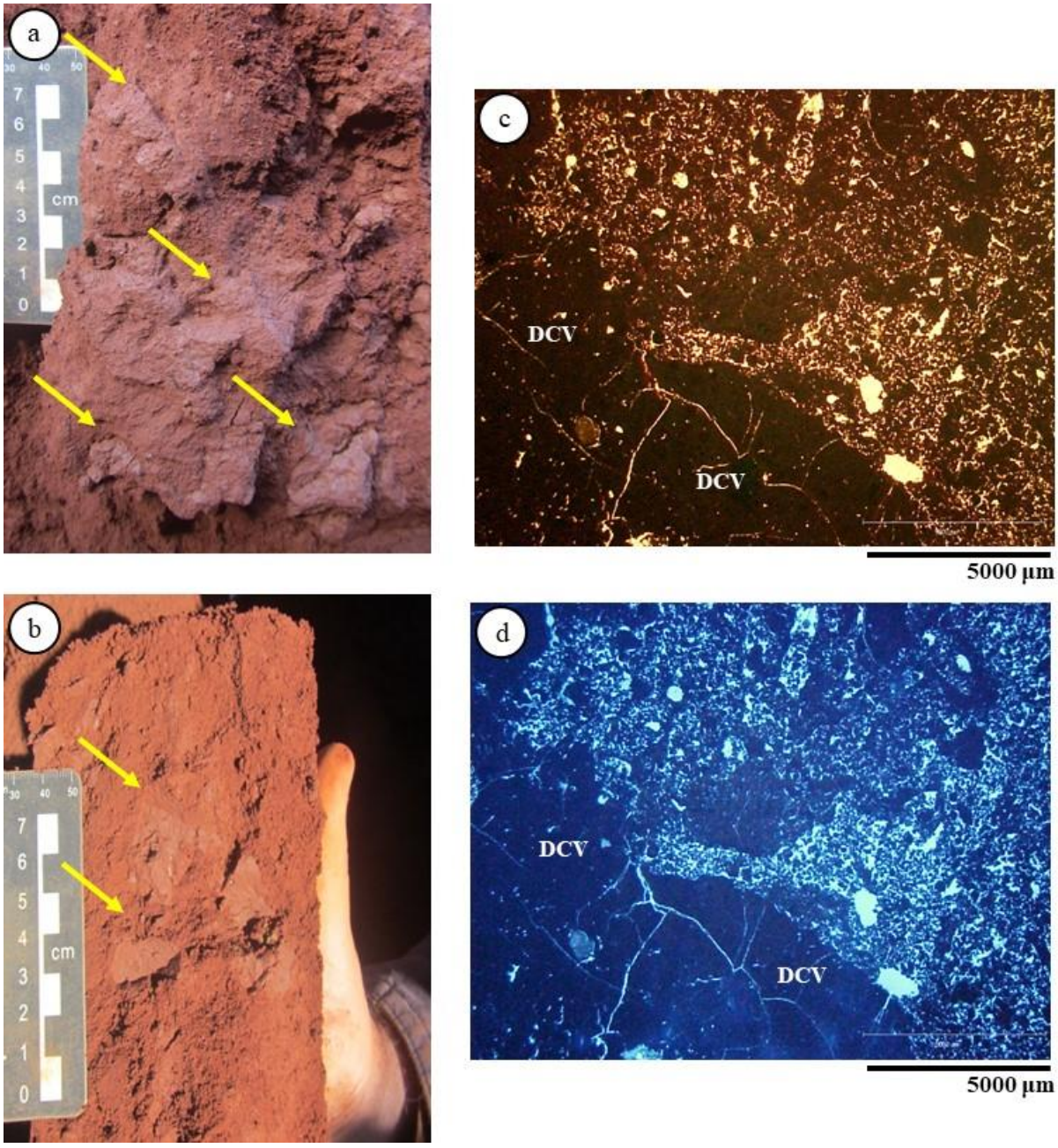

Figure 9. Relict dense clayey volume (DCV and yellow arrows) with waxy and shiny peds appereance in the middle of the ferralic B horizon at 300 cm of depth in P3 soil profile from Palotina (a) e (b); c) e d) Photomicrographs from soil thin sections from (b) showing the dense clayey volume without clay coatings and infillings (PPL and UV).

Iron oxides nodules were also observed from weathering front (BC and BC_r horizons) to upper horizons, with similar groundmass, quartz grains (when present), decreasing the size towards soil surface and remaining stable along the soil profile (Figure 10). In the BC_r horizons of G4, C3 and P3 profiles, and BC_1-BC_g horizon of G1 profile, iron concentrations were observed and developed into amiboidal and typic iron nodules along the soil profiles varying in mineralogy and colour, as hematitic nodules (reddish), goethitic nodules (yellowish) and with intermediate composition (varying in color) (Figures 10d, 10e

and 10f). In C1, C3, P1 and P3 soil profiles, a layer of iron oxides nodules was observed above the BCr horizon with continuous lateral configuration and a thickness ranging from 20–30 cm. According to Nahon (1991), Riggi and Riggi (1964), Marengo et al. (2005) and Morrás et al. (2009), the layer of iron oxides nodules is a result of the nodulation process with iron concentration related to the spheroidal weathering of basalt under a humid climate (redoximorphic conditions). Our observations differs from the main researches performed in other ferralsols which considered the dense clayey and iron nodules as a relict pedofeature from allochthonous weathered reworked materials (Stoops et al., 1994; Vidal-Torrado, 1994; Muggler, 1998; Vidal-Torrado and Lepsch, 1999).

In addition to clayey and iron nodules, basaltic and rhyo-dacitic lithorelicts were also observed in the coarse material of the representative soil profiles (Figure 11; Appendix M–O). They appear as isolated spots in different soil depths (profile G1 from 150–500 cm; G4 profile from 150–360 cm; C3 profile from 965–1035 cm; P3 profile from 150–620 cm), degree of alteration, varying from 0.5 mm to 5 mm in size and its limits are mostly diffuse in relation to the soil matrix. The lithorelicts and the pedorelicts (iron and dense clayey nodules) are rock fragments inherited (residual) from the *in situ* weathering from the underling parent material, which may have been moved by the bioturbation process from the deepest horizons (Stoops, 1989). In addition, the lithorelicts may also originate from the differential weathering of ancient basalt and rhyo-dacite fragments distributed along the soil profile.

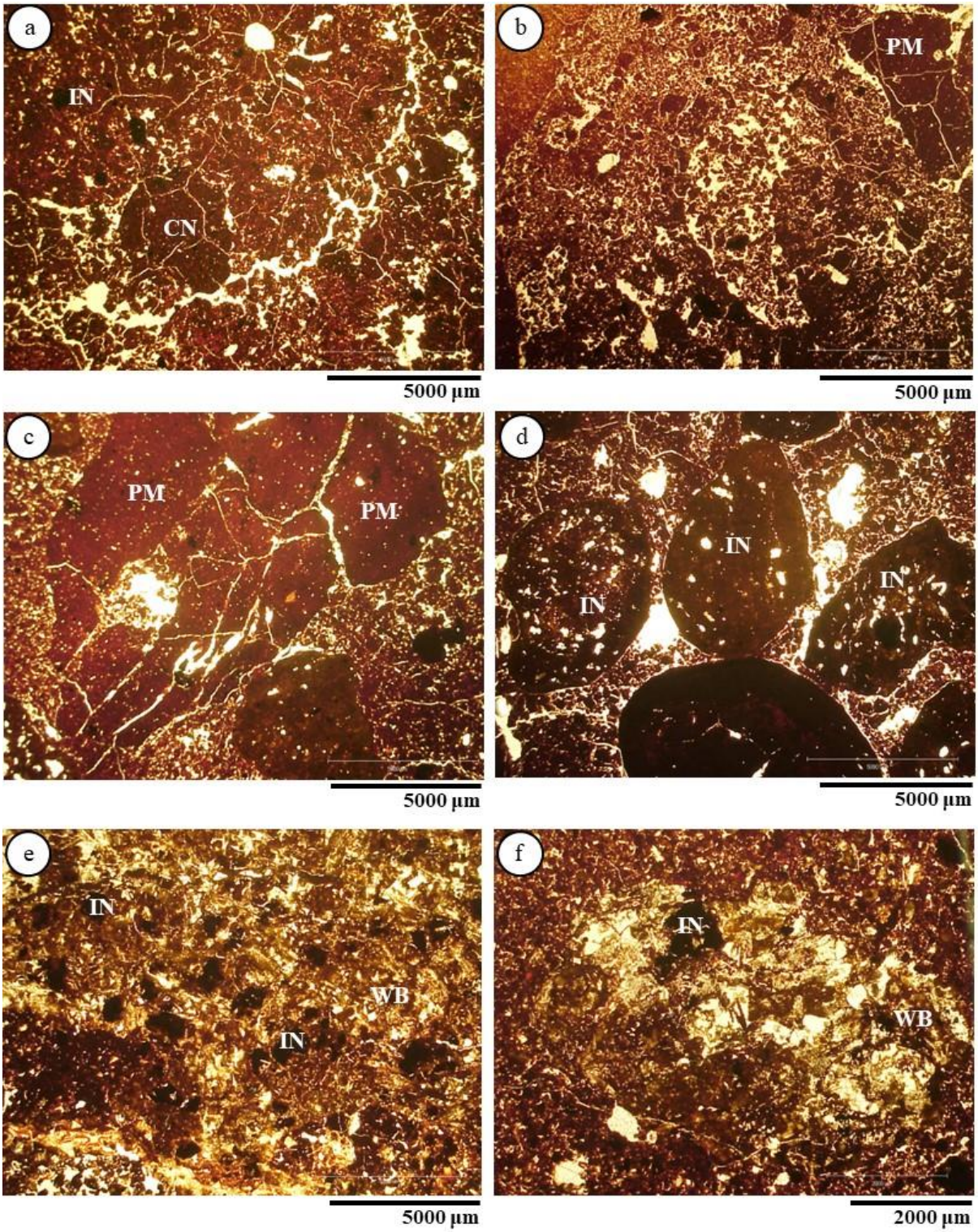

Figure 10. The evolution of iron and dense clayey nodules from the saprolite zone to upper horizons in the Rhodic Ferralsol (Eutric) (soil profile P3 from Palotina). a) dense clayey nodules formed from the fissuration and bioturbation the porphyric matrix in the Bfl_1 horizon (30 cm deep), PPL; b) enaulic matrix with a relict porphyric matrix and dense clayey nodules in the Bfl_5 horizon (280 cm deep), PPL; c) porphyric matrix with fissures in the Bfl_7 horizon (600 cm deep), PPL; d) iron nodules in the Bfl_7 horizon (600 cm deep), probably formed by the influence of humid conditions (hydromorphism) PPL; e) and f) pedoplasmation and development of Fe nodules in the weathered rock fragment in the BCr horizon (630 cm deep). WB = weathered basalt; IN = iron nodule; PM = porphyric matrix; CN = dense clayey nodule.

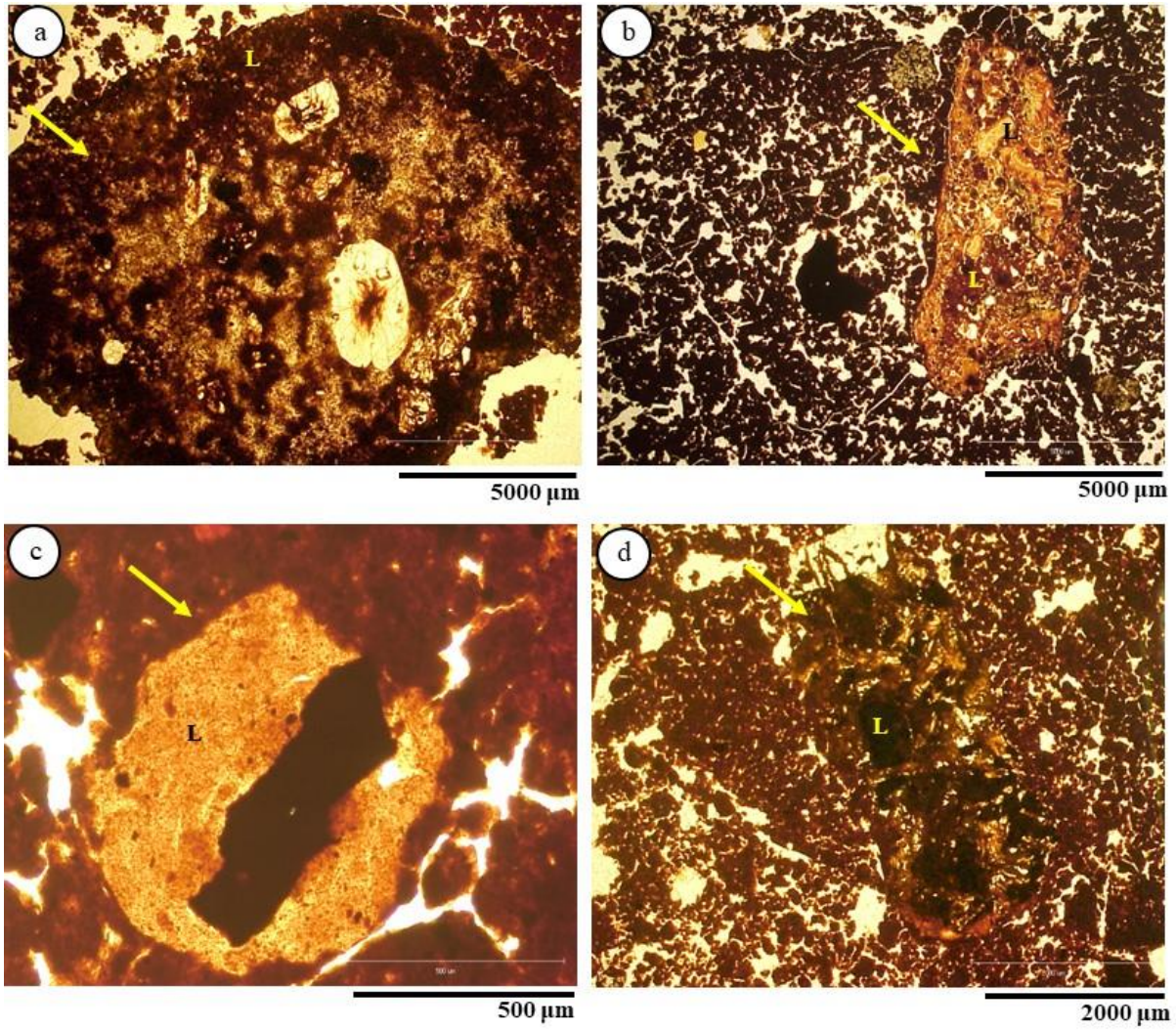

Figure 11. Photomicrographs of the lithorelicts (yellow arrows). a) Rhyo-dacitic lithorelict in the Bfl_2 horizon from profile G1 (~135–150 cm deep); b) Basaltic lithorelict in transition from Bfl_2/Bfl_3 horizons of profile G4 (~185–200 cm deep); c) Basaltic lithorelict in the Bfl_3 horizon of profile C3 (~455–470 cm deep); d) Basaltic lithorelict in the Bfl_4 horizon of profile P3 (~150–165 cm deep). L = lithorelict.

The micromorphological descriptions also demonstrated an intense bioturbation process contributing to the formation of ferralic structure and homogenization of soil profiles. All ten soil profiles presented loose continuous and discontinuous infillings, dense complete and incomplete infillings and excrements in the soil thin sections (Bullock et al., 1985; Silva and Vidal-Torrado, 1999). The representative biofeatures are shown in Figure 12. The process of bioturbation is considered in this work as short-term evidence that will be discussed in more details in section 3.5.

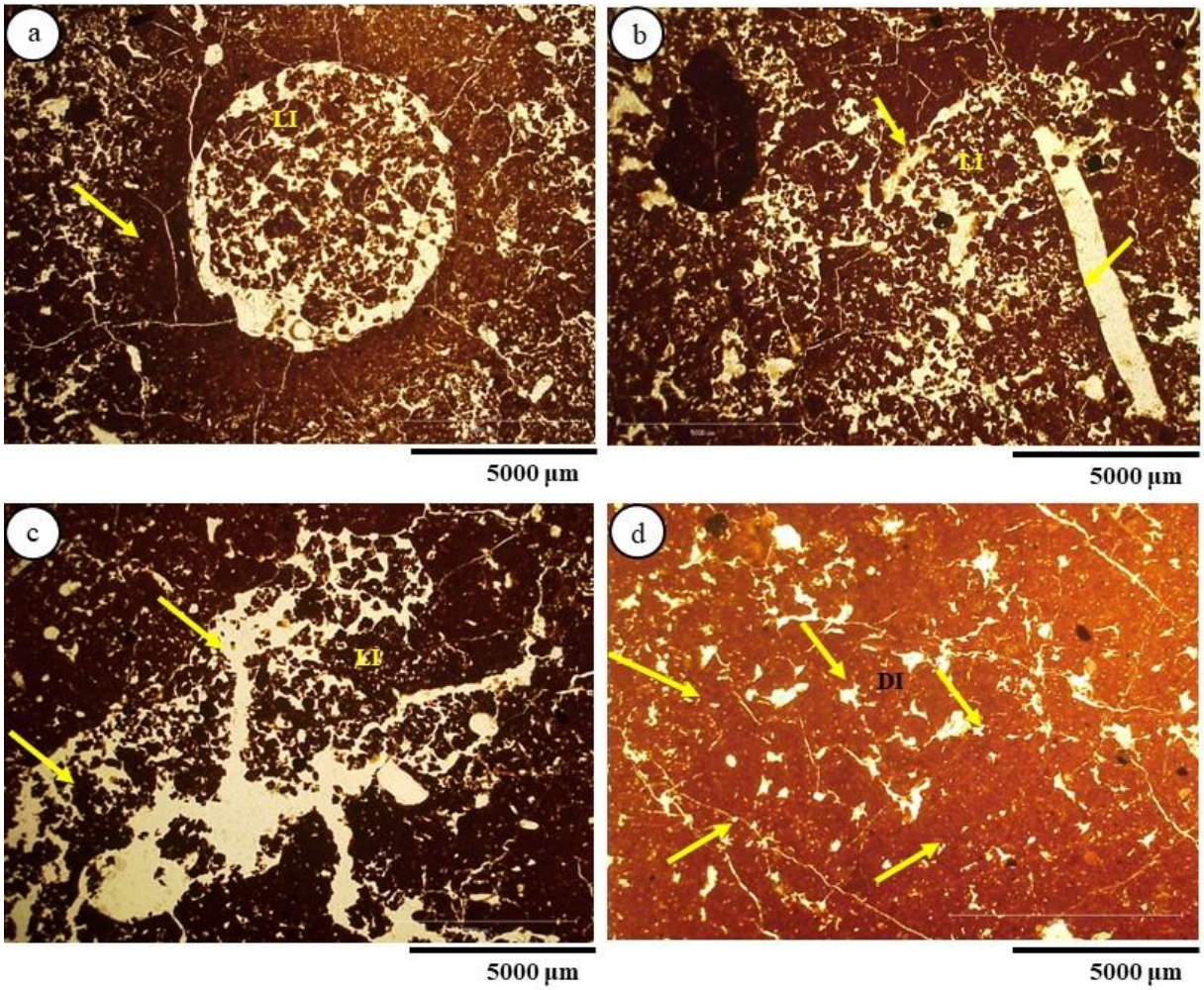

Figure 12. The bioturbation process in G1 (Guarapuava) soil profile. a) Loose continuous infilling in AB horizon (35–50 cm deep), PPL; b) Loose discontinuous infillings and bioporo in Bfl_1 horizon (105–120 cm deep), PPL; c) Loose discontinuous infilling in the Bfl_2 horizon (135–150 cm deep), PPL; d) Dense incomplete infilling in the BC_1 horizon (460–475 cm deep), PPL.

Table 3. General properties of the studied profiles in Guarapuava.

Profile	Hz	Depth	Colour[1]	Sturcture[2]	Ds	pH	pH	BS[3]	CEC[4]	Ct[5]	Clay	Silt/Clay
		cm			g cm^{-3}	H_2O	KCl	%	cmolc kg^{-1}	g kg^{-1}		
G1	A_{pa}	0–30	5YR 3/3	SB	0.8	5.9	4.8	40	14.6	31.6	725	0.2
	AB	30 –75	5YR 3/4	SB/G	0.9	5.3	4.3	25	10.7	20.1	725	0.2
	BA	75–105	5YR 3/3-4	SB/G	0.8	5.5	4.8	33	9.7	15.9	738	0.1
	Bfl_1	105–135*	2.5 YR 3/4-6	SB/G	0.8	5.2	5.2	13	4.8	10.1	788	0.1
	Bfl_2	135–180*	2.5 YR 3-4/6	SB/G	0.9	5.1	5.3	25	4.8	5.3	863	0.1
	Bfl_3	180–225	2.5 YR 3/4	SB/G	1.0	5.1	4.8	11	3.8	4.4	750	0.1
	Bfl_4	225–280	2.5 YR 3/4-6	SB/G	1.0	4.9	4.8	12	3.4	3.4	763	0.1
	Bfl_5	280–360	2.5 YR 3/4-6	SB/G	1.0	4.9	4.5	9	3.9	3.0	800	0.1
	Bfl_6	360–410	2.5 YR 3/6	SB	1.0	5.0	4.1	8	4.8	2.3	800	0.1
	BC_1	410–475	2.5 YR 5/6	SB	1.0	5.0	4.0	13	5.5	2.3	788	0.1
	BC_2	475–500	2.5 YR 4/4	SB	0.9	5.1	3.9	2	5.3	2.1	813	0.1
	BC_g	500 +	2.5 YR 5/3 5Y 5/1	M	1.0	5.0	3.8	12	5.9	1.3	775	0.1
G2	A_1	0–30	7.5 YR 2.5/3	G/G	0.8	4.6	3.8	7	16.9	39.0	700	0.2
	A_2	30–55	7.5 YR 3/3	SB/G	0.8	4.7	3.9	3	12.7	27.0	738	0.2
	A_3	55–75	5 YR 3/4	SB/G	0.8	4.9	4.0	6	10.3	19.5	725	0.1
	AB	75–100	5 YR 3/4	SB/G	0.8	5.2	4.4	12	9.3	17.8	675	0.2
	BA	100–120	5 YR 4/6	SB/G	0.9	5.1	4.7	16	6.9	14.1	788	0.2
	Bfl_1	120–170*	2.5 YR 3/6	SB/G	1.2	5.2	5.1	19	4.8	7.4	763	0.1
	Bfl_2	170–200*	2.5 YR 3/6	SB/G	-	5.2	5.0	12	3.5	6.0	763	0.1
	Bfl_3	200–260* +	2.5 YR 3/6	SB/G	-	5.6	5.0	8	3.4	3.9	763	0.1
G3	A_1	0–30	5 YR 3/4	SB/G	0.9	5.1	4.0	8	13.7	30.3	713	0.2
	A_2	30–55	5 YR 3/4	SB/G	0.9	5.1	4.1	7	11.6	25.6	713	0.2
	A_3	55–80	5 YR 3/4	SB/G	0.8	5.0	4.3	8	9.9	18.2	738	0.2
	AB	80–95*	5 YR 3/4	SB/G	0.8	5.3	5.0	14	5.8	11.9	750	0.1
	BA	95–120*	5 YR 3/4	SB/G	0.8	5.1	5.0	17	6.3	10.7	800	0.2
	Bfl_1	120–180*	2.5 YR 3/4	SB/G	0.9	5.4	5.1	10	3.8	5.2	713	0.1
	Bfl_2	180–240	2.5 YR 3/6	SB/G	0.9	5.3	4.9	10	3.8	4.1	738	0.1
	Bfl_3	240–260	2.5 YR 3/6	SB	1.1	5.3	4.6	20	3.5	1.8	613	0.2
	BCr	260 +	2.5 YR 3/6	SB	1.1	5.2	4.3	18	4.5	1.8	513	0.4
G4	A_1	0–25	5 YR 3/3-4	G	0.6	4.7	3.8	2	19.9	37.4	788	0.2
	A_2	25–55	5 YR 2.5-3/1-2	SB	0.8	4.0	3.8	2	19.6	33.5	750	0.2
	A_3	55–80	5 YR 3/3	SB/G	0.8	4.9	3.9	1	14.6	20.9	813	0.2
	AB	80–120	5 YR 3/3-4	SB/G	0.8	5.0	3.9	1	11.9	17.5	775	0.1
	BA	120–140	5 YR 3-4/3	SB/G	0.8	5.0	3.9	4	9.3	13.4	788	0.1
	Bfl_1	140–160	5 YR 3-4/4-6	SB/G	1.0	5.2	4.0	5	8.4	11.0	800	0.2
	Bfl_2	160–190	2.5 YR 2.5/4	SB/G	1.0	5.4	4.2	1	6.7	9.2	750	0.1
	Bfl_3	190–280	2.5 YR 2.5/4	SB/G	1.0	5.3	4.7	2	4.1	5.9	813	0.1
	BC_1	280–330	2.5 YR 2.5/4	SB/G	1.0	5.4	4.8	18	4.8	4.8	813	0.2
	BC_2	330–360	2.5 YR2.5/4	SB/G	1.0	5.4	4.8	2	3.8	3.8	913	0.1
	BCr	360* +	2.5 YR 3/4/6 7.5 YR 5/8	SB/G	1.5	5.2	5.5	13	3.0	2.5	525	0.4

[1]Munsell Colour; [2]Structure: G: granular; SB: subangular block; AB: angular block; PR: prismatic; M: massive;
[3]BS = base saturation (%); [4]Cation exchange capacity; *geric; [5] = total carbon (Ct).

Table 4. General properties of the studied profiles in Cascavel.

Profile	Hz	Depth	Colour[1]	Sturcture[2]	Ds	pH	pH	BS[3]	CEC[4]	Ct[5]	Clay	Silt/Clay
		cm			g cm^{-3}	H_2O	KCl	%	cmolc kg^{-1}	g kg^{-1}		
C1	A_{pa1}	0–35	5 YR 3/4	SB	1.0	4.8	4.1	9	17.9	36.0	800	0.1
	A_{pa2}	35–45	5 YR 3/2	SB	1.1	4.8	4.2	16	15.3	23.6	800	0.2
	A_{pa3}	45–55	5 YR 3/4	SB	1.1	5.0	4.4	14	12.1	18.1	838	0.1
	AB	55–65	2.5 YR 2.5/4	SB	1.1	5.2	4.6	17	10.6	16.0	825	0.1
	BA	65–85	2.5 YR 3/4	SB	1.0	5.4	4.9	20	9.1	14.5	825	0.2
	Bfl_1	85–135*	2.5 YR 3/4	SB/G	0.9	5.3	5.2	19	6.7	11.6	813	0.2
	Bfl_2	135–200*	2.5 YR 2.5/4	SB/G	0.9	5.1	5.5	18	5.4	6.9	825	0.1
	Bfl_3	200–290*	2.5 YR 2.5/4	SB/G	1.0	4.9	5.5	22	4.5	4.2	850	0.1
	Bfl_4	290–420*	2.5 YR 3/6	SB/G	1.1	5.1	5.0	10	3.8	3.0	875	0.1
	Bfl_5	420–540*	2.5 YR 3/6	SB/G	1.1	5.1	5.1	11	5.0	4.2	863	0.1
	BC	540 +	2.5 YR 3/6	SB/G	1.1	5.1	4.3	5	4.6	1.2	788	0.2
C2	A_1	0–15	2.5 YR 2.5/3	G	0.9	4.2	3.9	2	16.4	7.4	800	0.2
	A_2	15–40	2.5 YR 2.5/3	SB	0.9	4.4	4.0	2	12.4	6.7	850	0.1
	A_3	40–50	2.5 YR 2.5/4	SB	0.9	4.6	4.1	2	11.3	6.0	875	0.1
	AB	50–90	2.5 YR 2.5/4	SB/G	0.9	4.6	4.2	2	8.6	5.3	875	0.1
	BA	90–145	2.5 YR 2.5/4	SB/G	0.9	4.7	4.6	5	6.4	4.5	900	0.1
	Bfl_1	145–350*	2.5 YR 2.5/4	SB/G	0.9	5.3	5.2	4	4.8	3.8	875	0.1
	Bfl_2	350–500*	2.5 YR 2.5/4	SB/PR	1.0	5.4	5.1	6	4.5	3.1	888	0.1
	Bfl_3	500–620	2.5 YR 2.5/4	SB/PR	1.1	5.6	4.7	6	4.4	2.4	900	0.1
	Bfl_4	620–670	2.5 YR 2.5/4	SB/PR	1.1	5.8	4.4	4	4.9	1.6	875	0.1
	AS[6] 1	700	2.5 YR 2.5/4	-	-	5.5	4.3	3	5.1	1.5	800	0.2
	AS 2	750	2.5 YR 2.5/4	-	-	5.6	4.3	4	5.5	1.3	825	0.2
	AS 3	800	2.5 YR 2.5/4	-	-	5.7	4.2	5	5.7	-	750	0.3
	AS 4	850	2.5 YR 2.5/4	-	-	5.8	4.2	3	5.6	1.2	738	0.2
	AS 5	900–920	2.5 YR 2.5/4	-	-	5.6	4.1	4	5.6	1.1	738	0.3
	AS 6	1000–1050	2.5 YR 2.5/4	-	-	5.7	4.0	7	6.4	0.0	675	0.4
C3	A_{pa}	0–20	2.5 YR 2.5/3	G	0.9	5.7	4.8	39	12.9	25.3	763	0.2
	AB	20–60	2.5 YR 2.5/3	SB/G	1.0	4.9	4.2	14	12.3	18.6	813	0.1
	BA	60–120	2.5 YR 2.5/3	SB/G	0.9	5.2	4.6	23	9.3	12.5	850	0.1
	Bfl_1	120–265*	2.5 YR 2.5/3	SB/G	0.8	5.2	5.5	18	4.1	5.7	813	0.1
	Bfl_2	265–360*	2.5 YR 2.5/3	SB/G	0.9	5.0	5.4	15	4.2	4.4	838	0.1
	Bfl_3	360–745*	2.5 YR 2.5/3	SB/G	0.9	5.4	5.3	11	3.4	2.5	850	0.1
	Bfl_4	745–860	2.5 YR 2.5/3	SB/G	0.9	5.5	4.7	7	4.8	1.5	688	0.2
	BC_1	860–910	2.5 YR 2.5/3	SB/G	1.1	5.6	4.6	7	4.8	1.7	800	0.1
	BC_2	910–1025	2.5 YR 2.5/3	SB/AB	1.1	5.9	4.5	6	5.1	1.2	575	0.4
	BCr	1025 +	2.5 YR 2.5/3	SB/AB	0.6	5.6	4.4	7	5.9	1.1	475	0.3

[1]Munsell Colour; [2]Structure: G: granular; SB: subangular block; AB: angular block; PR: prismatic; M: massive; [3]BS = base saturation (%); [4]Cation exchange capacity; *geric; [5] = total carbon (Ct); [6]AS = auger sample.

Table 5. General properties of the studied profiles in Palotina.

Profile	Hz	Depth	Color[1]	Sturcture[2]	Ds	pH	pH	BS[3]	CEC[4]	Ct[5]	Clay	Silt/Clay
		cm			g cm^{-3}	H_2O	KCl	%	cmolc kg^{-1}	g kg^{-1}		
P1	A	0–30	2.5 YR 2.5/3	G	0.8	6.2	5.4	69	13.3	24.7	688	0.2
	AB	30–50	2.5 YR 2.5/3	SB/G	1.0	5.7	4.8	18	3.9	4.2	763	0.2
	Bfl_1	50–90	2.5 YR 2.5/4	SB/PR	1.1	6.1	5.2	73	5.4	5.5	825	0.1
	Bfl_2	90–140	2.5 YR 2.5/4	SB/G	1.2	5.7	4.8	50	6.2	4.0	825	0.1
	Bfl_3	140–290	2.5 YR 2.5/4	SB/G	1.0	5.3	4.5	40	6.0	3.6	800	0.1
	Bfl_4	290–430	2.5 YR 2.5/4	SB/G	0.9	5.9	5.1	57	5.1	2.0	675	0.3
	BCr	430 +	2.5 YR 2.5/4	SB/G	1.5	5.8	5.2	53	5.0	1.7	513	0.4
P2	A_{pa}	0–10	2.5 YR 2.5/3	G	0.7	5.8	4.9	55	10.9	17.0	763	0.2
	AB	10–40	2.5 YR 2.5/3	SB	1.1	5.8	4.8	55	9.1	13.1	775	0.1
	Bfl_1	40–90	2.5 YR 2.5/3	SB/PR	1.0	4.9	4.1	27	5.2	1.8	863	0.1
	Bfl_2	90–180	2.5 YR 2.5/3	SB/G	1.0	5.9	5.2	59	5.3	2.8	838	0.1
	Bfl_3	180–350	2.5 YR 2.5/3	SB/G	1.2	6.3	5.1	57	5.5	2.4	825	0.1
	Bfl_4	350–650	2.5 YR 2.5/4	SB/G	1.1	5.0	4.1	25	5.5	1.3	688	0.3
	Bfl_5	650 +	2.5 YR 2.5/4	SB/G	1.1	4.8	4.0	16	5.3	0.9	763	0.1
	AS[6] 1	850	2.5 YR 2.5/4	-	-	5.1	4.1	19	5.1	1.1	738	0.2
	AS 2	900	2.5 YR 2.5/4	-	-	5.4	4.0	15	4.7	0.9	700	0.3
	AS 3	960	2.5 YR 2.5/4	-	-	5.3	4.1	4	4.3	0.9	588	0.3
P3	A_{pa}	0–10	2.5 YR 2.5/3	G	1.1	4.7	4.0	26	12.7	22.4	788	0.1
	Bfl_1	10–45	2.5 YR 2.5/4	SB/PR	1.2	5.2	4.2	34	9.0	12.4	825	0.1
	Bfl_2	45–105	2.5 YR 2.5/4	SB/G	1.0	5.9	5.2	60	5.9	6.4	888	0.1
	Bfl_3	105–140	2.5 YR 2.5/4	SB/G	0.8	6.0	5.2	66	8.4	4.4	863	0.1
	Bfl_4	140–255	2.5 YR 2.5/4	SB/G	0.9	4.8	4.0	21	7.1	3.5	813	0.1
	Bfl_5	255–335	2.5 YR 2.5/4	SB/G	0.9	4.7	3.9	12	6.2	2.3	838	0.1
	Bfl_6	335–510	2.5 YR 2.5/4	SB/G	0.8	4.7	3.9	10	6.5	2.0	788	0.2
	Bfl_7	510–600	2.5 YR 2.5/4	SB/G	1.4	4.6	4.0	13	5.2	1.7	688	0.3
	BCr	600–640	2.5 YR 2.5/4	PR/AB	1.5	4.8	4.4	12	5.8	1.1	425	0.4

[1]Munsell Colour; [2]Structure: G: granular; SB: subangular block; AB: angular block; PR: prismatic; M: massive; [3]BS = base saturation (%); [4]Cation exchange capacity; [5] = total carbon (Ct); [6]AS = auger sample.

The main chemical and physical properties of the ten soil profiles are shown in Tables 3–5 and Appendix P–U. The high CEC values observed in A horizon in the profiles are related with the high OM content (Dalmolin et al., 2006). The Bfl horizons presented a low silt/clay ratio (~0.2) which is typical of highly weathered soils such as ferralsols (Fox, 1982). The pH_{KCl} ranged from 3.8 to 5.5 in the Guarapuava profiles, from 3.9 to 5.5 in the Cascavel soils and from 3.9 to 5.4 in the Palotina ones. In addition, the pH_{H2O} varied from 4.0 to 5.9, from 4.2 to 5.9 and from 4.6 to 6.3, in Guarapuava, Cascavel and Palotina, respectively, characterizing an acidic soil solution. A long period of weathering and intense basic cation leaching throughout the soil profiles G1–G4 and C1–C3 resulted in a low base saturation (< 50%) and geric property (except G4 profile) (Fox, 1982; Rolim-Neto et al., 2004; Schaefer et al., 2008). In the Palotina profiles (P1–P3), however, the base saturation was high (> 50%), characterized as a eutric property. According to Moura Filho and Buol (1975), Ker (1998) and Schaefer et al. (2008) the eutric property in ferralsols developed from

basic rocks is possible because of the effective protecting role of microaggregates. The K, Ca and Mg leaching is retarded or impeded in the interior of microaggregates. Furthermore, the basaltic rock of the Palotina profiles showed vesicles filled mainly with calcite, such as *Meláfiros* basalts (Gutmans, 1943; Ferreira et al., 2014), which may provide a high quantity of base cations during weathering, favoring the development of the eutric property. Another fact that may have contributed to the eutric property in Palotina profiles was the partial ferralitization combined with Ca^{2+} and Mg^{2+} cycling by the roots of the past vegetation in a dry climate with low rates of leaching (Ker, 1998) (see *sections 3.2.4 and 3.3.1*).

3.2.1.1. Soil classification

The classification of the ten soil profiles, according to the Brazilian Soil Classification System would result in the following reasoning:

Due to the presence of the *Latossólico* B horizon, the first category level (Order) is classified as *Latossolos* for the ten studied profiles. As the soils in Guarapuava (G1–G4) presented a carbon content greater than 10g kg^{-1} down to a depth of 70 cm and presenting a dark reddish brown (5YR) with value ≤ 4 and chroma < 6 in the upper part of B horizon, these soils were classified as *Bruno* (Brown) in the second level. Guarapuava profiles showed low base saturation (BS < 50%). Thus, the third category level they were classified as *Distrófico* (Dystrophic). For the fourth category level, the soil profiles at Guarapuava site (G1–G4) were classified as *rúbrico*, because the presence of *rúbrico* features (Table 6). In Cascavel (C1–C3) and Palotina (P1–P3) the *Latossólico* B horizon showed a red colour in the first 100 cm, which characterized a second level as *Vermelho* (Red). The Cascavel profiles showed *ácrico* features and Fe_2O_3 (data from sulphuric extract; Appendix Q) content between 180 and 360 g kg^{-1} in most of the first 100 cm of the B horizon, characterizing an *Acriférrico* third category level. The fourth category level in the Cascavel profiles were classified as *espesso-húmico* for C1, because the presence of humic A horizon with carbon content ≥ 10 g kg^{-1} down to a depth of 80 cm, and the profiles C2 and C3 as *típico* (Typical) (Table 6). The Palotina profiles showed high base saturation (BS > 50%) and Fe_2O_3 content (data from sulphuric extract; Appendix R) > 180 g kg^{-1} in most of the first 100 cm of the B horizon, the third category level was classified as *Eutroférrico.* At the fourth category level, the soil profiles at Palotina site (P1–P3) were classified as *típico* (Typical) (Table 6).

In the WRB classification (IUSS Working Group WRB, 2015), the presence of Ferralic B horizon allows characterisation in the Order of Ferralsols. At Guarapuava (G1–G3) and C1 profile from Cascavel, the classification was Umbric Geric Ferralsol, and G4 resulted in Umbric Ferralsol because of the presence of an umbric horizon and geric properties (similar to *ácrico* feature described by SiBCS (Santos et al., 2018)). As regards qualifiers, the soils (G1–G4) and C1 were classified as Humic, Rhodic and Dystric (Table 6). C2 and C3 classification was in Rhodic Geric Ferralsol with Dystric such as the qualifier. Palotina profiles the classification resulted in Rhodic Ferralsol, and the qualifier as Eutric (Table 6).

The classification of our soil profiles are similar to those obtained by other studies in areas closer to our sampling sites, such as Demattê and Garcia (1999), Ghidin et al. (2006a; 2006b), Behring (2007) and Testoni et al. (2017). Furthermore, as reported by Ker and Resende (1990) the qualitative "brown" (*Bruno*) has been used in the characterization of high altitude soils in subtropical climates. Generally, the yellowish brown color is found in hues 7.5 YR and 10YR, printed by the dominance of goethite in relation to hematite (Kämpf and Schwertmann, 1983). Thus, the soils located in Guarapuava were classified as *Latossolos Bruno* in accordance with definitions found in SiBCS (Santos et al., 2018), however the predominance of the type of iron oxide observed in the mineralogy data of the *Latossolos Brunos* from Guarapuava is the hematite (see *section 3.2.3.3*).

Table 6. Soil Classification in the Brazilian Soil Classification System (SiBCS; Santos et al., 2018) and WRB (IUSS Working Group WRB, 2015).

Profile		Classification	
		SiBCS	WRB
Guarapuava	G1	LATOSSOLO Bruno distrófico rúbrico	Umbric Geric Ferralsol (Humic, Rhodic, Dystric)
	G2	LATOSSOLO Bruno distrófico rúbrico	Umbric Geric Ferralsol (Humic, Rhodic, Dystric)
	G3	LATOSSOLO Bruno distrófico rúbrico	Umbric Geric Ferralsol (Humic, Rhodic, Dystric)
	G4	LATOSSOLO Bruno distroférrico rúbrico	Umbric Ferralsol (Humic, Rhodic, Dystric)
Cascavel	C1	LATOSSOLO Vermelho ácriférrico espesso-húmico	Umbric Geric Ferralsol (Humic, Rhodic, Dystric)
	C2	LATOSSOLO Vermelho ácriférrico típico	Rhodic Geric Ferralsol (Dystric)
	C3	LATOSSOLO Vermelho ácriférrico típico	Rhodic Geric Ferralsol (Dystric)
Palotina	P1	LATOSSOLO Vermelho Eutroférrico típico	Rhodic Ferralsol (Eutric)
	P2	LATOSSOLO Vermelho Eutroférrico típico	Rhodic Ferralsol (Eutric)
	P3	LATOSSOLO Vermelho Eutroférrico típico	Rhodic Ferralsol (Eutric)

3.2.2. Estimation of Fe forms

The results of Fe forms are presented in Table 7. Crystalline iron oxides or total pedogenetic Fe contents (Fe_{CBD}) prevailed in all the studied soil horizons. The Fe_{CBD} contents showed a gradual increase with depth in soil profiles C3 and P3 (except horizons BC_r in C3 and Bfl_7 in P3), indicating the prevalence of highly ordered Fe oxyhydroxides with depth (Curi and Franzmeier, 1987). In contrast, the Fe_{CBD} content decreased with depth in profiles G1 and G4, which is accompanied by an increase of Fe_{AO} content. All samples showed Fe_{AO}/Fe_{CBD} ratios with values <0.05 and low Fe_{AO} content, reflecting the predominance of highly ordered iron oxides in studied soil profiles, which is a common characteristic in highly weathered soils such as ferralsols (Smeck et al., 1994; Camêlo et al., 2017).

The content of Fe_P represents the short ordered range Fe oxides linked to OM (Table 7). The Fe_P content in upper horizons showed higher values than subsuperficial horizons in studied soil profiles. Differences were observed with contents in the Guarapuava profiles (G4 and G1) higher than in Cascavel (C3) and Palotina (P3) soils. This clear difference was associated with different current climatic conditions between the studied areas. At Guarapuava (profiles G1 and G4), the humid and cold climate favours the accumulation of organic matter (Ct, Table 3), the melanization process and the formation of a profundihumic A horizon in the Umbric Ferralsol. The OM inhibits partially the formation of highly ordered iron oxides, releasing Fe to the soil solution that can form organometallic complexes (Kämpf and Schwertmann, 1983; Inda Junior and Kämpf, 2003). As a result of this, the Guarapuava soil profiles showed the highest Fep levels. Thus, Cascavel (C3) and Palotina (P3), in areas with high temperatures and low organic matter content (Ct, Tables 4–5) showed lowest Fe_p values. This condition favours the formation of highly ordered iron oxides, with lower iron content released into the soil solution to form organometallic complexes (Schwertmann e Kämpf, 1985).

Table 7. Iron oxides dissolution of the studied soils.

Profile	Hz	Depth	Fe_{CBD}	Fe_{AO}	Fe_P	Fe_{AO}/Fe_{CBD}	Fe_P/Fe_{CBD}
		cm		%			
G1	A_{pa}	0–30	26.11	0.42	1.54	0.02	0.06
	AB	30–75	27.02	0.07	2.06	0.00	0.08
	BA	75–105	26.36	0.14	1.77	0.01	0.07
	Bfl_1	105–135	24.74	0.25	0.21	0.01	0.01
	BC_1	410–475	15.33	0.25	0.01	0.02	-
	BC_2	475–500	15.71	0.39	0.01	0.02	-
G4	A_1	0–25	21.23	0.41	3.59	0.02	0.17
	A_3	55–80	22.12	0.23	3.75	0.01	0.17
	AB	80–120	17.71	0.26	3.06	0.01	0.17
	BA	120–140	21.61	0.12	2.57	0.01	0.12
	Bfl_1	140–160	21.45	0.09	1.26	-	0.06
	Bfl_2	160–190	20.52	0.08	0.76	-	0.04
	Bfl_3	190–280	16.09	0.10	0.04	0.01	-
	BCr	360 cm+	21.82	0.19	0.03	0.01	-
C3	A_{pa}	0–20	17.02	0.34	0.83	0.02	0.05
	BA	60–120	17.06	0.11	0.44	0.01	0.03
	Bfl_1	120–265	17.40	0.14	0.01	0.01	-
	Bfl_2	265–360	19.06	0.13	0.03	0.01	-
	Bfl_3	360–745	23.37	0.11	0.01	-	-
	BC_2	910–1025	20.80	0.10	0.01	-	-
	BCr	1025 cm+	19.86	0.30	0.01	0.02	-
P3	A_{pa}	0–10	13.89	0.19	0.09	0.01	0.01
	Bfl_1	10–45	15.84	0.13	0.07	0.01	-
	Bfl_2	45–105	15.29	0.08	0.03	0.01	-
	Bfl_3	105–140	20.25	0.04	0.01	-	-
	Bfl_6	335–510	22.53	0.11	0.03	-	-
	Bfl_7	510–620	17.91	0.18	0.01	0.01	-

3.2.3. Mineralogical evidence

3.2.3.1. Mineralogy of volcanic rocks

Thin sections and XRD data of basalts in the soil profiles G4 and P3 indicated the presence of augite (Au), plagioclase (Pl), olivine (Ol), magnetite (Mt), ilmenite (Il), quartz (Qz), alkaline feldspar (Fd), calcite (Cl), 2:1 clay mineral (2:1 CM), kaolinite (Kt) and hematite (Hm) (Figure 13). For the porphyritic rhyo-dacite of the G1 soil profile, Au, Pl, Fd, Mt, Qz, 2:1 clay mineral, Kt, Hm, pigeonite (Pi) and apatite (Ap) were detected (Figure 13). The main primary minerals observed in the studied volcanic weathered rocks are consistent with the characterization by Clemente and Azevedo (2007), Nardy et al. (2008) and Caner et al. (2014). In addition, the presence of secondary minerals in the weathered rocks, such as 2:1 clay mineral, Kt and Hm revealed the initial weathering process of the studied rocks.

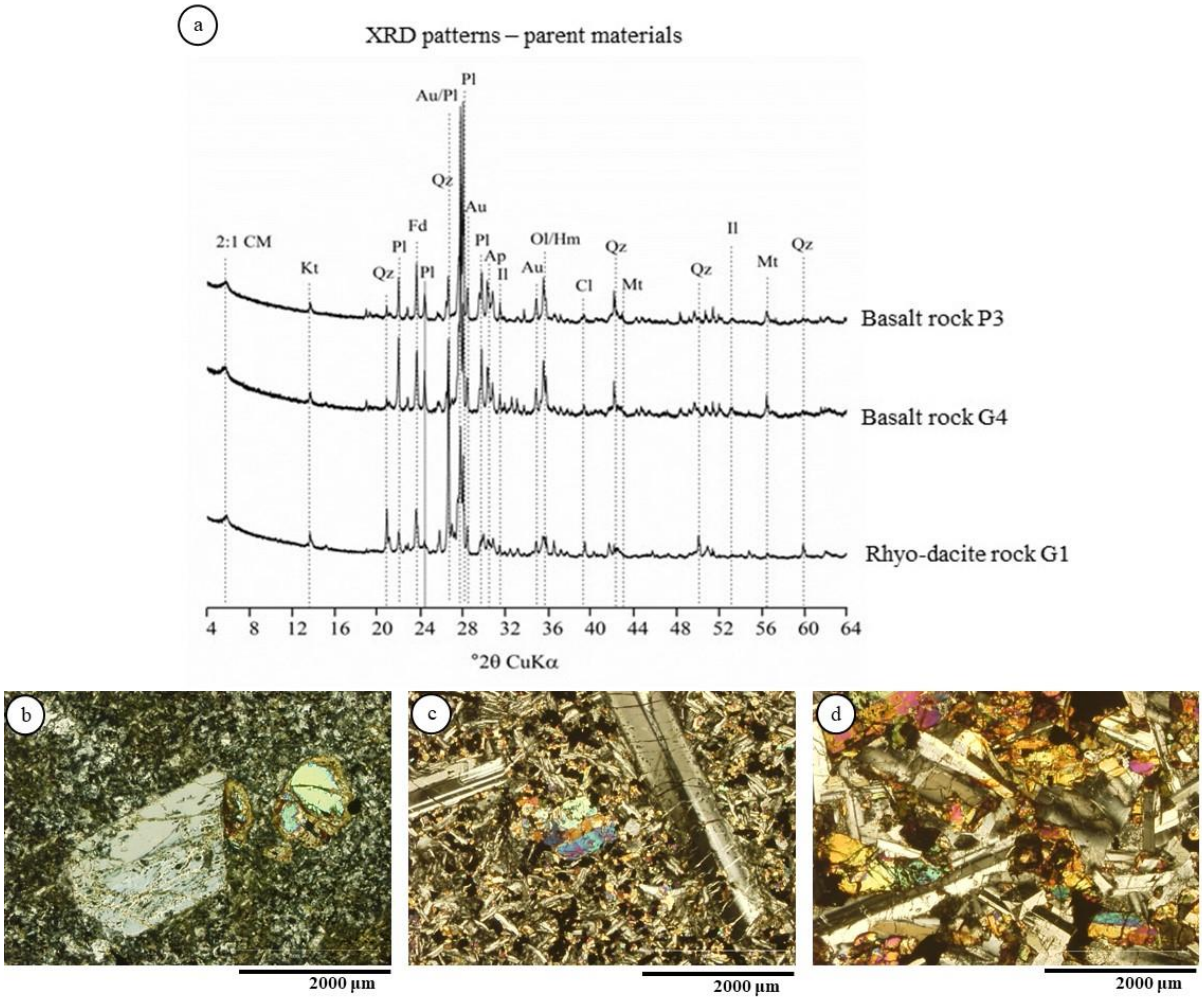

Figure 13. Constituent minerals of the weathered rock from studied soil profiles. a) XRD of the parent material (2:1 CM = 2:1 clay mineral; Kt = kaolinite; Qz = quartz; Pl = plagioclase; Fd = alkaline feldspar; Au = augite; Ap = apatite; Ol = olivine; Hm = hematite; Cl = calcite; Il = ilmenite; Mt = magnetite); b) Photomicrograph of the rhyo-dacite rock from G1 profile, XPL; c) Photomicrograph of the basaltic rock from the G4 profile, XPL; d) Photomicrograph of the basaltic rock from the P3 profile, XPL.

3.2.3.2. Evidence of transformation of primary minerals

The major primary silicates identified in the weathered rocks (G1, G4 and P3 profiles) were pyroxene group minerals (augite and pigeonite) and plagioclases, with the minor minerals K-feldspar (orthoclase) and quartz and some phyllosilicates. The most important primary minerals, the source for the transformations that lead to secondary mineral formation, are augite and plagioclases.

Augite was identified in the XRD patterns by ~29.88 °2 θ peak (d = 2.99 Å) and also observed in rock thin sections (Figure 13). The SEM-EDS images provided the chemical composition of a pyroxene mineral in G1 rock thin section (Figure 14, point 1). An alteration

fissure of the pyroxene mineral (Figure 14, point 2) showed the loss of Ca, Mg, Si, Fe, Na, Mn and an increase of Al. Amorphous materials, 2:1 clay minerals (smectites and vermiculite), Fe-(hydr) oxides, kaolinite and gibbsite may be the weathering products of pyroxenes (augite) depending the environmental conditions (Eswaran, 1979; Noack et al., 1993 and references therin). It was impossible to precisely identify the product of pyroxene weathering in the analysed fissure, but probably a 2:1 clay mineral may form during the alteration of augite in the G1 rock sample (observed at rock sample G1 a 2:1CM peak, Figure 13). In profiles derived from basaltic rocks (G4, C3 and P3), the likely early products of alteration of augite were mainly amorphous Fe-(hydr) oxides, due to the high contents of Fe-bearing primary silicates and the favorable drainage conditions. The short-range ordered Fe-(hydr) oxides probably transforms into hematite and goethite. The formation of 2:1 clay mineral may also occur during the first stages of basalt weathering, since peaks of 2:1 clay minerals (2:1 CM) were identified in the XRD rock patterns (Figure 13) (Eswaran, 1979; Noack et al., 1993 and references therein).

A plagioclase crystal was scanned in the G1 rock sample and the chemical composition is shown in Figure 15c. Two points were analyzed, one at the unaltered mineral surface and the other in a crystal fissure, showing the depletion of Na, Ca, Si, K, Al, Na, Mn and increase of Fe and Mg. Amorphous materials, gibbsite and kaolinite are the common weathering products from plagioclase (Eswaran and De Coninck, 1971; Eswaran, 1979; Rasmussen et al., 2010). Under high weathering rates, the plagioclases change uniformly and the first alteration feature is the appearance of fine fractures/fissures, a few micrometers thickness (Delvigne, 1965; Bellieni et al., 1986; Truffi and Clemente, 2002). Usually, the fractures are yellow or reddish yellow suggesting the infilling by Fe-(hydr) oxides from the alteration of neighboring minerals, as observed in Figure 15a. The advance of plagioclase alteration under good drainage conditions was observed in the BCr horizons from profiles G4, C3 and P3, suggesting the formation of kaolinite and gibbsite minerals (Figure 16). It is also possible that a 2:1 clay mineral (observed at rock samples 2:1CM, Figure 13) and/or an amorphous material may have formed, replacing the plagioclase under poor drainage conditions, during the first stages of the weathering of plagioclase crystals (Glasmann and Simonson, 1985). As the weathering proceeds, the progressive transformation from 2:1 mineral via mixed-layering can form kaolinite (Andrade et al., 2019 and references therein). Alternatively, the process of dissolution of the 2:1 mineral, and/or amorphous material under

low pH solution releases Si and Al into solution and can promote the recombination and precipitation of kaolinite (Delvigne, 1965).

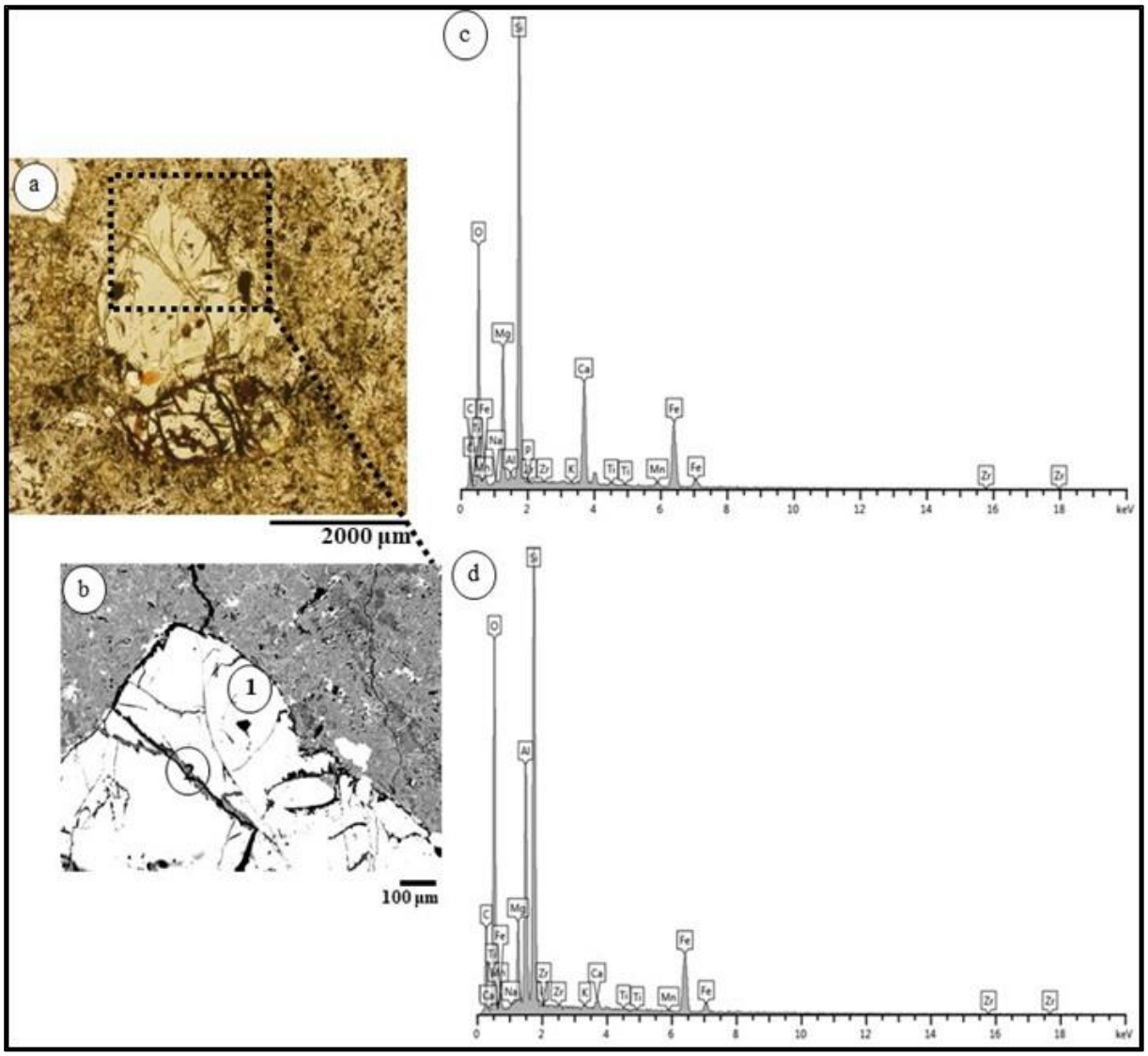

Figure 14. SEM-EDS analysis of a thin rock section from the G1 profile. a) Photomicrograph of the pyroxene in thin rock section from profile G1 (porphyritic rhyo-dacite) under petrography microscopy; b) Photomicrograph of the pyroxene under SEM-EDS; c) Geochemical composition of the pyroxene mineral (point 1); d) Geochemical composition of a fissure in a pyroxene mineral (point 2).

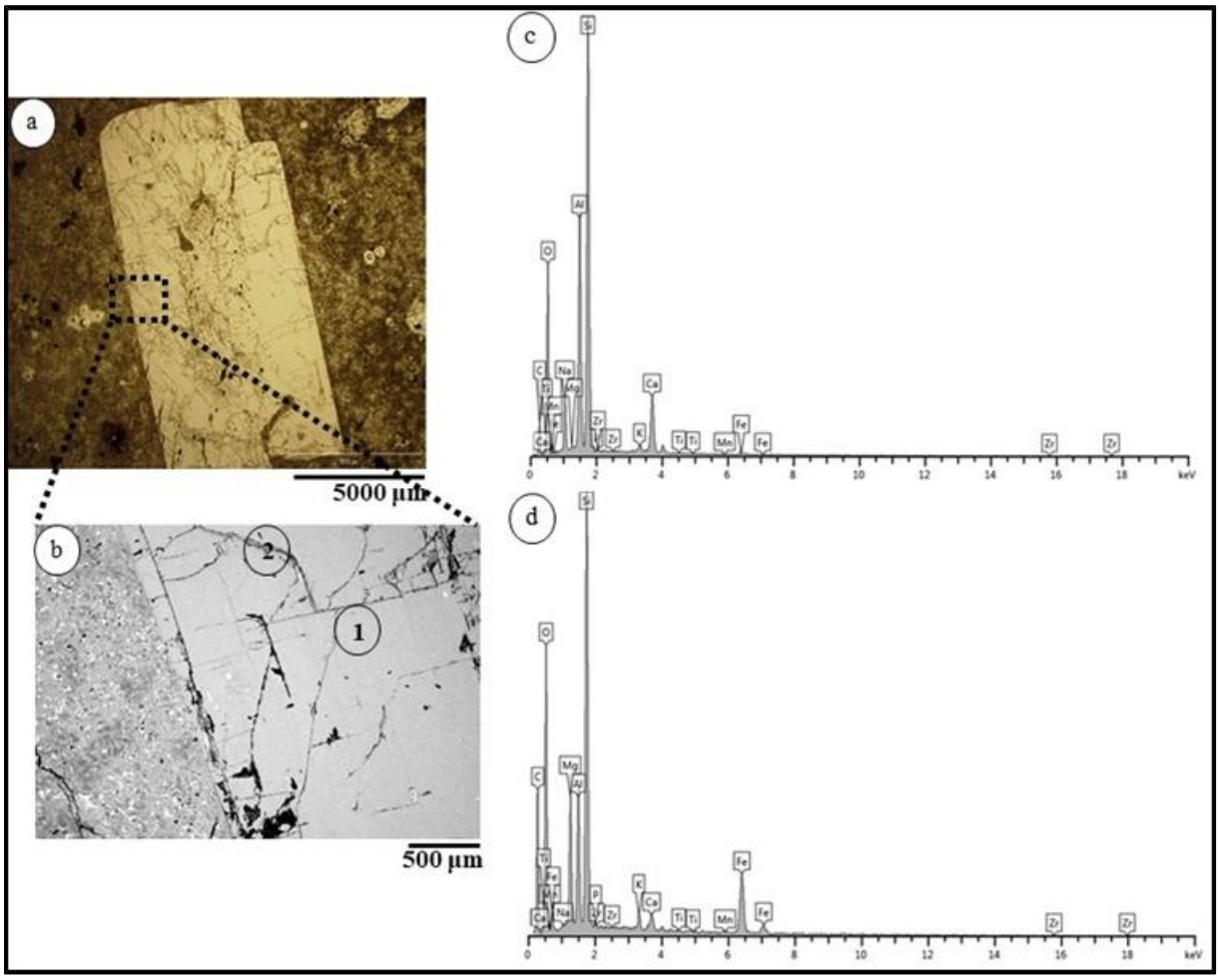

Figure 15. Geochemical composition and mineralogical transformations. a) Photomicrograph of the plagioclase phenocristal in a thin rock section from profile G1 (porphyritic rhyo-dacite) under petrograph microscopy; b) Photomicrograph of the plagioclase under SEM-EDS; c) Geochemical composition of the plagioclase mineral (point 1); d) Geochemical composition of a fissure in a plagioclase mineral (point 2).

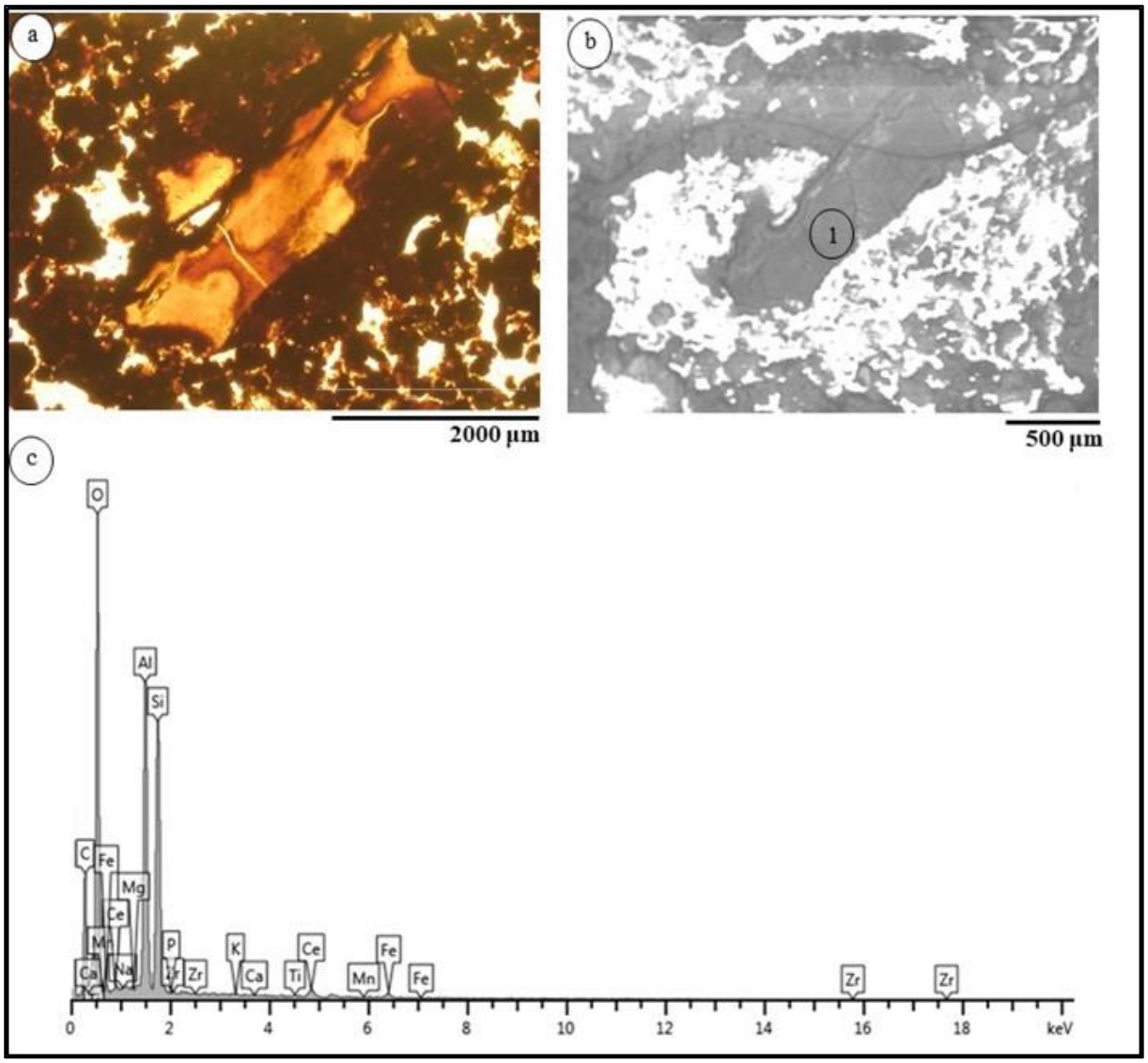

Figure 16. Geochemical composition of a weathered plagioclase mineral from the BCr horizon of the P3 profile developed under a basaltic rock. a) Photomicrograph of the weathered plagioclase from the BCr horizon of the profile P3 under petrography microscopy; b) Photomicrograph of the weathered plagioclase under SEM-EDS; c) Geochemical composition of the weathered plagioclase (point 1).

3.2.3.3. Soil clay mineralogy

XRD patterns of the oriented mounts of the clay fraction free of Fe oxyhydroxides in all soil profiles, reveal the existence of 001 peaks related to kaolinite (Kt) and hydroxy-interlayered 2:1 minerals (2:1 HI), and 002 peak related to gibbsite (Gb) (Figure 17). The Kt 001 peaks are evident ~12.2 ° 2θ and ~24.8 ° 2θ, collapsing after K 500 °C treatment, and are present from the bottom to top of the soil profiles. The intensity of Kt peaks decrease from the deep horizons to soil surface in G1, C3 and P3 profiles, while the opposite trend was observed in the G4 soil profile. The hydroxy-interlayered 2:1 minerals were confirmed after the

combination of Mg+EG and K500 °C. There was no expandability in Mg+EG and the partial collapse of ~ 6.1° 2θ towards 6.0 ° 2θ in the K500 °C treatment. The intensity of 2:1 HI peaks increase in samples from the bottom to the top in all soil profiles. This vertical variation in hydroxy-interlayered 2:1 minerals is a common feature observed in Ferralols, and it is considered to be a pedogenic origin (Morrás et a., 2009; Caner et al., 2014). In this way, the hydroxy-aluminium released during the weathering can be deposited in the interlayers of the 2:1 clay minerals hindering and/or preventing the formation of gibbsite, causing an antigibbsite effect (Jackson, 1963).

The gibbsite peaks were observed ~18.3 ° 2θ. After K 500 ° C treatment, a total collapse of ~18.3 ° 2θ Gb peak in all soil samples were observed. The intensity of the gibbsite peak increases from the bottom to the top of G1, C3 and P3 soil profiles. For the G4 soil profile the intensity of Gb peaks are relatively high in the samples from all analysed horizons. In addition, the identification of Kt and Gb was also confirmed by the thermal analysis (ATD-TG). The exothermic dehydroxylation events of Kt are evident at ~471 ° C and for Gb at ~256 °C (average values) (Appendix V–Y).

The mineral quantification in the clay fraction of the representative soil profiles are presented in Table 8. Kaolinite is the dominant mineral in all profiles, contributing to between 37.0% and 67.8% of the minerals. The quantitative trends of kaolinite differed between the profiles. It's known that the higher Si content in the soil solution facilitates the recombination of the element with Al for the kaolinite formation (Melo and Wypych, 2009). In the G1 and P3 profiles, Kt content below the control section was higher than in surface horizons. This resulted from the higher SiO_2 content in the deeper soil horizons, derived from the weathering of the parent material. Similar results were reported by Curi and Franzmeier (1984) and Guidin et al. (2006). Profile G4 showed the highest Kt content in the Bfl_1 horizon and this can be related to the leaching of Si from the surface horizons, which further concentrate and recombinate with Al in the Bfl_1 horizon, due to the high density of this horizon that allows the concentration of soil solution (neoformation) (Guidin et al., 2006). In profile C3, the highest Kt contents were observed in A_{pa}, Bfl_2 and BC_r horizons. In the BCr horizon the high content of Si that promotes Kt formation is associated with the presence of vesicles filled with quartz/chalcedony. The low crystallinity SiO_2 polymorphs (such as chalcedony) have higher solubility than well crystalized quartz (Siever, 1962; Eswaran and Stoops, 1979), providing soluble Si that can recombine with Al and promotes Kt formation. In the Bfl_2 horizon, the Si content probably resulted from the leaching of Si derived from the shallower soil horizons. In

the A_{pa} horizon, the soluble Si necessary for Kt formation is probably associated with the dissolution of biological amorphous SiO_2 (phytoliths), originated from the vegetation (Lucas et al., 1993).

Table 8. Mineralogical composition and Gt/(Gt+Hm) ratio of the clay fraction of the representative studied soil profiles.

			Kt	Gb	Hm	Gt	AO	Total	Gt/(Gt+Hm)
Profile	Hz	Prof.	%						
G1	A_{pa}	0–30	45.8	21.1	26.9	1.4	0.4	95.6	0.05
	AB	30–75	38.3	24.9	26.6	1.7	0.1	91.4	0.06
	BA	75–105	39.5	23.2	27.8	nd	0.1	90.6	nd
	Bfl_1	105–135	46.9	20.6	24.9	1.4	0.2	94.0	0.05
	BC_1	410–475	60.0	12.6	10.0	3.7	0.3	86.4	0.27
	BC_2	475–500	63.2	7.1	8.9	9.1	0.4	88.7	0.51
G4	A_1	0–25	45.1	16.7	19.3	3.9	0.4	85.4	0.17
	A_3	55–80	42.4	15.6	15.5	10.8	0.2	84.5	0.41
	AB	80–120	40.6	19.0	13.1	7.2	0.3	80.2	0.36
	BA	120–140	41.4	15.2	20.1	3.7	0.1	80.5	0.15
	Bfl_1	140–160	53.5	17.2	12.8	13.1	0.1	96.7	0.50
	Bfl_2	160–190	42.1	16.3	12.0	11.3	0.1	81.9	0.49
	Bfl_3	190–280	43.0	28.3	9.0	11.1	0.1	91.5	0.55
	BC_r	360 cm+	43.6	26.3	15.0	9.7	0.2	94.9	0.39
C3	A_{pa}	0–20	58.0	3.6	17.8	nd	0.3	79.8	nd
	BA	60–120	56.5	3.2	19.7	nd	0.1	79.6	nd
	Bfl_1	120–265	57.9	3.6	16.1	1.7	0.1	79.4	0.09
	Bfl_2	265–360	61.8	4.6	19.6	nd	0.1	86.2	nd
	Bfl_3	360–745	38.7	18.3	20.5	5.6	0.1	83.2	0.22
	BC_2	910–1025	57.2	4.6	17.0	6.2	0.1	85.1	0.27
	BC_r	1025 cm+	64.4	4.5	12.7	9.7	0.3	91.5	0.43
P3	A_{pa}	0–10	38.1	26.6	6.9	10.7	0.2	82.4	0.61
	Bfl_1	10–45	37.0	27.9	9.0	9.7	0.1	83.7	0.52
	Bfl_2	45–105	38.1	25.7	9.0	10.4	0.1	83.4	0.54
	Bfl_3	105–140	45.4	15.0	13.3	9.1	0.0	82.8	0.41
	Bfl_6	335–510	65.6	4.5	23.0	nd	0.1	93.2	nd
	Bfl_7	510–620	67.8	4.5	18.4	nd	0.2	90.9	nd

nd = not determined by the low intensity of reflection (Gt (110)).

The gibbsite content ranged from 3.2% to 28.3% in the studied soil profiles (Table 8; Figure 17). Kt and Gb showed a negative correlation (r = - 0.87) indicating the competitive formation between these two minerals in the soil profiles (Oliveira Junior et al., 2014). It is expected that the upper horizons and the more weathered horizons (Bfl horizons) of tropical/subtropical soils contain higher values of Gb than deeper horizons (Lucas et al., 1993) and this was observed in the G1, C3 and P3 soil profiles. For profile G4 an increase in Gb content below the control section in the saprolite zone was observed, indicating an environment with a rapid loss of Si in a strong dissected landscape (Furian et al., 2002).

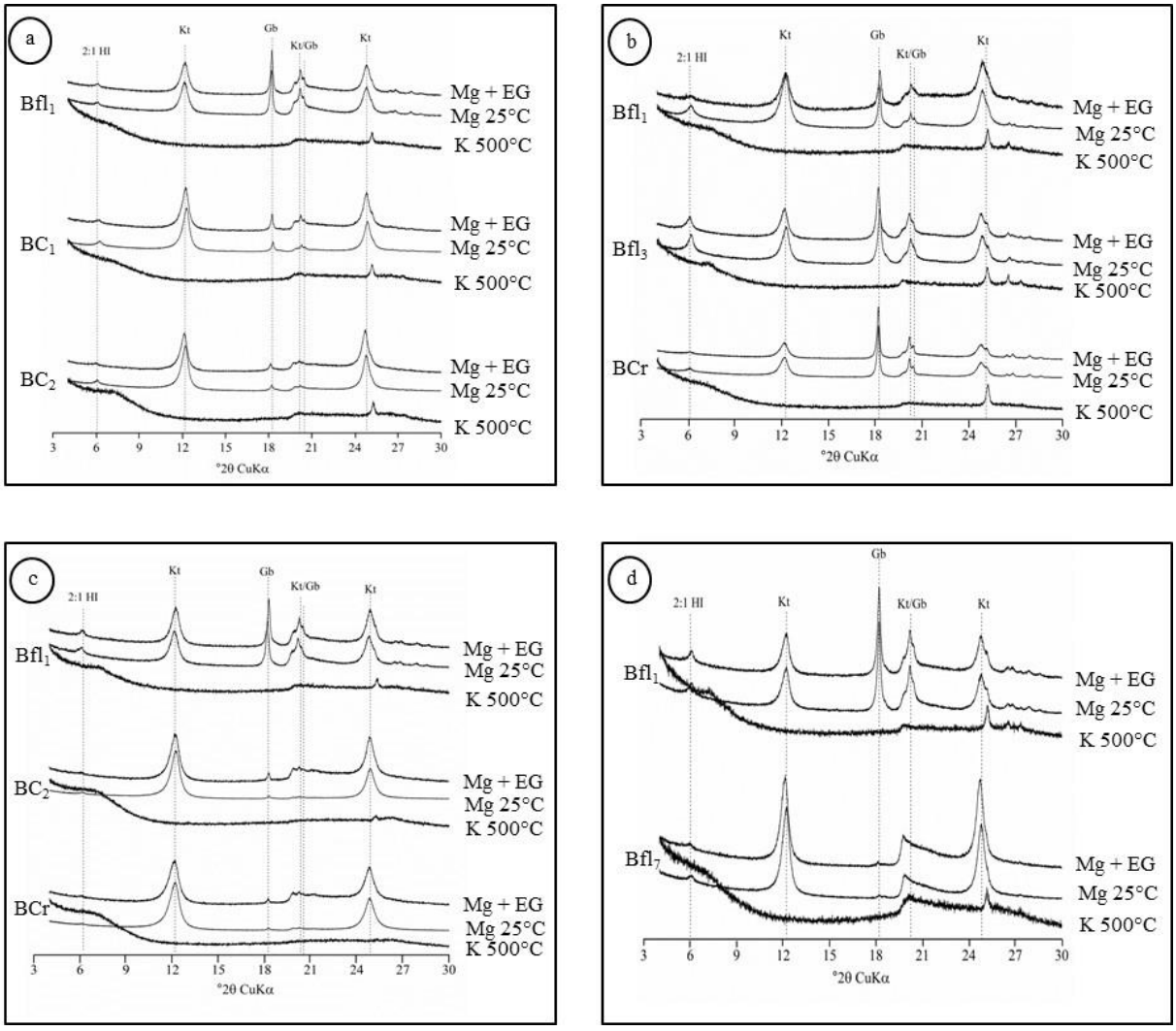

Figure 17. XRD patterns of the clay content of the main horizons (Bfl, BC and BC_r) from the four studied soil profiles saturated with Mg (Mg 25 °C), solvated with ethylene glycol (Mg + EG) and K heated until 500 ºC (K 500 °C). a) G1 soil profile; b) G4 soil profile; c) C3 soil profile and d) P3 soil profile.

XRD patterns of the samples with concentrated iron oxides revealed the existence of peaks related to goethite (Gt: ~21.3 ° 2θ and ~36.9 ° 2θ), hematite (Hm: ~33.2 ° 2θ and ~35.7 ° 2θ), maghemite (Mg: ~30.3 ° 2θ and ~43.4 ° 2θ) and minor existence of quartz (Qz: ~26.5 ° 2θ), rutile (Ru: ~27.4 ° 2θ) and anatase (An: ~25.3 ° 2θ) (Figure 18).

The values of the Gt/(Gt + Hm) ratio varied from 0.05 to 0.61. The high Hm content in relation to Gt promotes the rubification process associated with moderate ferralitization in the profiles G1, G4 and C3 characterizing the reddish color observed in the field (Table 8; Tables 3–5). In contrast, at profile P3 the Gt content was higher than hematite in the upper horizons wich can suggest the occurrence of xanthization process. For the upper horizons of profiles G1 and C3, and deep horizons from P3 profile, the hematite peaks and traces of goethite peaks were identified in the clay fraction, showing that the Fe activity in soil solution

was high enough to favour Hm formation. The higher Hm content in relation to Gt in the profiles from G1 (A_{pa}–BC_1) and G4 (A_1–BA and BC_r) were not expected in the upper horizons, because of the current humid climatic conditions and high C content, which favour the Gt formation. Guidin et al. (2006) observed similar results in Umbric Ferralsols in Guarapuava (PR) in a profile with Hm content higher than Gt in the B ferralic horizons, however, the authors not develop links with the possible origin. According to Kämpf and Schwertmann (1983), factors that favour hematite formation over goethite are the same that favour ferrihydrite formation, such as a high release rate of Fe and a low content of organic matter to complex the Fe. Once ferrihydrite is formed, hematite is favoured over goethite with increasing temperature in a drier climate. Therefore, the Hm content observed in the soil profiles G1 and G4 may have been formed under drier past climatic conditions during the Quaternary or older (see section 3.3.1) (Schwertmann, 1971; Behling, 1997; 1998; 2002; Ker, 1998; Ker and Resende, 1990; Calegari et al., 2017; Luz et al., 2019). However, Almeida (1979) apud Ker (1998), reported that Fe^{3+} contents in the system more than any other factor favour the formation of hematite. Thus, the past climatic conditions may have accelerated the formation of hematite, but this is not necessarily the most important factor. Therefore, the Hm content observed in soil profiles enhance the likely polygenetic history of study soils.

Maghemite (ferromagnetic Fe oxide - Mg) was detected in all the soils. G1 and C3 profiles presented sharper/more intense peaks than the G4 and P3 profiles (Figure 18). Mg formation is associated with magnetite oxidation inherited from the parent material and/or from transformation of other pedogenetic Fe oxides (Hm and Gt) under high temperatures in the presence of organic C (Curi and Franzmeier, 1987; Schwertmann and Taylor, 1989; Fontes and Weed, 1991; Costa et al., 1999; Fontes et al., 2000; Camêlo et al., 2017). Maghemite peaks were identified from the upper to deep soil horizons, probably formed from the oxidation of magnetite present in the parent material. The possibility of maghemite formation by transformation of other pedogenetic Fe oxides, such as Hm and Gt under high temperatures in the presence of organic C is not ignored, since, the Holocenic fires in a drier climate were recorded at the studied and nearby areas (*see section 3.3.1*) (Behling, 1997; 1998; 2002; Luz et al., 2019).

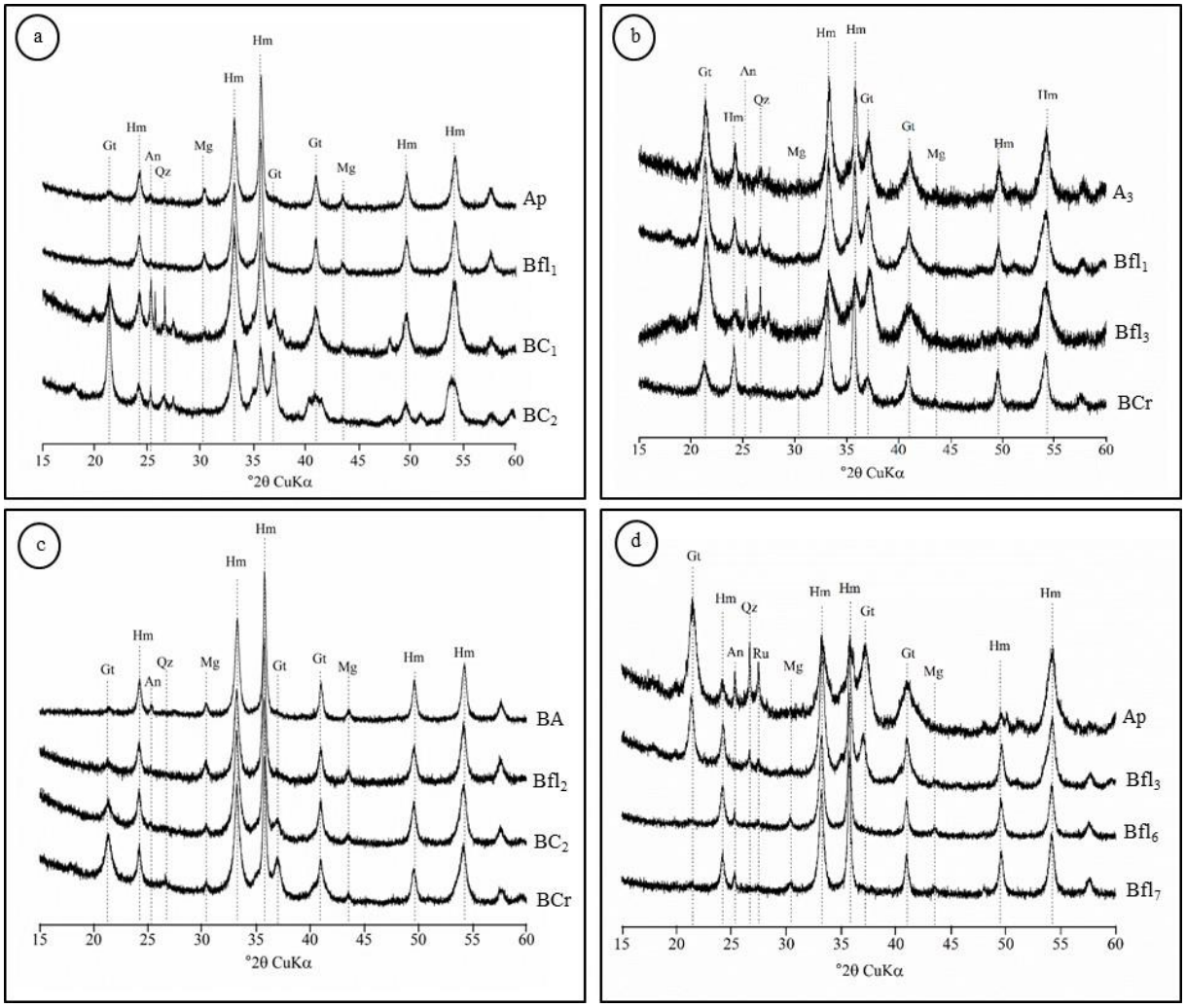

Figure 18. XRD patterns of samples with concentrated iron oxides. Hematite is the dominant iron oxide mineral in studied soil profiles; a) G1 soil profile; b) G4 soil profile; c) C3 soil profile and d) P3 soil profile. Hm = hematite; Gt = goethite; Qz = quartz; Ru = rutile; An = anatase; Mg = maghemite.

3.2.3.3.1. Crystallographic parameters of kaolinite and gibbsite

The d001 values for Kt in the clay fraction varied from 7.21–7.30 Å, throughout the studied soil profiles (Table 9). The range for d002 was 3.57–3.61 Å (Table 9). This variation in the d001 value is due to the presence of Fe and other elements in the structure of Kt, which is related to the size of the crystal (Trunz, 1976; Koppi and Skjemstad, 1981; Singh and Gilkes, 1992; Melo et al., 2001b; Ghidin et al., 2006). The MCD values of Kt did not showed a clear trend in the soil profiles. Samples from the P3 soil profile showed the highest average MCD values (Average MCD value= 13.81) followed by G1 (Average MCD value = 13.72), G4 (Average MCD value = 12.45) and C3 profile (Average MCD value = 12.27). Highest MCD values were observed in Bfl_1 horizon of G1 (MCD = 15.8), Bfl_3 and BCr horizon in G4 (MCD = 14.9 and 17.6, respectively), A_{pa} and Bfl_2 in C3 (MCD = 13.4) and A_{pa}, Bfl_1 and Bfl_2

in P3 profile (MCD = 16.8, 14.1 and 14.9, respectively). The high MCD values of Kt can be related to the favourable formation environment and consequently a greater lattice ordering. The average number of layers (ANL) of Kt is around 17. The WHH, MCD and ANL values of the soils in the present study were similar to those described by Melo et al. (2001b), Ghidin et al. (2006) and Testoni et al. (2017) for Kt in ferralsols derived from basaltic and rhyo-dacitic rocks.

Table 9. Crystallographic parameters of kaolinite in studied soils.

Profile	Hz	Depth	*d* 001	*d* 002	WHH[1]	MCD[2]	ANL[3]	Cristallinity index	AI[4]	SA	Dehydroxylation temperature
		cm	--------Å-------		°2θ	nm		(HBCI)		$m^2\ g^{-1}$	° C
G1	A_{pa}	0–30	7.23	3.58	0.54	14.9	20.6	11.8	0.30	52.5	466
	AB	30–75	7.23	3.58	0.54	14.9	20.6	12.8	0.15	52.5	466
	BA	75–105	7.26	3.58	0.63	12.8	17.7	13.7	0.08	60.7	466
	Bfl_1	105–135	7.25	3.58	0.51	15.8	21.8	14.3	0.02	49.5	469
	BC_1	410–475	7.21	3.59	0.62	13.0	18.0	11.4	0.16	60.2	472
	BC_2	475–500	7.23	3.59	0.74	10.9	15.1	10.4	0.11	71.4	474
G4	A_1	0–25	7.26	3.59	0.63	12.8	17.7	12.9	0.05	60.7	471
	A_3	55–80	7.24	3.58	0.67	12.0	16.6	15.1	0.10	64.7	472
	AB	80–120	7.21	3.59	0.57	14.1	19.5	15.7	0.19	55.4	473
	BA	120–140	7.26	3.58	0.81	10.0	13.8	19.3	0.01	77.7	473
	Bfl_1	140–160	7.30	3.61	1.17	7.0	9.5	13.7	0.08	110.6	475
	Bfl_2	160–190	7.26	3.57	0.73	11.1	15.3	14.7	0.01	70.1	473
	Bfl_3	190–280	7.24	3.57	0.54	14.9	20.6	13.7	0.00	52.4	465
	BC_r	360 cm+	7.27	3.57	0.46	17.6	24.2	21.6	0.22	44.7	475
C3	A_{pa}	0–20	7.23	3.58	0.6	13.4	18.6	9.7	0.07	58.2	472
	BA	60–120	7.23	3.59	0.64	12.6	17.4	9.5	0.06	62.0	472
	Bfl_1	120–265	7.23	3.58	0.64	12.6	17.4	9.6	0.00	61.9	472
	Bfl_2	265–360	7.24	3.59	0.6	13.4	18.6	8.6	0.03	58.1	472
	Bfl_3	360–745	7.26	3.58	0.61	13.3	18.3	13.3	0.05	58.8	466
	BC_2	910–1025	7.25	3.59	0.71	11.4	15.7	15.1	0.07	68.4	479
	BC_r	1025 cm+	7.27	3.58	0.88	9.2	12.7	16.3	0.16	84.1	477
P3	A_{pa}	0–10	7.23	3.59	0.48	16.8	23.2	14.6	0.04	46.8	466
	Bfl_1	10–45	7.24	3.58	0.57	14.1	19.5	14.8	0.16	55.3	466
	Bfl_2	45–105	7.21	3.59	0.54	14.9	20.6	12.6	0.15	52.6	468
	Bfl_3	105–140	7.24	3.58	0.69	11.7	16.1	15.4	0.13	66.6	471
	Bfl_6	335–510	7.29	3.59	0.62	13.1	18.0	8.3	0.06	59.5	476
	Bfl_7	510–620	7.26	3.58	0.66	12.3	16.9	8.9	0.06	63.6	473

[1]WHH = width at half maximum height of the 001 diffraction peak; [2]MCD = mean crystallite dimension along 001 direction; [3]ANL = average number of layers; [4]AI = assimetry index; [5]SA= surface area in $m^2\ g^{-1}$.

The Hughes and Brown crystallinity index (HBCI) (Hughes and Brown, 1979) of Kt showed values ranging from 8.3 (Bfl_6 horizon in the P3 profile) to 21.6 (BC_r horizon in the G4 soil profile). The average value was 13.2. These values are slightly above to those observed by Melo et al. (2001a; HBCI: 11.4 to 12.2) and Ghidin et al. (2006; HBCI: 5.7 to 9.9) in Brazilian ferralsols developed from basalt and rhyo-dacite. In addition, profile C3

showed in general, the lowest crystallinity index of the studied soil profiles, which is probably related to its higher Fe_2O_3 content than in the G1, G4 and P3 profiles (Table 12). As a result, the Fe substitutes the Al in the octaedral sheet, resulting in the lowest crystallinity. According to Hughes and Brown (1979), the low crystallinity of Kt is associated with a high degree of structural disorder, caused by defects in the layer stacking and inter-stratification with other minerals (Plançon and Zacarie, 1990). The reduction in crystallinity and the increase in Kt surface area may also be due to the presence of octaedral Fe, which comes from the Fe rich parent material (Mestdagh et al., 1980; Brindley et al., 1986) (Table 9 and Table 12). It was observed that the higher the dehydroxylation temperature, the lower the MCD for the most horizons (Table 9). The Kt dehydroxylation temperature in the clay fraction varied between 465 and 479° C, with an average value of ~471° C.

The asymmetry index (AI; Melo and Wypych, 2009) for Kt 001 peak ranged from 0 in Bfl_3 horizon of the G4 profile to 0.30 in the A_{pa} horizon of the G1 soil, indicating a high asymmetry. The average values showed that the AI in samples from the G1 profile (Average AI value = 0.14) are higher than those in the samples from the P3 (Average AI value = 0.10), G4 (Average AI value = 0.08) and C3 profiles (Average AI value = 0.06). Testoni et al. (2017) observed similar results of high asymmetry in Kt from Cascavel ferralsols, indicating the occurrence of inter-stratified minerals (kaolinite-smectite).

The Gb d002 values ranged from 4.84 to 4.87 Å, and the MCD Gb d002 ranged from 31.2 to 73.1 nm (average value of 46.4 nm) (Table 10). The highest MCD values were observed below the control section, in the less weathered horizons of profiles G1 (BC_2 horizon) and C3 (BC_r horizon), in the B ferralic horizons of profile P3 (Bfl_3, Bfl_6 and Bfl_7) and G4 profile (Bfl_2), and in the superficial horizon of the G4 profile. In general, the highest average MCD values were observed in the C3 profile (~49.2 nm) followed by P3 (~48.2 nm), G4 (~45.3 nm) and G1 soil (~44.4 nm). The values for MCD d002 of Gb are similar to higher than the the MCDs for Fe oxides, which is consistent with the values found by Fontes and Weeds (1991) and Melo et al. (2001a). The dehydroxylation temperature of Gb varied from 238°C to 271°C, showing generally a positive correlation with Gb contents (r = 0.77).

Table 10. Crystallographic parameters of gibbsite in studied soils.

Profile	Hz	Depth	*d* 002	WHH[1]	MCD[2] (002)	Dehydroxylation temperature
		cm	Å	°2θ	nm	° C
G1	A_{pa}	0–30	4.85	0.23	35.8	259
	AB	30–75	4.85	0.22	38.2	260
	BA	75–105	4.85	0.22	37.6	263
	Bfl_1	105–135	4.85	0.19	44.2	263
	BC_1	410–475	4.85	0.15	55.0	259
	BC_2	475–500	4.87	0.15	55.7	254
G4	A_1	0–25	4.86	0.16	51.9	260
	A_3	55–80	4.86	0.18	46.2	261
	AB	80–120	4.85	0.19	44.0	264
	BA	120–140	4.85	0.17	48.7	262
	Bfl_1	140–160	4.86	0.19	43.7	262
	Bfl_2	160–190	4.85	0.16	51.8	261
	Bfl_3	190–280	4.84	0.26	31.6	256
	BC_r	360 cm+	4.86	0.19	44.4	271
C3	A_{pa}	0–20	4.84	0.21	39.2	244
	BA	60–120	4.84	nd	nd	240
	Bfl_1	120–265	4.85	nd	nd	241
	Bfl_2	265–360	4.87	nd	nd	238
	Bfl_3	360–745	4.86	0.21	38.8	260
	BC_2	910–1025	4.85	0.17	49.6	251
	BC_r	1025 cm+	4.85	0.12	69.0	247
P3	A_{pa}	0–10	4.85	0.26	31.2	258
	Bfl_1	10–45	4.85	0.25	32.8	258
	Bfl_2	45–105	4.86	0.26	31.8	259
	Bfl_3	105–140	4.86	0.17	49.7	262
	Bfl_6	335–510	4.86	0.11	73.1	252
	Bfl_7	510–620	4.85	0.12	70.6	247

[1]WHH = width at half maximum height of 002 diffraction peak; [2]MCD = mean crystallite dimension along 002 direction; [3]Gibbsite (Gb) content determined in the CBD residue, via simultaneous differential thermal analysis (DTA) and thermogravimetric (TG) analysis. nd = not determined because of the low intensity of reflection.

3.2.3.3.2. Crystallographic parameters of hematite and goethite

The MCD Gt (110) values ranged from 26.9 to 66.8 nm. The MCD Gt (111) values varied from 11.0 to 22.1 nm (Table 11). The higher MCD Gt (110) suggest an isodimensional development of the crystal (Schwertmann and Kämpf, 1985; Singh and Gilkes, 1992). The lower MCD Gt value (111) shows a reduction in the size of the oxide with isomorphic substitution (IS) (Fitzpatrick and Schwertmann, 1982; Schwertmann and Taylor, 1989; Melo et al., 2001a). Isomorphic substitution values for Gt ranged from 10 to 310 mmol mol^{-1}. In profiles G1, G4 and C3, the IS did not show any trend with depth. In these three profiles, highest IS values were observed in upper horizons because of the high degree of weathering, and in the deepest ones probably because of the Al availability. On the other hand, the profile P3 showed a clear decrease in IS for Gt with depth. According to Schwertmann and Kämpf (1985), goethite with high IS is usually associated with gibbsite in the same sample. This fact

was observed in our studied soil samples (r = 0.75), and could characterize a moderate–strong pedogenetic environment of desilication in the study profiles and differ the areas by the weathering intensity.

The MCD Hm (110) values were higher than the MCD Hm (104) suggesting a platy morphology (Schwertmann and Taylor, 1989; Fontes and Weed, 1991) (Table 11). The MCD in the profiles G1, G4 and C3 did not showed a clear trend with depth, which suggests an effect of the bioturbation process when mixing the soil matrix and homogeneous conditions that favour the development of hematite. On the other hand, samples from the profile P3 showed a constant increase in MCD with depth. This difference may suggest that climatic and geochemical conditions might favour a highly ordered hematite in the deep soil horizons of profile P3. The measured WHH of Hm (110) was lower than the WHH of Hm (104) and Gt (110), enhancing the high degree of crystallinity of hematite in relation to goethite. The isomorphic substitution in Hm is relatively constant with values varying from 30 to 150 mmol mol^{-1}. Profiles G1 and C3 did not showed a clear trend between the IS and depth. In profiles G4 and P3 lower IS values were observed in the deepest horizons. According to Schwertmann and Kämpf (1985), this indicates that the Hm with a low degree of IS forms first, and as weathering proceeds, more Al becomes available for incorporation into the Hm structure. Thus, it is possible to observe that most of the Bfl and upper horizons from the studied profiles presented a high degree of IS in Hm.

Table 11. Crystallographic parameters of the hematite and goethite in the studied soil profiles.

Profile	Hz	Depth	WHH[1]				MCD[2]				IS[3]	
			Gt (110)	Gt (111)	Hm (104)	Hm (110)	Gt (110)	Gt (111)	Hm (104)	Hm (110)	Gt	Hm
		cm	----------° 2 θ----------				----------nm----------				mmol mol^{-1}	
G1	A_{pa}	0–30	0.60	nd	0.54	0.39	38.2	nd	23.6	35.5	270	120
	AB	30–75	0.72	nd	0.59	0.37	37.7	nd	20.7	39.5	10	60
	BA	75–105	nd	nd	0.54	0.38	nd	nd	23.7	37.7	140	90
	Bfl_1	105–135	nd	nd	0.59	0.35	nd	nd	21.3	39.7	90	100
	BC_1	410–475	0.73	0.38	0.60	0.50	35.1	22.1	22.2	52.8	180	-
	BC_2	475–500	0.37	0.42	0.78	0.41	64.6	20.4	18.0	32.9	140	150
G4	A_1	0–25	0.48	nd	0.50	0.33	45.1	nd	25.1	41.7	90	140
	A_3	55–80	0.64	0.62	0.51	0.36	40.5	13.4	26.0	37.7	230	150
	AB	80–120	0.67	0.56	0.50	0.50	34.0	14.9	27.3	27.4	230	120
	BA	120–140	0.51	0.44	0.49	0.38	52.2	19.5	29.0	35.6	90	130
	Bfl_1	140–160	0.55	0.56	0.52	0.37	45.9	14.8	26.3	37.6	270	100
	Bfl_2	160–190	0.60	0.53	0.51	0.39	42.3	16.0	26.3	37.3	170	60
	Bfl3	190–280	0.65	0.75	0.80	0.70	42.9	11.0	17.5	19.6	300	130
	BC_r	360 cm+	0.71	0.70	0.38	0.38	33.4	11.9	33.5	38.7	250	50
C3	A_{pa}	0–20	nd	nd	0.53	0.34	nd	nd	24.8	41.9	190	100
	BA	60–120	nd	nd	0.54	0.34	nd	nd	24.0	37.4	160	-
	Bfl_1	120–265	0.54	nd	0.53	0.34	51.6	nd	23.4	43.8	30	30
	Bfl_2	265–360	nd	nd	0.48	0.33	nd	nd	28.8	44.2	120	50
	Bfl_3	360–745	0.72	nd	0.52	0.39	40.1	nd	23.7	34.8	70	150
	BC_2	910–1025	0.69	0.48	0.49	0.33	42.5	17.6	24.7	42.5	160	100
	BC_r	1025 cm+	0.70	0.49	0.50	0.29	35.6	17.5	24.9	47.7	150	100
P3	A_{pa}	0–10	0.69	0.68	0.66	0.58	42.9	12.0	18.7	23.9	310	120
	Bfl_1	10–45	0.78	0.57	0.67	0.58	32.1	14.7	18.3	24.8	250	60
	Bfl_2	45–105	0.71	0.57	0.68	0.53	38.6	14.4	19.8	23.5	250	-
	Bfl_3	105–140	0.44	0.43	0.46	0.33	66.8	20.0	29.1	43.4	120	60
	Bfl_6	335–510	0.68	nd	0.46	0.29	42.8	nd	28.0	50.6	-	40
	Bfl_7	510–620	1.00	0.58	0.50	0.33	26.9	14.7	25.3	44.3	160	50

[1]WHH = width at half maximum height of the diffraction peak; [2]MCD = mean crystallite dimension; [3]Isomorphic substitution. Nd = not determined because of the low intensity of reflection.

3.2.4. Geochemical evidence: bulk chemical composition, geochemical mass balance calculations and weathering indices

The bulk chemical composition of weathered rocks and the soil samples are shown in Table 12. The rhyo-dacite weathered rock (G1) contains a high content of SiO_2, Al_2O_3 and K_2O. However, the content of CaO, MgO, Fe_2O_3, TiO_2 and MnO is low, especially when compared to that of the basaltic weathered rocks (basalts from G4 and P3). The four representative soil profiles present Al_2O_3, SiO_2, Fe_2O_3, and TiO_2 as the major elements, which represent > 80% of the bulk composition. The secondary elements are MnO, MgO, K_2O, CaO and ZrO_2, and their proportions do not exceed 2% in most of the soil horizons. SiO_2 increases with depth in profiles G1 and C3. The high SiO_2 content in the deep horizons of G1 are related to the parent material, which is rich in this element. In C3, the high SiO_2 content is associated with the presence of vesicles filled with quartz/chalcedony in the BC_r horizon. Profiles G4 and P3 presented the SiO_2 content that varies with depth, but does not present a clear tendency. The content of secondary elements (MgO, K_2O and CaO) tend to decrease towards soil surface. For Fe_2O_3, Al_2O_3, TiO_2 and ZrO_2 content, a tendency for accumulation was observed for the four representative soil profiles, increasing towards the surface, showing an association with the presence of kaolinite, iron oxides, and heavy minerals (anatase, rutile, ilmenite and zircon). The LOI values tend to increase from deep to upper soil horizons in these profiles (Table 12).

In general, the major elements (Al_2O_3, SiO_2, Fe_2O_3) which are mainly related to the parent material and the weathering process, presented few differences among the soil profiles. The ternary plot based on bulk chemical composition (Figure 19) allows the differentiation of the samples into three groups: 1) Samples from the G1 profile; 2) Samples from the G4 and C3 profiles; and 3) Samples from the P3 soil profile. The samples of group 1 (soil profile G1, derived from rhyo-dacite rock) are characterized by an Al_2O_3 content higher than that in the G4, C3 and P3 profiles, followed by SiO_2 content higher than that in the G4 and C3 profiles and finally, an Fe_2O_3 content lower than that in the G4, C3 and P3 profiles. Group 2 is characterized by the presence of samples from G4 and C3 profiles, which were derived from basaltic rock and presented an Fe_2O_3 content higher than that of the G1 and P3 soil profiles, Al_2O_3 content higher than that of the P3 profile and SiO_2 content lower than that of the G1 and P3 soil profiles. Group 3 (profile P3) also derived from basaltic rock is characterized by a SiO_2 content higher than that of the G4 and C3 profiles, Al_2O_3 content lower than that of the G4, C3 and G1 profiles and Fe_2O_3 content lower than that of the G1 profile. Thus, the groups

1 and 2 presented major element content in the order $Al_2O_3 > SiO_2 > Fe_2O_3$ and group 3 in the order $SiO_2 > Al_2O_3 > Fe_2O_3$.

Table 12. Total chemical composition of the studied representative soil profiles (G1, G4, C3 and P3).

Profile	Hz	Depth	K_2O	Fe_2O_3	TiO_2	Al_2O_3	SiO_2	ZrO_2	MnO	CaO	MgO	Total	LOI[1]
		cm					%						g
G1	A_{pa}	0–30	0.2	12.3	6.1	42.7	32.7	0.2	0.1	0.3	0.2	94.8	0.114
	AB	30 –75	0.2	12.5	6.2	45.7	32.9	0.2	0.1	0.1	0.6	98.4	0.107
	BA	75–105	0.2	12.6	6.2	46.1	31.9	0.2	0.1	0.1	1.0	98.4	0.108
	Bfl_1	105–135	0.1	12.6	6.2	46.1	31.6	0.2	0.1	0.1	0.3	97.2	0.102
	Bfl_2	135–180	0.1	12.5	6.0	48.3	32.8	0.2	0.1	0.0	0.4	100.5	0.090
	Bfl_3	180–225	0.2	12.1	6.1	47.3	34.1	0.2	0.1	0.0	0.8	100.9	0.097
	Bfl_4	225–280	0.2	12.9	6.4	49.3	33.0	0.2	0.1	0.0	0.7	102.8	0.090
	Bfl_5	280–360	0.2	12.4	5.9	50.3	33.9	0.2	0.1	0.0	0.2	103.2	0.089
	Bfl_6	360–410	0.2	12.1	5.8	46.8	34.5	0.2	0.1	0.0	1.2	101.0	0.089
	BC_1	410–475	0.2	11.3	5.9	44.9	37.2	0.2	0.1	0.0	0.5	100.3	0.083
	BC_2	475–500	0.2	9.0	7.1	44.3	41.6	0.3	0.1	0.0	0.2	102.8	0.078
	Weathered rock	-	3.8	6.1	1.3	12.4	63.2	0.1	0.1	2.1	0.6	89.6	0.013
G4	A_1	0–25	0.1	17.6	10.1	34.8	29.6	0.1	0.2	0.1	0.9	93.4	0.119
	A_2	25–55	0.1	17.7	9.7	37.3	29.6	0.1	0.2	0.0	1.4	96.1	0.113
	A_3	55–80	0.1	18.0	9.8	38.5	29.4	0.1	0.2	0.0	2.4	98.4	0.101
	AB	80–120	0.1	18.3	9.9	40.6	30.4	0.1	0.2	0.0	0.4	100.0	0.095
	BA	120–140	0.1	18.0	9.4	40.0	30.6	0.1	0.2	0.0	2.0	100.4	0.094
	Bfl_1	140–160	0.1	17.8	9.7	40.2	30.9	0.1	0.2	0.0	0.6	99.7	0.090
	Bfl_2	160–190	0.1	17.9	9.5	40.8	30.3	0.1	0.2	0.0	0.6	99.6	0.087
	Bfl_3	190–280	0.1	19.3	9.7	41.9	28.3	0.1	0.2	0.0	0.0	99.6	0.085
	BC_1	280–330	0.1	19.6	8.7	45.2	27.5	0.1	0.2	0.0	1.1	102.5	0.096
	BC_2	330–360	0.1	19.8	8.3	45.7	25.7	0.1	0.2	0.0	1.3	101.3	0.089
	BC_r	360 +	0.0	25.7	7.0	39.1	11.5	0.1	0.2	0.1	0.5	84.3	0.090
	Weathered rock	-	1.7	8.3	2.6	9.8	46.4	0.0	0.2	7.2	2.0	78.3	0.011
C3	A_{pa}	0–20	0.1	22.3	5.6	36.4	27.0	0.1	0.3	0.2	0.0	92.1	0.095
	AB	20–60	0.1	22.6	5.5	38.5	27.0	0.1	0.2	0.1	0.1	94.1	0.094
	BA	60–120	0.1	23.1	5.4	40.8	26.1	0.1	0.2	0.1	0.0	95.8	0.087
	Bfl_1	120–265	0.1	23.0	5.6	41.1	25.1	0.1	0.2	0.1	0.7	96.0	0.088
	Bfl_2	265–360	0.1	23.8	5.7	42.8	24.8	0.1	0.2	0.1	0.7	98.2	0.081
	Bfl_3	360–745	0.1	23.5	5.2	43.4	26.0	0.1	0.2	0.1	1.2	99.7	0.076
	Bfl_4	745–860	0.1	22.2	3.9	40.4	30.5	0.1	0.2	0.0	0.8	98.3	0.085
	BC_1	860–910	0.1	22.0	3.6	37.6	31.5	0.1	0.2	0.0	0.0	95.0	0.072
	BC_2	910–1025	0.1	22.7	3.4	37.5	32.4	0.1	0.2	0.0	0.5	97.0	0.073
	BCr	1025 +	0.1	21.1	2.4	36.8	33.7	0.1	0.3	0.0	1.7	96.2	0.014
P3	A_{pa}	0–10	0.1	16.3	5.6	35.6	38.5	0.1	0.3	0.3	0.3	97.1	0.085
	Bfl_1	10–45	0.1	15.5	5.0	38.1	38.6	0.1	0.2	0.2	0.9	98.6	0.077
	Bfl_2	45–105	0.1	15.2	4.5	40.7	39.5	0.1	0.1	0.2	0.9	101.3	0.073
	Bfl_3	105–140	0.1	15.6	5.0	39.7	39.8	0.1	0.1	0.1	0.7	101.3	0.068
	Bfl_4	140–255	0.1	15.7	4.7	40.3	40.1	0.1	0.1	0.1	0.8	101.9	0.069
	Bfl_5	255–335	0.1	15.5	4.5	40.7	39.4	0.1	0.1	0.1	0.0	100.5	0.069
	Bfl_6	335–510	0.1	16.1	4.6	38.9	37.9	0.1	0.1	0.1	1.0	98.8	0.068
	Bfl_7	510–600	0.1	16.4	5.2	40.2	38.6	0.1	0.1	0.0	0.5	101.3	0.058
	BC_r	600–640	0.1	22.5	2.0	38.2	32.6	0.0	0.1	0.1	0.0	95.7	0.123
	Weathered rock	-	1.0	7.7	1.6	10.1	46.0	0.0	0.2	8.4	3.3	78.5	0.084

[1] LOI = loss on ignition.

Geochemical mass balance calculations are presented in Table 13. The mass transfer coefficient (τ) values and mass flux (Mj, flux) are negative for SiO_2, MnO, MgO, K_2O, and CaO, showing the effect of the elemental loss rates in relation to parent material (Chadwick et al., 1990; Anderson et al., 2002; Caner et al., 2014; Andrade et al., 2019). For Fe_2O_3, Al_2O_3 and TiO_2 the τ values and mass flux are positive in most soil horizons indicating gains in relation to the parent material. Strain values (ε) are negative for soil profile P3 and some horizons from G1 (Bfl_3, Bfl_4, Bfl_5, Bfl_6, BC_1 and BC_2) and G4 (BCr) indicating loss of volume in relation to the parent material and contraction during weathering (Brimhall and Drietrich, 1987; Caner et al., 2014; Andrade et al., 2019). Positive ε values were observed in the G4 and C3 soil profiles and upper horizons from G1, denoting a net gain in volume. Positive ε values in the horizons from studied soil profiles can be associated to the presence of organic matter that presents less bulk density than mineral matter and the bioturbation process that is responsible for the volume increase (dilation/expansion) (Chadwick et al., 1990; Egli and Fitze, 2000; Caner et al., 2014). Furthermore, the presence of weathered rock fragments and iron nodules can influence the increased density values in the saprolite horizons (BC_r), which generates positive ε values (Andrade et al., 2019). The same trend for τ and mass flux values characterized the process of ferralitization that is marked by intense chemical weathering and loss of base cations (Ca, Mg and K) and Si, and residual accumulation of Fe- and/or Al-(hydro) oxides (Buol and Eswaran, 1999; Schaefer, 2001; Martinez and Souza, 2020).

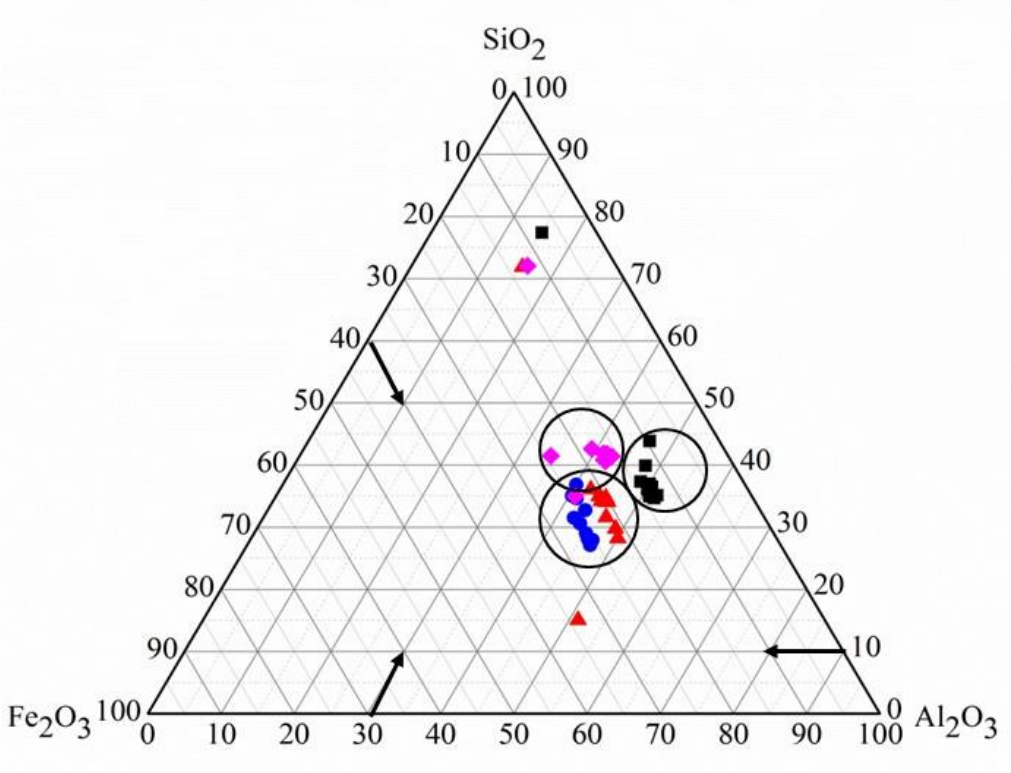

Figure 19. SiO_2, Al_2O_3 and Fe_2O_3 contents (%) in the studied soil profiles (■G1; ▲G4; ●C3 e ♦ P3).

Weathering index results are consistent with the geochemical mass balance calculations and are presented in detail in Appendix Z. For all indices, the high values reflect low weathering rates, and low values (near to zero) reflect strong weathering rates (Table 2). Low values of the Ruxton ratio reflect high desilication and accumulation of Al and Fe (Eswaran and de Coninck, 1971; Yost et al., 2019). Indeed, the R values ranged from 4.5 to 5.1 for the weathered rocks (parent materials), while A horizons ($1.08 < R < 0.7$), Bfl horizons ($1.01 < R < 0.60$) and BC horizons ($0.94 < R < 0.29$) showed much lower levels. The same trend was observed for the other indices (STI and A), with high values in parent material and low values in the A, Bfl and BC horizons of the soil profiles.

The results indicated different weathering zones when we compared the A, Bfl and BC horizons in the soil profiles (Table 14), with three distinct zones in each one. Profiles G1 and C3 presented: 1) a zone with high R values in the BC_r–BC_1 horizons (R = 0.89 at G1 and R = 0.88 at C3); 2) a second zone in Bfl horizons, with lower values than those observed in the BC_r–BC_1 horizons (R = 0.69 at G1 and R = 0.64 at C3); and 3) a third zone with the highest values, in the BA–A_{pa} horizons (R = 0.73 at G1 and R = 0.69 at C3). The G4 and P3 profiles also presented three different weathering zones, but an increase occurred towards surface (G4: 1) a value of R = 0.49 in the BC_r–BC1 horizons; 2) R = 0.73 in the Bfl horizons;

and 3) R = 0.78 in the BA–A_1 horizons; P3: 1) 0.85 in the BCr horizon; 2) R = 0.98 in the Bfl horizons; and 3) R = 1.08 in the A_{pa} horizon). Thus, the ordered sequence of the weathering intensity considering the Ruxton ratio (R) for the Bfl horizon was C3 > G1 > G4 > P3. However, the R ratio not reflect the geomorphology conditions, soil quantified mineralogy and geochemical mass balance calculations (Table 14). The high intensity of weathering should reflect a high relative content of gibbsite in clay fraction mineral suite, which was not observed in the profile C3 (Table 14 and Table 8). Another point is that the weathering indices were calculated from results of bulk chemical characterization, which includes the sand fraction and it may increase the Ruxton ratio (SiO_2/Al_2O_3) (G1 and G4 profiles presented a sand content in their Bfl horizons higher than that in the C3 profile; Appendix S–U). Therefore, the sequence proposed above for the weathering of the studied soils is not valid.

Thus, in order to understand the weathering degree of the studied soil profiles and the quantified mineralogy, a comparison with ferralsols profiles developed from basaltic rock from the Serra Geral formation in Brazil will be carried out. The collected data (mineralogical and chemical) are presented in Table 15 and included location of the profiles, climate classification with mean temperature and precipitation, Ki index and the quantification of the main minerals of the clay fraction (Kt, Gb, Hm and Gt). The methodology for the quantification of minerals in the clay fraction was different and can be seen according to each author.

The most weathered ferralsols developed from the basaltic rock presented in the Table 15 are those with gibbsitic-oxidic mineralogy with Ki values close to 0.4 including 12 ferralsols (6–9, 18, 19, 24, 27, 28 and 36–38) (Table 15) (Ker, 1998; Schaefer et al., 2008). Generally, these soil profiles are typical of the highland planation surfaces, where long-term weathering has resulted in intensive leaching and located under a tropical climate (Aw) (except one profile from Guidin et al., 2006). The quantified Gb content values of these ferralsols varied from 27.7% to 89.4%, which is the dominant mineral of the clay fraction. Therefore, according to our mineralogy results our study profiles do not fit like the most weathered ferralsols (gibbsic). Furthermore, the other 27 ferralsols presented in the Table 15, showed the kaolinite as the predominant mineral of the clay fraction. These soils still had varied contents of Gb, hematite and goethite. The climate under these 27 ferralols are located varied from tropical (Aw) to subtropical climate (Cfa-Cwa-Cfb). Thus, the most ferralsols derived from the basaltic rock are kaolinitic with variable contents of Gb, Hm and Gt. The

Paraná Magmatic province shows a gradient from the South to North in the gibbsite content increasing from the temperate (Cfb, South) to tropical climate (Aw, North).

The studied ferralsols are located in a climate sequence from the CFb to CFa, and the quantitative Kt and Gb content (ATD/TG) presented similar values with the most representative ferralsols derived from basaltic rock of the Serra Geral Fomation around the Paraná Basin (Tables 8 and 15). Kaolinite is the predominant mineral of the clay fraction and in general presented Gb contents < 25%. However, a difference was observed in the Gb contents in the studied ferralsols. Thus, a possible weathering intensity sequence according to our quantified clay mineralogy data would be G4 > G1 > P3 > C3.

In addition to the two analysed weathering intensity sequences, a third one will be considered using the data of SiO_2 and Al_2O_3 from the sulphuric extract calculating the Ki indice (Resende and Santana, 1988) (Table 14). According to Ki results the new weathering sequence is G1> G4 e C3> P3, which agrees with what was observed in the ternary graph and crystallographic parameters of the iron oxides (isomorphic substitution) (Figure 19; Table 11).

Table 13. Geochemical mass balance parameters calculations.

Profile	Hz.	K_2O		Fe_2O_3		TiO_2		Al_2O_3		SiO_2		MnO		CaO		MgO		$\varepsilon i,w$[3]
		τ[1]	M j, flux[2]	τ	M j, flux	τ	M j, flux	τ	M j, flux	τ	M j, flux	τ	M j, flux	τ	M j, flux	τ	M j, flux	
G1	A_{pa}	-0.97	-1.73	0.06	0.18	0.06	0.04	0.82	4.75	-0.73	-21.65	-0.55	-0.03	-0.91	-0.88	-0.82	-0.23	0.24
	AB	-0.98	-3.28	0.08	0.44	0.08	0.10	0.95	10.51	-0.72	-40.77	-0.59	-0.06	-0.97	-1.77	-0.46	-0.24	0.2
	BA	-0.98	-1.76	0.09	0.25	0.09	0.05	0.96	5.66	-0.73	-22.15	-0.61	-0.04	-0.98	-0.96	-0.09	-0.02	0.22
	Bfl_1	-0.98	-1.78	0.04	0.13	0.04	0.03	0.88	5.24	-0.75	-22.77	-0.64	-0.04	-0.99	-0.98	-0.78	-0.22	0.21
	Bfl_2	-0.98	-3.25	-0.02	-0.11	-0.02	-0.02	0.86	9.31	-0.75	-41.75	-0.66	-0.07	-0.99	-1.78	-0.65	-0.34	0.00
	Bfl_3	-0.98	-3.37	-0.05	-0.3	-0.05	-0.06	0.82	9.30	-0.74	-42.85	-0.64	-0.07	-0.99	-1.85	-0.36	-0.19	-0.04
	Bfl_4	-0.98	-4.00	0.06	0.40	0.06	0.09	1.00	13.44	-0.74	-50.63	-0.57	-0.08	-0.99	-2.20	-0.41	-0.27	-0.01
	Bfl_5	-0.98	-5.99	0.01	0.08	0.01	0.02	1.01	20.23	-0.73	-75.28	-0.61	-0.12	-0.99	-3.29	-0.81	-0.77	-0.04
	Bfl_6	-0.97	-3.82	-0.01	-0.04	-0.01	-0.01	0.89	11.43	-0.73	-47.93	-0.60	-0.08	-0.99	-2.12	0.03	0.02	-0.07
	BC_1	-0.97	-5.38	-0.17	-1.55	-0.17	-0.34	0.61	11.12	-0.74	-68.28	-0.63	-0.11	-0.99	-2.98	-0.65	-0.56	-0.14
	BC_2	-0.98	-2.66	-0.51	-2.24	-0.51	-0.48	0.18	1.56	-0.78	-35.52	-0.77	-0.07	-0.99	-1.46	-0.9	-0.38	-0.32
	WR*	0	0	0	0	0	0	0	0	0	0	0	0	0	0	0	0	0
G4	A_1	-0.96	-0.51	-0.03	-0.07	0.77	0.64	0.63	1.98	-0.71	-10.51	-0.58	-0.03	-1.00	-2.29	-0.8	-0.51	1.24
	A_2	-0.97	-0.85	-0.05	-0.21	0.65	0.92	0.70	3.67	-0.71	-17.71	-0.58	-0.06	-1.00	-3.82	-0.68	-0.73	0.61
	A_3	-0.97	-0.70	-0.02	-0.08	0.68	0.78	0.76	3.27	-0.71	-14.51	-0.58	-0.04	-1.00	-3.13	-0.47	-0.41	0.64
	AB	-0.97	-1.19	-0.01	-0.06	0.70	1.36	0.86	6.28	-0.71	-24.37	-0.56	-0.07	-1.00	-5.33	-0.90	-1.35	0.54
	BA	-0.96	-0.56	-0.03	-0.07	0.60	0.55	0.83	2.84	-0.70	-11.41	-0.57	-0.04	-1.00	-2.50	-0.56	-0.39	0.65
	Bfl_1	-0.96	-0.67	-0.02	-0.06	0.70	0.77	0.87	3.58	-0.70	-13.56	-0.59	-0.04	-1.00	-3.01	-0.86	-0.72	0.37
	Bfl_2	-0.96	-1.09	-0.04	-0.23	0.60	1.08	0.84	5.70	-0.71	-22.62	-0.59	-0.07	-1.00	-4.91	-0.86	-1.18	0.25
	Bfl_3	-0.96	-3.17	0.06	1.02	0.68	3.56	0.94	18.45	-0.72	-66.81	-0.52	-0.18	-1.00	-14.27	-1.00	-3.99	0.30
	BC_1	-0.96	-1.79	0.07	0.68	0.51	1.51	1.09	12.1	-0.73	-38.34	-0.56	-0.11	-1.00	-8.09	-0.74	-1.68	0.27
	BC_2	-0.96	-1.11	0.06	0.34	0.40	0.74	1.06	7.32	-0.75	-24.49	-0.59	-0.07	-1.00	-5.01	-0.72	-1.00	0.23
	BCr	-1.00	-1.6	0.46	3.74	0.25	0.65	0.88	8.40	-0.88	-40.00	-0.48	-0.08	-1.00	-6.98	-0.87	-1.70	-0.12
	WR*	0	0	0	0	0	0	0	0	0	0	0	0	0	0	0	0	0

Table 13. Geochemical mass balance parameters calculations (continuation).

Profile	Hz.	K_2O		Fe_2O_3		TiO_2		Al_2O_3		SiO_2		MnO		CaO		MgO		$\varepsilon i,w$[3]
		τ[1]	M j, flux[2]	τ	M j, flux	τ	M j, flux	τ	M j, flux	τ	M j, flux	τ	M j, flux	τ	M j, flux	τ	M j, flux	
C3	A_{pa}	-0.97	-0.49	0.14	0.49	0.68	0.40	0.24	1.22	-0.74	-13.42	-0.38	-0.03	-0.98	-2.71	-1.00	-0.68	0.33
	AB	-0.97	-1.05	0.21	1.50	0.70	0.87	0.36	3.99	-0.73	-28.00	-0.46	-0.08	-0.99	-5.79	-0.98	-1.41	0.25
	BA	-0.97	-1.50	0.19	1.95	0.62	1.10	0.39	6.14	-0.75	-40.98	-0.49	-0.12	-0.99	-8.28	-0.99	-2.04	0.32
	Bfl_1	-0.97	-3.53	0.14	3.42	0.61	2.56	0.35	12.82	-0.77	-98.88	-0.52	-0.29	-0.99	-19.5	-0.83	-4.00	0.35
	Bfl_2	-0.98	-2.50	0.17	2.91	0.63	1.84	0.40	10.27	-0.77	-70.21	-0.52	-0.20	-1.00	-13.79	-0.83	-2.84	0.25
	Bfl_3	-0.97	-10.42	0.19	13.62	0.53	6.51	0.46	49.48	-0.75	-286.61	-0.48	-0.79	-1.00	-57.68	-0.69	-9.83	0.22
	Bfl_4	-0.97	-2.96	0.15	3.08	0.19	0.66	0.39	11.94	-0.70	-75.87	-0.54	-0.25	-1.00	-16.37	-0.79	-3.20	0.28
	BC_1	-0.97	-1.41	0.21	2.03	0.14	0.23	0.37	5.43	-0.67	-34.84	-0.51	-0.11	-1.00	-7.84	-1.00	-1.94	0.16
	BC_2	-0.98	-3.37	0.24	5.56	0.09	0.35	0.36	12.37	-0.67	-81.46	-0.50	-0.26	-1.00	-18.52	-0.86	-3.94	0.13
	BCr	-0.98	-0.36	0.1	0.25	-0.28	-0.12	0.27	1.01	-0.67	-8.77	-0.29	-0.02	-1.00	-1.99	-0.56	-0.28	0.84
	WR*	0	0	0	0	0	0	0	0	0	0	0	0	0	0	0	0	0
P3	A_{pa}	-0.95	-0.32	-0.28	-0.70	0.16	0.09	0.20	0.66	-0.71	-10.75	-0.58	-0.04	-0.99	-2.70	-0.97	-1.06	-0.60
	Bfl_1	-0.97	-1.03	-0.18	-1.48	0.25	0.43	0.53	5.56	-0.66	-31.58	-0.63	-0.14	-0.99	-8.65	-0.89	-3.07	-0.56
	Bfl_2	-0.97	-1.39	-0.12	-1.33	0.22	0.49	0.79	11.11	-0.62	-39.65	-0.73	-0.22	-0.99	-11.55	-0.88	-4.10	-0.44
	Bfl_3	-0.96	-0.64	-0.15	-0.76	0.28	0.30	0.64	4.24	-0.64	-19.11	-0.75	-0.11	-0.99	-5.41	-0.91	-1.97	-0.30
	Bfl_4	-0.96	-2.44	-0.17	-3.30	0.18	0.72	0.62	15.55	-0.64	-73.49	-0.76	-0.41	-1.00	-20.66	-0.9	-7.46	-0.40
	Bfl_5	-0.97	-1.74	-0.21	-2.87	0.08	0.24	0.57	10.19	-0.66	-53.45	-0.76	-0.29	-1.00	-14.57	-1.00	-5.81	-0.41
	Bfl_6	-0.97	-3.77	-0.19	-5.42	0.10	0.64	0.50	19.19	-0.68	-118.02	-0.78	-0.64	-1.00	-31.59	-0.88	-11.08	-0.40
	Bfl_7	-0.97	-4.01	-0.21	-6.61	0.19	1.23	0.47	19.13	-0.69	-127.69	-0.77	-0.67	-1.00	-33.66	-0.94	-12.61	-0.65
	BCr	-0.98	-0.57	0.53	2.30	-0.35	-0.32	0.82	4.69	-0.60	-15.55	-0.18	-0.02	-1.00	-4.72	-0.93	-1.76	-0.54
	WR*	0	0	0	0	0	0	0	0	0	0	0	0	0	0	0	0	0

*WR = weathered rock; [1]τ – gain/losses in the elemental fraction; [2]Mj,flux – mass elemental fluxes, kg m^{-2}; [3]$\varepsilon i,w$ – strain of the soil horizons in relation to parent material.

Table 14. Weathering zones and mineralogical composition of the representative soil profiles.

Profile	Zones[1]	Weathering indices				Mineralogical composition[6]			
		R[2]	STI[3]	A[4]	Ki[5]	Kt[7]	Gb[8]	Hm[9]	Gt[10]
						%			
G1	1	0.885	43.87	0.475	-	62	10	9	6
	2	0.693	38.942	0.412	0.8	47	21	25	1
	3	0.727	39.733	0.423	-	41	23	27	2
G4	1	0.487	30.293	0.323	-	44	26	15	10
	2	0.73	38.337	0.423	1.2	46	21	11	12
	3	0.782	39.472	0.438	-	42	17	17	6
C3	1	0.877	44.887	0.467	-	61	5	15	8
	2	0.635	37.018	0.39	1.2	53	9	19	2
	3	0.693	38.643	0.41	-	57	3	19	nd
P3	1	0.85	44.96	0.46	-	nd	nd	nd	nd
	2	0.981	46.774	0.496	1.8	51	16	15	10
	3	1.08	48.06	0.52	-	38	27	7	11

[1]Zones = according to the text; [2]Ruxton ratio (Ruxton, 1968); [3]Silica and Titanium index (Jayawardena and Izawa, 1994); [4]A index proposed by Kronberg and Nesbitt (1981); [5]Ki index (Resende and Santana, 1988); [6]mineralogical composition (average values were presented); [7]Kt = kaolinite; [8]Gb = gibbsite; [9]Hm = hematite and [10]Gt = goethite; nd = not determined.

Table 15. Ferralsols developed from basalt and rhyo-dacite, mineralogical and geochemical properties.

References	Identification	Parent Material	Location	Landscape position	Altitude (m.a.s.l.)	Mean T[6] (°C)	Mean PPT[7] (mm)	Climate	Kt	Gb	Hm	Gt	Ki
									%				
Curi and Franzmeier (1984)[1]	1	Basalt	Itumbiara-Go	Summit	-	25	1123	Aw	22	22	-	-	-
Fontes and Weeds (1991; 1996)[1,2]	2	Basalt	Triângulo Mineiro-MG	-	-	20.0-24.0	1300-1700	Aw	49	49	21.3	5.9	-
	3	Basalt							62.7	34	17.7	5.8	-
	4	Basalt							55.6	41.2	15.4	5.7	-
	5	Basalt							69.9	23.1	18.3	5.4	-
Alleoni and Camargo (1995)[1]	6	Basalt	Ribeirão Preto-SP			22.7	1384	Aw		50			
	7		Guaíra-SP			-24.1	1300	Aw		64			
Ker (1998)	8	Basalt	Cravinhos-SP	-	-	21	1340	Cwa	-	-	-	-	0.4
	9	Basalt	Ribeirão Preto-SP	-	-	22.7	1384	Aw	-	-	-	-	0.5
	10	Basalt	Dourados-MS	-	-	23.4	1419	Am	-	-	-	-	1.9
	11	Basalt	Medianeira-PR	-	-	21.9	2003	Cfa	-	-	-	-	1.8
	12	Basalt	Londrina-PR	-	-	21.1	1723	Cfa	-	-	-	-	1.5
	13	Basalt	Cascavel-PR	-	-	22	2000	Cfa	-	-	-	-	0.6
Melo et al. (2001)[1]	14	Basalt	Capinópolis-MG		-	23.5	1434	Aw	57.4				-
Gomes et al. (2004)[3]	15	Basalt	Triângulo Mineiro-MG	Summit - Shoulder	510-525	20.0-24.0	1300-1700	Aw	34.1	18.5	30.6	0	0.9
	16	Basalt		Summit-Shoulder	540-560				14.2	15.4	30.2	0	1.1
Fontes e Carvalho Jr. (2005)[1,3]	17	Basalt	Minas Gerais	-	-	23	1200	Aw	35.1	26.2	10.1	4.8	-
	18	Basalt*		-	-	21	1370	Cwa	29.8	37.6	13.3	2.5	-

Table 15.Ferralsols developed from basalt and rhyo-dacite, mineralogical and geochemical properties (continuation).

References	Identification	Parent Material	Location	Landscape position	Altitude (m.a.s.l.)	Mean T[6] (°C)	Mean PPT[7] (mm)	Climate	Kt	Gb	Hm	Gt	Ki
									%				
Guidin et al. (2006)[1,4]	19	Basalt*	Cascavel-PR	shoulder	781	22	2000	Cfa	29.4	32.2	30.9		0.6
	20	Basalt							36.5	34.1	26.8		0.6
	21	Rhyo-dacite	Guarapuava-PR	shoulder	1068	18	2000	Cfb	38	31.7	9.5	14.2	1.6
	22	Rhyo-dacite							46.4	30.1	11.6	8.1	1
Calegari (2008)	23	Rhyo-dacite	Guarapuava-PR	Summit	1079	18	2000	Cfb	-	-	-	-	0.7
Schaefer et al. (2008)	24	Basalt	-	-	-	-	-	-	27.3	27.7	28.9	10.7	0.7
Alves et al. (2008)[1,2,6]	25	Basalt	Guaíra-SP	-	-	-24.1	1300	Aw	50.7/69.4/78.0	33.4/17.1/16.9	-	-	-
	26	Basalt	Ribeirão Preto-SP	-	-	22.7	1384	Aw	50.6/67.1/76.2	41.6/21.3/20.0	-	-	-
	27	Basalt*	Guaíra-SP	-	-	-24.1	1300	Aw	30.4/55.9/64.9	41.6/26.5/27.0	-	-	-
	28	Basalt*	Miguelópolis-SP	-	-	22	-	Aw	15.5/39.3/48.0	89.4/45.8/46.4	-	-	-
Boitt (2014)	29	Basalt	Vacaria-RS	-	1000	15.5	1897	Cfb	-	-	-	-	2
	30	Basalt	Campos Novos-SC	-	948	18	1886	Cfb	-	-	-	-	1.6
	31	Basalt	Pinhalzinho-SC	-	535	20.6		Cfa	-	-	-	-	1.5
	32	Basalt	Londrina-PR	-	610	21.1	1723	Cfa	-	-	-	-	1.6
	33	Basalt*	Ribeirão Preto-SP	-	546	19.3	1384	Aw	-	-	-	-	0.6
	34	Basalt*	Uberlândia-MG	-	768	24	1342	Aw	-	-	-	-	0.4
Camêlo et al. (2017)[3]	34	Basalt	Uberlândia-MG	-	725	24	1342	Aw	43.3	6.7	13.4	2.3	1.5
	36	Basalt*	Uberlândia-MG	-	888	24	1342	Aw	17.5	33.8	9.3	1.6	0.5
	37	Basalt*	Uberaba-MG	-	696	22.9	1681	Aw	20.9	27.3	9.8	1.2	0.6
	38	Basalt*	Uberaba-MG	-	849	22.9	1681	Aw	13.9	36.1	11.7	2.3	0.4
Testoni et al. (2017)[5]	39	Basalt	Cascavel-PR	-	-	22	2000	Cfa	31	26	-	-	-

[1] mineralogial quantification using ATD/TG; [2] mineralogial quantification using alocation (Resende et al., 1987); [3] mineralogial quantification according to Melo et al., (2001);[4] mineralogical quantification using the software highScore; [5] mineralogical quantification using Rietveld and software SIROQUANT™.*high weathered soil. [6]T=temperature; [7]PPT = precipitation.

3.3. Evidence of short-term pedogenetic processes in the studied ferralsols

3.3.1. Paleoenvironmental reconstruction: short-term vegetation and carbon changes

3.3.1.1. ^{14}C dating

Results of the ^{14}C datings of the humin fraction of the representative soils (G4, C3 and P3) are presented in Table 16. The minimum soil age indicated by the humin fraction showed a typical increase with soil depth until 500 cm in the G4, C3 and P3 profiles. The inversion of ^{14}C values for the two samples in the deepest part of the C3 soil profile (below 500 cm depth) suggests the relatively larger contribution from younger carbon introduced into the deepest part of the soil, which could be explained by bioturbation and/or percolation. The humin ^{14}C values ranged from ~2120 cal yrs BP to ~12,290 cal yrs BP, from ~6341 cal yrs BP to ~16,619 cal yrs BP, and from ~5515 cal yrs BP to ~14,422 cal yrs BP, in the G4, C3 and P3 soil profiles, respectively. The ^{14}C values showed the possibility of recovering proxies that can indicate the vegetation in the study area for at least ~12,290 cal yrs BP in Guarapuava (G4), ~14,422 cal yrs BP in Palotina (P3), and ~16,619 cal yrs BP in Cascavel (C3).

Table 16. ^{14}C dating of the representative studied soil profiles.

Local	Profile	Horizon	Depth (cm)	2 sigma calibrated age BP	Medium age calibrated BP
Guarapuava	G4	A_2	50	2106±29	2120
		BA	120	7412±35	7429
		Bfl_3	240	12,264±52	12,290
Cascavel	C3	BA	100	6323±37	6341
		Bfl_3	500	16,590±59	16,619
		Bfl_3	700	12,779±52	12,805
		BC_r	1020	15,188±38	15,214
Palotina	P3	Bfl_1	60	5500±31	5515
		Bfl_3	200	11,478±29	11,492
		Bfl_5	400	14,405±35	14,422

3.3.1.2. Total C and N and C/N ratio

Total C content in upper soil samples (first 50 cm) are shown in Table 17. Guarapuava soil profiles showed a total C content (average values) in the upper soil samples of 3.0%, 3.4%, 3.2% and 5.0%, in G1, G2, G3 and G4, respectively. In addition, Cascavel soils presented average values of total C content of 3.7% in C1, 2.3% in C2 and 2.1% in C3

profile. The Palotina upper soil samples showed (average values) a total C content in P1 (1.7%), P2 (1.0%) and P3 (1.3%) lower than those in the upper soil samples from Guarapuava and Cascavel profiles. Comparing the total C content in upper soil samples with current vegetation/land uses, little difference was observed between the soils under forest vegetation and agriculture systems. The soil profiles under forest vegetation (G2, G3, G4, and P1) showed higher C values than the soils under agriculture system (G1, C3, P2 and P3). The exception was the profiles C1 and C2 from Cascavel that presented higher C values under agricultural (C1) than under forest vegetation (C2). This fact may be related to the high altitude location of the soil profile C1 (790 m a.s.l.) in relation to profile C2 (674 m a.s.l.) favouring the C accumulation. With this, a positive correlation of total C content with altitude (m a.s.l.) was observed in the soil profiles (r = 0.79), showing that the difference in C accumulation is primarily related to the altitude (m a.s.l.) and consequently with climate and secondarily with land use.

Table 17. Total C content (%) in the first 50 cm of depth in the studied soil profiles.

Depth	% C									
	Guarapuava				Cascavel			Palotina		
cm	G1	G2	G3	G4	C1	C2	C3	P1	P2	P3
0–10	3.8	5.2	5.2	8.6	4.3	3.2	2.9	2.5	1.7	2.2
10–20	3.7	3.8	3.8	4.8	3.8	2.5	2.2	2.4	1.5	1.7
20–30	2.8	3.2	2.7	4.0	3.5	2.2	2.0	1.6	0.7	1.1
30–40	2.4	2.5	2.4	3.9	3.1	1.9	1.8	1.1	0.5	0.9
40–50	2.1	2.5	2.0	3.5	–	1.6	1.6	0.9	0.5	0.7
Average	3.0	3.4	3.2	5.0	3.7	2.3	2.1	1.7	1.0	1.3

The values of total C content (%) with depth are shown in Figure 20. In general, C (%) exponentially decreases with depth until the saprolite zone for all profiles ($r^2 > 0.92$), which is a common tendency observed in the soils of temperate and tropical regions (Parton et al., 1987). A steep linear decrease in C content occurred in the upper 200 cm in all soil profiles, with highest C values were observed in Guarapuava, followed by Cascavel and Palotina. The cold subtropical climate in the Guarapuava region favours the accumulation of carbon and the development of thick humic epipedons by melanization (Calegari et al., 2013), while the warmer subtropical climate observed in the Cascavel and mainly Palotina experimental areas promotes the more intense decomposition and loss of C in the soils (Six et al., 2000). From 200–380 cm of deep the total C content was similar in the Guarapuava and Cascavel profiles and lower in Palotina profiles (Figure 20a). Below 380 cm, the highest C

values (%) were observed in the Cascavel profiles, followed by the Guarapuava and Palotina profiles. This fact suggests that the environment conditions in Guarapuava, Cascavel and Palotina probably differed in the past. Total nitrogen content (Nt) showed a similar trend and positive correlation with Ct (for n = 551 samples: r^2 = 0.79) in the studied soil profiles, reflecting the organic matter content.

The C/N ratio values with depth are shown in Figure 21. In the Guarapuava soil profiles (G1–G4) presented a gradual increase in C/N ratio from the soil surface to 110 cm, with average values from 14.9 to 23.1. A decrease in the C/N ratio was observed below 110 cm in the G1–G4 profiles with values ranging from 21.3 to 6.3. At Cascavel sites, the gradual increase of the C/N ratio in the C1 profile was similar to C/N trend observed in the Guarapuava soils, showing an increase from the soil surface down to 110 cm, with average values from 13.9 to 20.0. In the C2 and C3 soil profiles, the gradual increase continued deeper than that observed for the G1–G4 and C1 profiles. The C2 site presented an increase in the C/N ratio from the soil surface down to 240 cm (C/N ratio from 13.3 to 18.3). The C3 soil profile presented a gradual increase in the C/N ratio from the soil surface down to 410 cm (C/N values from 12.1 to 20.3). Below these depths, the C/N values decreased from 19.0 to 6.3. The Palotina profiles presented an initial decrease in the C/N ratio over the first 80 cm in the P1 profile (C/N ratio from 9.6–7.7), 0–40 cm in P2 (C/N ratio from 9.2–7.5) and 0–60 cm in P3 (C/N ratio from 9.4–8.6). Below these soil depths, an increase was observed until 140 cm (from 7.7–9.0), 110 cm (from 7.5–10.1) and 150 cm (from 8.6–10.6) in P1, P2 and P3, respectively, and then a decrease until the saprolite zone, with average C/N values from 10.8 to 5.3. In general, the average C/N ratio (Guarapuava = 15.2; Cascavel = 13.8; Palotina = 7.8) showed that the organic matter of Palotina soils was more decomposed than that observed in the Cascavel (C1–C3) and Guarapuava soil profiles (G1–G4) (Dick et al., 2008; Chiapini et al., 2018). In addition, the decomposed organic matter in the Palotina profiles could reflect the current and past environment conditions, warmer and drier in relation to the sites at Guarapuava and Cascavel.

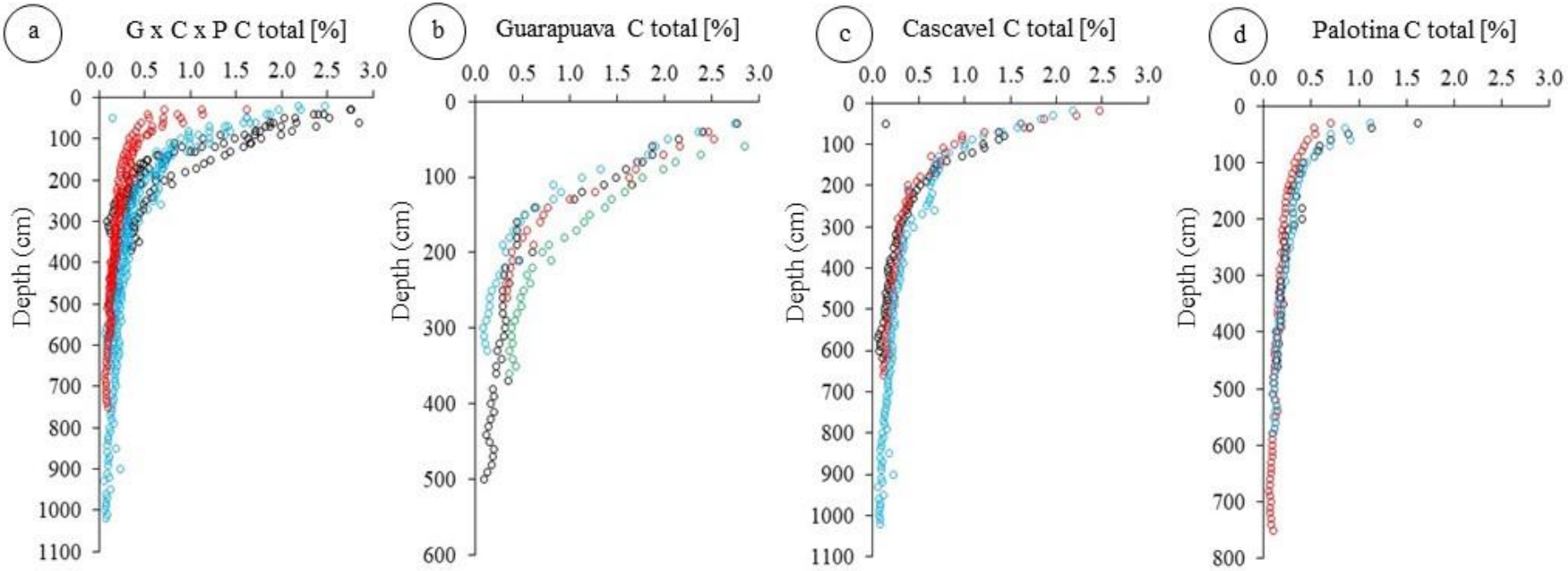

Figure 20. Total C content with depth in studied soil profiles. a) Total C content (%) at the Guarapuava, Cascavel and Palotina study sites: Black empty circles: Guarapuava profiles (G1-G4); Blue empty circles: Cascavel profiles (C1-C3); Red empty circles: Palotina profiles (P1-P3); b) Total C content (%) in the Guarapuava profiles; Black empty circles: G1; Red empty circles: G2; Blue empty circles: G3; Green empty circles: G4; c) Total C content (%) in the Cascavel profiles; Black empty circles: C1; Red empty circles: C2; Blue empty circles: C3; d) Total C content (%) in the Palotina profiles; Black empty circles: P1; Red empty circles: P2; Blue empty circles: P3.

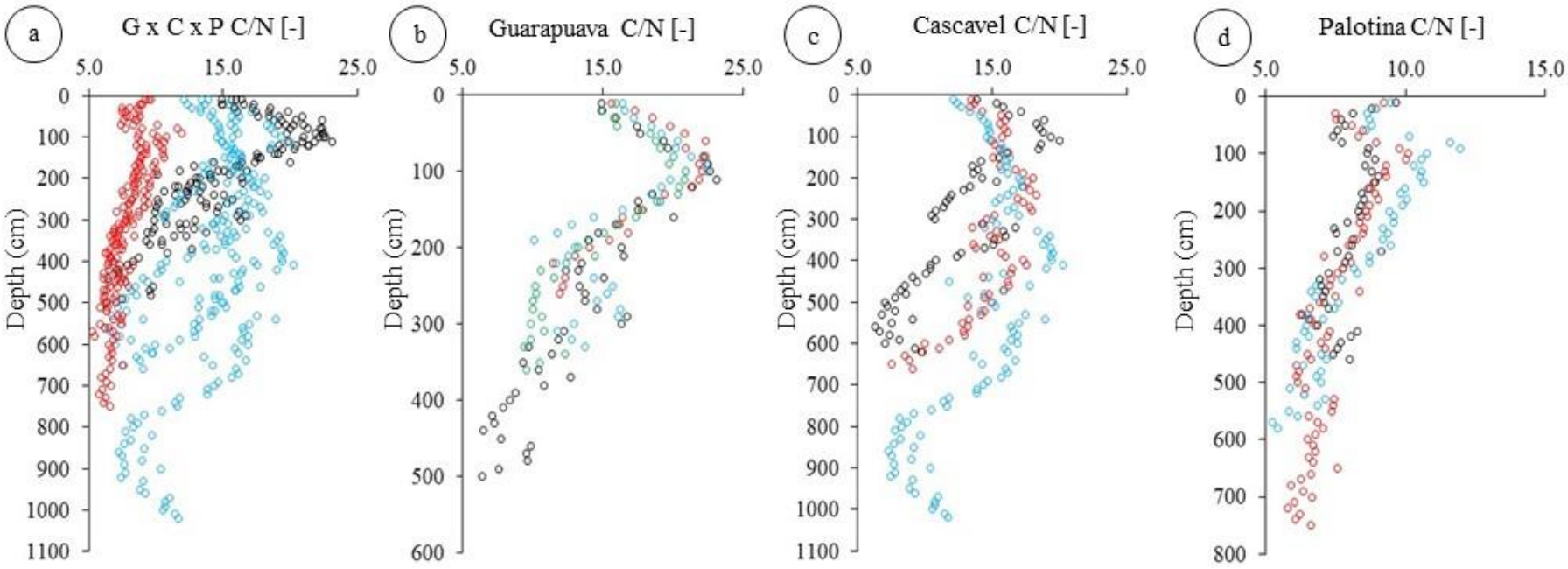

Figure 21. C/N ratio with depth in studied soil profiles. a) C/N ratio at Guarapuava, Cascavel and Palotina study sites: Black empty circles: Guarapuava profiles (G1-G4); Blue empty circles: Cascavel profiles (C1-C3); Red empty circles: Palotina profiles (P1-P3); b) C/N ratio in the Guarapuava profiles; Black empty circles: G1; Red empty circles: G2; Blue empty circles: G3; Green empty circles: G4; c) C/N ratio in the Cascavel profiles; Black empty circles: C1; Red empty circles: C2; Blue empty circles: C3; d) C/N ratio in the Palotina profiles; Black empty circles: P1; Red empty circles: P2; Blue empty circles: P3.

3.3.1.3. δ ^{13}C isotopic composition

Isotopic variations of $\delta^{13}C$ greater than 4‰ are associated with changes in vegetation (Desjardins et al., 1996; Saia et al., 2007; Souza, 2019). Thus, the isotopic variations $\delta^{13}C$ less than 4‰ are associated with isotopic fractionation that occurs naturally during the decomposition of organic matter and variations in the carbon isotopic composition of atmospheric CO_2 (Boutton, 1996). With this, plants with C_3 photosynthesis cycle (trees, shrubs and some grasses) show $\delta^{13}C$ values that vary from −22‰ to −32‰, while values of C_4 plant species (predominantly grasses) vary between −9‰ and −17‰ (Boutton et al., 1998). Therefore, depth records of $\delta^{13}C$ can be used to provide information about the vegetation that contributed to the soil profiles (Caner et al., 2003; Chiapini et al., 2018).

The records of $\delta^{13}C$ isotopic composition of the studied profiles are shown in Figure 22. The $\delta^{13}C$ isotopic values observed in the upper horizons reflect a native forest or shrub vegetation, or a mixture of soybean/mayze agricultural system. In the studied areas, the native forest/shrub vegetation corresponds to *Araucaria* forest at Guarapuava and Semideciduous forest with *Araucaria* trees at Cascavel and Semideciduous forest at Palotina (Behling, 2002; Dümig et al., 2008; Bertoldo et al., 2014). In soil profiles with agricultural system, the $\delta^{13}C$ isotopic values at the soil surface represent the mixture of soybean/mayze (Guareschi et al., 2014).

Apart from the soil surface (0 to ~50cm), the $\delta^{13}C$ isotopic composition in the soil profiles varied between 14.7 ‰ and -23.7 ‰. Periods with different contributions from C_4 plants and C_3 plants (*Periods I–IV*) were evident at the three studied areas (Table 18). In particular, the *Period IV* is characterized by the change to current vegetation.

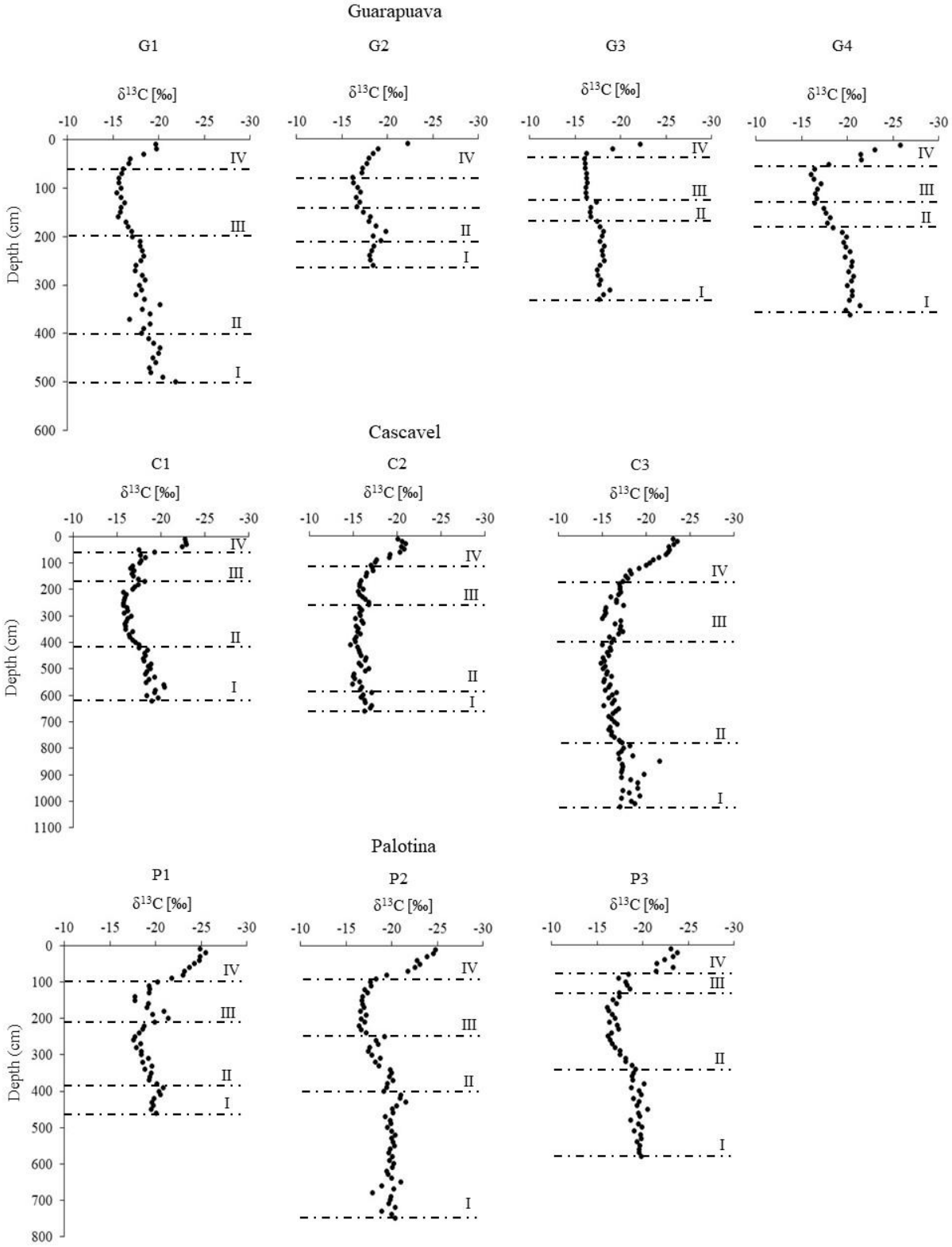

Figure 22. $\delta^{13}C$ isotopic composition with depth for the ten soil profiles indicating the different Periods with contribution from C4 plants. The periods are separated by dashed lines (Period I: I; Period II: II; Period III: III and Period IV: IV). The Period IV is characterized by the change to the current vegetation.

3.3.1.3.1. Guarapuava

Four periods with different contributions from C_4 and C_3 plants were evident and shown above (Figure 22 and Table 18):

Period I: characterized by a mixed vegetation (C_3 and C_4 plants), but with predominance of C_3 plants in the deep horizons during the Late Pleistocene indicating a more humid climate and probably the occurrence of *Araucaria* forest (between ~12,290 cal yrs BP; Table 16);

Period II: the values of $\delta^{13}C$ isotopic composition indicated a mixed vegetation of C_4 and C_3 plants with a predominance of C_4, but less than the *Period III*;

Period III: period with the largest contribution from C_4 plants that occurred during the Mid–Holocene with a drier climate characterizing the occurrence of a more open vegetation, dominated by C_4 grasses (~7429 cal yrs BP; Table 16);

Period IV: mixed vegetation (C_3 and C_4 plants), with predominance of C_3 plants during the Late Holocene indicating a more humid and colder climate than the previous period, showing the environmental change to the current vegetation (~2120 cal yrs BP; Table 16).

The $\delta^{13}C$ depth records from the Guarapuava ferralsols indicate a progressive change in vegetation since the Late Pleistocene. According to the results, at the end of the Pleistocene in all studied areas at Guarapuava location (G1–G4), the vegetation presented a predominance of C_3 plants. These results corroborate the studies of Bertoldo et al. (2014), Pagotto et al. (2020) and Wilson et al. (2021), indicating the presence of forests during this same period in agreement with humid conditions in the Late Pleistocene. In addition, Pinaya et al. (2019) observed the establishment of migration areas of montane forest, connecting different ecosystems on a continental scale, also found under the condition of high humidity in the south and southeast regions of Brazil between 18,000 and 14,000 cal yrs BP. However, on a regional scale, Behling (2002) and Rasbold et al. (2016) reported the predominance of grassland with the rare occurrence of Araucaria trees ~ 14,000 cal yrs BP, characterizing a drier and colder period than the Early Holocene in the region. With this, the presence of grassland during the Late Pleistocene at the Guarapuava site is not supported by our $\delta^{13}C$ results. In addition, an open vegetation, such as grassland, characterizes the next observed period (*Períod II*) until Mid–Holocene (*Period III*: ~7429 cal yrs BP; Table 16; Figure 22). According to Behling (1998; 2002), Calegari (2008), Bertoldo et al. (2014), Calegari et al.

(2017), Pagotto et al. (2020) and Wilson et al. (2021) a drier climate was registered in the Mid–Holocene with a predominance of C_4 plants, such as grassland in Southern Brazil. The modern predominant climatic conditions were stablished ~4000-3000 cal yrs BP in Paraná at the end of the Mid–Holocene (Pessenda et al., 1996; Behling, 1997; Stevaux, 2000; Calegari, 2008; Parolin et al., 2008; Beroldo et al., 2014; Luz et al., 2019; Calegari et al., 2017). The current expansion of *Araucaria* forest in Guarapuava soils (*Period IV*; Figure 22: G1–G4) over areas previously dominated by C_4 plants, such as grasslands (*Period III*; Figure 22: G1–G4) dated from the Late Holocene, ~2120 cal yrs BP (Table 16), associated with a more humid and colder climate in the region.

Table 18. $\delta^{13}C$ isotopic composition periods of the ten studied soil profiles.

Profile	$\delta^{13}C$ isotopic composition											
	Period I			*Period II*			*Period III*			*Period IV*		
	Min	Max	Depth (cm)	Min	Max	Depth (cm)	Min	Max	Depth (cm)	Min	Max	Depth (cm)
G1	-21.9	-18.9	500–410	-20.1	-16.3	400–210	-17.0	-15.4	200–60	-19.7	-16.0	50–0
G2	-18.5	-18.1	260–220	-19.7	-17.3	150–210	-17.0	-16.1	140–80	-22.2	-16.2	70–0
G3	-18.8	-17.4	330–170	-16.8	-16.6	160–140	-16.3	-16.0	120–30	-22.1	-16.2	20–0
G4	-21.4	-19.5	360–190	-18.5	-17.4	180–140	-17.1	-16.0	130–60	-25.8	-16.4	50–0
C1	-20.4	-18.1	610–420	-16.8	-15.7	410–200	-18.2	-16.5	190–60	-22.8	-17.5	50–0
C2	-17.1	-15.9	660–590	-16.7	-14.7	580–270	-17.3	-15.6	260–110	-20.9	-16.9	100–0
C3	-21.5	-16.9	1020–770	-16.8	-14.8	760–380	-18.3	-14.8	370–180	-23.5	-16.8	170–0
P1	-20.8	-19.4	460–380	-19.6	-18.2	370–220	-21.3	-17.7	210–100	-25.5	-20.1	90–0
P2	-21.5	-17.9	750–410	-20.1	-17.4	400–250	-18.2	-16.4	240–90	-24.7	-17.6	80–0
P3	-20.5	-18.7	580–330	-18.1	-16.1	320–130	-18.6	-17.3	120–80	-23.7	-18.4	70–0

3.3.1.3.2. Cascavel

The three profiles from Cascavel also showed four periods, though different compared to those of the Guarapuava profiles (Figure 22 and Table 18):

Period I: characterized by a mixed vegetation (C_3 and C_4 plants) with a predominance of C_4 plants during the Late Pleistocene (between ~15,214 cal yrs BP and ~12,805 cal yrs BP) in profiles C2 and C3, whereas profile C1 the mixed vegetation showed a predominance of C_3 plants;

Period II: showed the largest contribution from C_4 plants during the Early Holocene–Mid–Holocene probably related to a drier climate than *Period I* (~12,805 cal yrs BP to ~6341 cal yrs BP; Table 16);

Period III: the values of $\delta^{13}C$ isotopic composition indicated a mixed vegetation of C_4 and C_3 plants with a predominance of C_4 ones, probably related to a drier climate but less than the *Period II* and more than *Period IV*;

Period IV: mixed vegetation (C_3 and C_4 plants), with predominance of C_3 plants showing the environmental change to the current vegetation probably during the Late Holocene with more humid conditions.

The $\delta^{13}C$ depth records of the Cascavel soil profiles showed different vegetation changes since Late Pleistocene. The vegetation evolution registred in the C2 and C3 soil profiles are predominantly with C_4 photosynthetic plants (*Periods I, II and III*) during the Late Pleistocene to Mid–Holocene (between ~15,214 cal yrs BP to ~6341 cal yrs BP), indicating a drier climate. Pessenda et al. (1996), Ladchuk et al. (2016) and Luz et al. (2019) reported a drier climate with the predominance of C_4 plants suggesting the expansion of savanna (Cerrado) from the Late Pleistocene to Mid–Holocene in the region of Londrina and Campo Mourão, ~362 km and ~180 km distant from our study area, respectively. Apart from this moment, the modern humid conditions were established and the development of Semideciduous forest with *Araucaria* trees in the C2 and C3 soil profiles (*Period IV*) were observed over the areas previously dominated by C_4 plants (*Cerrado*/savanna or grassland).

Although soil profile C1 is similar to C2 and C3 soils, presented the largest contribution from C_4 plants in *Periods II* and *III*. Furthermore, the *Period I* of profile C1 was characterized by the predominance of C_3 plants, suggesting the occurrence of a more closed vegetation such as Semideciduous forest with *Araucaria* trees, probably related to altitude (meters above sea level = 790; Table 1) as the area where the C1 profile comes from is higher than the areas for profiles C2 and C3, which may have promoted a different microclimate. The coexistence of grasslands or *Cerrado*/savanna and forest has also been reported in this region (Luz et al., 2019). Thus, the vegetation development on the C1 soil profile was little different from that of the C2 and C3 soil profiles: Semideciduous forest with *Araucaria* trees during the Late Pleistocene, followed by an open vegetation during the Mid–Holocene, such as grassland (can be *Cerrado* or a grassland); and Semideciduous forest with *Araucaria* trees over the areas previously dominated by C_4 plants (*Period IV*).

3.3.1.3.3. Palotina

The four periods observed in the three profiles from Palotina are described below and are shown in Figure 22 and Table 18:

Period I: characterized by a mixed vegetation (C_3 and C_4 plants) with an increasing contribution from C_4 plants in the deeper horizons during the Late Pleistocene (between ~14,422 cal yrs BP; Table 16);

Period II: mixed vegetation (C_3 and C_4 plants), but with predominance of C_4 plants. This period is characterized by the largest contribution from C_4 plants in profiles P1 and P3, occurring in the Early Holocene associated with a drier and warmer climate (~11,492 cal yrs BP; Table 16);

Period III: the values of $\delta^{13}C$ isotopic composition indicated a mixed vegetation of C_4 and C_3 plants with a predominance of C_4, with the largest contribution from C_4 plants in profile P2 occurring in Early–Mid–Holocene, indicating a drier and warmer climate (between ~11,492 cal yrs BP and ~5515 cal yrs BP; Table 16);

Period IV: characterized by a mixed vegetation (C_3 and C_4 plants), with an increased contribution of C_3 plants showing the environmental change to the current vegetation with more humid conditions than previous period.

The $\delta^{13}C$ depth records from the Palotina ferralsols indicated vegetation changes since the Late Pleistocene. The results, from the end of the Pleistocene–Early–Mid–Holocene showed mixed vegetation (C_3 and C_4 plants) with an increasing contribution from C_4 plants (Figure 22). Profiles P1 and P3 showed the largest contribution of C_4 plants in the *Period II*, and profile P2 in the *Period III*, indicating probably drier and warmer climate. The studies by Stevaux (2000), Luz et al. (2019) and paleoenvironmental reconstruction researches carried out in southeast region (Pessenda et al., 1996; 1998; Rodrigues; 2019; Souza, 2019) indicate the presence of a vegetation adapted to a warm and dry climate during the Late Pleistocene until Mid–Holocene. According to the studies cited above, the start of the Early–Holocene (~11,492 cal yrs BP; Table 16) and in the Mid–Holocene (~5515 cal yrs BP; Table 16) the drier and warmer conditions affected the vegetation, causing a change in its structure, and this was observed in profiles P1–P3 with a larger participation of C_4 plants, indicating the occurrence of more open vegetation, which could be savanna (*Cerrado*). In addition, in *Period IV*, which occurs after the Mid–Holocene and probably in the Late Holocene (~1500 cal yrs BP, according to Stevaux, 2000) a more humid climate than that observed in the

previous phases was observed, characterizing the environmental change to the current vegetation with the predominance of C_3 plants (Semideciduous forest).

3.3.1.3.4. Synthesis of vegetation changes: Guarapuava x Cascavel x Palotina

The $\delta\ ^{13}C$ isotopic composition of the studied ferralsols indicate the vegetation changes since the Late Pleistocene in the three areas. Guarapuava profiles presented a predominance of C_3 plants during the Late Pleistocene, suggesting a more humid climate and the occurrence of *Araucaria* forest (Bertoldo et al., 2014; Pinaya et al., 2019; Pagotto et al., 2020; Wilson et al., 2021). In this same period, we observed a predominance of C_4 plants in the Cascavel profiles (except C1), and a mixed vegetation with C_3 and C_4 plants in the Palotina profiles, suggesting a drier environment in Cascavel and probably warmer and drier in Palotina (Pessenda et al., 1996; Stevaux, 2000; Ladchuk et al., 2016; Luz et al., 2019). The next periods, the Early–Mid–Holocene, a predominance of C_4 plants were observed in the three studied areas, suggesting a more open vegetation such as grasslands in Guarapuava, grassland or savanna (*Cerrado*) in Cascavel, and *Cerrado*/savanna in Palotina (Behling, 1998; 2002; Pessenda et al., 1996; Stevaux, 2000; Calegari, 2008; Bertoldo et al., 2014; Ladchuk et al., 2016; Calegari et al., 2017; Luz et al., 2019). During the Late Holocene, the current expansion of the *Araucaria* forest in Guarapuava, Semideciduous forest with *Araucaria* tress in Cascavel, and Semideciduous forest in Palotina, occurred over the areas previously dominated with C_4 plants, such as grasslands and Cerrado, in a more humid climatic conditions (Pessenda et al., 1996; Behling, 1997; Stevaux, 2000; Calegari, 2008; Parolin et al., 2008; Beroldo et al., 2014; Ladchuk et al., 2016; Luz et al., 2019; Calegari et al., 2017).

3.4. Molecular composition of SOM: evidence of short-term carbon composition changes

3.4.1. General composition of SOM

Mean values of groups of pyrolysis products from the studied areas are shown in Table 19. The composition of SOM presented a dominance of aromatic compounds, N-containing compounds, (poly) aromatics and polysaccharides with a low contribution from

lignin compounds suggesting that the OM from the studied ferralsols is degraded (Dick et al., 2005; Marques et al., 2015; Justi et al., 2017; Schellekens et al., 2017).

The high abundance of aromatic compounds has been previously reported by several authors (Zegouagh et al., 2004; Dick et al., 2005; Justi et al., 2017; Schellekens et al., 2017). According to Schellekens et al. (2017), most aromatic pyrolysis products may originate from several sources including lignin, polysaccharides, proteins and black carbon (BC). The quantified aromatic compounds included seven different products (benzene (Ar1), toluene (Ar2), indene (Ar3), C_2 benzenes (Ar4–6) and benzene,1,3-bis(1,1-dimethyl) (Ar7); Appendix K), and their mean abundance varied between 42.1% and 48.9% of TIC. The quantified N-containing compounds included five products (pyrrole (N1), benzonitrile (N2), pyridine (N3) and C_1 pyridines (N4–5)), which presented a large contribution in pyrolysates of SOM, varying from 16.8% to 22.4% of TIC. N-containing compounds originate from proteins of various sources. The large contribution of N-containing compounds suggests a considerable contribution from microbial material in the studied profiles (Schulten and Schnitzer, 1992; Buurman et al., 2007; Vancampenhout et al., 2016; Schellekens et al., 2017). The (poly) aromatics products include eight different compounds (naphthalene (PAH1), C_1 naphthalenes (PAH2–3), biphenyl (PAH4), anthracene (PAH5), phenanthrene (PAH6), terphenyl, 4-phenyl (PAH7) and 2,4-diphenyl-4-methyl-2(z)-pentene (PAH8); Appendix K). As reported by González-Pérez et al. (2014), the (poly) aromatics compounds are well-known pyrolysis products of black carbon (BC) and the relatively large abundance of PAHs observed in our samples can suggests the occurrence of fire in the studied areas. The mean abundance of PAHs varied between 12% and 16.2%, which is high compared with BC- rich soils analysed up 2 m depth (Marques et al., 2015; Justi et al., 2017; Schellekens et al., 2017; Chiapini et al., 2018). However, the (poly) aromatics in combination with aromatic compounds represent more than 50% of the sum of all quantified products (% TIC) in our samples, which can be an indicative of highly degraded SOM associated with a SOM affected by fire.

The polysaccharide compounds were low in number and included five products (2-furaldehyde (Ps1), 5-methyl-2-furaldehyde (Ps2) and unidentified carbohydrates (Ps3–5); Appendix K). The mean abundance of Ps varied between 3.0% and 10.6% of TIC. As reported by Vancampenhout et al. (2016) and Schellekens et al. (2017), the soil Ps compounds originate from plant and microbial sources. As the Ps compounds presented low molecular weight and an association with N-containing compounds indicated by factor analysis, in this dataset the Ps are most likely of microbial origin.

Lignin phenols were presented in low abundance varying between 0.3% and 1.1% of TIC. Lignin phenols are exclusively of plant origin and the low abundance suggests a considerable degree of decomposition. Phenol compound showed a moderate contribution to the pyrolysates, ranging from 2.4% to 8.8% of TIC and may have various sources.

The mean abundance of groups of pyrolysis products showed a clear difference in the molecular composition of soil organic matter in the studied areas. As reported by Dick et al. (2005), the soil type, the vegetation and climatic conditions may effect the quantity and quality of the SOM. Therefore, as the soil class is the same in the three studied areas (ferralsols), the vegetation type and current and past climatic conditions are most likely to be responsible for the differences between the studied profiles. Knowing this, the Guarapuava soil profiles presented SOM with a lower level of decomposition with a greater contribution from lignin phenols and phenols compounds, and a lower contribution from N-containing compounds and aromatic compounds than in the Cascavel and Palotina profiles. This fact is in agreement with the climatic conditions, where Guarapuava presented more humid and colder conditions and more forest vegetation than the Cascavel and Palotina profiles.

Table 19. Mean abundance of groups of the pyrolysys products in the studied areas, expressed as proportion of the sum of all quantified products (% TIC).

Chemical group	Guarapuava		Cascavel		Palotina	
	%TIC	SD[2]	%TIC	SD	%TIC	SD
Aromatics	42.1	22.5	43.9	22.4	48.9	26.0
Benzofurans	0.6	0.4	0.6	0.4	0.6	0.4
PAHs[1]	16.2	22.8	12.0	18.5	16.1	26.0
N-containing compounds	16.8	10.2	20.8	10.8	22.4	15.7
Lignins phenols	1.1	2.9	0.9	1.6	0.3	1.2
Polysaccharides	10.6	13.7	10.4	12.7	3.0	7.3
Phenols	8.8	17.3	7.5	12.0	2.4	4.8

[1]PAHs = (poly) aromatics; [2]SD = standard deviation (%).

3.4.2. Factor analysis

Factor analysis was applied to all 28 pyrolysis products from soil samples treated with 3:1 HF/HCl solution, to verify the major chemical diferences within sample set (profile, depth and area). Prior to factor analysis, the seven lignin phenols were summed to a single variable (Lg1–Lg7), because of their low abundance and occurrence. In addition, the surface samples (5 cm of depth) were excluded, because they exhibited an outlier type of behaviour, which would bias the interpretation of FA. The first four factors explained 60.5% of the total

variance. The distribution of pyrolysis products (loadings) for the first two factors are plotted in Fig. 23. The depth records of factor scores for F1 and F2 are displayed in Figure 24.

The compounds related with plant materials (lignin phenols and phenol) and microbial materials (polysaccharides and N-containing compounds, except for N2) (Ralph and Hatfield, 1991; Marques et al., 2015; Vancampenhout et al., 2015; Chiapini et al., 2018) all had negative loadings on F1, while the (poly) aromatic compounds that are associated with BC were separated on F1. Indene (Ar3), C_2 benzenes (Ar4–6), C_1 naphthalenes (PAH2–3), and 2,4-diphenyl-4-methyl-2(z)-pentene (PAH8) showed negative loadings, while compounds with positive loadings on F1 included benzonitrile (N2), benzene (Ar1), benzene,1,3-bis (1,1-dimethyl) (Ar7), naphthalene (PAH1), biphenyl (PAH4), anthracene (PAH5), phenanthrene (PAH6) and terphenyl, 4-phenyl (PAH7). This separation of products on F1, suggests that F1 reflects decomposition, with a higher degree of decomposition for positive loadings. This interpretation is supported by depth records of the F1 scores that showed a clear increase with depth (Figure 24). The separation of products associated with BC showed a clear trend, PAHs and aromatics with alkyl side-chain showing negative loadings and PAHs and aromatics without alkyl side-chain and without functional group showed positive loadings (Marques et al., 2015; Justi et al., 2017; Chiapini et al., 2018). As reported by Justi et al. (2017), the loss of alkyl side-chains and hydroxyl functional groups from PAHs and aromatics is indicative of degraded BC. This is in agreement with the interpretation of F1, and with the generally high degradation state as indicated by the dominance of (poly) aromatics (Table 19), and reflects an increase of the degraded BC pyrolysates with depth.

The depth records of F1 showed a clear difference in the degree of decomposition in the studied profiles. G1–G4 and C1–C3 profiles showed negative scores values in most samples between the A and Bfl_2 horizons (~25–185 cm depth), while profiles P1–P3 showed negative scores in samples between A and Bfl_2 horizons, but at shallower depths (~25–85 cm of depth), suggesting that profiles G1–G4 and C1–C3 presented conditions which are less favorable for decomposition when compared to soil profiles P1–P3. Less decomposed OM in profiles G1–G4 and C1–C3 is supported by the larger C/N values found in these profiles (C/N average values: Guarapuava = 15.2; Cascavel = 13.8) in relation with Palotina ones (C/N average values: Palotina = 7.8). This difference is in agreement with the mean abundance of groups of pyrolysis products and climatic conditions of the studied areas, where Guarapuava and Cascavel profiles are located in more humid and colder climate than the Palotina profiles (Table 19; *section 2.1.3*).

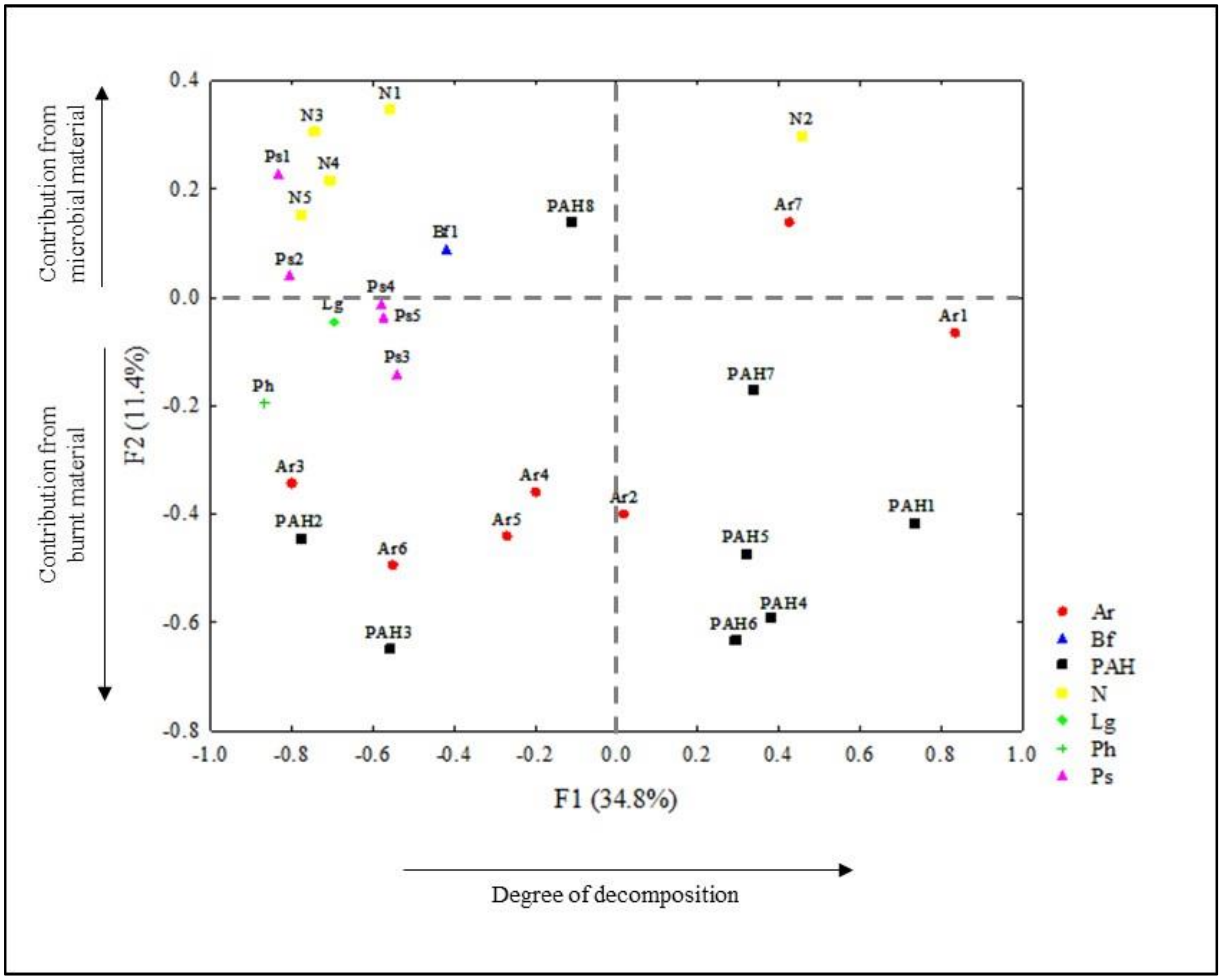

Figure 23. Factor loadings for the F1–F2 projection of a factor analysis applied to the quantified pyrolysis products of all samples. Ar = aromatic; Bf = benzofuran; PAH = (poly) aromatic; N = N-containing compound; Lg = lignin phenol; Ph = phenol; Ps = polysaccharide.

The loadings show that F2 separates products associated with burnt material (negative loadings for most PAHs and aromatics) from those associated with microbial material (positive loadings for most N-containing compounds and polysaccharides) (Vancampenhout et al., 2016). Thus, F2 is interpreted to reflect the contribution from burnt material, with the unburnt material most strongly represented by microbial material (positive loadings) (Figure 23). The fact that lignin has low loadings in F2 may indicate that it is mostly present in charcoal and plant material that is not protected as such has already been lost, while microbial material is continuously refreshed.

The depth records from F2 scores clearly showed a different trend in the studied profiles (Figure 24). The depth records from F2 showed no general depth trend in the profiles G1–G4 and C1–C2. In contrast, a general decrease in the depth records of F2 was observed in

the profiles C3, P1, P2 and P3. In addition, this latter group of profiles (C3, P1–P3) clearly presented more positive values. The scores suggest that soil profiles C3, P1, P2 and P3 received more contribution from microbial material and less contribution from materials derived from black carbon than the profiles G1–G4 and C1–C2. However, soil profiles C3 and P1–P3 showed a negative correlation in F2 with ^{13}C isotopic composition (C3 = -0.57; P1 = -0.70; P2 = -0.56 e P3 = -0.62), and in associated with our paleoenvironmental reconstruction data, these soil profiles presented a past vegetation often dominated by C_4 plants, which results in a lower charcoal in the soils after fire. In addition, the soil profiles with more negative values (G1–G4 and C1–C2) probably presented more material derived from charcoal.

In relation to soil depth, we observed negative scores in F2 in Periods with a higher contribution of C_4 plants in the paleoenvironmental reconstruction data, suggesting the moments when fire occurred. However, the G2, G4, C1 and C2 soil profiles showed negative scores in the superficial samples, which correspond to Period IV (dominance of C_3 plants) in the paleoenvironmental reconstruction data, indicating that despite having a C_3 vegetation dominance and a humid climate, we still find current fire records.

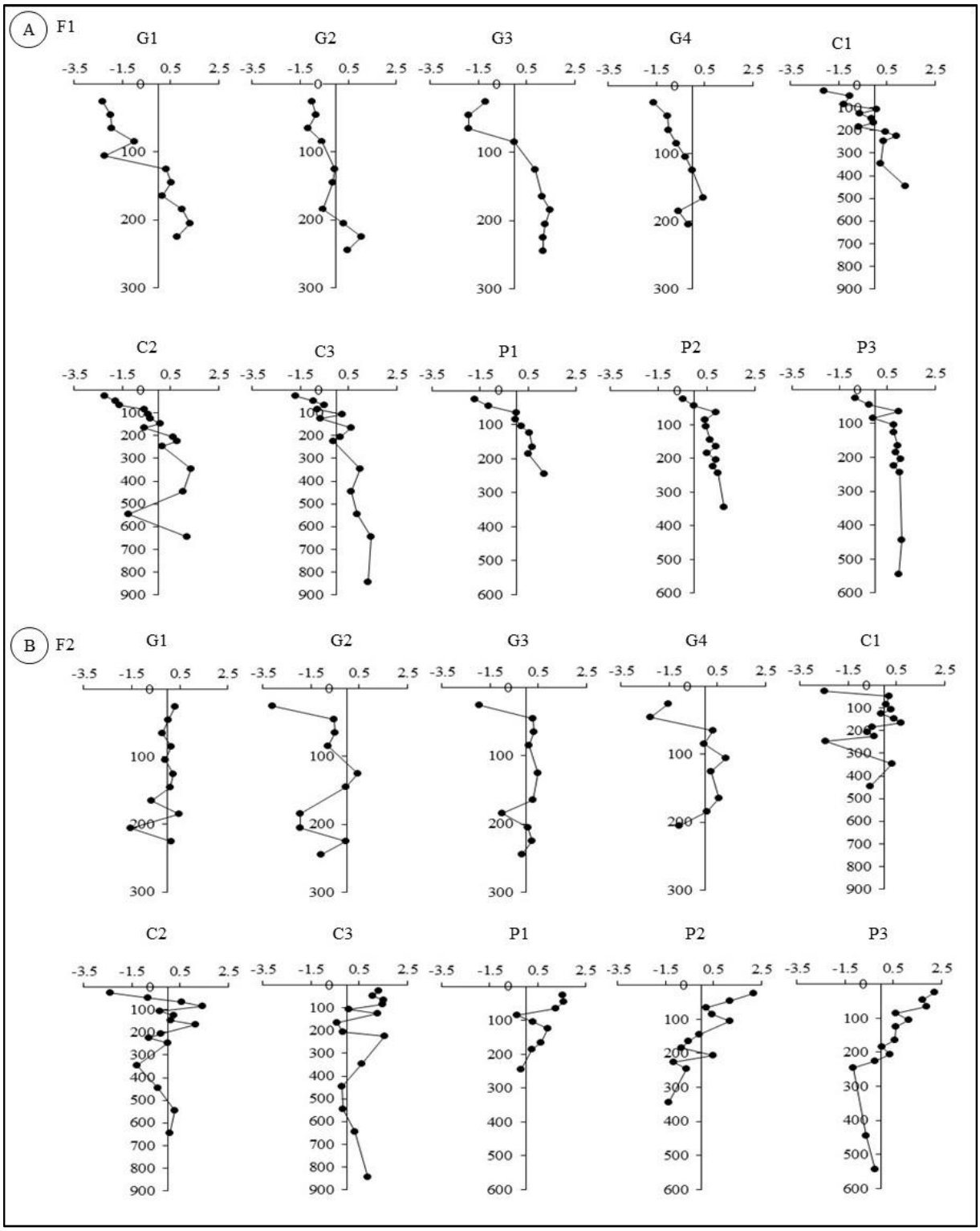

Figure 24. Depth records of factor scores for F1–F2 of a factor analysis applied to pyrolysates from all soil samples.

3.5. Bioturbation: evidence of short-term fauna and flora activity in the studied ferralsols

3.5.1. Identification of biofeatures (BFs) and bioturbating agents (Ba) on a macro- and microscale

The identification of biofeatures and bioturbating agents mainly on a microscale were carried out according to the existing literature, the ant (micro) aggregates produced during our lab experiment, and online meetings with renowned researches of the soil fauna, such as Patrick Lavelle, George Brown, Luiz Carlos Forti, Og F.F. de Souza and Tiago F. Carrijo.

Thin section was made from the ant (micro) aggregates and the photomicrographs are shown in Figure 25. The ant (micro) aggregates showed an aggregation of smaller microaggregates and were characterized by irregular shape with or without pores, surface roughness identified as serrate–mammilate and size < 2.00 mm in diameter.

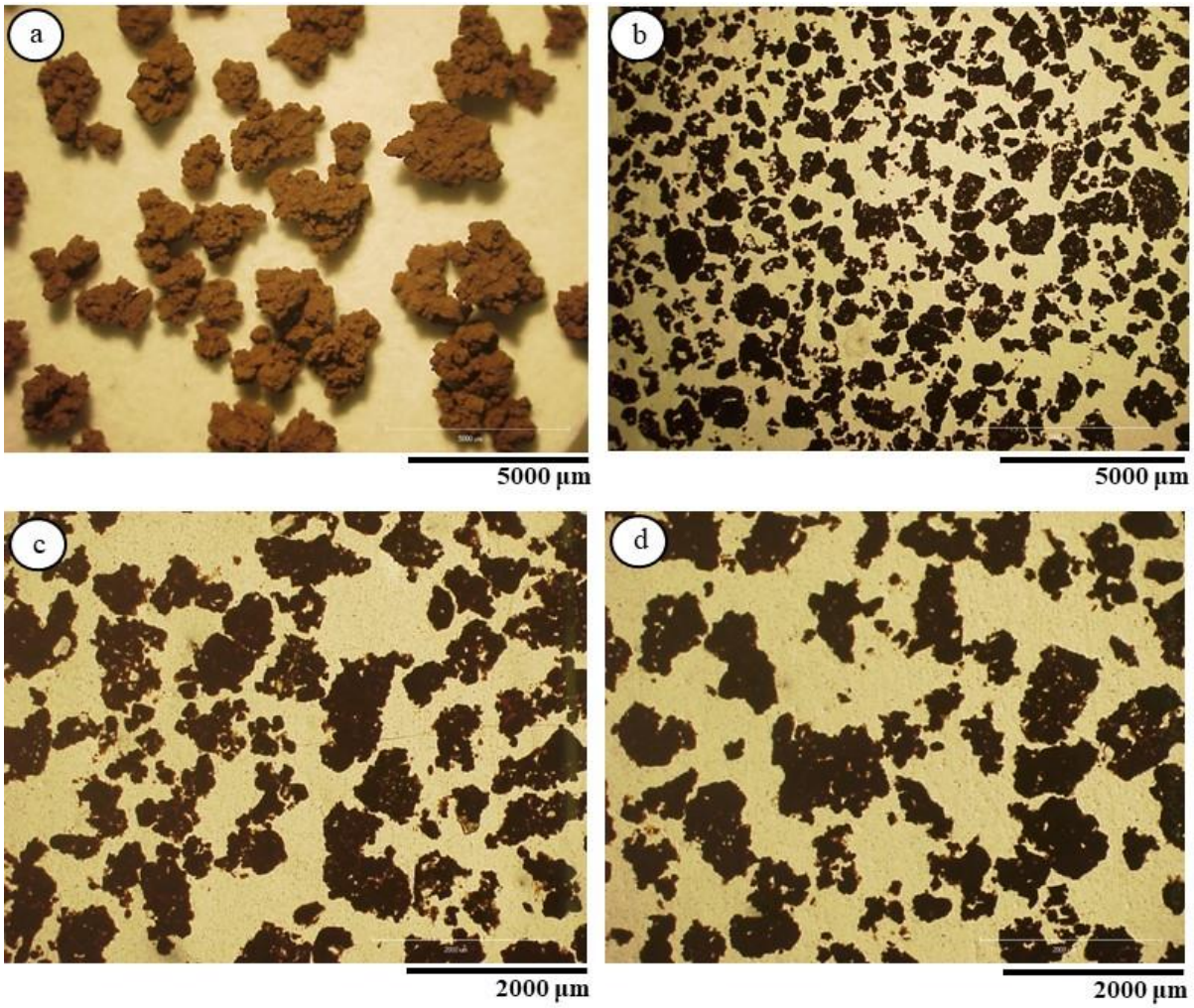

Figure 25. The ant (micro) aggregates. a) ant (micro) aggregates under magnifying glass, PPL. b), c) and d) photomicrographs of ant (micro) aggregates thin section, PPL. Attention to the roughness (serrate/mammilate) and porosity of the (micro) aggregates (c and d).

3.5.1.1. Identification of BFs and Ba in the macroscale

3.5.1.1.1. Roots

The occurrence of fresh roots in the studied soil profiles varied with depth, reaching 140 cm (BA horizon) in the Guarapuava profile (G4), 120 cm (BA horizon) in the Cascavel profile (C3) and 105 cm (Bfl_2 horizon) in the Palotina profile (P3) (Figure 26). BFs derived from roots, such as, charcoal and burnt roots were also observed. Fine fresh roots (1 < ø 2 mm) were most common in upper horizons while thick roots (5 < ø 10 mm) were observed in deeper horizons, creating vertical and horizontal burrows. Fresh roots are important bioturbating agent of soil, because when these roots decay, infillings of macropores occurs allowing transport and mixing of soil material (Roering et al., 2002; Gabet et al., 2003;

Phillips et al., 2005; Phillips and Marion, 2006; Wilkinson et al., 2009). Additionally, roots decay attracts macro and mesofauna from the topsoil in search of food, which induces its deeper distribution and bioturbing action. Tree uprooting can also occur and can mix or inverting soil horizons causing soil displacement and creating mounds mainly in the soil profiles under forest vegetation (Guarapuava profiles (G2–G4); Cascavel profile (C2) and Palotina profile (P1)) (Shaler, 1891; Putz, 1983; Schaetzl and Follmer, 1990; Schaetzl et al., 1990; Norman et al., 1995; Gabet et al., 2003; Wilkinson et al., 2009).

3.5.1.1.2. Soil fauna groups

In the field, krotovinas (dense and loose infillings) and ant chambers BFs were observed and associated with soil fauna activity (Figure 26). In a Guarapuava soil profile (G4) the krotovinas occurred until 340 cm in depth (BC_2 horizon), while Cascavel (C3) and Palotina (P3) profiles they were observed until 810 cm (BC_1 horizon) and 210 cm (Bfl_4 horizon), respectively. The observation of this type of BFs below two meters depth is the first indication of the occurrence of soil fauna activity at greater depths in our studied soils. However, the identification and description of BFs in the field were difficult in profiles with a reddish and homogeneous colour, leading to the non-identification of BFs below 210 cm depth in the Palotina profile (P3).

The soil fauna groups associated with activities at greater soil depths are endogeic and anecic organisms. Endogeic bioturbating agents are active diggers in short vertical distances, while anecic ones explore and construct their nests and galleries in deep layers. The most common endogeic and anecic organisms are earthworms, termites and ants (Lavelle, 1988; Lavelle et al., 1992; Tonneijck and. Jongmans, 2008). The specific BFs of each endogeic and anecic organisms cited above can be verified on a microscale in thin soil sections.

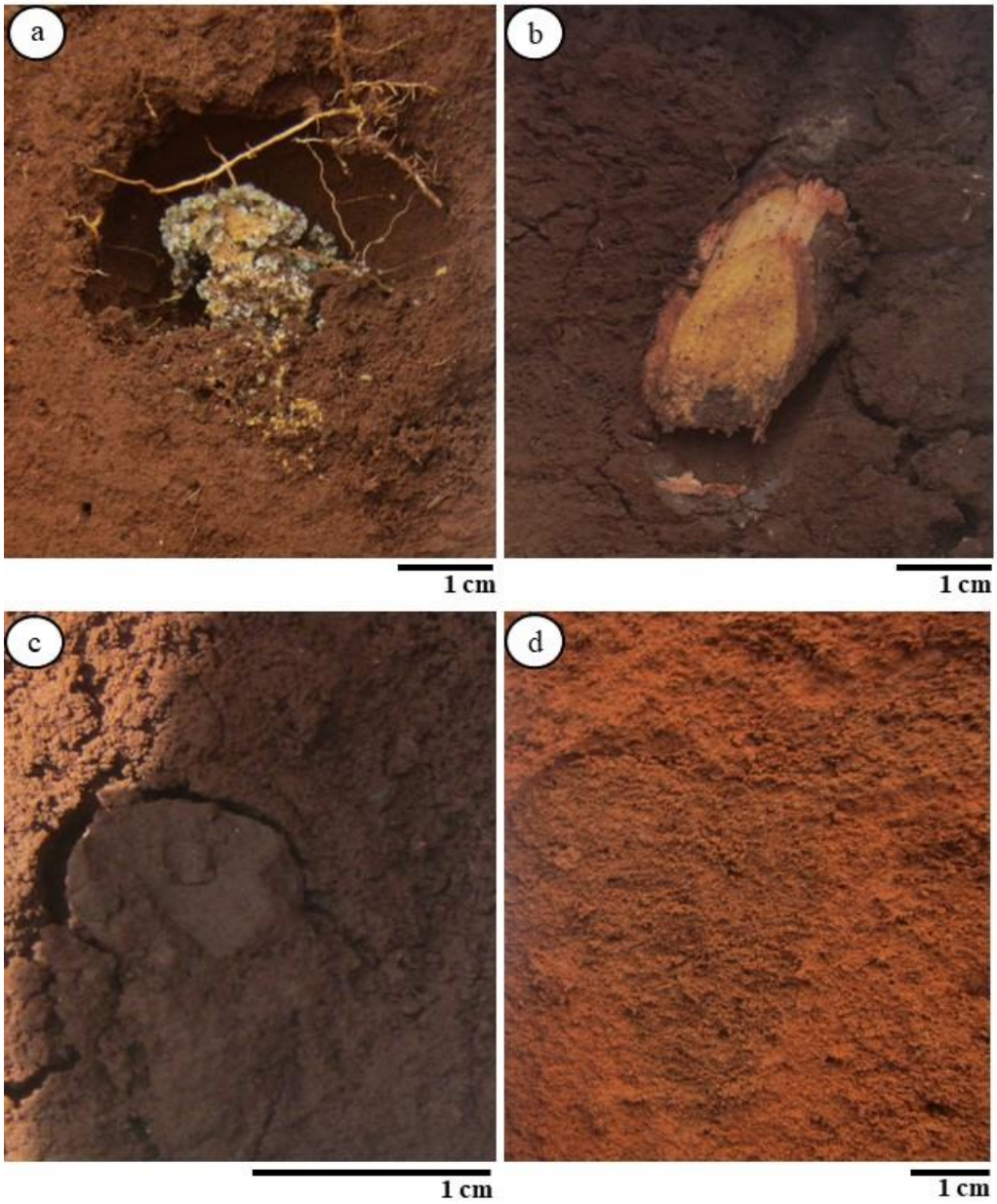

Figure 26. Examples of biological features observed on the macroscale in the Guarapuava soil profiles. a) Ant chamber (with fungus) from G3 profile in the A horizon (20 cm deep); b) root and c) krotovina (dense infilling) from G4 in the AB and A_3 horizon, respectively (90 cm and 60 cm of depth); d) krotovina (loose infilling) observed in G1 in the BA horizon (75 cm deep).

3.5.1.2. Identification of BFs and Ba on the microscale

3.5.1.2.1. Roots

The dominant occurrence of roots, root channels and root voids were observed in upper horizons similar to our field descriptions (macroscale) (Figure 27). Furthermore, these BFs in soil thin sections were observed until 235 cm in Guarapuava (G4; Bfl_3 horizon), 955

cm in Cascavel (C3; BC_2 horizon) and 445 cm at Palotina soil profile (P3; Bfl_6 horizon) and varied from 8 to 1 mm in diameter with a simple recognizable pattern, creating vertical and horizontal burrows. The BFs of fine roots were more visible at upper horizons. A smooth lining and the presence of a compaction of the surrounding walls of the soil matrix characterize the channels and voids of roots and sometimes they were empty of soil microaggregates. The decayed roots were rarely observed in the studied soil profiles, because microarthropods, termites, earthworms and ants probably fed these materials (Humphreys, 1993). In addition, the natural decomposition process may also contribute to the rare occurrence of the decayed roots.

3.5.1.2.2. Soil fauna groups

Based on the depth distribution and the heterogeneity of the BFs encountered at the microscale, the process of bioturbation is carred out by several groups of fauna. Some biofeatures are specific for a particular bioturbating agent:

_Individual small smooth ellipsoidal light brown excrements were observed at 70 cm deep (A_3 horizon) in profile G4, associated and inside the root debris, varying from 0.2 to 0.1 mm in diameter (Figure 28a). Epigeic and small endogeic decomposer species such as microarthropods (acari, collembola and enchytraeids) that lives in litter and soil horizons produce this type of biofeature (Bullock et al., 1985; Lavelle, 1997; Lavelle and Spain, 2003; Rusek, 1985; Stoops et al., 2018). Excrement morphology, size characteristics and the depth occurrence showed that the observed feature resulted from acari activitiy. According to Bullock et al. (1985) and Rusek (1985) the excrements of acari have been described as egg-shaped (ellipsoidal) or spherical, with smooth surface, very compact, and without mineral particles inside, light brown colour and up to 0.2 x 0.14 mm in size, which is very similar to those observed BF of the Guarapuava soil profiles. In the profiles from Cascavel and Palotina this type of BFs was not observed.

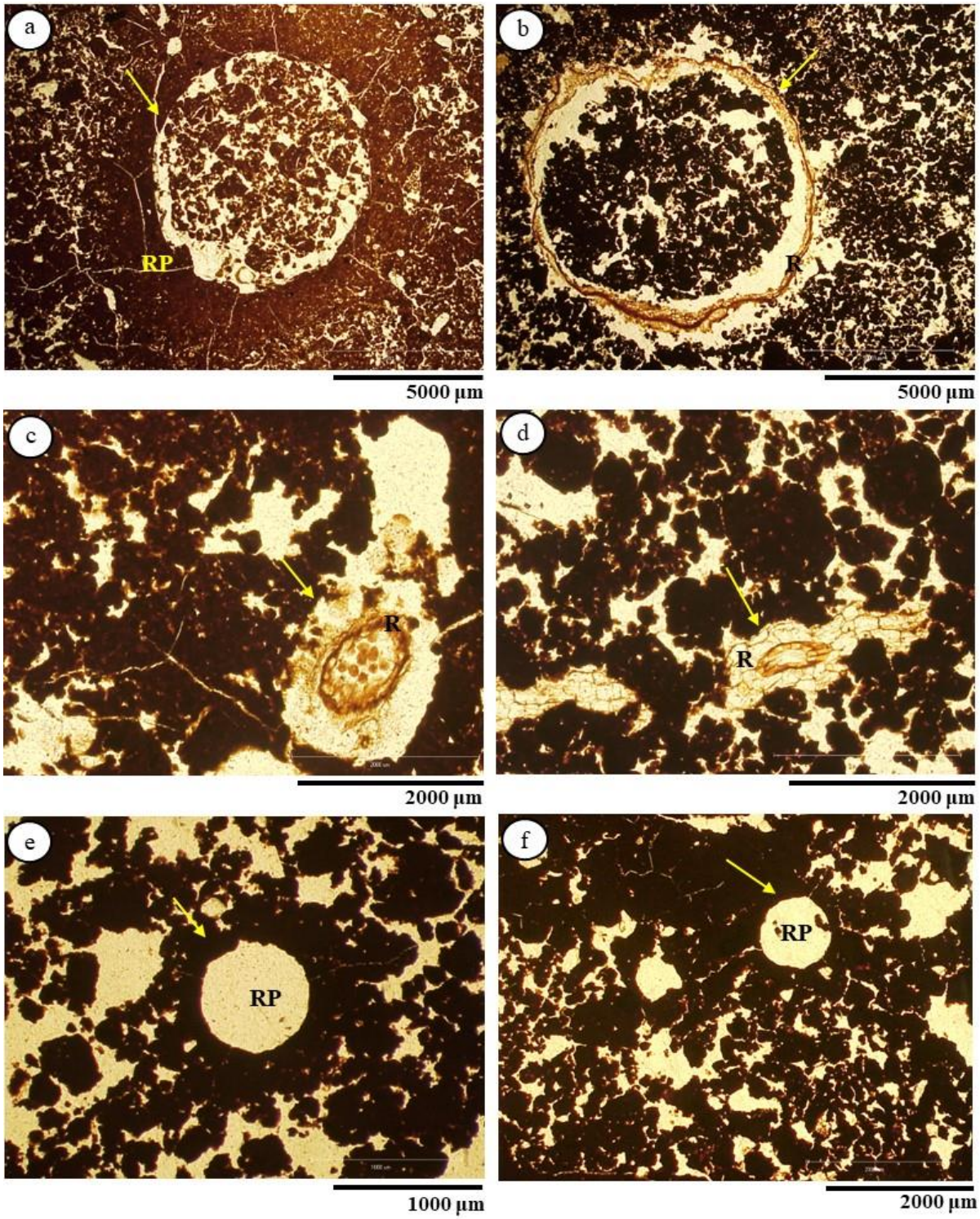

Figure 27. Photomicrographs of root biofeatures in the studied soil profiles (yellow arrows), PPL. a) Horizon AB, profile G1 (35–50 cm deep); b) Horizon A_3, profile G3 (50–65 cm deep); c) Horizon A_3, profile G4 (65–80 cm deep); d) Horizon A_2, profile C2 (35–40 cm deep); e) Horizon BA, profile C2 (135–150 cm deep); f) Horizon AB, profile P2 (12–25 cm deep). RP = root pore; R = root. Note the nearly circular cross section of roots channels and equal compressed zones; root tissues in b), c) and d) photomicrographs.

_Individual small (< 0.1 mm in diameter) smooth spherical/oblong excrements with sharp boundaries and a brown colour, were observed at ~50 cm deep (A_2/A_3 horizons) in the

G2 profile (Figure 28b). The excrement morphology, size characteristics and the depth occurrence were probably the result of collembola or enchytraeid activity (Babel, 1975; Bullock et al., 1985; Rusek, 1985; Pawluk, 1987; Davidson et al., 2002; Lavelle and Spain, 2003; Stoops, 2021). However, Babel (1975) pointed that the enchytraeids and collembola excrements were very similar, but the enchytraeids excrements is more distinctive in soil horizons with high organic matter content, which is observed in profile G2. In the profiles from Cascavel and Palotina enchytraeid excrement was not observed.

_Dense complete and incomplete infillings with bow-like structure and vermicular microstructure (Stoops, 2021) with little and/or any compaction in the soil surrounding matrix were observed frequently from the surface to deep horizons in the soil profiles from Guarapuava. In profiles from Cascavel and Palotina the occurrence of this type of BFs was very low (scarce). The size of the dense infillings varied from 13.0 to 0.9 mm in diameter and the colour is similar to that of the soil matrix (Figure 28c–f).

_Loose continuous and discontinuous infillings occurred in the upper horizons until the weathering front in the three representative soil profiles (G4, C3 and P3), and the others seven studied profiles, varying from 19.6 to 0.6 mm in diameter (Figure 29). Generally, the loose infillings were associated to complex vertical and horizontal channels and chambers, presenting ellipsoidal and spherical shapes, and sometimes the loose infillings presented a coating (MO + clay) on the inner wall. In the C3 and P3 soil profiles (representing Cascavel and Palotina sites), the presence of loose infillings with ellipsoidal shape were more frequent than in the G4 soil profile. The soil material that formed the loose infillings was composed of microaggregates/excrements that differ in morphology and size.

According to Bullock et al. (1985), Barros et al. (2001), Kooistra and Pulleman (2018), Castro and Cooper (2019) and Stoops (2021), these dense and loose infillings types were formed by endogeic and anecic species, in particular earthworm excrement (dense infillings), excrements or activity of termites, ant activity and roots (loose infillings). The fauna organisms play an important role in the soil process because they ingest soil particles with organic matter and during an efficient symbiotic digestion produce stabilized excrements (earthworms and termites), and create diverse and abundant structures, which interfere with the soil physical structure (mainly ants) (Lavelle, 1997).

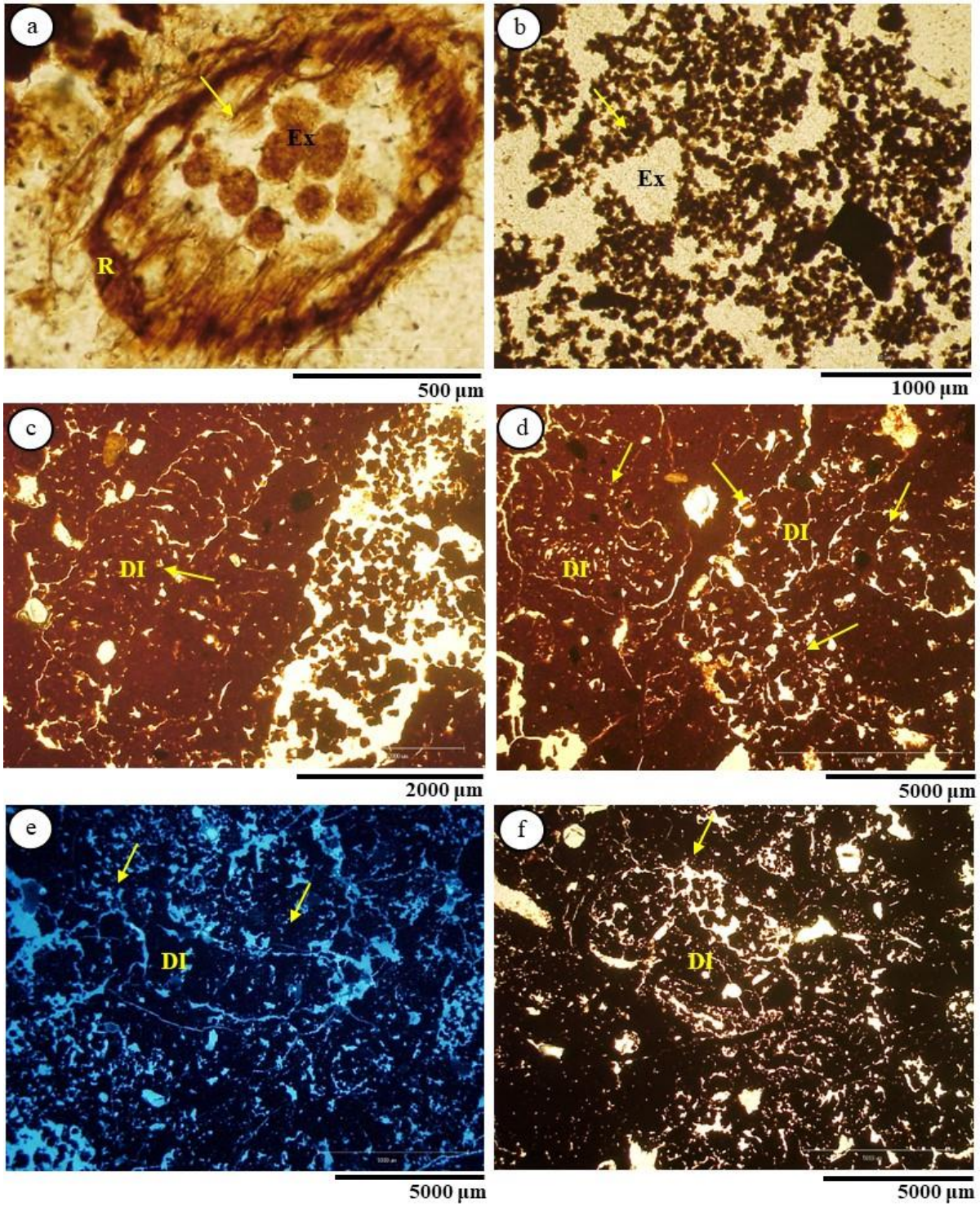

Figure 28. Photomicrographs of biofeatures from fauna in the studied soil profiles. a) excrements of Acari in a root in A_3 horizon, profile G4 (~70 cm deep), PPL; b) excrements of enchytraeids in the A_2/A_3 horizons, profile G2 (45–60 cm deep), PPL; c) e d) earthworm excrement (DI) with bow-like and vermiform microstructure in the Bfl_2 horizon, profile G2 (175–190 cm deep), PPL; e) earthworm excrement (DI) with bow-like and vermiform microstructure in the BC_2 horizon, profile G4 (330–345 cm deep), UV; f) earthworm excrement (DI)with bow-like and vermiform microstructure in the Bfl_3 horizon, profile C3 (590–600 cm deep), PPL. DI = dense infilling; R = root; Ex = excrement.

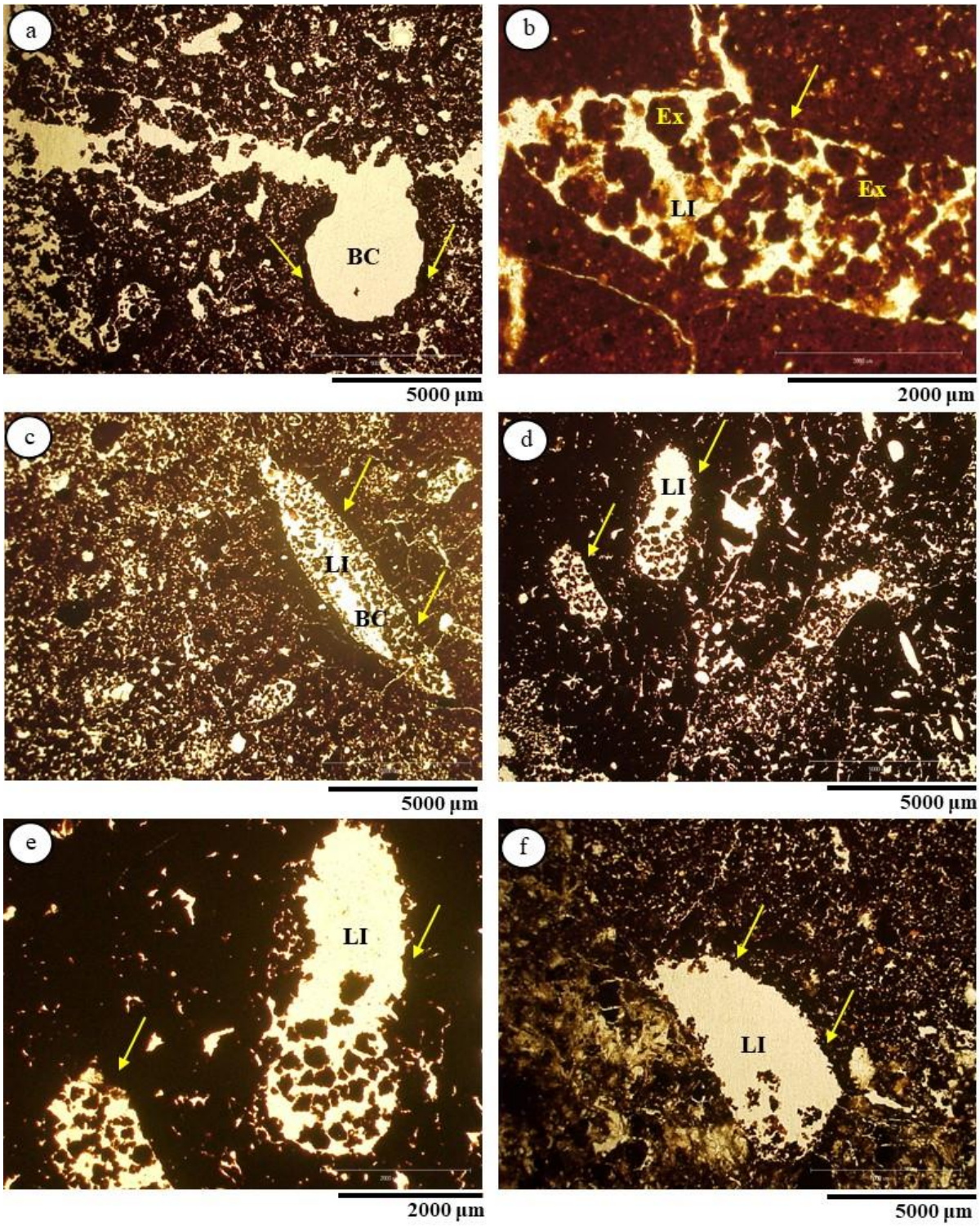

Figure 29. Photomicrographs of biofeatures from fauna activity in the studied soil profiles, PPL. a) BC (Mo + clay), suggesting termite activity in the Bfl_3 horizon, profile P3 (105-120 cm deep); b) LI with excrements in the Bfl_3 horizon, profile G2 (230–245 cm deep); c) ellipsoidal BC (Mo + clay) and LI in the Bfl_2 horizon, profile P2 (170–180 cm deep); d) and e) LI with serrate-mammilate microaggregates, polyhedral microaggregates and complex microaggregates, and bioporos with serrate walls, suggesting mainly ant activity in the Bfl_3 horizon, profile C3 (730–740 cm deep); f) LI with serrate-mammilated microaggregates and bioporos with serrate walls in the BC_r horizon, profile P3 (630–645 cm deep); LI = loose infilling; BC = bioporo with coating; Ex = excrement.

The specific biofeatures suggested that the acari, enchytraeids and earthworms activity occurred with more frequency in the Guarapuava soil profiles than in Cascavel and Palotina. This difference was expected due to the more favorable soil moisture, temperature and organic matter content in the Guarapuava soil profiles that influence de biology of these organisms, mainly enchytraeids and earthworms, which are considered semi aquatic animals presenting a cutaneous respiration (Lavelle and Spain, 2003). Furthermore, the low occurrence of enchytraeids and earthworms biofeatures in Cascavel and Palotina soil profiles is also associated with a dry period during the year and/or the period of quiescence/diapause of these organisms (Saussey, 1966; Bouché, 1984; Lavelle and Spain, 2003). The biofeatures of ants occurred in the three studied areas because ants have a wide longitudinal distribution and have adapted to the most diverse ecosystems since their origin ~120 million years ago (Lavelle and Spain, 2003; Grimaldi and Engel, 2005). In addition, the termite biofeatures occurred with more frequency in Cascavel and Palotina profiles. It is known that termites are more adapted to warm climates, which is observed at these two sites, presenting temperatures higher than those at the Guarapuava site (Wood, 1979; Lobry de Bruyn and Conacher, 1990; Eggleton et al., 1994).

Furthermore, the overlapping of BFs and the re-bioturbation of these features over time, does not allow the identification of the initial bioturbation agent, but only the current one.

3.5.2. Bioturbation (%) and biomantle: quantitative evidence on the macro- and microscale

3.5.2.1. Bioturbation

Quantitative results of bioturbation (%) on the macro- and microscale are shown in the Figure 30 and demonstrating that the bioturbation process reaches the weathering front. In the Palotina and Cascavel soil profiles the average bioturbation values were higher than those for the Guarapuava profiles (Palotina bioturbation average values = 55.7%, Cascavel = 55.0% and Guarapuava 47%), suggesting that the current temperature influences the bioturbation process. In addition, as reported by Bachelier (1978) and Humphreys (1993), the soil fauna is mostly found where the energy source is high, which corresponds to the upper horizons rich in plant materials, roots at an adequate temperature and soil moisture. Generally, the highest

level of bioturbation (%) was observed in the uppermost two meters decreasing non-linearly with depth in the studied profiles, corroborating with the studies of Humphreys and Field (1998), and Wilkinson et al. (2009). On the other hand, Rodrigues (2019), showed a linear decrease of bioturbation (%) with depth, which was not observed in our studied profiles.

Zones with high bioturbation (%) occurred at different soil depths in the studied areas and may be associated with past environmental conditions and/or with the specific soil ecology. The zones with the highest bioturbation (%) were sometimes the same on both the macro- and microscale, Table 20. The zones with high bioturbation (%) were considered when we observed an increase of bioturbation (%) in relation to above depth/sample analysed in the microscale. The soil profiles showed important variations in bioturbation (%) with depth (zones). According to our environmental reconstruction data (*section 3.3.1*) apart from the soil surface (0 to ~50 cm), the soil profiles G1 and G2 from Guarapuava, C1–C3 from Cascavel, and profiles P1–P3 from Palotina showed the zones with highest bioturbation (%, Table 20), mainly occurred in the zones with high C_4 plants contribution. The periods with higher C_4 plant contribution in the environmental reconstruction data, which correlated with the bioturbation zones in G1, G2, C1, C2 and P2 profiles were Periods II and III. In profiles C3, P1 and P3, the periods with C_4 plants contribution were Periods I and III. It is known that C_4 vegetation contributes with more roots than C_3 plants, which increases the availability of plant material to be used as na energy source by the soil fauna, thus increasing its action and consequently increasing bioturbation (high %) (Lavelle and Spain, 2003). However, the dominance of C_4 plants suggest a drier environment, which can interfere with the development of macrofauna. In addition, it is known that the soil macrofauna and roots can go deeper into the soil profiles in drier environmental periods. The fauna go deeper to find adequate temperatures and mainly humidity for nest construction, while the roots go deeper to find water. Examples of this are ants from the *Atta* genus that need wetter soil conditions for the development of their colonies and fungi cultivation for food (Lach et al., 2009; Miklós, 2012; Swanson et al., 2019).

In contrast, profiles G3 and G4, showed the zones with high bioturbation (%) occurring mainly in the zones with high contribution from C_3 plants, which is related to Period I in our environmental reconstruction data, suggesting a wetter period, favouring greater development of the root system and soil macrofauna (Lavelle and Spain, 2003; Miklós, 2012).

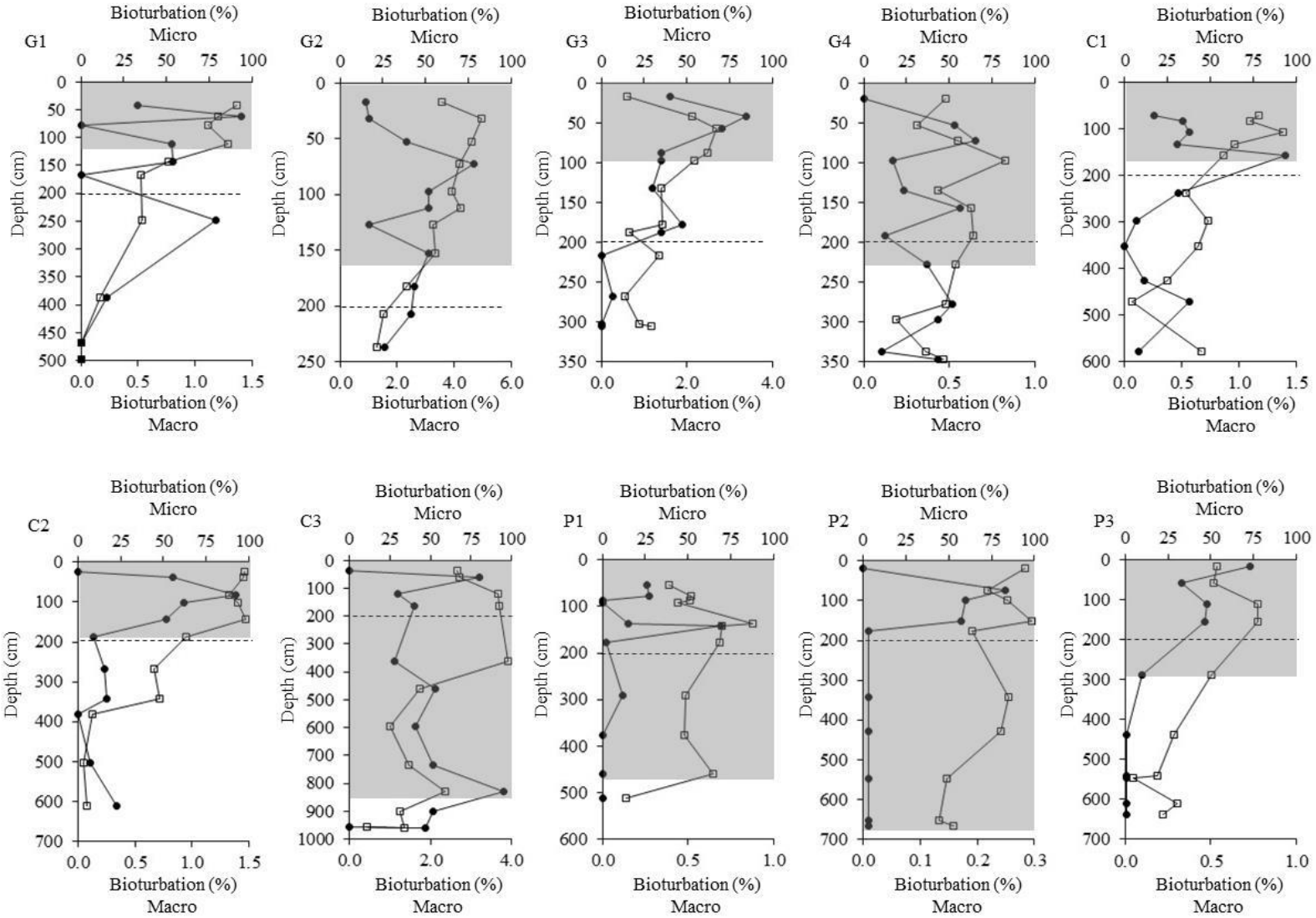

Figure 30. Bioturbation (%) on the macroscale (filled circles) and microscale (empty squares) in the studied soil profiles. The biomantle is indicated by the grey band and the control section (2 m depth) is indicated by the dashed line.

Table 20. Zones with high bioturbation (%) of the ten studied soil profiles.

Study sites	Zones with high bioturbation (%)	
	Depth (cm)	
	Macroscale	Microscale
G1	62, 112 , 142 and 247	42, 112 and 247
G2	72 and 152	32, 112 and 152
G3	42 , 177 and 267	57, 177, 217 and 305
G4	72 , 157 , 277 and 347	97, 192 and 347
C1	107, 157 and 472	107, 297 and 577
C2	82, 267 , 342 and 612	22, 142 and 342
C3	60 , 165, 462 and 800	120, 360, 830 and 960
P1	77 and 142	77, 137 and 460
P2	72	18, 150, 342 and 667
P3	18 , 112 and 155	112 and 610

Correlations of bioturbation (%) with dry soil bulk density and carbon content were observed in our studied soil profiles (Table 21). A negative correlation of bioturbation (%) and dry soil bulk density on a macro- and microscale was observed and expected, indicating that soils with higher levels of invertebrate, vertebrate and root activity (process of bioturbation) show a lower dry soil bulk density (Gabet et al., 2003; Wilkinson et al., 2009). On the other hand, fine texture and clayey soil horizons with higher values of dry soil bulk density (which is observed in some studied deep horizons) can hinder the gas (oxygen and carbon dioxide) and water flow rates and consequently the availability of an energy source (roots and plant materials) for the development of soil fauna and bioturbation process, which can explain the lower bioturbation (%) at greater depths (van Noordwijk et al., 1993; Lavelle and Spain, 2003; Lal and Shukla, 2004). In addition, a positive correlation of bioturbation (%) with total carbon content was observed suggesting that the bioturbation (%) tends to reduce when total carbon content decreases (Bachelier, 1978).

Table 21. Correlation of bioturbation (%) and total C content and soil bulk density (Ds) of the studied soil profiles.

Profiles	Bioturbation (%) on a macroscale		Bioturbation (%) on a microscale	
	Total C	Ds	Total C	Ds
G1			0.87	-0.65
G2			0.71	-0.57
G3	0.74	-0.61		-0.66
G4				
C1		-0.69	0.75	-0.54
C2	0.45	-0.43	0.85	-0.87
C3			0.51	-0.63
P1				
P2		-0.69	0.49	
P3	0.87		0.47	-0.70

In addition to the correlations observed above, the process of bioturbation produces the greatest effect on soil chemistry by increasing the organic carbon content of the soils through the production of BFs (Whitforf and Eldridge, 2013). The krotovinas (dense and loose infillings; BFs) observed in the field, were collected from the three representative soil profiles to investigate the input of carbon by soil fauna in the studied ferralsols. The results of the total carbon content (%) from the collected BFs *vs.* surrounding soil matrix are shown in Figure 31. In general, the BFs contained more total C content than the surrounding soil matrix. The exception was one BF from the G4 profile (35 cm deep), which presented a total C content lower than surrounding soil matrix. Similar observations were reported by Lavelle (1997), Jouquet et al. (2002) and Pulleman et al. (2005), suggesting that the activity of ecosystem engineers in the production of Bfs tends to accumulate and stabilize organic matter. The accumulation and stabilization of C in the soil, through the bioturbation process, often involves the ingestion of soil particles containing organic matter and an efficient digestive process involving a symbiotic relationship with microorganisms (Lavelle, 1997; Lavele and Spain, 2003 and references therein).

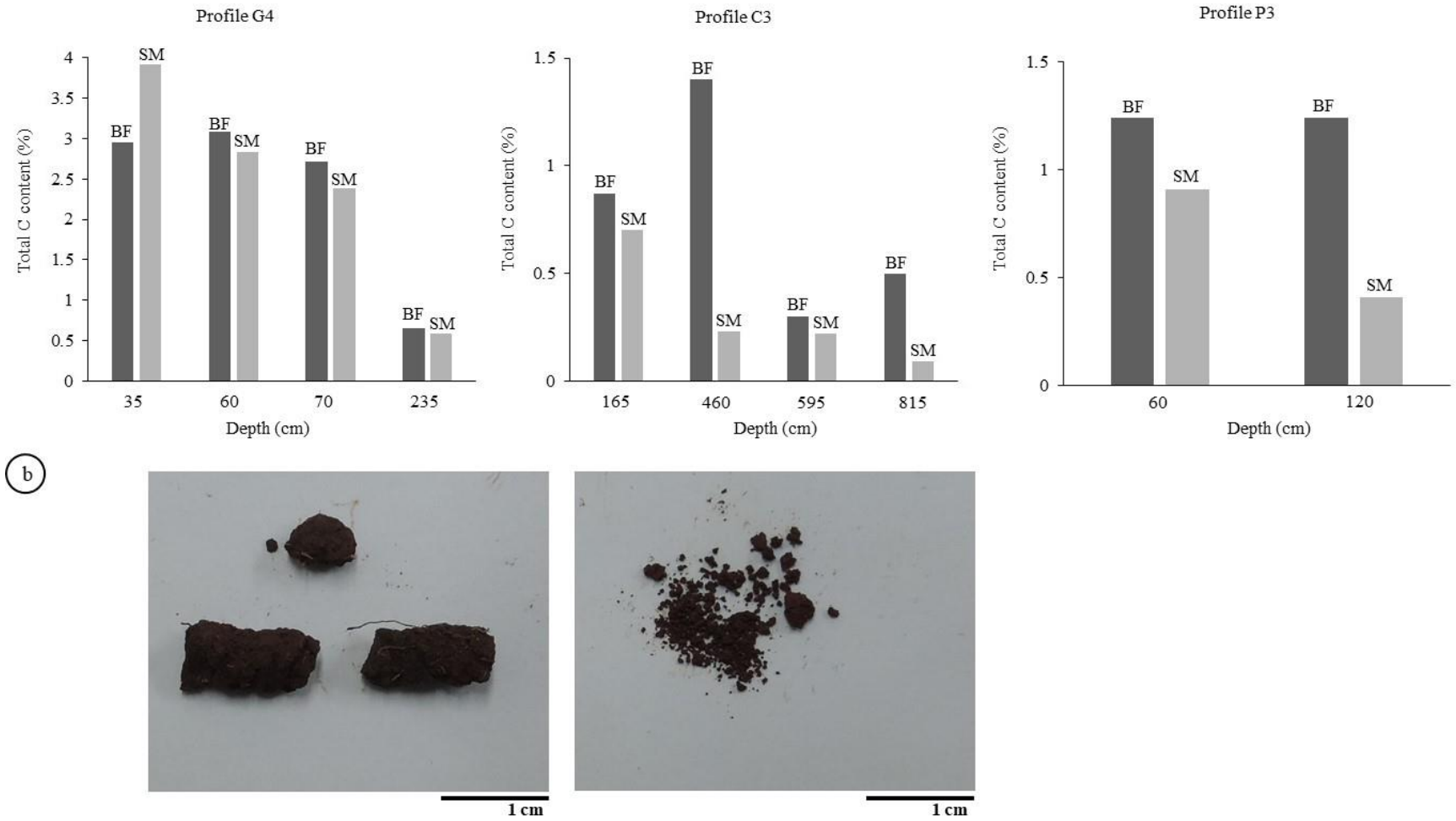

Figure 31. Total C content (%) of the biofeatures collect from three representative soil profiles and total C content (%) of the surrounding soil matrix (a); Examples of krotovinas (dense and loose infillings) collected in the fildwork fom the studied soil profiles (b).

3.5.2.2. Biomantle

The biomantle definition used here is based on the studies of Johnson (1990; 2002), Humphreys (1994), Paton et al. (1995) and Johnson et al. (2005b; 2005c). According to these authors, the biomantle is the differentiated zone in upper part of the soil produced by the bioturbation process containing at least 50% of BFs. In addition, the biomantle can be classified in seven types, such as: 1) one-layered faunalmantle; 2) two-layered faunalmantle; 3) multilayered faunalmantle; 4) one-layered floralmantle; 5) two-layered floralmantle; 6) multilyered floralmantle; and 7) complex biomantle (conjoined or coevolved faunalmantles and floralmantles). The identification and classification of biomantle will be done on a microscale, because in the macroscale was not possible to clearly identify horizons/layers with more than 50% BFs.

The biomantles on a microscale (layers with ≥ 50% of BFs or bioturbation (%); Johnson et al., 2005b; 2005c) can be observed down to 150 cm, 160 cm, 100 cm and 230 cm in the Guarapuava profiles G1–G4, respectively. In the Cascavel profiles, the biomantle reaches until 160 cm, 190 cm and 830 cm in C1, C2 and C3, respectively. In contrast, the biomantle in the Palotina soil profiles were observed down to 460 cm, 670 cm and 290 cm in P1, P2 and P3, respectively (Figure 30). The studied soil profiles presented one layered and homogeneous complex biomantles because of the occurrence of fauna and flora BFs in the same soil profile and the same depth (Johnson, 1990). The water content and oxygenation fluxes in addition to the presence of roots and vegetation type can influence the variations in the depth of the biomantle and bioturbation (%) in the soil profiles. The high presence of roots and the availability of plant material, as well as, high rates of oxygenation and water content favour the concentration of the bioturbation process at up two meters depth. The action of the roots create pores and preferential paths for the occupation and later homogenization of the fauna (Bachelier, 1978; Humphreys, 1995; Rodrigues, 2019). However, below 200 cm of deep, fauna and root activity (current and past) is still very expressive and intense, mainly in the Cascavel and Palotina soils, even with the reduced presence of roots and total C content. In these areas, the edaphic current and even paleoconditions seems to control the activity of the fauna in the subsurface, as well as, the intrinsic characteristics of each bioturbating agent (Wilkinson et al., 2009).

Our results demonstrate that the biomantle concept extends to several meters deep (~7 m) in clayey ferralsols under subtropical conditions. This contrasts with the studies by

Humphreys (1993) in soils located in subtropical climate, where he observed the presence of biomantle occurring at a depth of 37 cm and fauna activity down to 100 cm.

3.5.3. Origin of soil microaggregates: a long-term bioturbation process indicated by short-term biofeatures

3.5.3.1. Soil micromorphology evidence

Soil profile G4: the micromorphology description is shown in Appendix M. Two distinct zones in the BC_r horizon were described. The first zone, occupying 48% of the thin soil section, characterized by the yellow blocks of altered soil matrix with conserved parent material structure. The second zone was characterized by the decrease in the altered blocks of the parent material and the formation of a fine red porphyric material and an incipient microstructure with loose discontinuous/continuous infillings. Some blocks of the altered parent material showed rounded iron concentrations, dissolution cavities and pedoplasmation (Delvigne, 1998; Stoops et al., 2018) (Figure 32). The rounded iron concentrations varied from 0.3 to 0.02 mm in diameter, indicating a mobilization of iron during the weathering process. The incipient microstructure showed subangular blocky aggregates and polyhedral microaggregates (Figure 32). The polyhedral microaggregates varied from 0.6 to 0.3 mm in diameter. In the BC_2 and BC_1 horizons, the porphyric related distribution is individualized by cracks (fissures) forming the polyhedral microaggregates with the diameter varying from 1.4 to 0.1 mm. Zones with enaulic related distribution and microgranular structure were observed. The microgranular structure (the microaggregates) of the enaulic zones are characterized by oval granular, polyhedral and complex morphology with diameter varying from 0.03 to 1.4 mm (Figure 33). The same situation was observed in the Bfl_3, Bfl_2, Bfl_1 and A_3 horizons, where the soil matrix was characterized by a porphyric-enaulic related distribution in the Bfl_3 horizon and enaulic-porphyric in the Bfl_2, Bfl_1 and A_3 horizons. In the enaulic domains, different microaggregates were observed: oval granular, polyhedral and complex microaggregates varying from 0.06 to 1.2 mm in diameter. In the Bfl_2 horizon, lithorelicts were described with rounded iron concentrations, similar to those found in the BC_r horizon. On the upper horizon (A_3), the coalescence of complex, polyhedral and oval microaggregates was observed (Figure 33). Polyconcave vughs, chambers, cracks, mamelonar and biological vughs were observed in the porphyric related distribution, and packing voids dominate the

enaulic domains. The speckled b-fabric is common in the soil horizons, porostriated and granostriated b-fabrics occurred in the BC_1, BC_2 and Bfl_1 horizons.

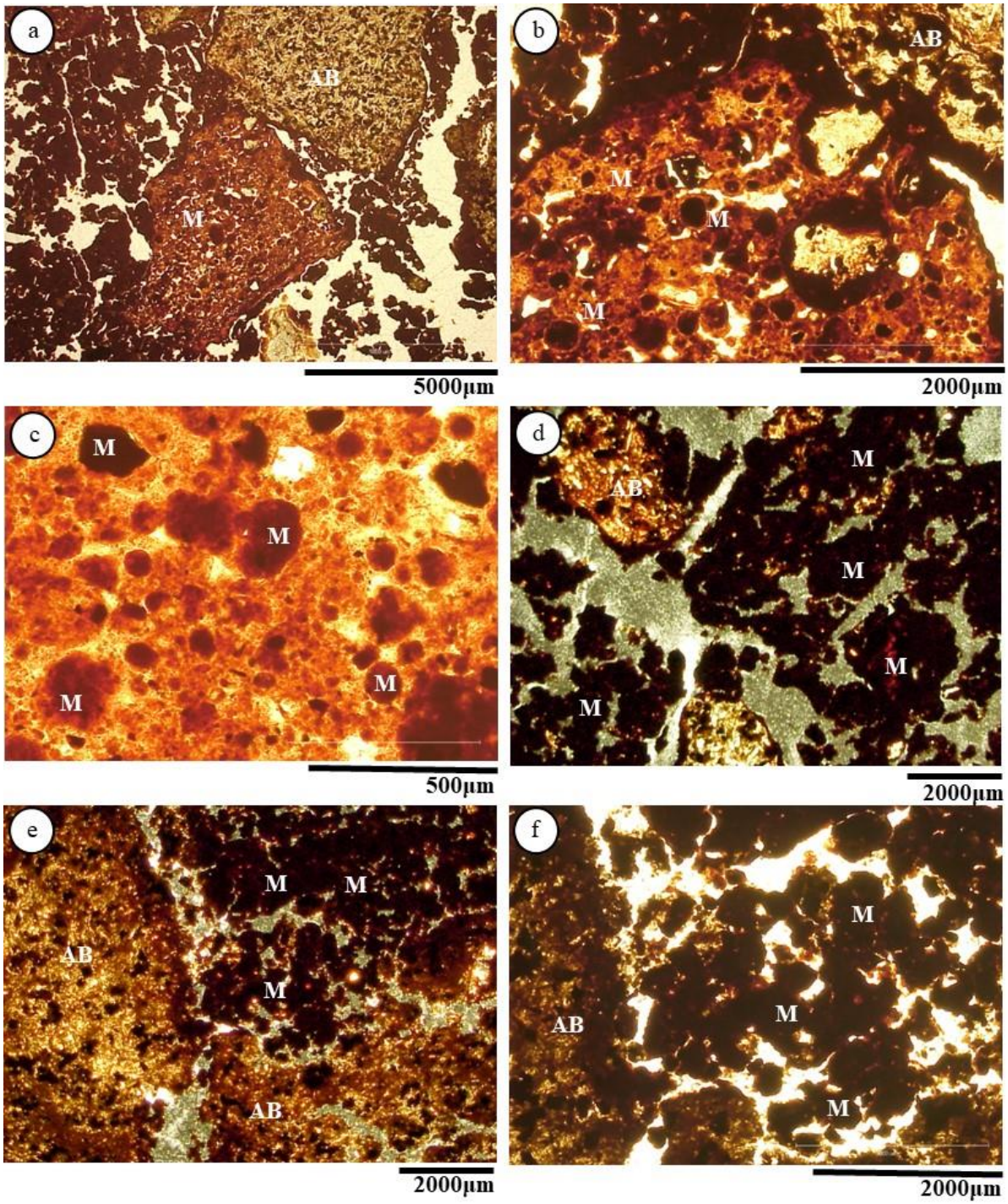

Figure 32. Photomicrographs from the weathering front (360 cm deep) from the Guarapuava G4 profile at (BC_r horizon). a) geochemical formation of rounded microaggregates inside the altered basaltic rock fragment, PPL; b) detailed of the geochemical rounded microaggregates inside the altered basaltic rock fragment, PPL; c) detailed of the geochemical rounded microaggregates inside the altered basaltic rock fragment, PPL; d) and e) altered basaltic rock fragment with the formation of polyhedral microaggregates, XPL; f) detailed of the altered basaltic rock fragment with formation of polyhedral microaggregates, PPL; AB = altered basalt; M = microaggregates.

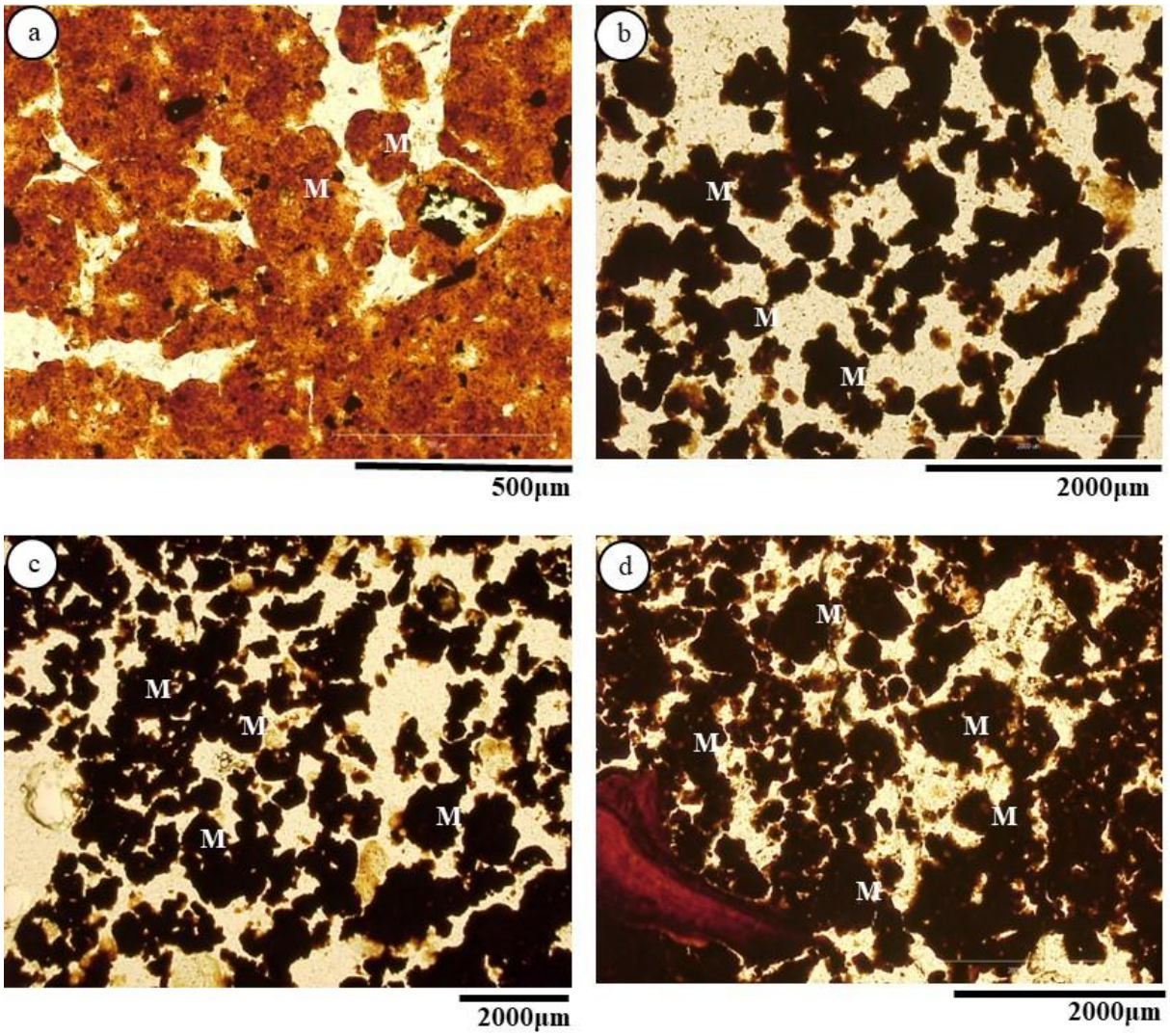

Figure 33. Photomicrographs from Guarapuava G4 profile. a) Photomicrograph from the BC_2 horizon (~330 cm deep), showing the porphyric course/fine related distribution with polyhedral microaggregates, PPL; b) photomicrograph from the Bfl_3 horizon (~200 cm deep), showing polyhedral and rounded microaggregates, PPL; c) photomicrograph from the Bfl_1 horizon (~150 cm deep), showing polyhedral, rounded and complex microaggregates, PPL; d) photomicrograph from the A_3 horizon (~65 cm deep), showing a coalescence of polyhedral, rounded and complex microaggregates, PPL; M = microaggregates.

Soil profile C3: the description of the micromorphology is shown in Appendix N. The BC_r horizon presented two distinct zones, one with the altered parent material with conserved structure of rock minerals occupying 60% of the thin soil section. The second zone was characterized by the formation of the fine red porphyric matrix and microstructure with loose continuous/discontinuous infillings. Dissolution cavities and pedoplasmation were observed similar to soil profile G4. The iron concentrations were observed with an irregular morphology (Figure 34a–b). Oval granular/rounded microaggregates were observed inside the loose infilling of the altered parent material in the second zone, varying from 0.04 to 1.0 mm in diameter (Figure 34c, e and f). Furthermore, polyhedral microaggregates were observed in

the second zone varying from 0.2 to 1.6 mm in diameter (Figure 34d). BC_2 and Bfl_4 horizons showed a porphyric related distribution with loose continuous/discontinuous infillings (Figure 35). Polyhedral microaggregates varying from 0.2 to 1.3 mm in diameter, oval granular from 0.08 to 0.4 mm and complex microaggregates varying from 0.1 to 0.3 mm were observed in the BC_2 horizon. The same microaggregates morphology were observed in the Bfl_4 horizon, varying from 0.3 to 0.7 mm in diameter in polyhedral microaggregates, in the oval granular microaggregates the diameter varied from 0.1 to 0.6 mm and in the complex ones the diameter varied from 0.3 to 0.9 mm. The transition between the Bfl_4 to Bfl_3 horizon was characterized by the passage of a porphyric to enaulic related distribution with the same types of microaggregates, commonly oval granular/rounded and complex ones. In the Bfl_1 and AB horizons the related distribution was enaulic with isolated porphyric domains (enaulic-porphyric related distribution) and coalescence of the microaggregates. The packing voids dominated the Bfl_3 horizon and the enaulic domains of the other horizons. Chambers, polyconcave, mamelonar and biological vughs, channels and fissures dominated the porphyric related distribution. Speckled b-fabric is common in soil horizons, porostriated and granostriated b-fabrics occurred in the BC_2 and Bfl_1 horizons.

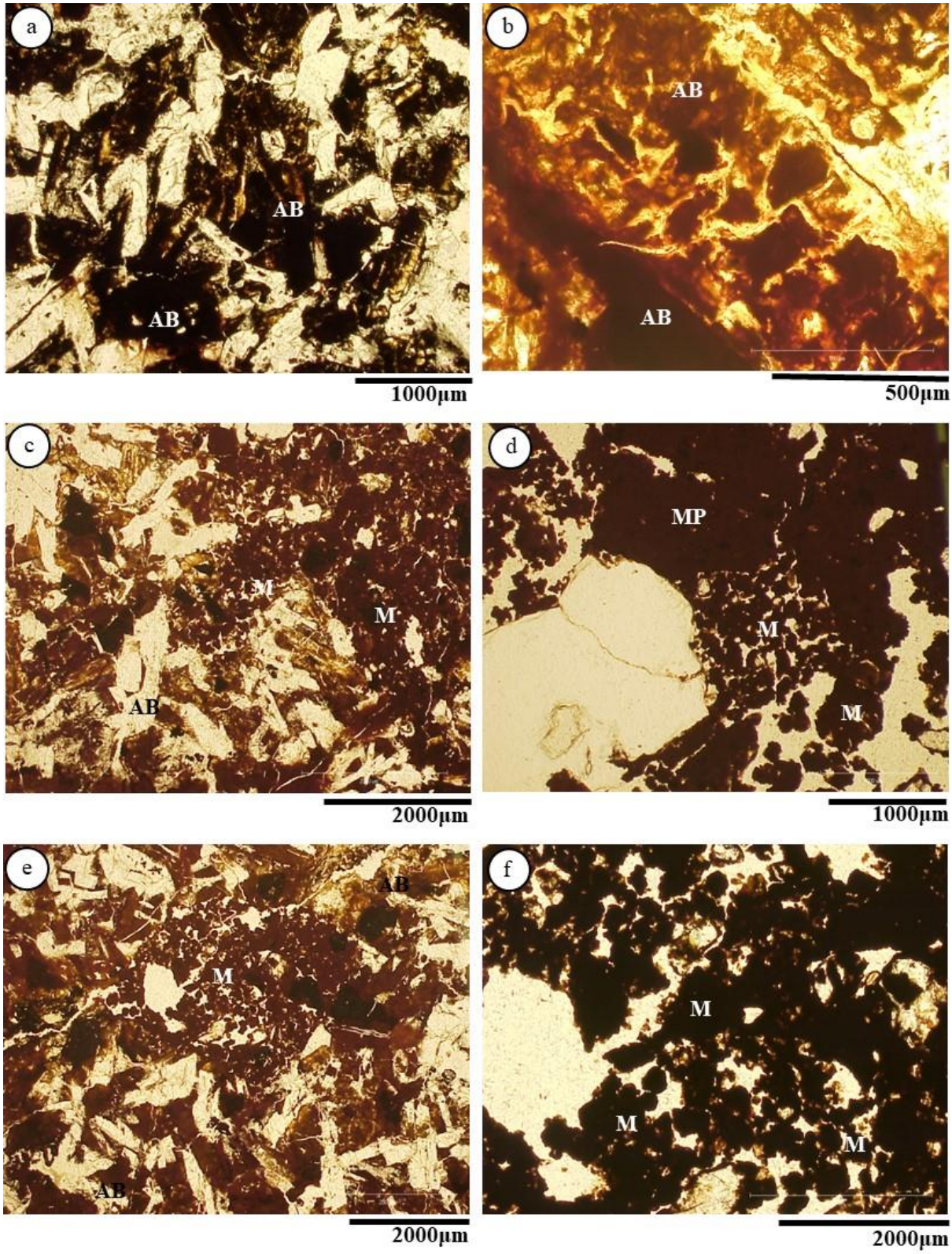

Figure 34. Photomicrographs from the weathering front (1020 cm deep) from the Cascavel C3 profile (BC_r horizon). a) altered basaltic rock fragment, PPL; b) detailed of altered basaltic rock fragment, PPL; c) geochemical formation of rounded microaggregates inside the altered basaltic rock fragment, PPL; d) polyhedral microaggregates, PPL; e) rounded microaggregates formed by biological activity, PPL; f) detailed of rounded microaggregates formed by biological activity (soil fauna), PPL; AB = altered basalt; M = microaggregates; MP = porphyric matrix.

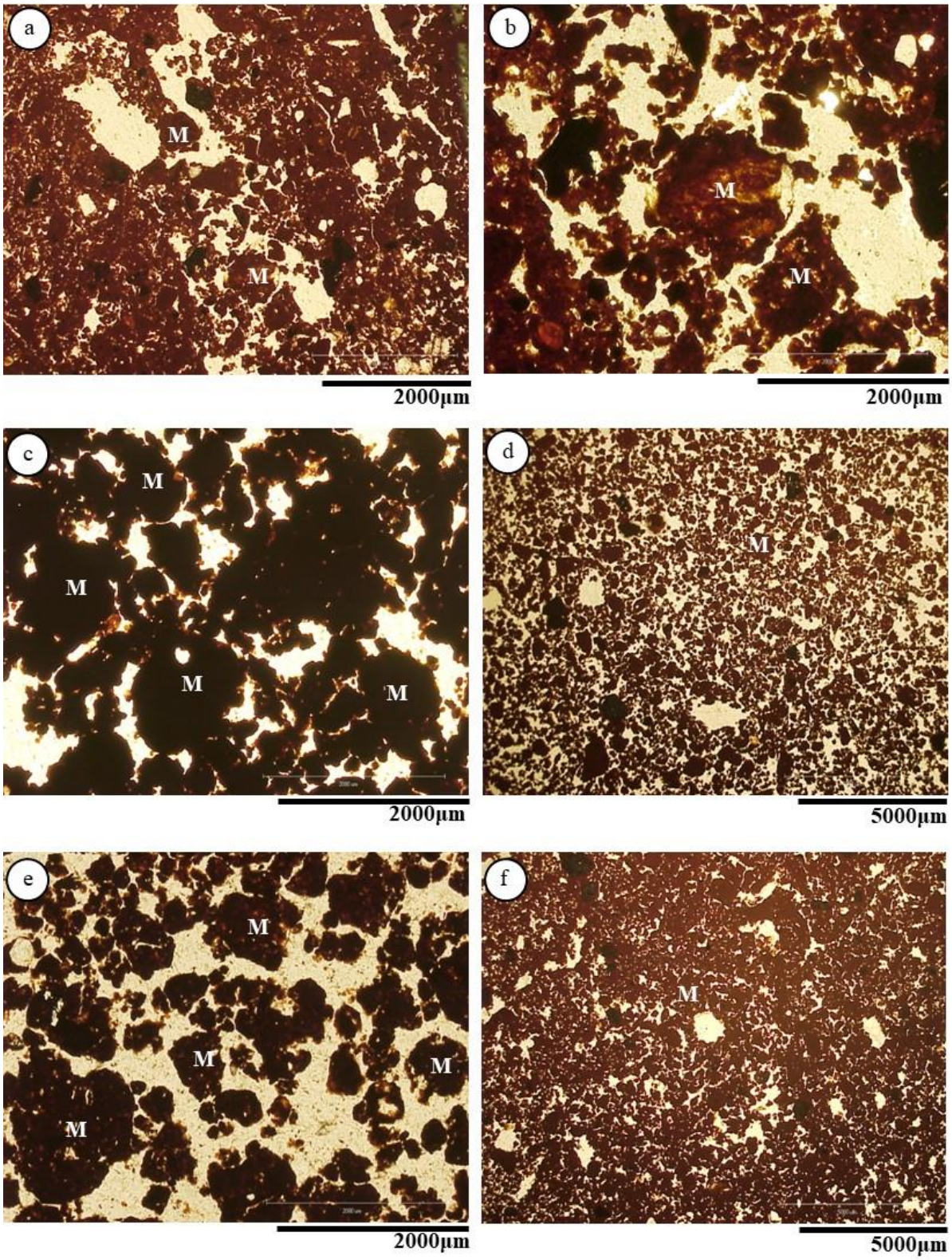

Figure 35. Photomicrographs from C3 profile (Cascavel); a) photomicrograph from the BC_2 horizon (~950 cm deep), showing polyhedral microaggregates formed by fragmentation of porphyric matrix in a channel (drainage channel), PPL; b) detail of the polyhedral microaggregates in a channel (drainage channel), PPL; c) photomicrograph of the Bfl_3 horizon (~600 cm deep), showing polyhedral, rounded and complex microaggregates, PPL; d) photomicrograph of the Bfl_2 horizon (~350 cm deep), showing polyhedral, rounded and complex microaggregates, PPL; e) detail of the polyhedral, rounded and complex microaggregates from the Bfl_2 horizon (~350 cm deep), PPL; f) photomicrograph from the BA horizon (~115 cm deep), showing the coalescence of polyhedral, rounded and complex microaggregates, PPL; M = microaggregates.

Soil profile P3: the micromorphology description is shown in Appendix O. The BC_r horizon presented two distinct zones, similar to BC_r horizon from the C3 soil profile. Altered parent material with preserved rock mineral structure occupied 58% of the thin section with rounded iron concentrations, dissolution cavities and pedoplasmation characterized the first zone. The second zone was characterized by the development of red porphyric soil matrix and microgranular structure inside the loose continuous/discontinuous infillings (Figure 36). The Bfl_7 horizon presented a porphyric related distribution with block structure and some zones with enaulic domains. Polyhedral, oval granular and complex microaggregates were observed in the Bfl_7 horizon varying from 0.1 to 0.5 mm, from 0.03 to 0.3 mm and from 0.1 to 0.3 mm in diameter, respectively. The transition between Bfl_7, Bfl_6 with Bfl_5, Bfl_4 and Bfl_2 horizons were characterized by the change of a porphyric to enaulic-porphyric related distribution with the same three morphological types of microaggregates (Figure 37). The porphyric domains were more common in this soil profile (P3) than in the other two studied profiles (G4 and C3). On the upper horizon, the coalescence of complex, polyhedral and oval microaggregates were observed. Chambers, polyconcave, mamelonar and biological vughs, channels and cracks dominated the porphyric related distribution. The packing voids dominated the enaulic domains. Speckled, porostriated and granostriated b-fabric are common to the soil horizons.

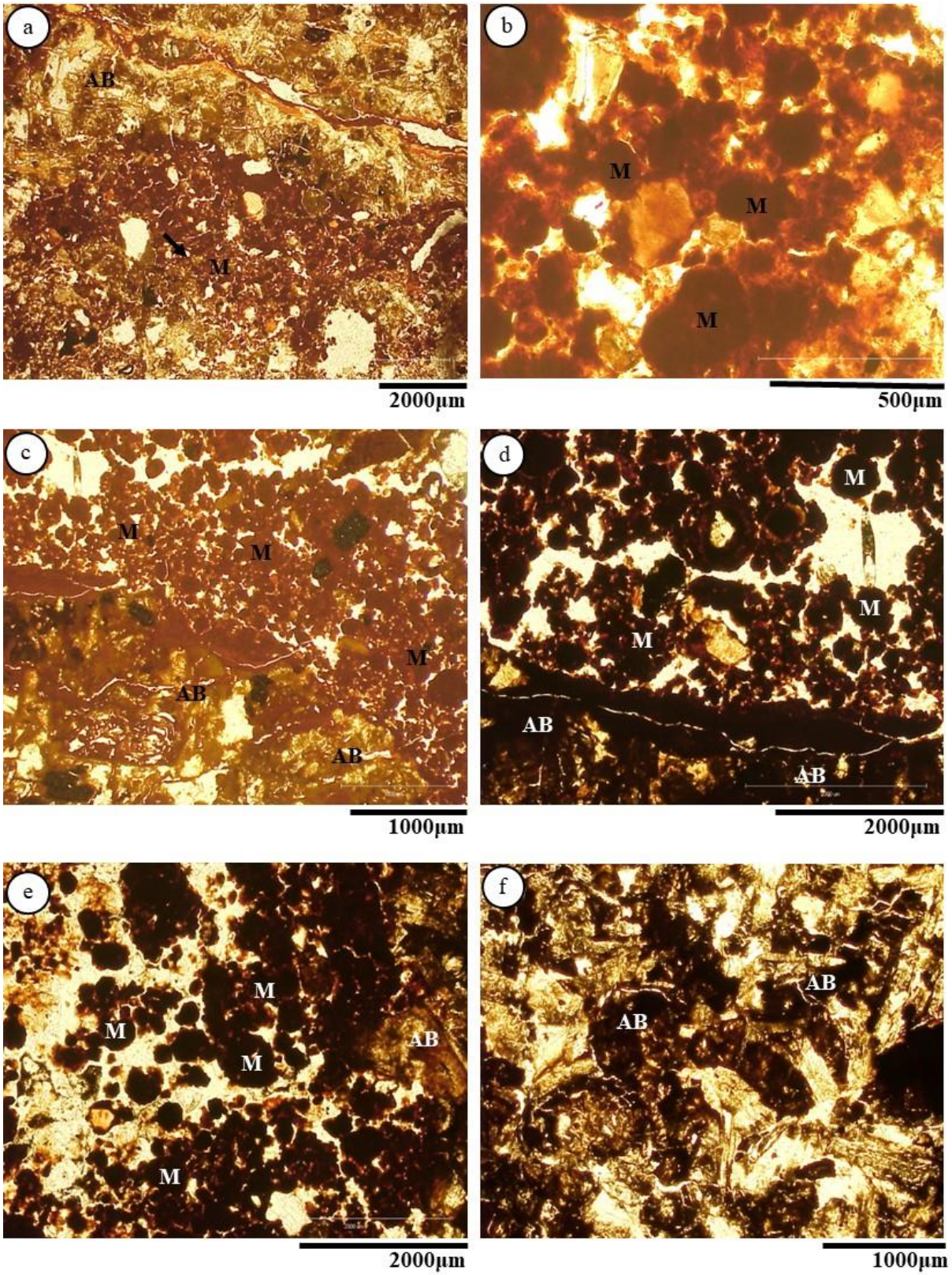

Figure 36. Photomicrographs from the weathering front (640 cm deep) from the soil profile P3 (horizon BC_r). a) geochemical formation of the rounded microaggregates inside the altered basaltic rock fragment, PPL; b) details of the geochemical formation of the rounded microaggregates inside the altered basaltic rock fragment, PPL; c) polyhedral and rounded microaggregates separating from the weathered basaltic fragment, PPL; d) details of polyhedral and rounded microaggregates separating from the weathered basaltic fragment PPL; e) rounded and polyhedral microaggregates separating from the weathered basaltic fragment, PPL; f) basaltic rock fragment in alteration PPL; AB = altered basalt; M = microaggregates.

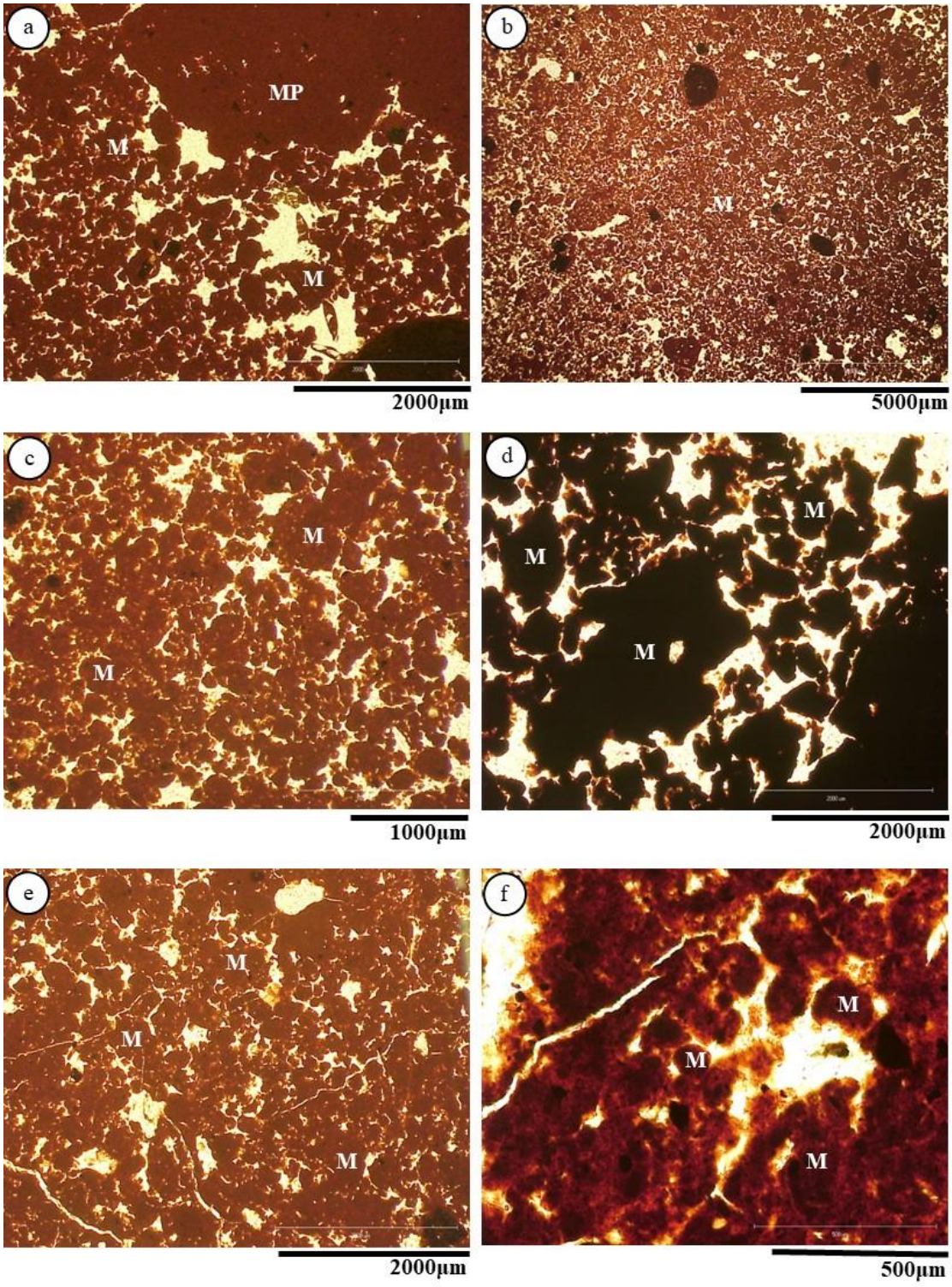

Figure 37. Photomicrographs from P3 profile (Palotina). a) photomicrograph from the BCr horizon (~600 cm deep), showing the polyhedral microaggregates originated by the mechanical fracturing of the porphyric matrix, PPL; b) photomicrograph from the Bfl4 horizon (~150 cm deep), showing polyhedral, rounded and complex microaggregates, PPL; c) detail of the polyhedral, rounded and complex microaggregates from the Bfl4 horizon (~150 cm deep), PPL; d) detail of the polyhedral and rounded microaggregates from the Bfl4 horizon (~150 cm deep), PPL; e) photomicrograph of the Bfl2 horizon (~50 cm of deep), showing a coalescence of polyhedral and rounded microaggregates, PPL; f) detail of the coalescence of polyhedral and rounded microaggregates from the Bfl2 horizon (~50 cm of deep), PPL; M = microaggregates; MP = porphyric matrix.

3.5.3.2. Origin of the soil microaggregates

Three morphological types of microaggregates were identified in the studied soil profiles: oval granular/rounded, polyhedral and complex microaggregates. The oval granular and complex microaggregates predominate in relation to the polyhedral type.

The polyhedral microaggregates were formed by the individualization/fissuration of the porphyric matrix, resulting from the expansion and contraction of the soil material into smaller aggregates due to alternating wet and dry conditions. A similar process of polyhedral microaggregates formation was reported by Muller (1977), Trapnell and Webster (1986), Bitom and Volkoff, (1991), Vidal-Torrado (1999) and Cooper et al. (2005). According to Cooper et al. (2005), the presence of polyhedral microaggregates inside the loose continuous/discontinuous infillings and enaulic domains is the result of pedoturbation after the porphyric soil matrix fissuration.

The oval granular microaggregates, similar with those observed by Cooper et al. (2005), did not showed sorted quartz grains distributed in their interior. The formation of these microaggregates as mentioned by these authors is uncertain, and could be zoogenetic (biological) and/or geochemical. The rounded iron concentrations inside the weathered parent material, observed in the BC_r horizon of the G4, C3 and P3 soil profiles were considered as geochemical microaggregates (Figures 32, 34 and 36). According to Chauvel et al. (1978), Pedro et al. (1976), Cambier and Prost (1981), Cambier (1986), Dexter (1988) and Santos et al. (1989) the geochemical origin of the oval granular (rounded) microaggregates occurs from physical-chemical interactions between the secondary minerals (iron hydro (oxide), gibbsite and kaolinite) exposed to high weathering and drainage conditions under wetter climatic conditions. In addition, Muller (1977) pointed out that the geochemistry formation could be a simple rearrangement of the plasma with colour changes reflecting a possible movement of iron, which is common in the studied soils in the BC_r horizon. Furthermore, some lithorelicts with rounded concentrations of iron (oval granular microaggregates) observed in the Bfl_2 horizon from the G4 soil profile, according to Muller (1977) can be considered relict microaggregates, residues of the weathering of the parent material.

On the other hand, the zoogenetic origin of the oval granular microaggregates has been reported by Eschenbrenner (1986), Miklós (1992), Schaefer (2001) and Cooper et al. (2005), but the five characteristics pointed out by the Miklós (1992), only the shape and size were described in our soil microaggregates. The presence of neostrians on the periphery of the

microaggregates, different coloured microaggregates and well-sorted coarse material in the interior of the microaggregates were not described here. In addition, as reported by Cooper et al. (2005), the high iron content could mask the neostrians in the microaggregates; the clayey soil material with a lower carbon content could influence the lack of a different colour and well-sorted quartz grains inside the microaggregates. With this, the origin of oval granular microaggregates in the studied ferralsols is difficult to determine, and here we considered: a geochemical origin for the oval granular microaggregates in the BC_r horizon; a zoogenetic origin of the microaggregates in the biological pores inside the BC_r horizon and zoogenetic origin of the microaggregates in the ferralic horizons, mainly the microaggregates inside the loose infillings and enaulic domains.

Complex microaggregates are common in the ferralic and upper horizons often associated with biological features, such as loose continuous and discontinuous infillings, and enaulic domains. The origin of these types of microaggregates can be associated with the aggregation of smaller microaggregates and when more than one process occurred (Muller, 1977; Vidal-Torrado, 1994). The ant (micro) aggregates (irregular shape with serrate/mammilate roughness) produced by our lab experiment showed an aggregation of smaller microaggregates, and their similarities with soil microaggregates inside the loose infillings (Figure 29), suggests that the action of ants in soils can produce complex microaggregates assisting pedoturbation and reworking the previously produced microaggregates originated from other processes beyond the control section.

4. FINAL CONSIDERATIONS

Old landscapes usually present ferralsols with very complex histories, because of the extremely long and contrasting periods during soil formation. Due to the uncertainties about the distinction between the soil formation phases, these soils are considered polygenetic (Duchaufour, 1988; Johnson et al., 1990; Muggler, 1998).

The ferralsols studied in the Paraná Magmatic Province have been developing since at least the Quaternary (Late Pleistocene), responding to climatic changes. The evidence of parent material uniformity in the studied profiles suggests that our soils do not present lithological discontinuity, emphasizing the homogeneity of soil material. Thus, the studied ferralsols are developed *in situ* from basaltic and rhyo-dacitic rocks, without the contribution of allochthonous material, which allows a continuous interpretation from the surface to the weathering front. Furthermore, these observations allows the assertion that the soils may have evolved according to morphoclimatic processes (Bigarella and Andrade, 1965), with the humid epochs favouring the development of thick regoliths by the etchplanation process (Büdel, 1982). Thus, chemical weathering acts constantly at high intensity in the wet periods and during relative tectonic stability, creating a thick weathering mantle that suffered laminar erosion later. In addition, the dissection of the relief would have been conditioned by the morphological and the structural differences presented by the flood basalts (Silva et al., 2021), in association with recent tectonic (Riffel et al., 2016; Peyerl et al., 2018), which were more evident in the Guarapuava region.

Considering a temporal scale of formation of ferralsols, the ferralitization process can be considered as a long-term formation process, together with the bioturbation. However, as the evidences of the bioturbation process are considered short-term, in this work we consider the bioturbation process to be a short-term process. In addition to these two pedogenetic processes, the melanization, were considered a short-term pedogenetic process, and the rubification and brunification processes as long-term one. We still observed the processes of contraction and expansion and formation of microaggregates that can be considered both long and short-term pedogenetic processes. With this, the most evident of a long and short-term pedogenetic processes in the studied ferralsols are ferralitization, bioturbation, melanization, moderate-weak shrinking/swelling, brunification, rubification and microaggregate formation.

The pedogenetic processes of brunification and rubification were observed in the soils of the Paraná Magmatic Province. The rubification process which is expressed by the reddish colour, due to the presence of hematite in the studied profiles of Cascavel, Palotina and in deeper horizons of Guarapuava profiles, originate from the weathering of the parent material rich in Fe-bearing primary minerals (mainly pyroxenes) under conditions of free drainage, which hematite accumulate due to the ferralitization process. Associated to the rubification in deep, the brunification process occurred only in the Guarapuava at the upper part of the profiles. The climatic conditions with lower temperature and high precipitation favours the formation of a profundihumic A horizon (varying from 75 to 120 cm of thickness), the melanization process and goethite and hematite occurrence at Guarapuava site, characterizing the brunification process.

Pedological features such as iron and dense clayey nodules are present in the studied soils of the Paraná Magmatic Province and both features decreasing the size towards soil surface and were developed *in situ* showing a hierarchical affiliation. The iron nodules are a heritage of the wetter periods and redoximorphic conditions of the weathering front. The decreasing the size towards soil surface is probably promoted by the gradual dissolution and mixing caused by the activity of soil fauna. On the other hand, the dense clayey nodules are a result of porphyric soil matrix fissuration with the mechanic and geochemical evolution of soil structure and also the bioturbation process. Therefore, dense clayey nodules are also considered a heritage of the weathering of the parent material (from the intense pedoplasmation originating a very dense porphyric matrix), which affiliation can only be identified by the investigation from the soil surface to weathering front. Thus, the dense clayey and iron nodules are not evidence of weathered reworked materials.

Contrasting chemical characteristics were observed in the study ferralsols. Geric and eutric properties occurred in the Guarapuava/Cascavel and Palotina profiles, respectively. We hypothesized that the eutric property observed in the Palotina soil profiles resulted from partial ferralitization combined with the more effective cycling of Ca and Mg performed by a higher activity of roots of past vegetation (C_4 plants) under a drier climate, and the role of the microaggregates protecting Ca and Mg from the leaching process. This can only be hypothesized because we analysed the profile from the surface to the weathering front, because this issue is often discussed in soil profiles down to 200 cm in the literature. On the other hand, the geric property observed in some soil profiles from Guarapuava and Cascavel resulted from more intense ferralitization. A common mineralogy observed in ferralsols with

geric properties in the literature is the predominance of Gb (values up to 30% of the clay fraction), and minor values of Kt, Hm and Gt, which were not observed in the kaolinitic ferralsols from the Paraná Magmatic Province.

The mineralogical assemblage of the clay fraction of the ferralsols presented Kt, Gb, Hm, Gt, maghemite, hydroxy-interlayered 2:1 mineral, anatase, rutile, ilmenite and quartz. The occurrence of quartz was identified in basalt as acessory mineral and in the weathering front thin sections, varying in size where the coarse fragments are related to the presence of amygdaloidal basalt levels filled with quartz/chalcedony. Kaolinite is the main component of the clay fraction and differed between profiles and depth, which is primarily related to the geochemical composition of the parent material and secondarily to the climatic conditions across the time gradient. The hydroxy-interlayered 2:1 minerals (2:1 HI) were not quantified, but the intensity of 2:1 HI peaks increases in samples from the bottom to the top in all the soil profiles. The presence of 2:1 HI mineral probably causes an anti-gibbsite effect (Jackson, 1963), justifying the lower content of Gb compared to kaolinite. Hematite and goethite are the predominant iron oxides in the clay fraction. The drier periods and the high levels of iron released from the parent material favoured the formation of hematite and the high quantified values mainly in Guarapuava profiles. Thus, the Hm content observed in soil profiles enhance the likely polygenetic history of study soils. The quantitative mineralogical data from the studied ferralsols presented a predominance of Kt and variable contents of Gb, Hm and Gt, characterizing an environment of moderate ferralitization under subtropical climates (CFb–CFa).

The bioturbation process varied between the studied areas and depth until reaching the weathered front. Bioturbation was more intense in the Palotina soil profiles, followed by Cascavel and Guarapuava, and in the upper 2 meters. Environmental conditions seem to interfere with the activity of soil fauna. Zones with high bioturbation were observed throughout the study profiles, certainly associated with drier environmental conditions, with the predominance of grasslands and *Cerrado*. Furthermore, the presence of biofeatures below the control section (two meters deep) suggests that the bioturbation process is controlled by edaphic (soil moisture) and environmental (precipitation and temperature) conditions, as well as, the intrinsic characteristics of each bioturbating agent. Biofeatures from epigeic, endogeic and anecic organisms were observed in the soil profiles. The biofeatures of the main bioturbating agents, such as roots, earthworms, termites, ants, acari and enchytraeids were identified characterizing the occurrence of one layered and homogeneous complex biomantles

in the ferralsols from the Paraná Magmatic Province. The biomantle of the studied clayey ferralsols under subtropical climate extends to several meters deep (~7 m) differing from biomantles studied in the same climatic zone, which studies have observed its occurrence down to 100 cm. Biofeatures of some bioturbating agents have been identified occurring in depths that are not common, such as the earthworm biofeatures below six meters deep. In addition, the presence of biofeatures below the control section also suggests that the bioturbation process occurred at least since the Late Pleistocene in the studied ferralsols and part of these biofeatures can persist for a long time in deep soil horizons.

The formation of the soil microaggregates is complex. In the weathering front of the basaltic weathered blocks (BCr horizons) the geochemical origin of the rounded/oval granular microaggregates was observed. Furthermore, the occurrence of polyhedral and rounded/oval granular microaggregates in the weathering front was observed, originating from the mechanical individualization/fissuration of porphyric matrix (physical origin) and the action of soil fauna (zoogenetic origin), respectively. Thus, the origin of soil microaggregates in the weathering front is not only of geochemical origin as initially hypothesized, but also a zoogenetic and physical origin. The microaggregates formed in the weathering front are reworked, remodeled and moved by the soil fauna into different soil depths. Thus, in the most bioturbed horizons, there is a common occurrence of polyhedral microaggregates of physical origin, rounded microaggregates of zoogenetic origin, and complex microaggregates, suggesting that more than one process occurred in their formation. In addition, complex microaggregates originating from the aggregation of smaller microaggregates and from ant activity were also observed in horizon with very intense bioturbation.

The most recent evidence of a short-term pedogenetic process in the studied ferralsols are the nature and dynamics of SOM, which played an important role in understanding the past vegetation and the climate that influenced part of the genesis of the ferralsols in the Paraná Magmatic Province. With this, the SOM of the PMP ferralsols can be used as environmental records down to the deepest horizons. In addition, from the molecular study of the SOM of the ferralsols it was possible to confirm that these soils are large carbon reservoirs, presenting the expected SOM decomposition process with depth and between the study areas. SOM was also influenced by the climatic changes since the Late Pleistocene, recording the driest periods with C_4 plants and highest contributions (%) of fire-affected compounds present in the ferralsols.

REFERENCES

Ab'Sáber, A. N., 1969. Megageomorfologia do território brasileiro, in A. J. T. Cunha, Sandra Batista; Guerra (Eds.), Geomorfologia do Brasil. Rio de Janeiro: Bertrand Brasil, pp. 71–106.

Alleoni, L. R. F., Camargo, O. A., 1995. Óxidos de ferro e de alumínio e a mineralogia da fração argila deferrificada de Latossolos ácricos. Sci. Agric. 52, 416–421.

Almeida, J.R., 1979. Cronocromosequência de solos originários de rochas pelíticas do Grupo Bambuí. Dissertação de mestrado. Universidade Federal de Viçosa, UFV.

Alves, M. E., Mascarenhas, Y. P., Vaz, C. M. P., 2008. Comparação de procedimentos de quantificação de caulinita e gibbsita na fração argila desferrificada de Latossolos. R. Bras. Ci. Solo 32, 569–577.

Anda, M., Chittleborough, D. J., Fitzpatrick, R. W., 2009. Assessing parent material uniformity of red and black soil complex in the landscapes. Catena 78, 142–153.

Anderson, S. P., Dietrich, W. E., Brimhall, G. H., 2002. Weathering profiles, mass balance analysis, and rates of solute loss: linkages between weathering and erosion in a small, steep catchment. Geol. Soc. Am. Bull. 114, 1143–1158.

Andrade, G. R. P., Azevedo, A. C., Lepchak, J. K., Assis, T. C., 2019. Weathering of Permian sedimentary rocks and soil clay minerals transformations under subtropical climate, southern Brazil (Paraná State). Geoderma 336, 31–48.

Anjos, L. H. C., Jacomine, P. K. T., Santos, H. G., Oliveira, V. A., Oliveira, J. B., 2012. Sistema Brasileiro de Classificação de solos, in: Ker, J. C., Curi N., Schaefer, C. E. G. R., Vidal-Torrado, P. (Eds.), Pedologia: Fundamentos. Viçosa: Sociedade Brasileira de Ciência do Solo, pp. 303–343.

Aubert, G. 1963. Soil with ferruginous or ferrallitic crusts of tropical regions. Soil Sci. 95, 235–242.

Aubert, G., Segalen, P. 1966. Projet de classification des sols ferrallitiques. ORSTOM, sér. Pédol., 4, 97–112.

Babel, U., 1975. Micromorphology of soil organic matter, in: Gieseking, J.E. (Ed.), Soil Components, Vol. 1. Organic Components. Springler, Berlin, pp. 369–473.

Bachelier, G. 1978. La faune des sols. Son ècologie et son action, ORSTOM, Paris.

Barros, E., Curmi, P., Hallaire, V., Chauvel, A., Levelle, P., 2001. The role of macrofauna in the transformation and reversibility of soil structure of an oxisol in the process of forest to pasture conversion. Geoderma 100, 193–213.

Barthès, B.G., Kouakoua, E., Larré-Larrouy, M.-C., Razafimbelo, T.M., Luca, E.F. de, Azontonde, A., Neves, C. S. V. J., Freitas, P.L. de, Feller, C.L., 2008. Texture and sesquioxide effects on water-stable aggregates and organic matter in some tropical soils. Geoderma 143, 14–25.

Behling, H., 2002. South and southeast Brazilian grasslands during Late Quaternary times: a synthesis. Palaeogeogr. Palaeoclimatol. Palaeoecol. 177, 19–27.

Behling, H., 1998. Late Quaternary vegetational and climatic changes in Brazil. Review of Palaeob. Palynol. 99, 143–156.

Behling, H., 1997. Late Quaternary vegetation, climate and fire history in the Araucaria forest and campos region from Serra Campos Gerais (Paran/t), South Brazil. Rev. Palaeobot. Palynol. 97, 109–121.

Behring, S.V., 2007. Mapa de solos do Estado do Paraná. Embrapa Solos, Rio de Janeiro.

Bellieni, G., Comin–CHiaramonti, P., Marques, L. S., Martinez, L. A., Melfi, A. J., Nardy, A. J. R., Papatrechas, C., Piccirillo, E., Roisenberg, A., Stolfa, D., 1986. Petrogenetic aspects of acid and basaltic lavas from the Paraná plateau (Brazil): geological, mineralogical and petrochemical relationships. J. of Petrol. 27, 915–944.

Bellieni, G., Brotzu, P., Comin-Chiaramonti, P., Ernesto, M., Ernesto, M., Melfi, A.J., Pacca, I. G., Piccirillo, E. M., 1984. Flood basalt to rhyolites suites in the southern Paraná plateau (Brazil): paleomagnetism, petrogenis and geodynamic implications. J. Petrol. 25, 579–618.

Bennema, J., 1974. Organic carbon profiles in Oxisols. Pédologie 24, 119–146.

Bertoldo, E. Paisani, J., C., Oliveira, P., E., 2014. Registro de Floresta Ombrófila Mista nas regiões sudoeste e sul do Estado do Paraná, Brasil, durante o Pleistoceno/Holoceno. Hoehnea 41, 1–8.

Besser, M. L., Vasconcellos, E. M. G., Nardy, A. J. R., 2015. Platô de São Joaquim, Província Magmática do Paraná: Feições de Campo e Questões Genéticas. Boletim Paranaense de Geociências 72, 13–28.

Bigarella, J.J., Andrade, G.O., 1965. Contribution the study of the Brazilian Quaternary. The Geolog. Societ.of America, Special Paper 84, 433–451.

Bigarella, J.J. et al., 2003. Estrutura e origem das paisagens tropicais e subtropicais. Ed. da UFSC, Florianópolis.

Bisdom, E. B. A., Ducloux, J., 1983. Submicroscopic studies of soils. Developments in Soil Science, vol. 12. Elsevier, Amsterdam.

Bitom, D., Volkoff, B., 1991. Mise en évidence de deux modes de microstructuration dans une couverture de sols ferralitiques rouges du Sud-Cameroun. Sci. du Sol 29, 289–300.

Boitt, G., 2014. Mineralogia e distribuição das formas de fósforo em Latossolos com diferentes graus de intemperismo. Dissertação de mestrado. Universidade do Estado de Santa Catarina.

Bouché, M. B., 1984. The subterranean behaviour of the earthworm, in: A.M. Bonvicini Pagliai and P. Omodeo (Eds.), On Earthworms, Mucchi, Modena, pp. 159–69.

Boutton, T. W., Archer, S. R., Midwood, A. J., Zitzer, S. F., Bol, R., 1998. $^{\delta}$13C values of soil organic carbon and their use in documenting vegetation change in a subtropical savana ecosystem. Geoderma 82, 5–41.

Boutton, T. W., 1996. Stable carbon isotope ratios of soil organic matter and their use as indicators of vegetation and climate change, in: Boutton, T.W.; Yamasaki, SI. (Eds.), Mass spectrometry of soils. New York: Marcel Dekker, pp.47–82.

Brewer, R., 1976. Fabric and Mineral Analysis of Soils. Robert E. Krieger Publishing Co., New York.

Brimhall, G. H., Dietrich, W. E., 1987. Constitutive mass balance reactions between chemical composition, volume, density, porosity, and strain in metasomatic systems: results on weathering and pedogenesis. Geochim. Cosmochim. Acta 51, 567–587.

Brindley, G. W., Kao, C. C., Harrison, J. L., Lipsicas, M. L., Raythatha, R., 1986. Relation between structural disorder and other characteristics of kaolinites and dickites. Clays Clay Miner. 34, 239–249.

Büdel, J., 1982. Climatic geomorphologie. Tradução de L. Fischer e D. Busche. New Jersey: Princenton University Press.

Bullock, P., Fedoroff, N., Jongerius, A., Stoops, G., Tursina, T., 1985. Handbook for Soil Thin Section Description. Waine Research, Albrington.

Buol, S. W. et al. 2011. Soil-Forming Factors: Soil as a Component of Ecosystems, in: Soil Genesis and Classification. 6 ed. Oxford: Wiley-Blackwell, 89–140.

Buol, S.W., Eswaran, H., 1999. Oxisols. Advances in Agronomy, 68, pp. 151–195.

Buurman, P., Peterse, F., Almendros, G., 2007. Soil organic matter chemistry in allophonic soils: a pyrolysis-CG/MS study of a Costa Rica Andosol catena. Eur. J. Soil Sci. 58, 1330–1347.

Calegari, M. R.; Paisani, S. D. L; Cecchet, F.; Ewald, P. L. de L.; Osterrieth, M. L.; Paisani, J. C.; Pontelli, M. E., 2017. Phytolith Signature on the Araucarias Plateau – Vegetation Change Evidence in Late Quaternary (South Brasil). Quat. Int. 434, 117–28.

Calegari, M.R., Madela, M., Brustolin, L.T., Pessenda, L.C.R., Buso, A.A., Francisquini, M., Vidal-Torrado, P., 2017. Potential of soil Phytoliths, organic matter and carbon isotopes for small-scale differentiation of tropical rainforest vegetation: A pilot study from the campos nativos of the Atlantic Forest in Espirito Santo State (Brazil). Quat. Int. 437, 156–164.

Calegari, M. R., Madella M., Buso, A. A., Osterrieth, M. L., Lorente, F. L., Pessenda, L. C. R., 2015. Holocene Vegetation and Climate inferences from Phytoliths and Pollen from Lagoa do Macuco, North Coast of Espírito Santo State (Brazil). Quat. and Environ. Geosci. 6, 41–50.

Calegari, M. R., Madella M., Vidal-Torrado, P., Pessenda, L. C. R., Marques, F. A., 2013. Combining phytoliths and $\delta^{13}C$ matter in Holocene palaeoenvironmental studies of tropical soils: An example of an Oxisol in Brazil. Quat. Inte. 287, 47–55.

Calegari, M. R., 2008. Ocorrência e significado paleoambiental do Horizonte A húmico em Latossolos. Tese de doutorado. Escola Superior de Agricultura "Luiz de Queiroz", Universidade de São Paulo.

Cambier, P. Organisation des constituants et interactions physicochimiques au sein des microagrégats de sols. Application au système ferralitique kaolinite-oxyde de fer. Paris: Université de Paris.

Cambier, P., Prost, R., 1981. Etude des associations argile-oxyde: organisation des constituants d'un matériau ferrallitique. Agronomie, EDP Sciences 1, 713–722.

Camêlo, D. L., Ker, J. C., Fontes, M. P. F., Costa, A. C. S., Corrêa, M. M., Leopold, M., 2018. Mineralogy, magnetic susceptibility and geochemistry of Fe-rich Oxisols developed from several parent materials. Sci. Agric. 75, 410–419.

Caner, L., Radtke, L. M., Vignol-Lelarge, M. L., Inda, A. V., Bortoluzzi, E. C., Mexias, A. S., 2014. Basalt and rhyo-dacite weathering and soil clay formation under subtropical climate in southern Brazil. Geoderma 235–236, 100–112.

Caner, L., Toutain, F., Bourgeon, G., Herbillon, A.J., 2003. Occurrence of sombric-like subsurface A horizons in some andic soils of the Nilgiri Hills (southern India) and their palaeoecological significance. Geoderma 117, 251–265.

Castro, S. S. de, Cooper, M., 2019. Fundamentos de micromorfologia de solos. Sociedade Brasileira de Ciência do Solo, Viçosa, Minas Gerais.

Chadwick, O. A., Brimhall, G. H., Hendricks, D. M., 1990. From a black to a gray box – a mass balance interpretation of pedogenesis. Geomorphol. 3, 369–390.

Chapman, S. L., Horn, M. E., 1968. Parent material uniformity and origin of silty soils in northwest Arkansas based on zirconium–titanium contents. Soil Sci. Soc. Am. Proc. 32, 265–271.

Chauvel, A., Pedro, G., 1978. Genèse de sols beiges (ferrugineux tropicaux lessivés) par transformation des sols rouges (ferrallitiques) de Casamance (Sénégal): Modalités de leur propagation. Cah. ORSTOM 16, 231–249.

Chiapini, M., Oliveira Junior, J.C., Schellekens, J., Almeida, A., Buurnam, P., Vidal-Torrado, P., 2021. Sombric-like horizon and xanthization in polychrome subtropical soils from Southern Brazil: implications for soil classification. Sci. Agric. 78, e2019011. https://doi.org/10.1590/1678-992X-2019-0115.

Chiapini, M., Schellekens, J., Calegari, M., R., Almeida, J., A., Buurman, P., Barbosa, P., B., Vidal-Torrado, P., 2018. Formation of black carbon rich ‘sombric’ horizons in the subsoil – A case study from subtropical Brazil. Geoderma 314, 232–244.

Chittleborough, D. J., Oades, J. M., Walker, P. H., 1984. Textural differentiation in chronosequences from eastern Australia. III. Evidence from elemental chemistry. Geoderma 32, 227–248.

Clemente, C., Azevedo, A. C., 2007. Mineral weathering in acid saprolites from subtropical, Southern Brazil. Sci. Agric. 64, 601 – 607.

Cooper, M., Vidal-Torrado, P., Chaplot, V., 2005a. Origin of microaggregates in soils with ferralic horizons. Sci. Agric. 62, 256–263.

Cooper, M., Vidal-Torrado, P., 2005b. Caracterização morfológica, micromorfológica e físico-hídrica de solos com horizonte B nítico. R. Bras. Ci. Solo 29, 581–595.

Cooper, M. 1999. Influência das condições físico-hídricas nas transformações estruturais entre horizontes B latossólico e B textural sobre diabásio. Tese de doutorado. Escola Superior de Agricultura "Luiz de Queiroz", Universidade de São Paulo.

Costa, A. C. S., Bigham, J. M, Rhoton, F. E., Traina, S. J., 1999. Quantification and characterization of Maghemite in soils derived from volcanic rocks in southern Brazil. Clays Clay Miner. 47, 466–73.

Curi, N., Franzmeier D. P., 1987. Effect of parent rocks on chemical and mineralogical properties of some Oxisols in Brazil. Soil Sci. Soc.of Am. J. 51,153–158.

Dalmolin, R. S. D., Gonçalves, C. N., Dick, D. P., Knicker, H., Klamt, E., Kögel-Knabner, I., 2006. Organic matter characteristics and distribution in Ferralsol profiles of a climosequence in southern Brazil. Eur. J. of Soil Sci. 57, 644–654.

Davidson, D. A, Bruneau, P. M. C, Grieve, I. C, Young, I. M., 2002. Impacts of fauna on an upland grassland soil as determined by micromorphological analysis. Appl. Soil Ecol. 20, 133–143.

Darwin C., 1838. On the formation of mould. Proc. Geol. Soc. Lond. 2, 274–576.

Darwin, C., 1881. The Formation of Vegetable Mould, Through the Action of Worms with Observations on Their Habits. Murray, London.

Delvigne, J., 1965. Pédogenèse em zone tropicale: La dormation des minéraux secondaires em milieu ferrallitique. Paris: Dunod.

Delvigne, J., 1998. Atlas of micromorphology of mineral alteration and weathering. Orstom, France.

Demattê, J. A. M., Garcia, G. J., 1999. Avaliação de atributos de latossolo bruno e de terra bruna estruturada da região de Guarapuava, Paraná, por meio de sua energia refletida. R. Bras. Ci. Solo 23, 343–355.

Desjardins, T., Filho, A. C., Mariotti, A., Chauvel, A., Girardim, C., 1996. Changes of the Forest-savanna bourdary in Brazilian Amazonia during the Holocene as revealed by soil organic carbon isotope ratios. Oecol. 108, 749–756.

Dexter, A. R., 1988. Advances in characterization of soil strucuture. Soils & Tillage Res. 11, 199–238.

Dick, D. P., Silva, L. B., Inda, A. V., Knicker, H., 2008. Estudo comparativo da matéria orgânica de diferentes classes de solos de altitude do Sul do Brasil por técnicas convencionais e espectroscópicas. R. Bras. Ci. Solo 32, 2289–2296.

Dick, D. P., Gonçalves, C. N., Dalmolin, R. S. D., Knicker, H., Klamt, E., Kögel-Knabner, I., Simões, M. L., Martin-Neto, L., 2005. Characteristics of soil organic matter of different Brazilian Ferralsols under native vegetation as a function of soil depth. Geoderma 124, 319–333.

Drees, L. R., Wilding, L. P., 1978. Elemental distribution in the light isolate of soil separates. Soil Sci. Soc. Am. J. 42, 976–978.

Driessen P., Deckers J., Spaargaren O., Nachtergaele F.,2001. Lecture Notes on the Major Soils of the World. World Soils Resources Reports 94. FAO, Rome.

Duchaufour, P., 1988. Pédologie. Masson, Paris.

Dümig, A., Schad, P., Rumpel, C., Dignac, M. F., Kögel-Knabner, I., 2008. Araucaria forest expansion on grassland in the southern Brazilian highlands as revealed by 14C and $^{\delta}$13C studies. Geoderma 145, 143–157.

Eggleton, P., Williams, P. H., Gaston, K. J., 1994. Explaining global termite diversity: productivity or history? Biodivers. and Conserv. 3, 318–330.

Egli, M., Fitze, P., 2000. Formulation of pedogenic mass balance based on immobile elements: a revision. Soil Sci. 165, 437–443.

Eschenbrenner, V., 1996. Termite activity and soil morphology in tropical areas, in: congresso latinoamericano de ciência do solo, solo-suelo, 96, 13, Águas de Lindóia, 1996. Resumos e Conferências. Águas de Lindóia, Soc. Bra. de Ci. do Solo, pp. 14.

Eschenbrenner, V., 1986. Contribution des termites à la micro-agrégation des sols tropicaux. Cahiers ORSTOM, Série Pédologie 22, 397–408.

Eswaran, H., Stoops, G. Surface textures od quartz in tropical soils. Soil Sci. Soc. Am. J. 43, 420–424.

Eswaran, H. 1979. The alteration of plagioclases and augites under differimg pedo-environmental conditions. J. of Soil Sci. 30, 547–555.

Eswaran, H. 1972. Micromorphological indicators of the pedogenesis in some tropical soils derived from basalts from Nicaragua. Geoderma 7, 15–31.

Eswaran, H., De Coninck, F. 1971. Clay mineral formations and transformations in basaltic soils in tropical environments. Pedol. 11, 181–21.

Ferreira, C. H. N., Mesquita, M. J. M., Gomes, M. E. B., Hillebrandt, P., Vasconcellos, E. M. G., 2014. Arquitetura interna e petrografia do derrame Salto do Lontra, sudoeste do estado do Paraná. Boletim Paranaense de Geociências 71, 46–59.

Fitzpatrick, R. W., Schwertmann, U., 1982. Al-substituted goethite – An indicator of pedogenic and other weathering environments in South Africa. Geoderma 27, 335–347.

Fontes, M. P. F., Carvalho Jr., I. A., 2005. Color attributes and mineralogical characteristics, evaluated by radiometry, of highly weathered tropical soils. Soil Sci. Soc. of Am. J. 69, 1162–1172.

Fontes, M. P. F., Oliveira, T., S., Costa, L. M., Campos, A. A.G., 2000. Magnetic separation and evaluation of magnetization of Brazilian soils from different parent materials. Geoderma 96, 81–99.

Fontes, M. P. F., Weed, S. B., 1996. Phosphate adsorption by clays from Brazilian Oxisols: relationships with specific surface area and mineralogy. Geoderma 72, 37–51.

Fontes, M. P. F., Weed, S. B., 1991. Iron oxides in selected Brazilian Oxisols: I. Mineralogy. Soil Sci. Soc. Am. J. 55, 1143–1149.

Fox, R. L., 1982. Some highly weathered soils of Puerto Rico: 3. Chemical properties. Geoderma 27, 139–176.

Furian, S., Barbiéro, L., Boulet, R., Grimaldi, P. C. M., Grimaldi, C., 2002. Distribution and dynamics of gibbsite and kaolinite in an Oxisol of Serra do Mar, southeastern Brazil. Geoderma, 106, 83–100.

Gabet, E. J., Reichman, O. J., Seabloom, E. W., 2003. The effects of bioturbation on soil processes and sediment transport. Annual Review of Earth and Planetary Sciences 31, 249–273.

Gallo, D., O., Nakano, S., Silveira Neto, R. P. L., Carvalho, G. C., Batista, E., Berti Filho, J. R. P., Parra, R. A., Zucchi, S. B., Alves, J. D. Vendramim, 1988. Manual de entomologia agrícola. Agronômica Ceres, São Paulo.

Garcia, I. P., Forti, L. C., Engel, V. L., Andrade, A. P., Wilcken, C. F., 2003. Ecological interaction between Atta sexdens (Hymenoptera: Formicidae) and the vegetation of a mesophyll semideciduous forest fragment in Botucatu, SP, Brazil. Sociobiol. 42, 265–283.

Gaucher, G., 1977. Vers une classification pedologique naturelle basee sur la geochemie de la pedogenese. Catena 4, 1–27.

Ghidin, A. A., 2003. Influência dos minerais da fração argila nas propriedades físicas de duas classes de Latossolos no estado do Paraná. Dissertação de mestrado. Universidade Federal do Paraná.

Ghidin, A. A., Melo, V. F., Lima, V. C., Lima, J. M. J. C., 2006. Toposseqüências de Latossolos originados de rochas basálticas no Paraná. I — Mineralogia da fração argila. Rev. Bras. Ci. Solo 30, 293–306.

Ghidin, A. A., Melo, V. F., Lima, V. C., Lima, J. M. J. C., 2006. Toposseqüência de Latossolos originados de rochas basálticas no Paraná. II e relação entre mineralogia da fração argila e propriedades físicas dos solos. Rev. Bras. Ci. Solo 30, 307–319.

Glasmann, J. R., Simonson, G. H., 1985. Alteration of basalt in soils ofWestern Oregon. Soil Sci. Soc. of Am. J. 49, 262–273.

Gomes, A. S., Licht, O. A. B., Vasconcellos, E. M. G., Soares, J.S., 2018. Chemostratigraphy and evolution of the Paraná Igneous Province volcanism in the central portion of the state of Paraná, Southern Brazil. J. of Volcanol. and Geotherm. Res. 355, 253–269.

Gomes, J. B. V., Curi, N., Motta, P. E. F., Ker, J. C., Marques, J .J. G. S. M., Shulze, D. G., 2004. Análise de componentes principais de atributos físicos, químicos e mineralógicos de solos do bioma Cerrado. R. Bras. Ci. Solo, 28, 137–153.

Gonçalves, C., Dalmolin, R., Dick, D. P., Knicker, H., Klamt, E., Kögel-Knabner, I., 2003. The effect of 10% HF treatment on the resolution of CPMAS ^{13}C NMR spectra and on the quality of organic matter in Ferralsols. Geoderma 116, 373–392.

Gonfiantini, R., 1978. Standards for stable isotope measurements in natural compounds. Nat. 271, 534–536.

Gouveia, S. E. M., Pessenda, L. C. R., Aravena, R., 1999. Datação da fração humina da matéria orgânica do solo e sua comparação com idades ^{14}C de carvões fósseis. Quím. Nova, 22, 810–814.

Grimaldi, D., Engel, M. S., 2005. Evolution of the Insects. Cambridge University Press, Cambridge.

Guareschi, R. F., Pereira, M. G., Perin, A., 2014. Carbono, nitrogênio e abundância natural de $\delta^{13}C$ e $\delta^{15}N$ em uma cronossequência de agricultura sob plantio direto no cerrado goiano. Rev. Bras. Ci. Solo, 38, 1135–1142.

Guimarães, D., 1933. Província magmática do Brasil Meridional. Instituto Geológico e mineralógico do Brasil, Boletim no 64, Rio de Janeiro.

Gutmans, M., 1943. Rochas-Mater da "Terra Roxa". Bragantia 3, 271–321.

Heinrich, E.W., 1965. Microscopic identification of minerals. New York: McGraw-Hill.

Hughes, J. C., Brown, G., 1979. A crystallinity index for soil kaolinite and its relation to parent rock, climate and soil maturity. J. Soil Sci. London 30, 557–563.

Humphreys, G. S., Hart, D. M., Simons, N. A., Field, R. J., 2003. Phytoliths as indicators of process in soils, in: D. M. Hart and L. A. Wallis (Eds.), Phytolith and Starch Research in the Austalian-Pacific-Asian Regions: The State of the Art. The Australian National Univ., Canberra, pp. 93–104.

Humphreys, G.S., Field, R., 1998. Mixing, mounding and other aspects of bioturbation: implications for pedogenesis. 16th World Congress of Soil Science. International Society of Soil Science, Montpellier.

Humphreys, G. S., 1994. Bioturbation, biofabrics and the biomantle: An example from the Sydney Basin, in: A. J. Ringrose-Voase and G. S. Humphreys (Eds.), Micromorphology: Studies in management and genesis. Amsterdam: Elsevier, pp. 421–436.

Inda Junior, A.V., Kämpf, N., 2003. Evaluation of pedogenic iron oxide extraction procedures with sodium dithionite-citratebicarbonate. Rev. Bras. Ci. Solo 27, 1139–1147.

IUSS Working Group WRB., 2015. World Reference Base for Soil Resources 2014, update 2015. International soil classification system for naming soils and creating legends for soil maps. World Soil Resources Reports No. 106. FAO, Rome.

Jackson, M. L., 1979. Soil chemical analysis: advanced course. Madison: By author.

Jayawardena, U., Izawa, E., 1994. A new chemical index of weathering for metamorphic silicate rocks in tropical regions: A study from Sri Lanka. Eng. Geol. 36, 303–310.

Johnson, D. L., Domier, J. E. J., Johnson, D. N., 2005a. Reflections on the nature of soil and its Biomantle. Annals of the Association of Am. Geographers 95, 11–31.

Johnson, D. L., Domier, J. E. J., Johnson, D. N., 2005b. Animating the biodynamics of soil thickness using process vector analysis: a dynamic denudation approach to soil formation. Geomorphol. 67, 23–46.

Johnson, D. L., 2002. Darwin would be proud: bioturbation, dynamic denudation, and the power of theory in science. Geoarchaeol. 17, 7–40.

Johnson, D. L., 1990. Biomantle evolution and the redistribution of Earth materials and artifacts. Soil Sci. 149, 84–102.

Johnson, D. L., Keller, E. A., Rockwell, T. K., 1990. Dynamic pedogenesis: New views on some key concepts, and a model for interpreting Quaternary soils. Quat. Res. 33, 306–319.

Jones, C. G., Lawton, J. H., Shachak, M., 1994. Organisms as ecosystem engineers. Oikos 69, 373–386.

Jouquet, P., Chintakunta, S., Bottinelli, N., Subramanian, S., Caner, L., 2016. The influence of fungus-growing termites on soil macro and micro-aggregates stability varies with soil type. Appl. Soil Ecol. 101, 117-123.

Jouquet, P., Dauber, J., Lagerlöf, J., 2006. Soil invertebrates as ecosystem engineers: intended and accidental effects on soil and feedback loops. Appl. Soil Ecol. 32, 153–164.

Jouquet, P., Lepage, M., Velde, B., 2002. Termite soil preferences and particle selections: strategies related to ecological requirements. Insectes soc. 49, 1–7.

Justi, M., Schellekens, J., Camargo, P.B., Vidal-Torrado, P., 2017. Long-term degradation effects on the molecular composition of black carbon in Brazilian Cerrado soils. Org. Geochem. 113, 196–209.

Justus, J. O, Machado, M. L. A., Franco, M. S. M., 1986. Geomorfologia, in: SEPLAN/FIBGE. Folha SH.22 Porto Alegre e parte das Folhas SH.21 Uruguaiana e SI.22 Lagoa Mirim: geologia, geomorfologia, pedologia, vegetação, uso potencial da terra. Levantamento de recursos naturais, 33, 313–404, IBGE, Rio de Janeiro.

Kämpf, N., Schwertmann, U., 1983. Goethite and hematite in a climosequence in southern Brazil and their application in classification of kaolinitic soils. Geoderma 29, 27–39.

Kämpf, N., Schwertmann, O., 1982. Quantitative determination of goethite and hematite in kaolinitic soils by X-ray diffraction. Clay Miner. 17, 359–363.

Kämpf, N., Schwertmann, U., 1982. The NaOH concentration method for iron oxides in soils. Clays and Clay Miner. 30, 401–408.

Kämpf, N., Klamt, E., 1978. Mineralogia e gênese de latossolos (oxisols) e solos podzólicos da região nordeste do planalto sul-riograndense. Rev. Bras. de Ci. do Solo 2, 68–73.

Karathanasis, A. D., MacNeal, B. R., 1994. Evaluation of parent material uniformity criteria in loess-influenced soils of westcentral Kentucky. Geoderma, 64, 73–92.

Ker, J. C., 1997. Latossolos do Brasil: uma revisão. Geonomos 5, 17–40.

Ker, J. C., Resende, M. 1990. Caracterização química e mineralógica de solos brunos subtropicais do Brasil. Rev. Bras. de Ci. do Solo 14, 215–225.

King, L. C., 1956. A Geomorfologia do Brasil Oriental. Rev. Bras. de Geogr. 147–265.

Klug, H. P., Alexander, L. E., 1954. X-ray, diffraction procedures for polycrystalline and amorphous materials. John Wiley & Sons, New York.

Kooistra, M. J., Pulleman, M. M., 2018. Features related to fauna activity, in: Stoops, G., Marcelino, V., Mees, F. (Eds.), Interpretation of micromorphological features of soils and regoliths. Elsevier Science. 397–418.

Koppi, A. J., Skjemstad, J. O., 1981. Soil kaolins and their genetic relationships in southeast Queensland, Australia. J. Soil Sci. 32, 661–672.

Kronberg, B. I, Nesbitt, H. W., 1981. Quantification of weathering, soil geochemistry and soil fertility. J. of Soil Sci. 32, 453–459.

Lach, L., Parr, C. L., Abbott, K. L., 2009. Ant ecology. Oxford University Press Inc. Oxford.

Ladchuk, D. P. P.T., Parolin, M., Bauermann, S. G., 2016. Recuperação de palinomorfos e dados isotópicos ($\delta^{13}C$ e $\delta^{15}N$) em sedimentos turfosos e seu significado paleoambiental para a região de Campo Mourão-PR. Rev. Bras. de Geogr. Fis. 9, 1183–1196.

Lal, R., Shukla, M. K., 2004. Principles of Soil Physics. Marcel Dekker, New York.

Lal, R., 2004. Soil Carbon sequestration impacts on global climate change and food security. Sci. 304, 1623–1627.

Lavelle, P., Spain, A.V., 2003. Soil Ecology. Kluwer Academic Publishers.

Lavelle P., 1988. Earthworm activities and the soil system. Biol. Fertil. Soils 6, 237–251.

Lavelle, P., 1997. Faunal activities and soil processes: adaptive strategies that determine ecosystem function. Adv. in Ecol. Res. 27, 93–132.

Lavelle, P., Spain, A.V., Blanchart, E., Martin, A. and Martin, S., 1992. The impact of soil fauna on the properties of soils in the humid tropics, in: P.A. Sanchez and R. Lal (Eds.), Myths and Science of Soils of the Tropics, Special Publication, Madison, Wisconsin, pp. 157–185.

Lavelle, P., Spain, A.V., Blanchart, E., Martin, A., Martin, S., 1992. The impact of soil fauna on the properties of soils in the humid tropics, in: P.A. Sanchez and R. Lal. (Eds), Myths and Science of Soils of the Tropics. Special Publication, Madison, Wisconsin, pp. 157–185.

Lavelle P. 1988. Earthworm activities and the soil system. Biol. Fertil. Soils 6, 237–251.

Leinz, V., 1949. Contribuição à geologia dos derrames basálticos do sul do Brasil. Boletim da Faculdade de Filosofia, Ciências e Letras, Universidade de São Paulo, Boletim 103, Geol. 5, 1–61.

Lobry de Bruyn, L. A.; Conacher, A. J., 1990. The role of termites and ants in soil modification: a review. Aust. J. of Soil Res. 28, 55–93.

Lucas, Y., Luizão, F. J., Chauvel, A., Rouiller, J., Nahon, D., 1993. The relation between biological activity of the rain forest and mineral composition of soils. Sci., 260, 521–523.

Luz, L., D., Parolin, M., Pessenda, L., C., R., Rasbold, G., G., Lo, E., 2019. Multiproxy analysis (phytoliths, stable isotopes, and c/n) as indicators of paleoenvironmental changes in a cerrado site, Southern Brazil. Rev. Bras. de Paleontol. 22, 15–29.

Maack, R., 1947. Breves notícias sobre a geologia dos estados do Paraná e Santa Catarina. Arq. Inst. Biol. Pesqui. Tecnol. 2, 66–154.

Macedo, R. S., Teixeira, W. G., Corrêa, M. M., Martins, G. C., Vidal-Torrado, P., 2017. Pedogenetic processes in anthrosols with pretic horizon (Amazonian Dark Earth) in Central Amazon, Brazil. PloS ONE 12: e0178038.

Magdoff, F., Weil, R. R., 2004. Soil Organic Matter in Sustainable Agriculture. Boca Raton: CRC Press.

Mantovani, M. S. M., Marques, L. S., de Sousa, M. A., Civetta, L., Atalla, L., Innocenti, F., 1985. Trace elements and strontium isotope constraints on the origin and evolution of Paraná continental flood basalts of Santa Catarina state (southern Brazil). J. Petrol. 26, 187–209.

Marengo, H., Palma, Y., Tchilingurian, P., Helms, F., Kruck, W., Roverano, D., 2005. Geologia del area de San Ignacio, Provincia de Misiones, in: Actas XVI Congreso Geológico Argentino, La Plata, I, pp. 141–148.

Marques, F.A., Buurman, P., Schellekens, J., Vidal-Torrado, P., 2015. Molecular chemistry in humic Ferralsols from Brazilian Cerrado and forest biomes indicates a major contribution from black carbon in the subsoil. J. Anal. Appl. Pyrolysis 113, 518–528.

Marques, L. M., Piccirillo, E. M., Melfi, A. J., Comin-Chiaramonti, P., Bellieni, G., 1989. Distribuição de terras raras e outros elementos traços em basaltos da Bacia do Paraná (Brasil Meridional). Geochim. Bras. 3, 33–50.

Martinez, P., Souza, I.F., 2020. Genesis of pseudo-sand structure in Oxisols from Brazil – A review. Geoderma Reg. 22, 1–11.

McKeague, J.A., Day, J. H., 1966. Dithionite and oxalateextractable Fe and Al as aids in differentiating various classes of soils. Can. J. of Soil Sci. 46, 13–22.

Mehra, O. P., Jackson, K. L., 1960. Iron oxide removal from soils and clays by dithionite-citrate system buffered with sodium bicarbonate. In: National Conference on Clay and Clay Minerals 7, 1958. Proceedings, Washington, 317–327.

Melfi, A. J., Piccirillo, E. M., Nardy, A. J. R., 1988. Geological and magmatic aspects of the Paraná Basin an introduction, in: Piccirillo, E., M., Melfi, A., J. (Eds.), The Mezosoic Flood Volcanism of tha Paraná Basin: Petrogenetic and Geophysical Aspects. São Paulo, IAG-USP. pp. 1–13.

Melo V. F., Oliveira Junior, J. C., Batista, A. H., Cherobim, V. F., Favaretto. N., 2020. Goethite and hematite in bichromic soil profiles of Southern Brazil: Xanthization or yellowing process. Catena 188, 1–15.

Melo V.F., Wypych F., 2009. Caulinita e Haloisita, in: Melo, V., F., Alleoni, L.,R.,F.(Eds), Química e Mineralogia do Solo. Viçosa, MG: Sociedade Brasileira de Ciência do Solo, pp. 427–504.

Melo, V. F., Fontes, M. P. F., Novais, R. F., Singh, B., Schaefer, C. E. G. R., 2001. Iron and aluminum oxides of different Brazilian soils. Rev. Bras. de Ci. do Solo 25, 19–32.

Melo, V. F., Singh, B., Schaefer, C. E. G. R., Novais, R. F., Fontes, M. P. F. F., 2001. Chemical and mineralogical properties of kaolinite-rich Brazilian soils. Soil Sci. Soc. Am. J. 65, 1324–1333.

Mestdagh, M. M., Vielvoye, L., Herbillon, A. J., 1980. Iron in kaolinite: II. The relationship between kaolinite crystallinity and iron contente. Clay Miner. 15, 1–13.

Miklós, A. A. DE W., 2012. Biogênese do solo. Revista do Departamento de geografia – USP, volume especial 30 anos, p.190-229.

Miklós, A. A. DE W., 1992. Biodynamique d'une coverture pédologique dans la région de Botucatú, Brésil. Tese de dooutorado. Paris: Université de Paris.

Millot, G., 1977. Géochimie de la surface et formes du relief. Présentation. Sci. Géol., Bull. 30, 229–233.

Moniz, A. C., 1980. Formation of na Oxisol-Ultisol transition in São Paulo, Brasil. Tese de doutorado, North Caroline State University, Raleigh.

Moore, D. M., Reynolds, R. C., 1997. X-Ray Diffraction and the Identification and Analysis of Clay Minerals, Second ed. Oxford University Press, Oxford.

Moreira, A., Forti, L. C., Andrade, A. P., Boaretto, M. A., Lopes, J., 2004. Nest architecture of *Atta laevigata* (F. Smith, 1858) (Hymenoptera: Formicidae). Stud. on Neotropical Fauna and Environ. 39, 109–116. https://doi.org/10.1080/01650520412331333756.

Morrás, H., Moretti, L., Píccolo, G, Zech, W., 2009. Genesis of subtropical soil with stony horizons in NE Argentina: Autochthony and polygenesis. Quat. Int. 196, 137–159.

Moura Filho, W., Buol S.W., 1976. Studies of a Latosol Roxo (Eutrustox) in Brazil; micromorphology effect on ion release. Exp., 21, 161 – 177.

Muggler, C. C., 1998. Polygenetic oxisols on tertiary surfaces, Minas Gerais, Brazil. Tese de doutorado. Wageningen, Wageningen Agricultural University.

Muller, J. P., 1977. Microstructuration des stutichrons rouges ferralitiques, a` l'amont des modele´s convexes (Centre-Cameroun). Aspects morphologiques. Cahiers ORSTOM, Série Pédol. 15, 239–258.

Nahon, D., 1991. Introduction to the Petrology of Soils and Chemical Weathering. Wiley, New York.

Nardy, A. J. R., Moreira, C. A., Machado, F. B., Luchetti, C. F., Hansen, M. A. F., Rossini, A. J., Barbosa Jr, V., 2014. Gamma-ray spectrometry signature of Paraná volcani rocks: preliminar results. Geociênc. 33, 216–227.

Nardy, A. J. R., 1988. Petrologia e paleomagnetismo das rochas vulcânicas da região centro-sul do estado do Paraná: formação serra geral. Dissertação de mestrado. Universidade de São Paulo.

Nardy, A. J. R., 1995. Geologia e petrologia do vulcanismo mesozóico da região central da bacia do Paraná. Rio Claro. Tese de doutorado. Universidade Estadual Paulista.

Nardy, A. J. R., Oliveira, M. A. F., Betancourt, R. H. S., Verdugo, D. R. H., Machado, F. B., 2002. Geologia e estratigrafia da Formação Serra geral. Geociênc. 21,13–30.

Nardy, A. J. R., Machado, F. B., Oliveira, M. A. F., 2008. As rochas vulcânicas mesozoicas ácidas da Bacia do Paraná: litoestratigrafia e considerações geoquímico-estratigráficas. Rev. Bras. Geoc. 38, 178–195.

Nardy, A. J. R., Rosa, M. C., Luchetti, A. C. F., Ferreira, M. L. C., Machado, F. B., Oliveira, M. A. F., 2011. Parâmetros físicos pré-eruptivos do magmatismo ácido da Província Magmática do Paraná: resultados preliminares. Geociênc. 30, 575–588.

Nesbitt, H.W., Young, G.M., 1982.Early proterozoic climates and plate motions inferred from major element chemistry of lutites. Nat. 299, 715–717.

Nitsche, P. R., Caramori, P. H., Ricce, W. S., Pinto, l. F. D. 2019. Atlas climático do estado do Paraná. IAPAR, Londrina.

Noack, Y., Colin, F., Nahon, D., Delvigne, J., Michaux, L., 1993. Secondary-mineral formation during natural weathering of pyroxene: review and thermodynamic approach. Am. J. of Sci. 293, 111–134.

Nóbrega, J., Schiavo, D., Amaral, C. D. B., Barros, J. A. V. A., Nogueira, A. R. A., Virgilio, A., Machado, R., 2017. Determination of Rare Earth Elements in Geological and Agricultural Samples by ICP-OES. Spectrosc. 32, 32–36.

Norman, S.A., Schaetzl, R.J., Small, T.W., 1995. Effects of slope angle on mass movement by tree uprooting. Geomorphol. 14, 19–27.

Oades, J.M., 1993. The role of biology in the formation, stabilization and degradation of soil structure. Geoderma 56, 377–400.

Norrish, K., Taylor, M., 1961. The isomorphous replacement of iron by aluminium in soil goethites. Eur. J. of Soil Sci. 12, 294–306.

Novais Filho, J. P., Couto, E. G., Rodrigues, L. C. M., Chig, L. A., Johnson, M. S. 2012. Indicativos de descontinuidade litológica de regolitos derivados de granitos emu ma microbacia sob floresta amazônica, em Juruena-MT. R. Bras. Ci. Solo 36, 317–324.

Oliveira Junior, J. C.; Melo, V. F.; Souza L. C. P.; Rocha, H. O., 2014. Terrain attributes and spatial distribution of soil mineralogical attributes. Geoderma 213, 214–225.

Pagotto, D., Paisani, J.C., Sordi, M.V., 2020. Dinâmica da paisagem do planalto do rio Canoas (SC) no quaternário tardio com base em registros pedoestratigráficos de paleocabeceira de drenagem. Geosul, 35, 481–505.

Paisani, J. C., Santos, L. J. C., Goudard, G., Goulart, A. Á., Biffi, V. H. R., 2019. Subtropical Araucaria Plateaus, in: A. A. R. Salgado; L. J. C. Santos; J. C. Paisani (Eds.), The Physical Geography of Brazil - Geography of the Physical Environment. pp.222.

Paisani, J. C., Pontelli, M. E., Osterrith, M. L., et. al. 2014. Paleosols in low-order streams and valley heads in the Araucaria Plateau - record of continental environmental conditions in southern Brazil at the end of MIS 3. J. of South Am. Earth Sci. 54, 57–70.

Paisani, J. C., Pontelli, M. E., Corrêa, A. C. B., Rodrigues, R. A. R., 2013b. Pedogeochemistry and micromorphology of oxisols e a basis for understanding etchplanation in the Araucarias Plateau (Southern Brazil) in the Late Quaternary. J. of South Am. Earth Sci. 48, 1–12.

Paisani, J. C., Pontelli, M. E., Andres, J., 2008. Superfícies aplainadas em zona morfoclimática subtropical úmida no Planalto Basáltico da Bacia do Paraná (SW Paraná/ NW Santa Catarina): primeira aproximação. Geociênc. 27, 541–553.

Parolin, M., Volkmer-Ribeiro, C., Stevaux, J. C., 2008. Use of spongofacies as a proxy for river-lake paleohydrology in quaternary deposits of Central-Western Brazil. Rev. Bras. de Paleontol. 11,187–98.

Parton, W.J., Schimel, D. S., Cole, C. V., Ojima, D. S., 1987. Analysis of factors controlling soil organic matter levels in Great Plains grasslands. Soil Sci. Soc. of Am. J. 51, 1173–1179.

Paton, T. R., Humphreys, G. S., Mitchell, P. B., 1995. Soils: a new global view. Yale University Press.

Pawluk, S., 1987. Faunal micromorphological features in moder humus of some western Canadian soils. Geoderma 40, 3–16.

Peate, D. W., Hawkesworth, C. J., Mantovani, M. S. M., 1992. Chemical stratigraphy of the Paraná lavas (South America): classification of magma types and their spatial distribution. Bull. Volcanol. 55, 119–139.

Pedro, G., Delmas, A.B., Seddon, F.K., 1975. Sur la necessite et l' importance d' une distinction fondamentale entre type et degre d' alteration. Application au probleme de la definition de la ferrallitisation. Comptes Rendus Hebdomadaires des Seances de l'Academie des Sciences, Serie-D. 280, 825–828.

Pessenda, L. C. R., et al., 1998. ^{14}C Dating and Stable Carbon Isotopes of Soil Organic Matter in Forest-Savana Boundary Areas in the Southern Brazilian Amazon Region. Radiocarb. 40, 1013–1022.

Pessenda, L. C. R., 1996. The use of carbon isotopes (^{13}C, ^{14}C) in soil to evaluate vegetation changes during the Holocene in Central Brazil. Radiocarb. 38, 191–201.

Peyerl, W.R.L., Salamuni, E., Sanches, E., do Nascimento, E.R., Santos, J.M., Gimenez, V. B., Farias, T.F.S., 2018. Reativation of Taxaquara fault and its morphotectonic influence on the evolution of Jordão river catchment, Paraná, Brasil. Braz. J. Genet. 48, 553–573.

Phillips, J. D., Marion, D. A., 2006. Biomechanical effects of trees on soil and regolith: beyond treethrow. Annals of the Association of Am. Geographers 96, 233–247.

Plançon, A., Zacharie, C., 1990. An expert system for the structural characterization of kaolinites. Clay Miner. 25, 249–261.

Poldervaart, A., 1964. Chemical definition of alkali basalts and tholeiites. Geol. Soc. of Am. Bulletin 75, 229–232.

Price, J.R., Velbel, M.A., 2003. Chemical weathering indices applied to weathering profiles developed on heterogeneous felsic metamorphic parent rocks. Chem. Geol. 202, 397–416.

Pulleman, M. M., Six, J., Uyl, A., Marinissen, J. C. Y., Jongmans, A. G., 2005. Earthworms and management affect organic matter incorporation and microaggregate formation in agricultural soils. Appl. Soil Ecol. 29, 1–15.

Putz, F.E., 1983. Treefall pits and mounds, buried seeds, and the importance of soil disturbance to pioneer trees on Barro ColoradoIsland, Panama. Ecol. 64, 1069–1074.

Pinaya, J. L. D., Cruz, F. W., Ceccantini, G. C. T. et al., 2019. Brazilian montane rainforest expansion induced by Heinrich Stadial 1 event. Sci Rep 9, 17912. https://doi.org/10.1038/s41598-019-53036-1

Rabbi, S. M. F., Wilson, B. R., LockWood, P.V., Daniel, H., Young, I. M., 2015. Aggregate hierarchy and carbon mineralization in two Oxisols of New South, Australia. Soil & Tillage Res. 146, 193–203.

Ralph, J., Hatfield, R. D., 1991. Pyrolysis–Gc–MS Characterization of forage materials. J. Agric. Food Chem. 39, 1426–1437.

Rasbold, G. G., Parolin, M., Caxambu, M. G., 2016. Reconstrução paleoambiental de um depósito sedimentar por análises multiproxy, Turvo, estado do Paraná, Brasil. Rev. bras. paleontol. 19, 315–324.

Rasmussen, C., Dahlgren, R. A., Southard, R. J., 2010. Basalt weathering and pedogenesis across an environmental gradiente in Southern Cascade Range, California, USA. Geoderma 154, 473–485.

Resende, M., Santana, D.P., 1988. Uso das relações Ki e Kr na estimativa da mineralogia para classificação dos latossolos. In: Reunião de classificação, correlação de solos e interpretação de aptidão agrícola, Rio de Janeiro. EMBRAPA-SNLCS, 225–232.

Riffel, S. B., Vasconcelos, P. M., Carmo, I. O., Farley, K. A., 2016. Goethite (U-Th)/He geochronology and precipitation mechanisms during weathering of basalts. Chem. Geol. 446, 18–32.

Riggi, J., Riggi, N., 1964. Meteorización de basaltos en Misiones. Revista de la Asociación Geol. Argent. 19, 57–70.

Rodrigues, B. M. 2019. Bioturbação e distribuição de fitólitos em Latossolos da Depressão Periférica Paulista. Dissertação de mestrado. Universidade de São Paulo.

Roering, J. J., Almond, P., Tonkin, P., McKean, J., 2002. Soil transport driven by biological processes over millennial time scales. Geol. 30, 1115–1118.

Rolim Neto F. C., Schaefer C. E. G. R., Costa L. M., Correa M. M., Fernandes Filho E. I., Ibriamo M. M., 2004. Adsorção de P, superfície específica e atributos mineralógicos em solos desenvolvidos de rochas vulcânicas de Alto Paranaíba MG. Braz. J. Soil Sci. 28, 953–964.

Rüegg, N. R., 1969. Aspectos geoquímicos, mineralógicos e petrográficos de rochas basálticas da Bacia do Paraná. Tese de doutorado. Universidade de São Paulo.

Rüegg, N. R., Amaral, G., 1976. Variação regional da composição química das rochas basálticas da Bacia do Paraná. Boletim IG, USP 7,131–147.

Rusek, J., 1985. Soil microstructures-contributions of specific soil organisms. Quaest. Entomol. 21, 497–514.

Ruxton, B. P., 1968. Measures of the degree of chemical weathering in rocks. J. Geol. 76, 518–527.

Saia, S. E. M. G., Pessenda, L. C. R., Gouveia, S. E. M., Aravena, R., Bendassolli, J. A. 2008. Last glacial maximum (LGM) vegetation changes in the Atlantic Forest, southeastern Brazil. Quat. Int. 184, 195–201.

Santos, H. G., et al., 2018. Sistema Brasileiro de Classificação de Solos. Brasília, DF: Embrapa.

Santos, R. D., Lemos, R. C., Santos, H. G., Ker, J. C., Anjos, L. H. C., Shimizu, S. H., 2013. Manual de descrição e coleta de solo no campo. 6.ed. Sociedade Brasileira de Ciência do Solo, Viçosa.

Santos L. J. C., Oka-Fiori C., Canali N. E., Fiori A. P., Silveira C. T., Silva J. M. F., Ross J. L. S., 2006. Mapeamento Geomorfológico do Estado do Paraná. Rev. Bras. de Geomorfol. 7, 03–11.

Santos, M. C. D, Mermut, A. R, Ribeiro, M. R., 1989. Submicroscopy of clay microaggregates in na Oxisol from Pernambuco, Brazil. Soil Sci. Am. J. 53, 1895–1901.

Saussey, M., 1966. Contribution à l'étude des phénomènes de diapause et de régénération caudale chez Allolobophora icterica (Savigny). Mémoires de la Société linnéenne de Normandie 1, 1–158.

Schaefer, C. E. G. R., Fabris, J. D., Ker, J. C., 2008. Minerals in the clay fraction of Brazilian Latosols (Oxisols): a review. Clay Miner. 43, 137–154.

Schaefer, C. E., 2001. Brazilian latosols and their B horizon microstructure as long-term biotic constructs. Soil Res. 39, 909–926.

Schaetzl, R. J., Anderson, S., 2005. Soils Genesis and Geomorphology. Cambridge.

Schaetzl, R. J., 1998. Lithologic discontinuities in some soils on drumlins. Theory, detection, and application. Soil Sci. 163, 570–590.

Schaetzl, R. J., Follmer, L. R., 1990. Longevity of treethrow microtopography: implications for mass wasting. Geomorphol. 3, 113–123.

Schaetzl, R. J., Burns, S. F., Small, T. W., Johnson, D. L., 1990. Tree uprooting: review of types and patterns of soil disturbance. Phys. Geograp. 11, 277–291.

Schellekens, J., Almeida-Santos, T., Santana Macedo, R., Buurman, P., Kuyper, T.W., Vidal-Torrado, P., 2017. Molecular composition of several soil organic matter fractions from anthropogenic black soils (Terra Preta de Índio) in Amazonia – a pyrolysis- GC/MS study. Geoderma 288, 154–165.

Schoeneberger, P. J., Wysocki, D. A., Benham, E. C., Broderson, W. D., 2002. Field Book for Describing and Sampling Soils, Version 2.0.Natural Resources Conservation Service, National Soil Survey Center, Lincoln.

Schulten, H. R., Schnitzer, M., 1992. Structural studies on soil humic acids by curie-point pyrolysis-gas chromatography/mass spectrometry. Soil Sci.153, 205–224.

Schulze, D. G. 1984. The influence of aluminium on iron oxides. VIII – Unit-cell dimensions of Al-substituted goethites and estimation of Al from them. Clays Clay Miner. 32, 36–44.

Schmidt, M. W. I., Torn, M. S., Abiven, S., Dittmar, T., Guggenberger, G., Janssens, I. A., Kleber, M., Kögel-Knabner, I., Lehmann, J., Manning, D. A. C., Nannipieri, P., Rasse,

D.P., Wiener, S., Trumbore, S.E., 2011. Persistence of soil organic matter as na ecosystem property. Nat. 478, 49–56.

Schwertmann U., Taylor, R. M., 1989. Iron oxides, in: Dixon, J., B., Weed, S., B.(Eds.), Minerals in soil environments. Madison: Soil Sci. Soc. of Am. pp. 379–438.

Schwertmann U., 1988. Some properties of soil and synthetic iron oxides, in: Stucki, J.,W., Goodman, B.,A,, Schwertmann U. (Eds.), Iron in soils and clay minerals. Dordrecht: D. Reidel Publishing Company, pp. 203–50.

Schwertmann, U., Kämpf, N., 1985. Properties of goethite and hematite in kaolinitic soils of southern and central Brazil. Soil Sci. 139, 344–350.

Schwertmann, U., Fitzpatrick, R. W., Taylor, R. M., Lewis, D. G., 1979. The influence of aluminium on iron oxides. Part II. Preparation and properties of Al-substituted hematites. Clays and Clay Miner. 29, 269–276.

SCHWERTMANN, U. Transformation of hematite to goethite in soils. Nature, 232:64-65, 1971.

Ségalen P., 1966. Le processus de ferrallitisation et ses limites, in: Les sols ferrallitiques. Cahiers ORSTOM. Série Pédologie, 4, 15–20. Les Sols Ferrallitiques: Réunion Annuelle, Paris.

Shaler, N. S., 1891. The origin and nature of soils, in: Powell, J.W. (Ed.), USGS 12th Annual report 1890–1891. Government Printing Office, Washington, D.C., pp. 213–245.

Siever, R., 1962. Silica solubility, 0º–200ºC, and the diagenesis of silicious sediments. The J.of geol. 70, 127–150.

Silva, B.A., Calegari, M.R., Pinheiro, M.R., Fujita, R.H., 2021. Lithostructural and tectonic determinants in the geomorphic evolution of the Basalt Plateau – Southern Brazil. J. of South Am. Earth Sci., 110, 103351.

Silva, A. C., Vidal-Torrado, P., 1999. Gênese dos Latossolos húmicos e sua relação com a evolução da paisagem numa área cratônica do Sul de Minas Gerais. R. Bras. Ci. Solo, 23, 329–341.

Singh, B., Gilkes, R. J., 1992. Properties of soil kaolinites from south-western Australia. J. Soil Sci. 43, 645–667.

Singh, B., Gilkes, R. J., 1991. Concentration of iron oxides from soils clays by 5 M NaOH treatment: the complete removal of sodalite and kaolin. Clay Miner. 26, 463–472.

Six, J., Elliott, E. T., Paustian, K., 2000. Soil macroaggregate turnover and microaggregate formation: a mechanism for C sequestration under no-tillage agriculture. Soil Biol. Biochem. 32, 2099–2103.

Smeck, N. E., Torrent, J., Barron, V., 1994. Interactions and weathering losses of iron and phosphorus in Palexeralfs of southern Spain. Soil Sci. Soc. Am. J. 58, 1723–1729.

Smykatz-Kloss, W., 1975. The DTA determination of the degree of (dis-) order of kaolinites: Method and application to some kaolin deposits of Germany, in: Proc. Int. Clay Conf. Wilmette, IL. pp. 429–438

Soil Survey Staff, 1999. Keys to soil taxonomy.8.ed. Washington, United States Department of Agriculture/Pocahontas Press.

Soil Survey Staff, 1975 Soil Taxonomy: A Basic System of Soil Classification for Makingand Interpreting Soil Surveys. US Department of Agriculture, Natural Resources Conservation Service Handbook no. 436. (US Department of Agriculture, Washington DC).

Souza, E., 2019. Reconstituição paleoambiental a partir do sinal fitolítico na ESEC Caetetus – Gália (SP). Dissertação de mestrado. Universidade Estadual do Oeste do Paraná.

Stevaux, J. C., 2000. Climatic events during the Late Pleistocene and Holocene in the Upper Parana River: correlation with NE Argentina and South-Central Brazil. Quat. Int. 72, 73–85.

Stoops, G., 2021. Guidelines for Analysis and Description of Soil and Regolith Thin Sections. Second edition. Soil Sci. Soc. of Am. Inc. Madison.

Stoops, G., V. Marcelino, F. Mees, editors. 2018. Interpretation of micromorphological features of soils and regoliths. Second Edition. Elsevier, Amsterdam.

Stoops, G., 1997. Application of micromorphological methods to the study of soil sequences in the tropics. Edafologia. Soc. Española de Ci. del Suelo, Granada.

Stoops, G., V. Marcelino, S. Zauyah, and A. Maas., 1994. Micromorphology of soils of the humid tropics, in: Ringrose-Voase, A., J., Humphreys, G., S., (Eds.), Soil micromorphology: Studies in management and genesis. Developments in Soil Science. Vol. 22. Elsevier, Amsterdam. pp. 1–15.

Stoops, G., 1989. Relict properties in soils of humid tropical regions with special reference to Central Africa. Catena Suppl. 16, 95-106.

Stoops, G., 1983. - Micromorphology of the oxic horizon. Proc. Vlth Int. Work. Meet. Soi1 Micromorph., London, P. Bullock and C.P. Murphy (Eds), AB Academic Publishers, Rothamsted, pp. 419-440.

Stoops, G., 1967. Le profile d'altération au Bas-Congo (Kinshasa). Sa description et sa genèse. Pedol. 17, 60–105.

Stork, N.E., Eggleton, P., 1992. Invertebrates as determinants and indicators of soil quality. Am. J. of Altern. Agric. 7, 38–47.

Swanson, A. C., Schwendenmann, L., Allen, M. F.,Aronson, E. L., Artavia-León, A., Dierick, D., Fernandez-Bou, A., Harmon, T. C., Murillo-Cruz, C., Oberbauer, S. F., Pinto-Tomás, A. A., Rundel, P. W., Zelikova, T. J., 2019. Welcome to the *Atta* world: A framework for understanding the effects od leaf-cutter ants on ecosystem functions. Funct. Ecol. 33, 1386–1399.

Teixeira, P. C., Donagemma, G. K., Fontana, A., Teixeira, W. G., 2017. Manual de métodos de análise de solo. 3. ed. Embrapa, Brasília, Distrito Federal.

Testoni S. A., Almeida J. A., Silva L., Andrade G. R. P., 2017. Clay mineralogy of Brazilian Oxisols with shrinkage properties. Rev. Bras. Ci. Solo 41, e0160487. https://doi.org/10.1590/18069657rbcs20160487

Tonneijck, F. H., Jongmans, A. G., 2008. The influence of bioturbation on the vertical distribution of soil organic matter in volcanic ash soils: a case study in northern Ecuador. Eur. J. of Soil Sci. 59, 1063–1075.

Torrent, J., Cabedo, A., 1986. Sources of iron oxides in reddish brown soil profiles from calcarenites in southern Spain. Geoderma 37, 57–66.

Trapnell, C. G., Webster, R., 1986. Microaggregates in red earths and related soils in East and Central Africa, their classification and occurrence. J. of Soil Sci. 37, 109–123.

Truffi, S. A., Clemente, C.A., 2002. Alteração de plagioclásios dos riodacitos da Formação Serra Geral (JKsg) da região de Piraju-SP. Sci. Agric. 59, 383–388.

Trunz, V., 1976. The influence of crystallite size on the apparent basal spacing of kaolinite. Clays Clay Miner. 24, 84–87.

Tsai, C., Chen, Z., 2000. Lithologic discontinuities in Ultisols along a toposequence in Taiwan. Soil Sci. 165, 587–596.

United States Department of Agriculture [USDA]. 1996. Soil Survey Laboratory Methods Manual. USDA, Washington, DC, USA.

Vancampenhout, K., Schellekens, J., Slaets, J., Hatté, C., Buurman, P., 2016. Fossil redox conditions influence organic matter composition in loess paleosols. Quat. Int. 418, 105–115.

van Noordwijk, M., Brouwer, G., 1993. Gas-filled root porosity in response to temporary low oxygen supply in different growth stages. Plant and Soil, 152, 187–99.

van Wambeke, A., Eswaran, H., Herbillon, A.J., Comerma, J., 1983. Oxisols. Reprinted from: Pedogênesis and Soil Taxonomy. II. The Soil Orders, by Wilding, L.P., Smeck, N.E., Hall, G.F., (Editors), pp. 325–354.

Vidal-Torrado, P., Cooper, M., 2008. Ferralsol. In: Chesworth, W. (Org.). Encyclopedia of Soil Science. Dordrecht: Springer, pp. 237–240.

Vidal-Torrado, P., Lepsch, I. F., 1999. Relações material de origem solo e pedogênese em uma sequência de solos predominantemente argilosos e latossólicos sobre psamitos na Depressão Periférica Paulista. R. Bras. Ci. Solo 23,357–369.

Vidal-Torrado, P., 1994. Pedogênese e Morfogênese no distrito de Tupi (Piracicaba, SP). Tese de doutorado. Universidade de São Paulo.

Wada, K., Kakuto, Y., 1983. Intergradient vermiculite-kaolin mineral in a Korean Ultisol. Clays and Clay Minerals 31, 183–190.

Wang, C., Arnold, R. W., 1973. Quantifying pedogenesis for soils with discontinuities. Soil Sci. Soc. Am. Proc. 37, 271–278.

Whitford, W. G., Eldridge, D. J., 2013. Effects of ants and termites on soil and geomorphological processes, in: Shroder, J., Butler, D.R., Hupp, C.R. (Eds.), Treatise on Geomorphology 12, Ecogeomorphology. Academic Press, San Diego, CA, pp. 281–292.

Wilkinson, M. T., Richards, P. J., Humphreys, G. S., 2009. Breaking ground: pedological, geological, and ecological implications of soil bioturbation. Earth Sci. Rev. 97, 257–272.

Wilson, O. J., Mayle, F. E., Walters, R. J., Lingner, D. V., Vibrans, A. C., 2021. Floristic change in Brazil's Southern Atlantic forest biodiversity hotspot: From the last glacial

maximum to the late 21st century. Quat. Sci. Rev. 264, 107005. https://doi.org/10.1016/j.quascirev.2021.107005

Wood, T.G., 1988.Termites and soil environment. Biol Fertil. Soils 6, 228–236.

Wood, T.G., 1979. The termite (Isoptera) fauna of Malesian and other tropical rainforests. Transactions of the 6th Aberdeen-Hull Symposium on Malesian Ecology (ed. A.G. Marshall), Aberdeen, pp. 113–32.

Wright, J. P., Jones, C. G., 2006. The concept of organisms as ecosystem engineers ten years on: progress, limitations, and challenges. BioSci.56, 203–209.

Yakushev, V. M., 1968. Influence of termite activity on the development of laterite soil. Sov Soil Sci 1, 109–111.

Yost, J. L., Roden, E. E., Hartemink, E., 2019. Geochemical Fingerprint and Soil Carbon of Sandy Alfisols. Soil Syst. 3, 1–22.

Zegouagh, Y., Derenne, S., Dignac, M. F., Baruiso, E., Mariotti, A., Largeau, C., 2004. Demineralisation of crop soil by mild hydrofluoric acid treatment: influence on organic matter composition and pyrolysis. J. Anal. Appl. Pyrolysis 71, 119–135.

Zhou, Y., Retallack, G. J., Huang, C., 2015. Early Eocene paleosol developed from basalt in southeastern Australia: implications for paleoclimate. Arab. J. Geosci, 8, 1281–1290.

APPENDIX

Appendix A. Guarapuava soil profiles.

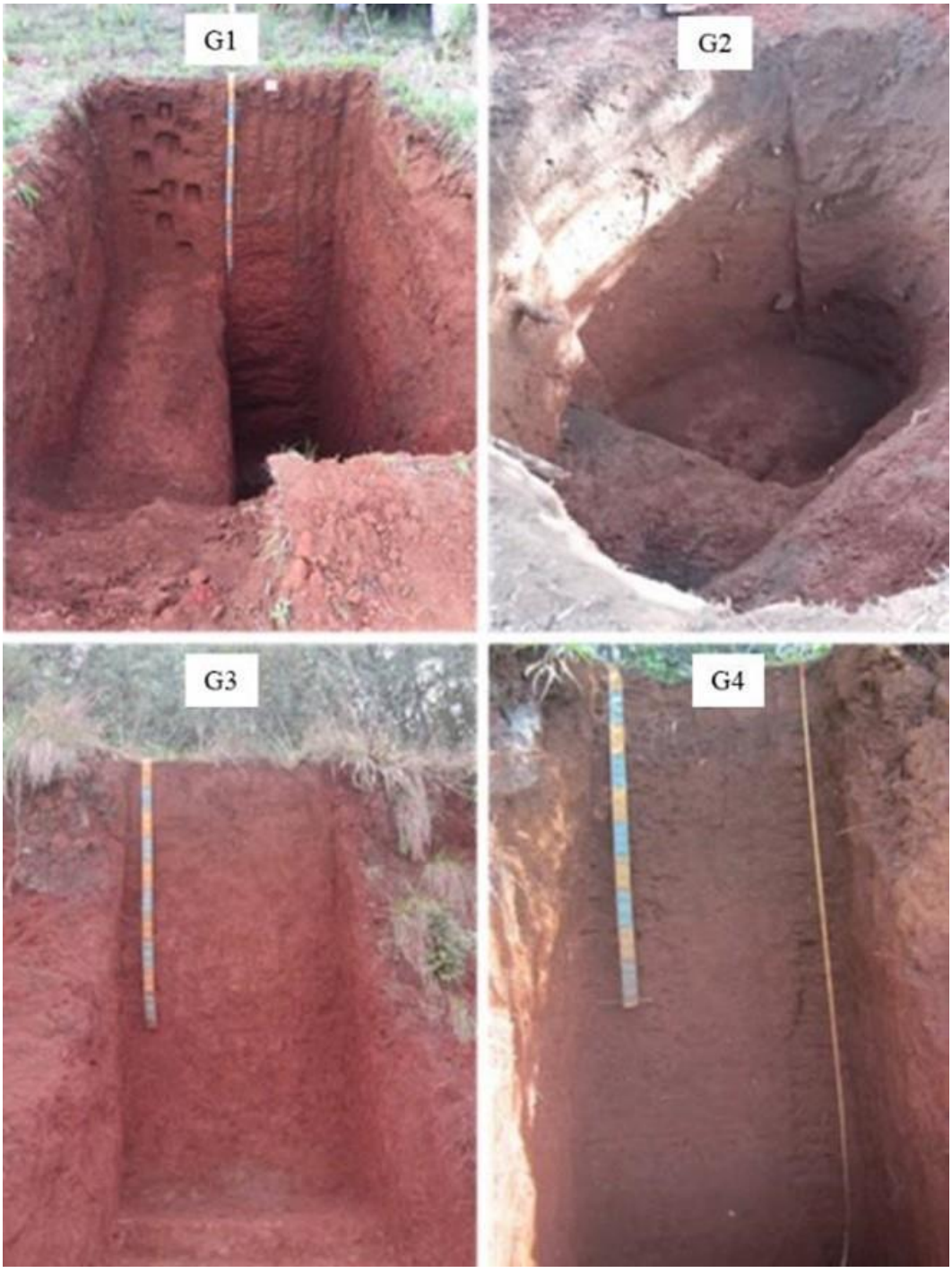

Appendix B. Cascavel soil profiles.

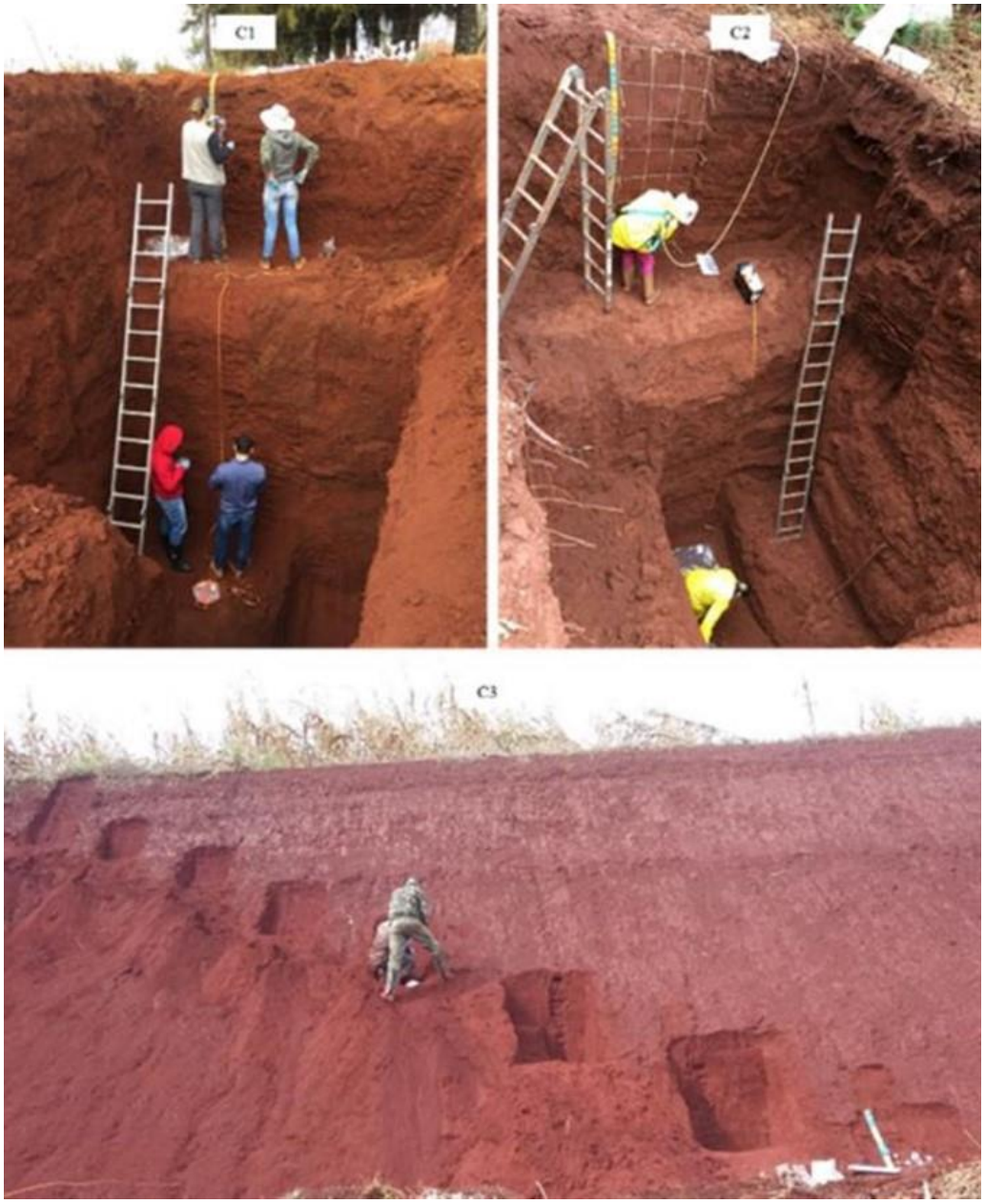

Appendix C. Palotina soil profiles.

Appendix D. Representative current vegetation of the Guarapuava areas.

Appendix E. Representative current vegetation of the Cascavel studied sites.

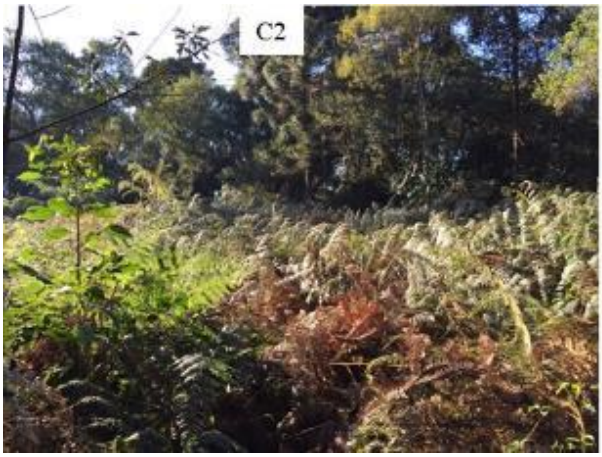

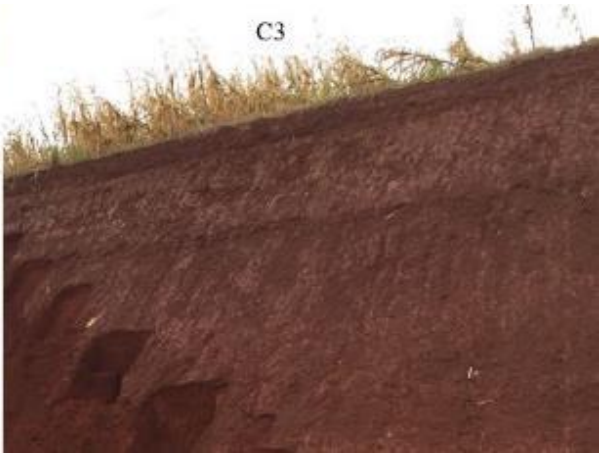

Appendix F. Representative current vegetation of the Palotina studied sites.

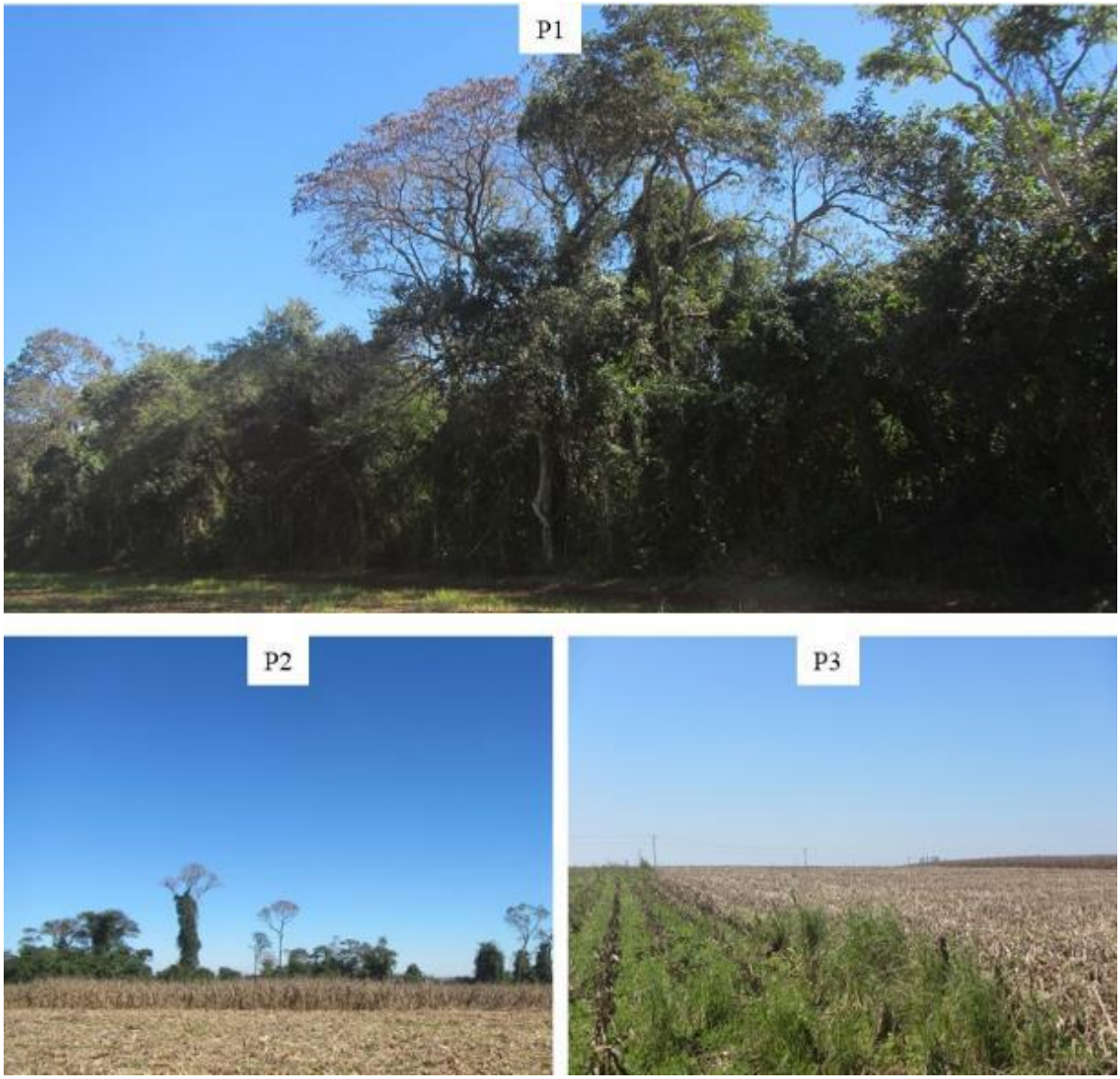

Appendix G. Five size fractions of the sand fraction of the G1 profile from Guarapuava.

Profile	Depth	Sand[1]				
		VC	C[1]	M[1]	F[1]	VF[1]
	cm	g kg^{-1}				
G1	10	6.7	17.4	18.7	25.9	12.6
	20	6.5	16.0	17.4	26.1	16.3
	30	4.1	10.5	13.4	16.3	9.9
	40	7.8	10.5	10.8	14.3	9.6
	50	7.8	9.2	8.1	10.4	8.7
	60	5.6	8.9	7.4	9.7	8.9
	70	7.4	8.7	7.1	9.7	7.4
	80	8.4	8.1	7.1	9.1	8.9
	90	8.3	9.7	7.1	9.7	10.3
	100	6.2	9.1	7.8	10.6	9.6
	110	5.7	8.1	7.8	11.2	9.6
	120	5.7	7.4	7.4	10.0	8.5
	130	6.6	5.7	6.3	9.2	8.6
	140	3.8	3.5	5.3	8.6	7.6
	150	4.6	3.1	4.9	8.2	9.0
	160	3.9	3.4	5.4	8.5	9.0
	170	4.6	4.3	6.1	9.0	9.2
	180	5.3	4.5	6.4	9.5	9.0
	190	5.0	4.7	6.3	9.6	9.4
	200	3.6	4.9	6.4	9.8	9.5
	210	6.6	4.2	6.9	9.5	9.0
	220	4.0	4.5	7.1	9.8	8.7
	230	5.9	4.0	6.2	9.3	8.8
	240	4.4	4.1	6.4	9.6	8.2
	250	6.4	4.9	5.8	9.4	7.9
	260	3.7	4.0	6.8	9.4	9.1
	270	3.1	4.6	6.6	9.7	8.9
	280	4.9	3.8	6.2	9.2	8.5
	290	4.6	3.7	6.0	8.9	8.4
	300	3.7	3.7	6.2	9.3	9.0
	310	3.5	4.0	6.1	9.0	9.0
	320	3.9	4.1	6.5	9.3	9.3
	330	5.0	3.6	6.4	8.9	10.1
	340	4.6	3.8	6.3	9.6	10.2
	350	3.5	4.1	6.7	10.2	11.7
	360	3.8	4.1	7.1	10.7	10.7
	370	3.4	4.0	6.7	10.7	10.4
	380	3.8	3.5	6.8	10.3	9.7
	390	3.0	3.6	6.0	10.9	10.9
	400	3.6	3.9	6.9	10.7	10.1
	410	2.1	3.5	6.2	10.2	10.2
	420	2.8	4.1	6.4	10.4	9.4
	430	7.2	4.0	5.6	9.6	9.1
	440	2.3	2.6	4.9	8.6	8.0
	450	2.6	2.4	5.0	8.8	9.1
	460	2.1	3.6	5.6	9.2	9.2
	470	3.6	3.1	5.1	8.9	8.7
	480	1.9	2.5	4.1	7.4	8.7
	490	1.1	1.9	3.4	6.6	6.6
	500	2.3	1.3	2.6	6.2	6.5

[1]Sand fractions: very coarse (VC: 2–1 mm), coarse (C: 1–0.5 mm), medium (M: 0.5–0.25 mm), fine (F: 0.25–0.10 mm) and very fine (VF: 0.10–0.05 mm) sand.

Appendix H. Five size fractions of the sand fraction of the G4 profile from Guarapuava.

Profile	Depth	Sand[1]				
		VC	C	M	F	VF
	cm	g kg^{-1}				
G4	10	8.7	23.0	17.9	13.8	41.6
	20	13.0	5.4	6.6	9.2	62.6
	30	5.1	4.6	6.1	8.4	31.4
	40	6.1	4.8	4.8	7.4	88.9
	50	3.3	3.8	4.8	7.3	17.4
	60	4.5	5.0	4.8	7.3	24.1
	70	6.2	5.1	4.8	7.0	18.3
	80	3.8	4.5	3.8	6.6	41.4
	90	4.6	2.8	3.3	6.1	43.2
	100	5.3	3.8	3.3	6.3	109.7
	110	5.8	4.3	3.0	5.8	26.0
	120	5.6	4.3	3.1	5.9	22.6
	130	5.8	3.6	2.8	5.8	99.4
	140	23.5	3.0	2.3	4.8	19.7
	150	25.2	2.8	2.0	4.5	46.2
	160	46.1	2.0	1.3	2.5	45.4
	170	17.4	3.5	2.3	5.5	103.4
	180	27.7	3.0	1.5	3.0	85.1
	190	25.1	2.5	1.8	4.1	86.3
	200	28.1	2.8	1.5	3.8	63.2
	210	19.0	3.0	2.0	4.1	83.7
	220	10.2	3.6	2.8	6.4	63.9
	230	13.5	3.3	2.8	6.1	35.6
	240	22.5	2.3	1.8	4.1	68.4
	250	27.1	2.3	1.5	3.6	15.0
	260	12.4	2.5	2.5	5.6	62.3
	270	16.7	2.8	2.3	5.3	18.3
	280	31.8	0.8	0.5	1.0	20.3
	290	27.0	1.8	1.3	3.1	8.4
	300	30.7	2.5	1.5	3.6	23.3
	310	13.9	1.8	1.3	3.3	10.6
	320	14.4	2.3	2.0	5.3	8.1
	330	25.9	2.0	1.5	3.8	19.3
	340	30.1	2.3	1.3	3.6	14.5
	350	28.5	1.3	1.0	2.8	20.6
	360	41.3	1.8	1.0	1.8	3.8

[1]Sand fractions: very coarse (VC: 2–1 mm), coarse (C: 1–0.5 mm), medium (M: 0.5–0.25 mm), fine (F: 0.25–0.10 mm) and very fine (VF: 0.10–0.05 mm) sand.

Appendix I. Five size fractions of the sand fraction of the C3 profile from Cascavel.

Profile	Depth	Sand[1]				
		VC	C	M	F	VF
	cm	g kg^{-1}				
C3	10	3.5	24.8	35.5	37.4	19.9
	20	5.4	21.3	31.5	30.8	13.8
	30	1.9	18.3	27.4	27.1	13.3
	40	3.1	15.9	26.1	26.1	13.6
	50	3.6	19.0	25.9	26.8	12.0
	60	2.8	16.1	25.2	26.6	12.7
	70	4.2	16.6	25.0	25.8	12.6
	80	2.7	17.1	24.1	26.3	12.7
	90	3.7	18.4	26.1	26.9	13.0
	100	4.6	18.5	25.5	26.6	13.4
	110	3.3	18.0	24.5	25.9	13.6
	120	3.3	18.0	26.8	27.1	13.4
	130	4.2	18.0	26.9	26.6	13.8
	140	4.3	16.9	25.4	26.2	14.4
	150	2.3	18.7	26.1	26.3	15.0
	160	2.4	15.8	23.3	26.7	15.0
	170	2.7	19.6	25.8	26.1	15.5
	180	1.9	17.8	25.2	26.0	15.1
	190	4.3	17.1	24.1	26.3	15.7
	200	4.3	15.7	24.6	25.9	15.2
	210	4.7	17.8	25.6	30.6	16.1
	220	4.1	17.8	22.7	24.7	13.4
	230	4.5	15.8	23.1	24.8	13.5
	240	3.3	18.6	26.1	25.0	13.6
	250	3.2	17.1	23.8	25.7	14.7
	260	3.4	15.2	23.4	26.8	14.1
	270	2.2	17.6	23.6	25.7	14.9
	280	3.7	16.1	22.0	26.2	15.5
	290	4.4	18.4	25.2	27.9	15.3
	300	7.1	14.4	21.7	27.1	16.4
	310	3.1	16.1	25.2	31.2	17.4
	320	3.0	17.1	24.4	29.8	16.5
	330	2.9	16.3	25.7	32.0	16.8
	340	4.6	16.2	25.9	33.7	18.0
	350	5.4	17.1	25.3	33.3	18.5
	360	5.2	21.7	29.3	34.8	18.6
	370	5.0	16.4	26.5	35.1	18.7
	380	3.7	18.5	27.3	32.9	17.9
	390	3.9	15.8	25.4	33.2	18.2
	400	4.5	17.5	26.6	33.6	19.8
	410	4.2	17.8	27.2	33.4	18.7
	420	4.2	18.7	26.3	32.2	17.7
	430	6.1	19.0	27.6	31.5	16.7
	440	3.4	17.1	24.3	32.2	19.1
	450	4.3	15.9	23.4	33.7	17.9
	460	6.8	20.1	22.1	34.2	15.9
	470	5.5	17.0	26.3	31.2	17.3
	480	4.9	19.5	25.7	31.4	15.7
	490	5.4	16.7	23.9	30.6	24.7
	500	6.3	19.6	24.6	31.5	11.9
	510	4.9	17.8	20.1	31.2	18.8

Appendix I. Five size fractions of the sand fraction of the C3 profile from Cascavel (continuation).

Profile	Depth	Sand[1]				
		VC	C	M	F	VF
	cm	g kg^{-1}				
C3	520	4.2	19.3	26.0	31.5	19.1
	530	3.6	18.0	26.2	29.8	21.1
	540	4.2	17.9	28.0	33.0	23.0
	550	4.8	17.7	26.2	32.0	21.7
	560	3.0	16.2	25.5	31.6	22.2
	570	5.6	16.6	25.1	31.8	23.5
	580	4.6	16.6	25.2	31.9	20.9
	590	5.5	19.7	26.0	30.6	21.3
	600	4.6	18.9	26.1	32.6	22.9
	610	4.8	17.4	27.1	32.4	23.3
	620	6.9	19.2	27.4	31.5	22.3
	630	4.1	19.0	27.0	33.4	22.4
	640	5.7	16.7	26.4	32.9	23.4
	650	5.2	19.0	27.7	34.5	23.7
	660	3.7	19.9	28.1	34.1	21.8
	670	3.8	19.0	28.7	32.0	23.6
	680	6.3	16.0	27.9	33.0	27.9
	690	6.1	18.0	28.4	29.2	39.8
	700	7.4	17.7	33.0	31.5	28.3
	710	5.9	19.2	32.8	31.8	25.1
	720	5.7	19.1	32.6	32.6	24.5
	730	7.8	17.1	33.4	30.5	30.5
	740	7.5	17.7	32.6	29.6	36.0
	750	7.8	16.2	31.8	29.3	46.4
	760	5.3	19.1	30.7	41.2	36.1
	770	4.4	17.8	30.0	43.1	40.5
	780	3.6	19.4	31.5	42.0	38.6
	790	6.1	19.9	32.2	45.0	43.7
	800	4.5	19.6	32.3	45.8	44.7
	810	4.7	21.0	32.4	44.3	42.7
	820	4.1	19.3	31.9	45.0	50.4
	830	5.5	20.6	32.9	44.7	56.4
	840	4.5	19.4	32.6	45.2	61.7
	850	5.9	20.4	33.2	45.4	62.4
	860	7.5	22.0	32.1	44.2	65.9
	870	8.0	20.9	33.1	46.0	62.2
	880	8.6	21.7	34.2	52.0	52.8
	890	12.1	23.7	34.2	49.7	54.0
	900	10.5	28.2	39.2	52.6	53.6
	910	22.3	16.9	28.7	41.5	52.2
	920	365.1	3.1	4.1	5.1	21.9
	930	282.2	17.1	22.7	25.9	43.6
	940	82.0	15.0	28.4	38.7	49.3
	950	20.4	23.3	42.2	55.8	52.1
	960	31.1	27.3	40.1	51.5	49.7
	970	12.9	32.6	45.0	65.4	56.1
	980	4.2	31.9	45.1	73.6	60.1
	990	27.2	39.0	48.1	68.7	57.3
	1000	22.2	52.2	64.6	83.0	57.4
	1010	34.1	55.6	73.0	89.8	52.5
	1020	20.4	66.3	82.0	94.0	49.0

[1]Sand fractions: very coarse (VC: 2–1 mm), coarse (C: 1–0.5 mm), medium (M: 0.5–0.25 mm), fine (F: 0.25–0.10 mm) and very fine (VF: 0.10–0.05 mm) sand.

Appendix J. Five size fractions of the sand fraction of the P3 profile from Palotina.

Profile	Depth	Sand[1]				
		VC	C	M	F	VF
	cm	g kg^{-1}				
P3	20	17.3	18.8	16.3	21.6	16.3
	30	17.4	14.8	13.3	16.1	12.0
	40	12.3	11.5	11.0	14.3	11.8
	50	24.1	12.5	22.3	15.4	1.3
	60	33.3	13.7	13.1	16.8	13.1
	70	10.7	13.5	12.0	15.1	11.2
	80	11.0	11.0	11.5	14.0	10.5
	90	10.8	12.5	10.8	15.1	11.3
	100	19.6	13.5	9.7	12.5	11.5
	110	33.5	12.0	9.5	13.6	12.0
	120	17.6	12.5	10.2	14.0	12.2
	130	21.7	12.8	10.0	14.3	13.5
	140	11.7	12.2	11.0	14.5	12.2
	150	14.3	12.0	11.2	14.8	14.8
	160	7.1	14.0	12.7	15.3	13.7
	170	10.9	13.2	12.2	15.7	14.5
	180	13.7	12.4	11.9	14.2	13.5
	190	15.2	13.2	11.2	14.7	12.9
	200	7.4	10.7	11.5	14.8	16.0
	210	27.2	14.3	10.2	13.2	13.7
	220	19.4	11.2	10.2	13.5	14.3
	230	32.2	13.0	10.5	13.5	14.3
	240	20.6	11.4	9.7	13.5	13.7
	250	12.5	12.7	11.2	15.3	15.8
	260	23.2	11.2	9.2	11.5	15.6
	270	14.5	10.7	10.2	13.5	14.5
	280	12.2	11.5	9.7	13.8	14.5
	290	14.0	11.2	9.4	13.0	12.5
	300	31.5	9.7	7.9	10.2	14.2

Appendix J. Five size fractions of the sand fraction of the P3 profile from Palotina (continuation).

Profile	Depth	Sand[1]				
		VC	C	M	F	VF
	cm	g kg^{-1}				
P3	310	28.5	9.7	7.4	9.7	14.0
	320	14.5	10.4	9.4	13.0	13.7
	330	15.3	9.7	8.7	12.5	16.3
	340	29.5	9.2	7.6	9.7	14.0
	350	14.2	11.7	10.7	14.7	15.3
	360	16.1	10.7	10.2	13.5	15.3
	370	20.4	9.2	8.1	12.0	16.3
	380	24.0	11.2	9.2	12.2	13.3
	390	16.5	12.5	10.2	12.7	39.1
	400	23.9	11.9	9.9	13.2	16.5
	410	23.9	11.2	10.7	14.2	15.0
	420	20.4	11.0	10.7	14.6	16.1
	430	13.7	12.7	10.9	15.0	17.1
	440	7.1	10.7	10.4	16.1	21.9
	450	23.7	13.3	11.2	13.8	17.3
	460	21.9	11.2	9.7	13.2	15.3
	470	34.8	11.2	10.2	12.5	11.4
	480	25.2	10.7	9.4	13.5	14.3
	490	21.9	12.7	9.7	13.5	14.3
	500	43.0	10.4	8.7	11.2	12.0
	510	25.4	12.1	9.5	13.6	13.8
	520	21.7	11.2	8.9	13.8	15.3
	530	23.5	12.0	11.2	14.3	12.7
	540	30.0	11.2	9.4	13.2	13.5
	550	28.1	10.7	9.2	14.3	14.8
	560	24.8	9.0	8.4	14.1	15.9
	570	43.3	10.9	8.9	10.9	12.5
	580	76.8	9.0	6.4	6.9	8.4

[1]Sand fractions: very coarse (VC: 2–1 mm), coarse (C: 1–0.5 mm), medium (M: 0.5–0.25 mm), fine (F: 0.25–0.10 mm) and very fine (VF: 0.10–0.05 mm) sand.

Appendix K. Quantified pyrolysis products of HF/HCl residue.

Code	Pyrolysis product	m/z[1]
Ar1	Benzene	78
Ar2	Toluene	91+92
Ar3	Indene	115+116
Ar4	C_2 benzene	91+106
Ar5	C_2 benzene	91+106
Ar6	C_2 benzene	91+106
Ar7	Benzene,1,3-bis(1,1-dimethyl)	175+190
Bf1	Benzofuran	89+118
PAH1	Naphthalene	128
PAH2	C_1 naphthalene	141+142
PAH3	C_1 naphthalene	141+142
PAH4	Biphenyl	154
PAH5	Anthracene	178
PAH6	Phenanthrene	178
PAH7	Terphenyl, 4-phenyl	306
PAH8	2,4-diphenyl-4-methyl-2(z)-pentene	221+143
N1	Pyrrole	67
N2	Benzonitrile	76+103
N3	Pyridine	52+79
N4	C_1 pyridine	66+93
N5	C_1 pyridine	66+93
Lg1	Guaiacol	109+124
Lg2	4-vinylphenol	91+120
Lg3	4-vinylguaiacol	135+150
Lg4	Syringol	139+154
Lg5	4-vinylsyringol	165+180
Lg6	C_3Guaiacol Trans	164
Lg7	C_3Syringol Trans	194
Ph	Phenol	66+94
Ps1	2-Furaldehyde	95+96
Ps2	5-methyl-2-Furaldehyde	109+110
Ps3	Unidentified carbohydrate	74+87
Ps4	Unidentified carbohydrate	74+101
Ps5	Unidentified carbohydrate	74+101

[1] Fragment ions used for quantification.

Appendix L. XRD patterns of the sand fraction of the representative soil horizons of the studied soils (G1, G4 and C3: Bfl_1 horizon; P3: Bfl_2 horizon). Mg: magnetite; Kt: kaolinite; Qz: quartz; Gt: goethite; Il: ilmenite; Na: anatase; Ru: rutile; Hm: hematite; Zr: zircon.

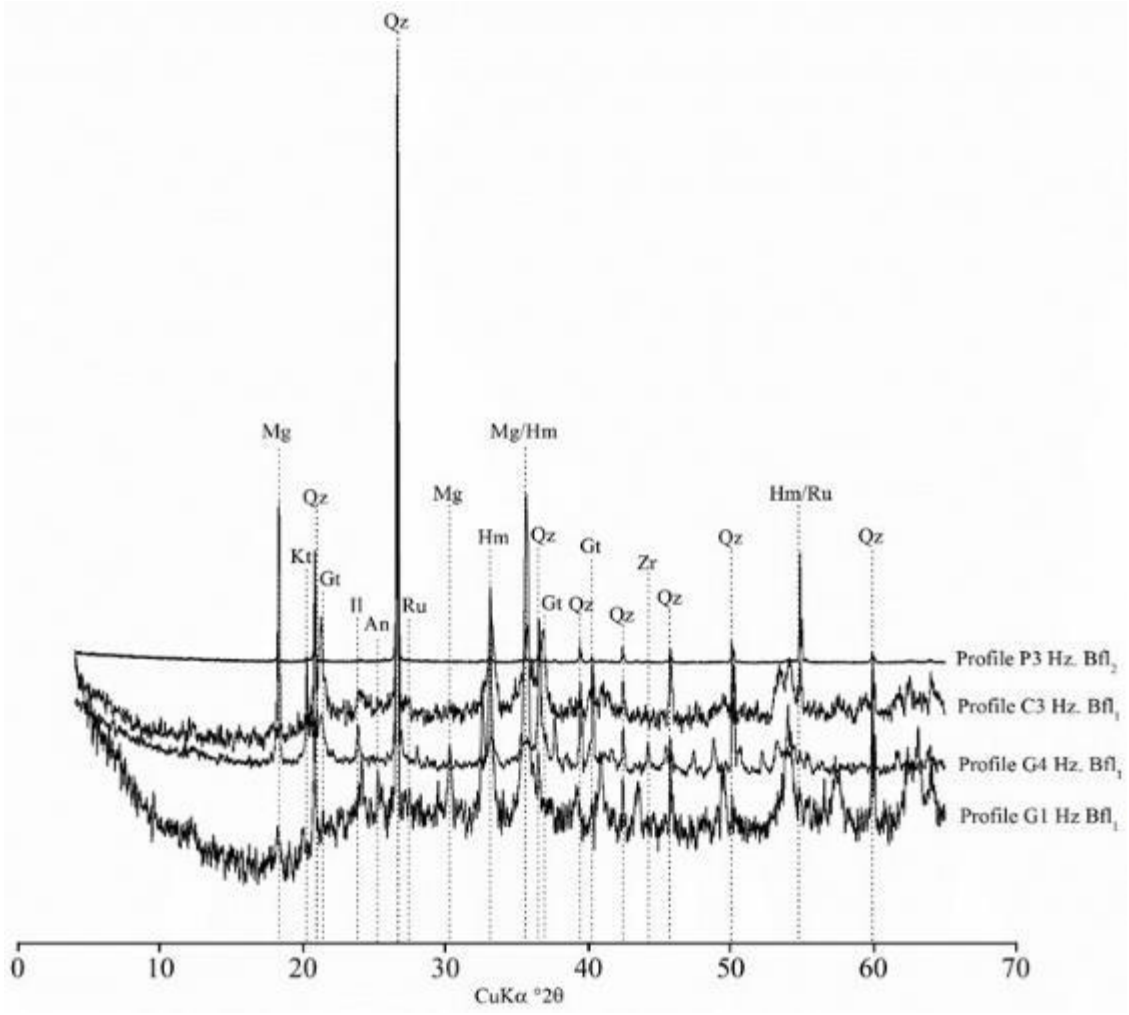

Appendix M. Micromorphological characteristics of the representative Guarapuava studied soils (G4 profile).

Profile G4	Hz. A3 (65-80cm)	Hz. Bfl_1 (150-165 cm)	Hz. Bfl_3 (220-235 cm)
Groundmass	Coarse material: 5 % Fine material: 65 % Porosity: 30 %	Coarse material: 5 % Fine material: 62 % Porosity: 33 %	Coarse material: 7 % Fine material: 65 % Porosity: 28 %
c/f* related distribution	Enaulic-Porphyric 1/13	Enaulic-Porphyric 1/12.4	Enaulic-Porphyric 1/9.2
Coarse Material	Quartz: 95 % (dominance of fine and very fine sand, subrounded shape and well-sorted) Nodules of Fe/Mn: 3% Charcoal: 2 %	Quartz: 95% (dominance of fine and very fine sand, subrounded shape and well-sorted) Nodules of Fe/Mn: 3 % Fragments of weathered rocks: 2%	Quartz: 95 % (dominance of fine and very fine sand, subrounded shape and well-sorted) Nodules of Fe/Mn: 3 % Fragments of weathered rocks: 2%
Fine Material	Clay, Fe and Al oxyhydroxides and organic matter	Clay and Fe and Al oxyhydroxides	Clay and Fe and Al oxyhydroxides
Pores	Packing voids dominate; policoncave vughs, chambers, fissres and channels	Packing voids dominate; policoncave vughs, chambers, fissres and channels	Packing voids dominate; policoncave vughs, chambers, fissres and channels
Microstructure	Medium-small subangular blocky peds and coalesced microaggregates/granules with moderately-strongly developed pedality	Medium-small subangular blocky peds and coalesced microaggregates/granules with moderately-strongly developed pedality	Medium-small subangular blocky peds and coalesced microaggregates/granules with moderately-strongly developed pedality
***b*-fabrics**	speckled	speckled, porostriated, granostriated	speckled
Pedofeatures	Presence abundant of loose continuous and discontinuous of channels and cavities resulted from the fauna activity. Presence of root biological features. Common presence of typic iron/manganese nodules	Presence abundant of loose continuous and discontinuous of channels and cavities resulted from the fauna activity. Presence of root biological features. Common presence of typic iron/manganese nodules and dense clay nodules. Presence of basaltic lithorelicts	Presence abundant of loose continuous and discontinuous of channels and cavities resulted from the fauna activity. Presence of root biological features. Common presence of typic iron/manganese nodules and dense clay nodules. Presence of basaltic lithorelicts

*2μm

Appendix M. Micromorphological characteristics of the representative Guarapuava studied soils (G4 profile) (continuation).

Profile G4	Hz. BC_1 (290-305 cm)	Hz. BC_2 (330-345 cm)	Hz. BC_r (360 cm)
Groundmass	Coarse material: 5 % Fine material: 70 % Porosity: 25 %	Coarse material: 3 % Fine material: 75 % Porosity: 22 %	Coarse material: 32 % Fine material: 50 % Porosity: 18 %
c/f* related distribution	Porphyric-Enaulic 1/14	Porphyric 1/25	Porphyric 1/1.5
Coarse Material	Quartz: 95 % (dominance of fine and very fine sand, subrounded shape and well-sorted) Nodules of Fe/Mn: 3% Fragments of weathered rocks: 2%	Quartz: 94 % (dominance of fine and very fine sand; presence of phenocrystals; subrounded shape and well-sorted) Nodules of Fe/Mn: 3% Fragments of weathered rocks: 3%	Quartz: 5 % (dominance of fine and very fine sand; subrounded shape and well-sorted) Nodules of Fe/ Mn: 5 % Fragments of weathered rocks: 90 %
Fine Material	Clay and Fe and Al oxyhydroxides	Clay and Fe and Al oxyhydroxides	Clay and Fe and Al oxyhydroxides
Pores	Packing voids, vughs, chambers and fissures	Chambers, vughs and fissures	Policoncave vughs, chambers and fissures
Microstructure	Medium-small subangular blocky peds and samll microaggregates/granules, with moderately-weakly developed pedality	Medium subangular blocky peds, with moderately-weakly developed pedality	Medium subangular blocky peds, with moderately-weakly developed pedality
***b*-fabrics**	speckled, Porostriated and granostriated	speckled, mosaic speckled, porostriated, granostriated	speckled
Pedofeatures	Presence abundant of loose continuous and discontinuous of channels and cavities, dense incomplete infillings from fauna activity. Dense incomplete infillings with bow-like structure and vermicular microstructure. Common presence of typic iron/manganese nodules. Presence of basaltic lithorelicts	Presence abundant of loose continuous and discontinuous of channels and cavities resulted from the fauna activity. Dense incomplete infillings with bow-like structure and vermicular microstructure. Presence of root biological features. Common presence of typic iron/manganese nodules. Presence of basaltic lithorelicts	Presence abundant of loose continuous and discontinuous of channels. Common presence of typic iron/manganese

*2μm

Appendix N. Micromorphological characteristics of the representative Cascavel studied soils (C3 profile).

Profile C3	Hz. AB (30-45cm)	Hz. Bfl_1 (160-170 cm)	Hz. Bfl_3 (590-600 cm)
Groundmass	Coarse material: 3 % Fine material: 70 % Porosity: 27 %	Coarse material: 3 % Fine material: 66 % Porosity: 31 %	Coarse material: 3 % Fine material: 66 % Porosity: 31 %
c/f* related distribution	Enaulic- Porphyric	Enaulic- Porphyric	Enaulic
G/F*	1/23.3	1/22	1/23.3
Coarse Material	Quartz: 95 % (dominance of fine and very fine sand; subrounded shape and well-sorted) Nodules of Fe/Mn: 2 % Charcoal: 3 %	Quartz: 97 % (dominance of fine and very fine sand; subrounded shape and well-sorted) Nodules of Fe/Mn: 3 %	Quartz: 97 % (dominance of fine and very fine sand; presence of phenocrystals; subrounded shape and well-sorted) Nodules of Fe/Mn: 3 %
Fine Material	Clay, Fe and Al oxyhydroxides and organic matter	Clay and Fe and Al oxyhydroxides	Clay and Fe and Al oxyhydroxides
Pores	Packing voids dominate; chambers and fissures	Packing voids dominate; chambers and fissures	Packing voids dominate; chambers, fissures and chambers
Microstructure	Medium subangular blocky peds and coalesced microaggregates/granules, with moderately-strongly developed pedality	Medium subangular blocky peds and coalesced microaggregates/granules, with moderately-strongly developed pedality	Microgranular with strongly developed pedality
***b*-fabrics**	speckled	speckled, porostriated, granostriated	undifferentiated
Pedofeatures	Presence abundant of loose continuous and discontinuous of channels and cavities resulted from the fauna activity. Common presence of typic iron/manganese nodules.	Presence abundant of loose continuous and discontinuous of channels and cavities resulted from the fauna activity. Common presence of typic iron/manganese nodules and dense clay nodules.	Presence abundant of loose continuous and discontinuous of channels and cavities resulted from the fauna activity. Dense incomplete infillings with bow-like structure and vermicular microstructure. Common presence of typic iron/manganese nodules. Presence brown-yellowish dense clay nodules with diffuse boundaries. Presence of basaltic lithorelicts

*2μm

Appendix N. Micromorphological characteristics of the representative Cascavel studied soils (C3 profile) (continuation).

Profile C3	Hz. Bfl_4 (825-835 cm)	Hz. BC_2 (955-965 cm)	Hz. BC_r (1025-1035 cm)
Groundmass	Coarse material: 5 % Fine material: 70 % Porosity: 25 %	Coarse material: 7 % Fine material: 68 % Porosity: 25 %	Coarse material: 30 % Fine material: 50 % Porosity: 20 %
c/f* related distribution	Porphyric	Porphyric	Porphyric
G/F*	1/14	1/9.7	1/8.5
Coarse Material	Quartz: 97 % (dominance of fine and very fine sand; presence of phenocrystals; subrounded and rounded shape and well-sorted) Nodules of Fe/Mn: 3 %	Quartz: 97 % (dominance of fine and very fine sand; presence of phenocrystals; subrounded shape and well-sorted) Nodules of Fe/Mn: 3 %	Quartz: 10 % (dominance of fine and very fine sand; presence of phenocrystals; subrounded shape and well-sorted) Nodules of Fe/Mn: 5 % Fragments of weathered rocks: 85 %
Fine Material	Clay and Fe and Al oxyhydroxides	Clay and Fe and Al oxyhydroxides	Clay and Fe and Al oxyhydroxides
Pores	Chambers and fissures dominate	Chambers dominate; fissures and small channels	Vughs dominate; chambers, fissures and small channels
Microstructure	Medium subangular blocky peds and coalesced microaggregates/granules, with moderately-weakly developed pedality	Medium subangular and angular blocky peds, with moderately-weakly developed pedality	Medium subangular and angular blocky peds, with moderately-weakly developed pedality
***b*-fabrics**	speckled	speckled, porostriated, granostriated	speckled
Pedofeatures	Presence abundant of loose continuous and discontinuous of channels and cavities resulted from the fauna activity. Common presence of typic iron/manganese nodules. Presence reddish dense clay nodules with diffuse boundaries. Presence of basaltic lithorelicts	Presence abundant of loose continuous and discontinuous of channels and cavities resulted from the fauna activity. Common presence of typic iron/manganese nodules. Some nodules showed pores and fissures.	Presence abundant of loose continuous and discontinuous of channels and cavities resulted from the fauna activity. Common presence of typic iron/manganese nodules.

*2μm

Appendix O. Micromorphological characteristics of the representative Palotina studied soils (P3 profile).

Profile P3	**Hz. Bfl_1 (13-23cm)**	**Hz. Bfl_2 (50-65 cm)**	**Hz. Bfl_4 (150-160 cm)**
Groundmass	Coarse material: 3 % Fine material: 66 % Porosity: 31 %	Coarse material: 2 % Fine material: 68 % Porosity: 30 %	Coarse material: 2 % Fine material: 64 % Porosity: 34 %
c/f* related distribution	Porphyric - Enaulic	Enaulic - Porphyric	Enaulic - Porphyric
G/F*	1/22	1/34	1/32
Coarse Material	Quartz: 96 % (dominance of fine and very fine sand; subrounded and rounded shape and well-sorted) Nodules of Fe/Mn: 4 %	Quartz: 96 % (dominance of fine and very fine sand; subrounded and rounded shape and well-sorted) Nodules of Fe/Mn: 4 %	Quartz: 96 % (dominance of fine and very fine sand; subrounded and rounded shape and well-sorted) Nodules of Fe/Mn: 3 % Fragments of weathered rocks: 1 %
Fine Material	Clay, Fe and Al oxyhydroxides and organic matter	Clay and Fe and Al oxyhydroxides	Clay and Fe and Al oxyhydroxides
Pores	Policoncave vughs, chambers and fissures. Regions with packing voids.	Packing voids dominate; policoncave vughs, chambers and fissures.	Packing voids dominate; policoncave vughs, chambers and fissures.
Microstructure	Medium subangular blocky peds and microaggregates/granules with moderately developed pedality	Medium subangular blocky peds and microaggregates/granules with strongly developed pedality	Medium subangular blocky peds and microaggregates/granules with strongly developed pedality
***b*-fabrics**	Speckled, porostriated, granostriated	Speckled, porostriated, granostriated	Speckled, porostriated, granostriated
Pedofeatures	Presence abundant of loose continuous and discontinuous of channels and cavities resulted from the fauna activity. Common presence of typic iron/manganese nodules and dense clay nodules.	Presence abundant of loose continuous and discontinuous of channels and cavities resulted from the fauna activity. Common presence of typic iron/manganese nodules. Presence reddish dense clay nodules. Presence of root biological features.	Presence abundant of loose continuous and discontinuous of channels and cavities resulted from the fauna activity. Common presence of typic iron/manganese nodules and dense clay nodules. Presence of basaltic lithorelicts.

*2μm

Appendix O. Micromorphological characteristics of the representative Palotina studied soils (P3 profile) (continuation).

Profile P3	Hz. Bfl_5 (280-300cm)	Hz. Bfl_7 (540-555 cm)	Hz. BC_r (600-620 cm)
Groundmass	Coarse material: 2 % Fine material: 66 % Porosity: 32 %	Coarse material: 3 % Fine material: 67 % Porosity: 30 %	Coarse material: 30 % Fine material: 50 % Porosity: 20 %
c/f* related distribution	Enaulic - Porphyric	Porphyric	Porphyric
G/F*	1/33	1/22.3	1/1.66
Coarse Material	Quartz: 96 % (dominance of fine and very fine sand; presence of phenocrystals; subrounded and rounded shape and well-sorted) Nódulos de Fe/Mn: 4 %	Quartz: 96 % (dominance of fine and very fine sand; subrounded and rounded shape and well-sorted) Nódulos de Fe/Mn: 4 %	Quartz: 10 % (dominance of fine and very fine sand; subrounded and rounded shape and well-sorted) Nódulos de Fe/Mn: 5 % Fragments of weathered rocks: 85 %
Fine Material	Clay and Fe and Al oxyhydroxides	Clay and Fe and Al oxyhydroxides	Clay and Fe and Al oxyhydroxides
Pores	Packing voids dominate; policoncave vughs, chambers and fissures.	Vughs dominate; chambers and fissures	Vughs dominate; chambers, fissures and small channels
Microstructure	Subangular blocky peds and microaggregates/granules with strongly developed pedality	Medium subangular blocky peds, moderately-strongly developed pedality	Small prisms, moderately-weakly pedality
***b*-fabrics**	Speckled, porostriated, granostriated	speckled, porostriated, granostriated	crystallitic, speckled,
Pedofeatures	Presence abundant of loose continuous and discontinuous of channels and cavities resulted from the fauna activity. Common presence of typic iron/manganese nodules and dense clay nodules.	Presence abundant of loose continuous and discontinuous of channels and cavities resulted from the fauna activity. Common presence of typic iron/manganese nodules.	Presence abundant of loose continuous and discontinuous of channels and cavities resulted from the fauna activity. Common presence of typic iron/manganese nodules. Some nodules showed pores and fissures.

*2μm

Appendix P. Additional chemical properties of the studied profiles in Guarapuava.

Profile	Hz	Depth	H + Al	Al^{3+}	K^{+}	Na^{+}	Ca^{2+}	Mg^{2+}	Sum of bases	CEC effective[1]	SiO_2[2]	Al_2O_3[2]	TiO_2[2]	Fe_2O_3[2]
		cm					$cmol_c\ kg^{-1}$					%		
G1	Apa	0–30	8.7	0.1	0.3	0	3.4	2.2	5.9	6.0	-	-	-	-
	AB	30 –75	8.0	0.3	0.1	0	1.3	1.3	2.7	3.0	-	-	-	-
	BA	75–105	6.5	0.1	0.1	0	1.3	1.8	3.2	3.3	-	-	-	-
	Bfl_1	105–135	4.2	0.1	0.1	0	0	0.5	0.6	0.7	15.5	32.5	5.1	15.8
	Bfl_2	135–180	3.6	0.1	0.1	0	0.6	0.5	1.2	1.3	-	-	-	-
	Bfl_3	180–225	3.4	0.1	0.1	0	0	0.3	0.4	0.4	-	-	-	-
	Bfl_4	225–280	3.0	0.1	0.1	0	0	0.3	0.4	0.5	-	-	-	-
	Bfl_5	280–360	3.5	0.2	0.1	0	0	0.3	0.4	0.5	-	-	-	-
	Bfl_6	360–410	4.4	0.6	0.1	0	0	0.3	0.4	1.0	-	-	-	-
	BC_1	410–475	4.8	1.1	0.1	0	0.3	0.3	0.7	1.8	-	-	-	-
	BC_2	475–500	5.2	1.1	0.1	0	0	0	0.1	1.2	-	-	-	-
	BCg	500 +	5.2	2.4	0.1	0	0.3	0.3	0.7	3.1	-	-	-	-
G2	A_1	0–30	15.8	2.3	0.1	0	0.5	0.5	1.1	3.4	-	-	-	-
	A_2	30–55	12.3	1.6	0.1	0	0	0.3	0.4	2.0	-	-	-	-
	A_3	55–75	9.7	0.8	0.1	0	0	0.5	0.6	1.4	-	-	-	-
	AB	75–100	8.2	0.2	0.1	0	0	1.0	1.1	1.3	-	-	-	-
	BA	100–120	5.8	0.1	0.1	0	0	1.0	1.1	1.2	-	-	-	-
	Bfl_1	120–170	3.9	0	0.1	0	0.3	0.5	0.9	0.9	-	-	-	-
	Bfl_2	170–200	3.1	0.1	0.1	0	0	0.3	0.4	0.5	-	-	-	-
	Bfl_3	200–260 +	3.2	0.1	0.2	0	0	0	0.3	0.3	-	-	-	-
G3	A_1	0–30	12.6	1.1	0.1	0	0.4	0.5	1.0	2.1	-	-	-	-
	A_2	30–55	10.8	0.8	0.1	0	0.4	0.3	0.8	1.6	-	-	-	-
	A_3	55–80	9.1	0.3	0.1	0	0.4	0.3	0.8	1.1	-	-	-	-
	AB	80–95	5.0	0	0.1	0	0.4	0.3	0.8	0.8	-	-	-	-
	BA	95–120	5.2	0.1	0.1	0	0.5	0.5	1.1	1.2	-	-	-	-
	Bfl_1	120–180	3.4	0.2	0.1	0	0	0.3	0.4	0.5	-	-	-	-
	Bfl_2	180–240	3.4	0.3	0.1	0	0	0.3	0.4	0.6	-	-	-	-
	Bfl_3	240–260	2.8	0.1	0.1	0	0.3	0.3	0.7	0.8	-	-	-	-
	BCr	260 +	3.7	0.4	0.1	0	0.4	0.3	0.8	1.2	-	-	-	-
G4	A_1	0–25	19.5	3.7	0.1	0.1	0	0.3	0.5	4.2	-	-	-	-
	A_2	25–55	19.1	3.4	0.1	0.1	0	0.3	0.4	3.8	-	-	-	-
	A_3	55–80	14.5	2.8	0.1	0	0	0	0.1	2.9	-	-	-	-
	AB	80–120	11.8	2.2	0.1	0	0	0	0.1	2.3	-	-	-	-
	BA	120–140	8.9	1.6	0.1	0	0	0.3	0.4	2.0	-	-	-	-
	Bfl_1	140–160	8.0	1.1	0.1	0	0	0.3	0.4	1.5	18.3	25.8	11.6	23.0
	Bfl_2	160–190	6.6	0.6	0.1	0	0	0	0.1	0.7	19.2	26.2	10.2	23.2
	Bfl_3	190–280	4.0	0.8	0.1	0	0	0	0.1	0.9	17.8	27.1	9.2	25.7
	BC_1	280–330	4.0	0.1	0.1	0	0.5	0.3	0.9	1.0	-	-	-	-
	BC_2	330–360	3.7	0.2	0.1	0	0	0	0.1	0.3	-	-	-	-
	BCr	360 +	2.6	0	0.1	0	0	0.3	0.4	0.4	-	-	-	-

[1]CEC effective = effective cation exchange capacity; [2]SiO_2, Al_2O_3, TiO_2 and Fe_2O_3 = determined in sulphuric extract.

Appendix Q. Additional chemical properties of the studied profiles in Cascavel.

Profile	Hz	Depth	H + Al	Al^{3+}	K^+	Na^+	Ca^{2+}	Mg^{2+}	Sum of bases	CEC effective[1]	SiO_2[2]	Al_2O_3[2]	TiO_2[2]	Fe_2O_3[2]
		cm	$cmol_c\ kg^{-1}$								%			
C1	Apa_1	0–35	16.3	2.0	0.1	0	1.0	0.5	1.6	3.6	-	-	-	-
	Apa_2	35–45	12.8	1.2	0.1	0	1.8	0.6	2.5	3.7	-	-	-	-
	Apa_3	45–55	10.4	0.8	0.1	0	0.9	0.7	1.7	2.5	-	-	-	-
	AB	55–65	8.8	0.2	0.1	0	0.9	0.8	1.8	2	-	-	-	-
	BA	65–85	7.3	0.4	0.1	0	0.9	0.8	1.8	2.2	-	-	-	-
	Bfl_1	85–135	5.4	0	0	0	0.6	0.6	1.3	1.3	-	-	-	-
	Bfl_2	135–200	4.4	0	0	0	0.4	0.5	1.0	1.0	-	-	-	-
	Bfl_3	200–290	3.5	0	0	0	0.6	0.4	1.0	1.0	-	-	-	-
	Bfl_4	290–420	3.5	0	0	0	0.2	0.1	0.4	0.4	-	-	-	-
	Bfl_5	420–540	4.4	0	0	0	0.4	0.1	0.6	0.6	-	-	-	-
	BC	540 +	4.4	0.6	0	0	0.2	0	0.2	0.8	-	-	-	-
C2	A_1	0–15	16.1	3.5	0.1	0	0.2	0	0.3	3.8	-	-	-	-
	A_2	15–40	12.2	2.3	0	0	0.1	0	0.2	2.5	-	-	-	-
	A_3	40–50	11.1	1.7	0	0	0.1	0	0.2	1.9	-	-	-	-
	AB	50–90	8.5	1.0	0	0	0.1	0	0.2	1.2	-	-	-	-
	BA	90–145	6.1	0.6	0	0	0.2	0	0.3	0.9	-	-	-	-
	Bfl_1	145–350	4.6	0	0	0	0.2	0	0.2	0.2	-	-	-	-
	Bfl_2	350–500	4.3	0	0	0	0.2	0.1	0.3	0.3	-	-	-	-
	Bfl_3	500–620	4.1	0.1	0	0	0.2	0	0.3	0.3	-	-	-	-
	Bfl_4	620–670	4.7	0.3	0	0	0.1	0	0.2	0.5	-	-	-	-
	Trad 1	700	4.9	0.4	0	0	0.1	0	0.2	0.6	-	-	-	-
	Trad 2	750	5.3	0.6	0	0	0.2	0	0.2	0.8	-	-	-	-
	Trad 3	800	5.4	0.6	0	0	0.2	0	0.3	0.9	-	-	-	-
	Trad 4	850	5.4	0.9	0	0	0.1	0	0.2	1.1	-	-	-	-
	Trad 5	900–920	5.4	1.0	0	0	0.1	0	0.2	1.2	-	-	-	-
	Trad 6	1000–1050	6.0	1.7	0	0	0.3	0.1	0.4	2.1	-	-	-	-
C3	Apa	0–20	7.9	0.1	0.1	0	3.6	1.3	5.0	5.1	-	-	-	-
	AB	20–60	10.6	0.9	0.1	0	1.1	0.6	1.8	2.6	-	-	-	-
	BA	60–120	7.2	0.2	0.1	0	1.3	0.7	2.1	2.3	-	-	-	-
	Bfl_1	120–265	3.4	0	0	0	0.5	0.1	0.7	0.7	14.6	28.1	6.0	31.2
	Bfl_2	265–360	3.6	0	0	0	0.5	0.1	0.6	0.6	16.6	27.2	7.7	34.2
	Bfl_3	360–745	3.0	0	0	0	0.2	0.1	0.4	0.4	29.6	27.7	6.0	33.5
	Bfl_4	745–860	4.5	0.1	0	0	0.2	0.1	0.3	0.5	-	-	-	-
	BC_1	860–910	4.5	0.2	0	0	0.2	0	0.3	0.6	-	-	-	-
	BC_2	910–1025	4.8	0.4	0	0	0.2	0	0.3	0.7	-	-	-	-
	BCr	1025 +	5.5	0.5	0.1	0	0.3	0	0.4	1.0	-	-	-	-

[1]CEC effective = effective cation exchange capacity; [2]SiO_2, Al_2O_3, TiO_2 and Fe_2O_3 = determined in sulphuric extract.

Appendix R. Additional chemical properties of the studied profiles in Palotina.

Profile	Hz	Depth	H + Al	Al^{3+}	K^+	Na^+	Ca^{2+}	Mg^{2+}	Sum of bases	CEC effective[1]	SiO_2	Al_2O_3	TiO_2	Fe_2O_3
		cm	$cmol_c\ kg^{-1}$								%			
P1	A	0–30	4.1	0.1	0.2	0	7.3	1.7	9.2	9.3	-	-	-	-
	AB	30–50	3.2	0	0.1	0	0.2	0.4	0.7	0.7	-	-	-	-
	Bfl_1	50–90	1.5	0	0.6	0	2.2	1.1	3.9	4	-	-	-	-
	Bfl_2	90–140	3.1	0.1	0.1	0	1.7	1.3	3.1	3.2	-	-	-	-
	Bfl_3	140–290	3.6	0.1	0	0	1.6	0.8	2.4	2.5	-	-	-	-
	Bfl_4	290–430	2.2	0	0.2	0	1.5	1.2	2.9	2.9	-	-	-	-
	BCr	430 +	2.3	0	0.4	0	1.0	1.2	2.6	2.7	-	-	-	-
P2	Ap	0–10	4.9	0.1	0.5	0	3.5	2.0	6.0	6.1	-	-	-	-
	AB	10–40	4.1	0	0.4	0	2.8	1.8	5.0	5.0	-	-	-	-
	Bfl_1	40–90	3.8	0.8	0.1	0	0.7	0.6	1.4	2.2	-	-	-	-
	Bfl_2	90–180	2.2	0	0.1	0	1.8	1.2	3.1	3.2	-	-	-	-
	Bfl_3	180–350	2.4	0	0	0	1.6	1.5	3.1	3.2	-	-	-	-
	Bfl_4	350–650	4.1	0.9	0	0	0.5	0.8	1.4	2.3	-	-	-	-
	Bfl_5	650 +	4.5	1.1	0	0	0.3	0.5	0.9	1.9	-	-	-	-
	Trad 1	850	4.1	1.0	0.1	0	0.3	0.6	1.0	2.0	-	-	-	-
	Trad 2	900	4.0	1.5	0	0	0.2	0.4	0.7	2.2	-	-	-	-
	Trad 3	960	4.1	1.3	0.1	0	0.1	0	0.2	1.5	-	-	-	-
P3	Ap	0–10	9.4	0.8	0.2	0	2.1	1.0	3.3	4.1	-	-	-	-
	Bfl_1	10–45	5.9	0.4	0	0	2.4	0.6	3.1	3.4	19.1	19.1	5.8	19.3
	Bfl_2	45–105	2.4	0	0	0	3.0	0.5	3.5	3.5	28.3	24.1	5.3	20.8
	Bfl_3	105–140	2.8	0.1	0	0	3.8	1.6	5.5	5.6	29.1	25.6	4.5	20.1
	Bfl_4	140–255	5.6	1.4	0	0	0.7	0.8	1.5	2.9	-	-	-	-
	Bfl_5	255–335	5.5	1.9	0	0	0.4	0.3	0.8	2.7	-	-	-	-
	Bfl_6	335–510	5.8	2.2	0	0	0.4	0.2	0.6	2.8	29.8	26.7	4.7	19.4
	Bfl_7	510–600	4.5	1.2	0	0	0.2	0.5	0.7	1.9	25.2	25.2	5.7	22.7
	BCr	600–640	7.8	2.6	0.1	0	0.2	0.4	0.7	3.3	-	-	-	-

[1] CEC effective = effective cation exchange capacity; [2]SiO_2, Al_2O_3, TiO_2 and Fe_2O_3 = determined in sulphuric extract.

Appendix S. Physical properties of the Guarapuava soil profiles.

Profile	Hz	Depth	Clay	Silt	Total Sand	Silt/Clay
		cm		g kg^{-1}		
G1	A_{pa}	0–30	725	163	113	0.2
	AB	30 –75	725	138	138	0.2
	BA	75–105	738	100	163	0.1
	Bfl_1	105–135	788	100	113	0.1
	Bfl_2	135–180	863	100	38	0.1
	Bfl_3	180–225	750	75	175	0.1
	Bfl_4	225–280	763	75	163	0.1
	Bfl_5	280–360	800	63	138	0.1
	Bfl_6	360–410	800	75	125	0.1
	BC_1	410–475	788	88	125	0.1
	BC_2	475–500	813	50	138	0.1
	BCg	500 +	775	75	150	0.1
G2	A_1	0–30	700	138	163	0.2
	A_2	30–55	738	125	138	0.2
	A_3	55–75	725	100	175	0.1
	AB	75–100	675	125	200	0.2
	BA	100–120	788	138	75	0.2
	Bfl_1	120–170	763	100	138	0.1
	Bfl_2	170–200	763	88	150	0.1
	Bfl_3	200–260 +	763	100	138	0.1
G3	A_1	0–30	713	150	138	0.2
	A_2	30–55	713	150	138	0.2
	A_3	55–80	738	125	138	0.2
	AB	80–95	750	100	150	0.1
	BA	95–120	800	150	50	0.2
	Bfl_1	120–180	713	100	188	0.1
	Bfl_2	180–240	738	100	163	0.1
	Bfl_3	240–260	613	125	263	0.2
	BCr	260 +	513	188	300	0.4
G4	A_1	0–25	788	150	63	0.2
	A_2	25–55	750	163	88	0.2
	A_3	55–80	813	125	63	0.2
	AB	80–120	775	100	125	0.1
	BA	120–140	788	113	100	0.1
	Bfl_1	140–160	800	138	63	0.2
	Bfl_2	160–190	750	100	150	0.1
	Bfl_3	190–280	813	75	113	0.1
	BC_1	280–330	813	125	63	0.2
	BC_2	330–360	913	50	38	0.1
	BCr	360 +	525	188	288	0.4

Appendix T. Physical properties of the Cascavel soil profiles.

Profile	Hz	Depth	Clay	Silt	Total Sand	Silt/Clay
		cm		g kg^{-1}		
C1	A_{pa1}	0–35	800	100	100	0.1
	A_{pa2}	35–45	800	125	75	0.2
	A_{pa3}	45–55	838	113	50	0.1
	AB	55–65	825	88	88	0.1
	BA	65–85	825	125	50	0.2
	Bfl_1	85–135	813	125	63	0.2
	Bfl_2	135–200	825	113	63	0.1
	Bfl_3	200–290	850	100	50	0.1
	Bfl_4	290–420	875	75	50	0.1
	Bfl_5	420–540	863	88	50	0.1
	BC	540 +	788	138	75	0.2
C2	A_1	0–15	800	138	63	0.2
	A_2	15–40	850	100	50	0.1
	A_3	40–50	875	125	0	0.1
	AB	50–90	875	100	25	0.1
	BA	90–145	900	100	0	0.1
	Bfl_1	145–350	875	125	0	0.1
	Bfl_2	350–500	888	100	13	0.1
	Bfl_3	500–620	900	75	25	0.1
	Bfl_4	620–670	875	88	38	0.1
	AS* 1	700	800	163	38	0.2
	AS 2	750	825	150	25	0.2
	AS 3	800	750	188	63	0.3
	AS 4	850	738	163	100	0.2
	AS 5	900–920	738	213	50	0.3
	AS 6	1000–1050	675	250	75	0.4
C3	A_{pa}	0–20	763	125	113	0.2
	AB	20–60	813	113	75	0.1
	BA	60–120	850	88	63	0.1
	Bfl_1	120–265	813	113	75	0.1
	Bfl_2	265–360	838	88	75	0.1
	Bfl_3	360–745	850	88	63	0.1
	Bfl_4	745–860	688	163	150	0.2
	BC_1	860–910	800	100	100	0.1
	BC_2	910–1025	575	213	213	0.4
	BCr	1025 +	475	150	375	0.3

*AS = auger sample.

Appendix U. Physical properties of the Palotina soil profiles.

Profile	Hz	Depth	Clay	Silt	Total Sand	Silt/Clay
		cm		g kg^{-1}		
P1	A	0–30	687.5	125.0	187.5	0.2
	AB	30–50	762.5	175.0	62.5	0.2
	Bfl_1	50–90	825.0	100.0	75.0	0.1
	Bfl_2	90–140	825.0	62.5	112.5	0.1
	Bfl_3	140–290	800.0	75.0	125.0	0.1
	Bfl_4	290–430	675.0	175.0	150.0	0.3
	BCr	430 +	512.5	187.5	300.0	0.4
P2	A_{pa}	0–10	762.5	150.0	87.5	0.2
	AB	10–40	775.0	112.5	112.5	0.1
	Bfl_1	40–90	862.5	100.0	37.5	0.1
	Bfl_2	90–180	837.5	62.5	100.0	0.1
	Bfl_3	180–350	825.0	75.0	100.0	0.1
	Bfl_4	350–650	687.5	187.5	125.0	0.3
	Bfl_5	650 +	762.5	112.5	125.0	0.1
	AS* 1	850	737.5	150.0	112.5	0.2
	AS 2	900	700.0	175.0	125.0	0.3
	AS 3	960	587.5	175.0	237.5	0.3
P3	A_{pa}	0–10	787.5	112.5	100.0	0.1
	Bfl_1	10–45	825.0	100.0	75.0	0.1
	Bfl_2	45–105	887.5	62.5	50.0	0.1
	Bfl_3	105–140	862.5	87.5	50.0	0.1
	Bfl_4	140–255	812.5	112.5	75.0	0.1
	Bfl_5	255–335	837.5	100.0	62.5	0.1
	Bfl_6	335–510	718.75	168.75	112.5	0.2
	Bfl_7	510–600	687.5	187.5	125.0	0.3
	BCr	600–640	318.75	187.5	493.75	0.7

*AS = auger sample.

Appendix V. ATD-TG patterns of the clay content of the main horizons (Bfl_1, BC_1 and BC_2 from the G1 soil profile.

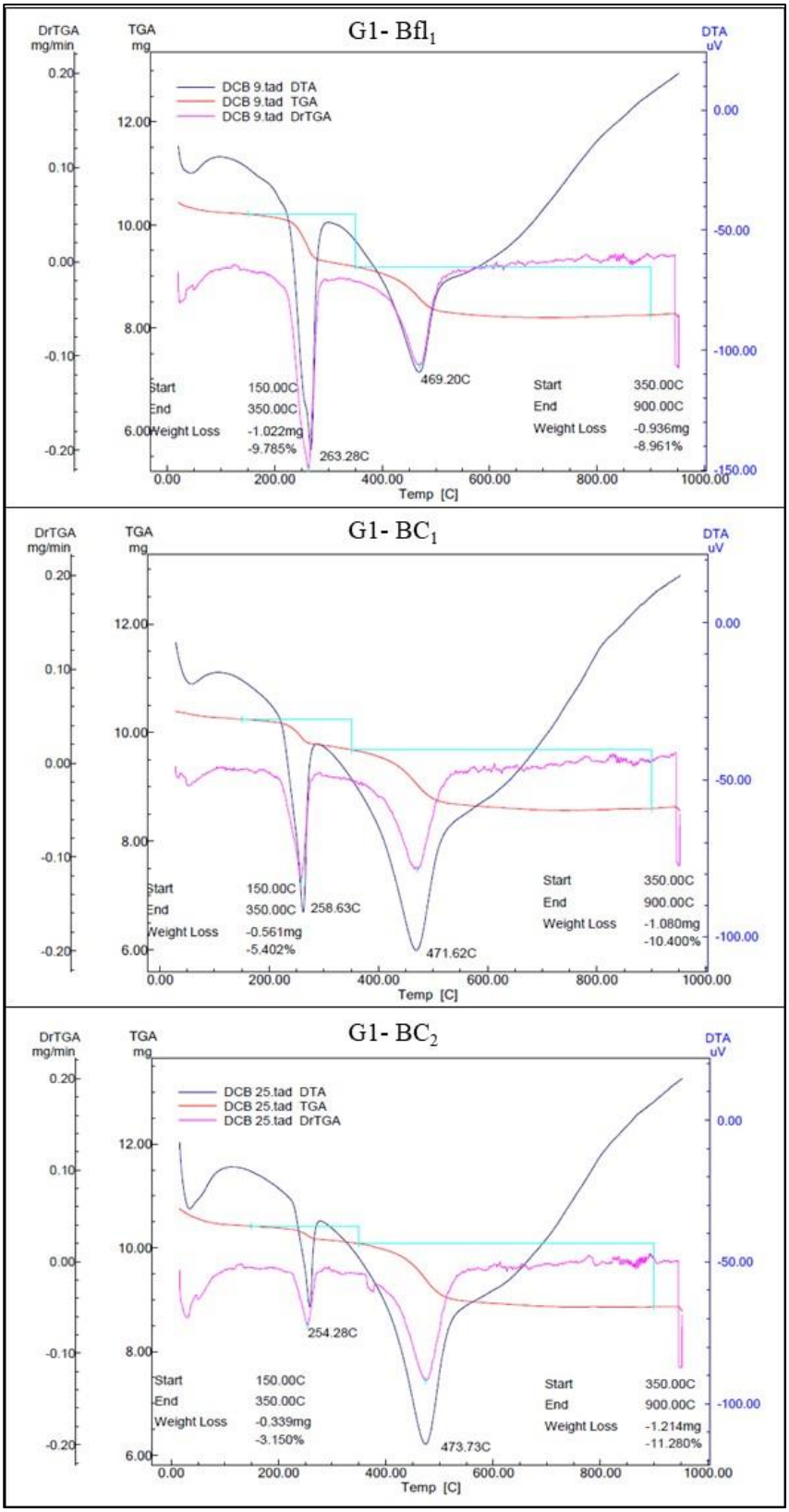

Appendix W. ATD-TG patterns of the clay content of the main horizons (Bfl_1, Bfl_3 and BC_r) from the G4 soil profile.

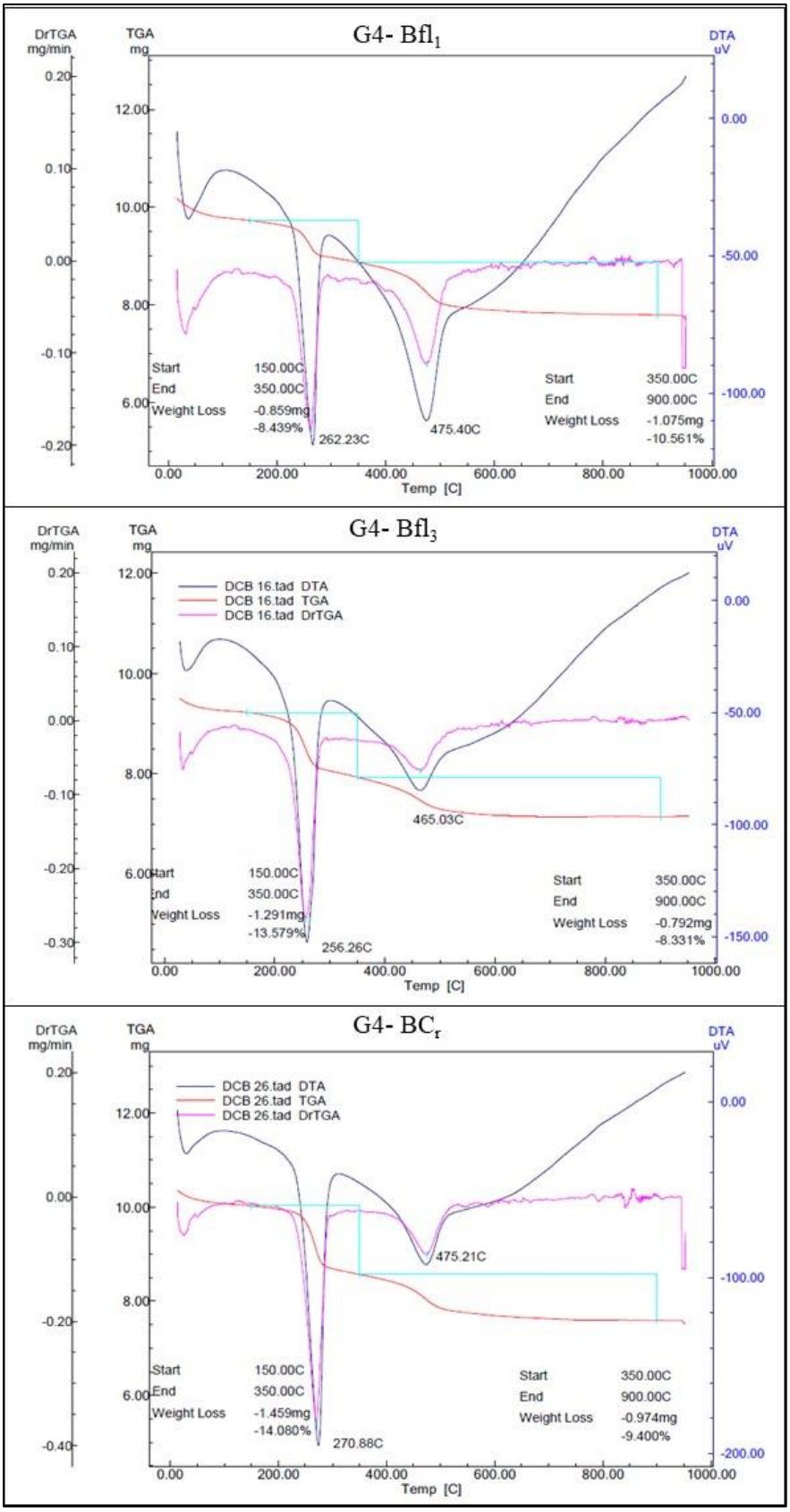

Appendix X. ATD-TG patterns of the clay content of the main horizons (Bfl_1, BC_2 and BC_r) from the C3 soil profile.

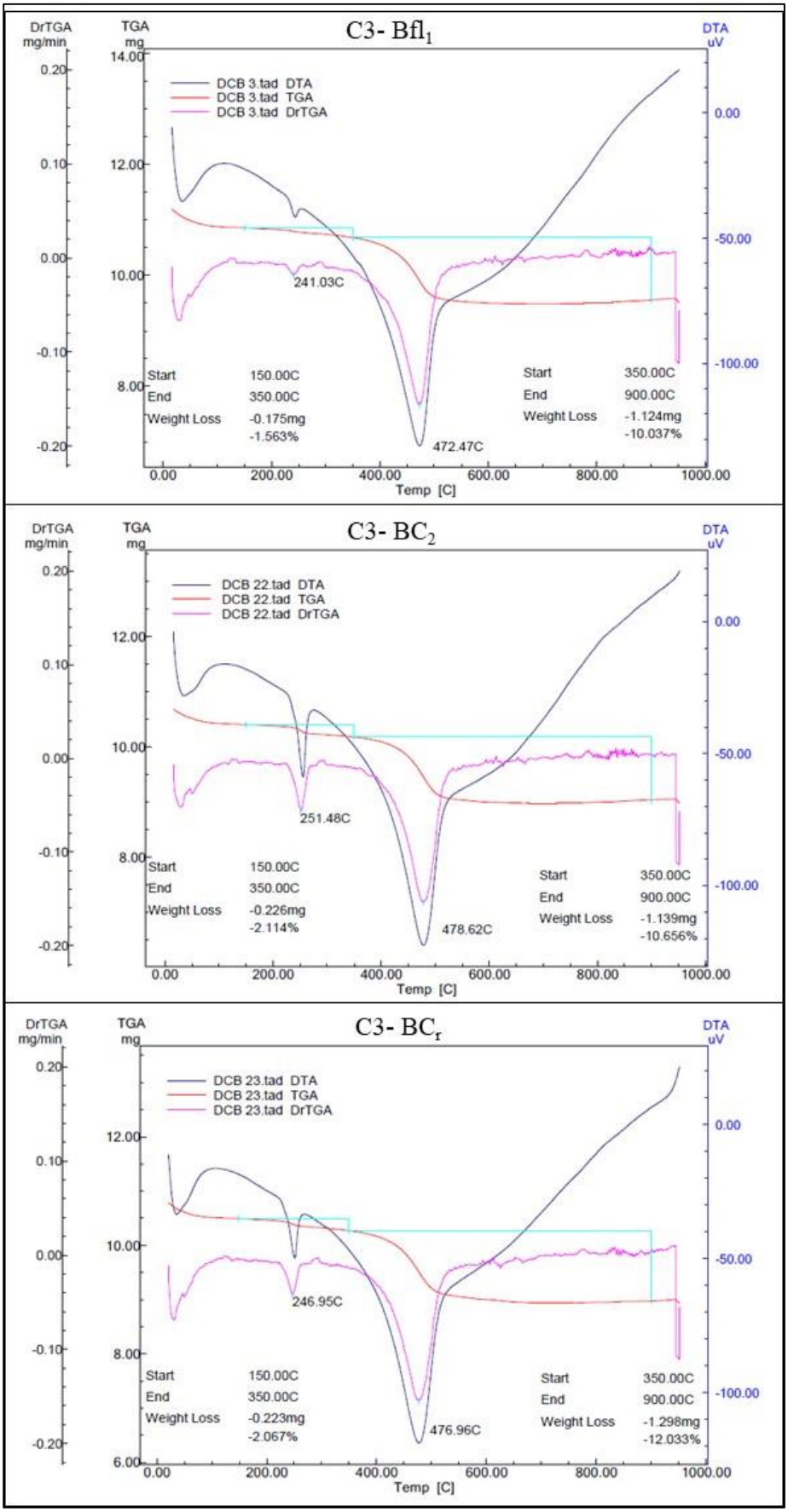

Appendix Y. ATD-TG patterns of the clay content of the main horizons (Bfl_1 and Bfl_7) from the P3 soil profile.

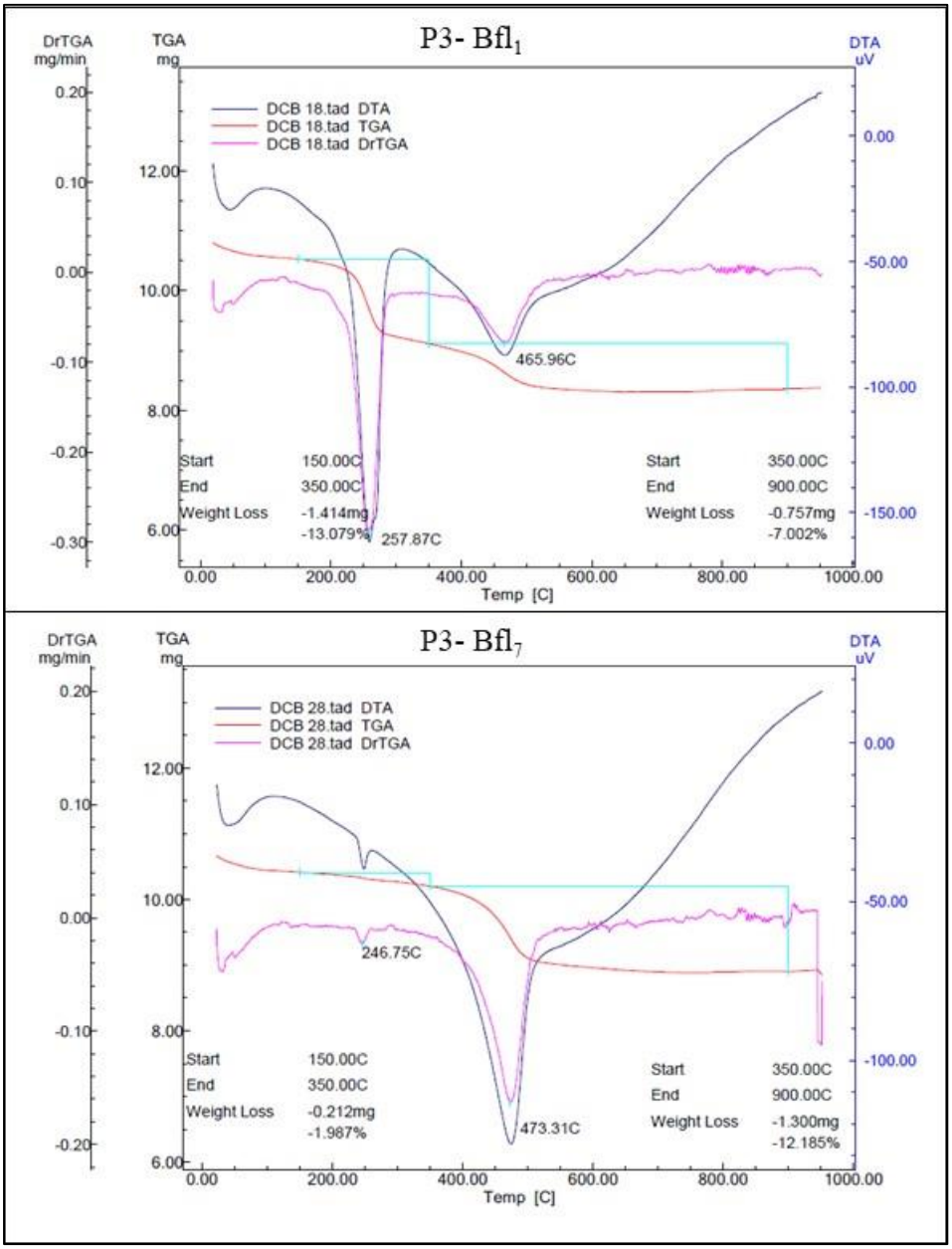

Appendix Z. Weathering indices for the four representative studied soil profiles.

Profile	Hz	Depth cm	R[1]	STI[2]	A[3]
G1	A_{pa}	0–30	0.77	40.83	0.44
	AB	30 –75	0.72	39.60	0.42
	BA	75–105	0.69	38.77	0.41
	Bfl_1	105–135	0.68	38.52	0.41
	Bfl_2	135–180	0.68	38.48	0.41
	Bfl_3	180–225	0.72	39.74	0.42
	Bfl_4	225–280	0.67	38.12	0.40
	Bfl_5	280–360	0.67	38.45	0.40
	Bfl_6	360–410	0.74	40.34	0.43
	BC_1	410–475	0.83	42.80	0.46
	BC_2	475–500	0.94	44.94	0.49
	Weathered rock		5.11	76.79	0.85
G4	A_1	0–25	0.85	40.56	0.46
	A_2	25–55	0.79	39.68	0.44
	A_3	55–80	0.76	39.03	0.43
	AB	80–120	0.75	38.78	0.43
	BA	120–140	0.76	39.31	0.43
	Bfl_1	140–160	0.77	39.34	0.44
	Bfl_2	160–190	0.74	38.77	0.43
	Bfl_3	190–280	0.68	36.90	0.40
	BC_1	280–330	0.61	35.24	0.38
	BC_2	330–360	0.56	33.80	0.36
	BCr	360 +	0.29	21.84	0.23
	Weathered rock		4.72	67.62	0.85
C3	A_{pa}	0–20	0.74	39.93	0.43
	AB	20–60	0.70	38.91	0.41
	BA	60–120	0.64	37.09	0.39
	Bfl_1	120–265	0.61	36.02	0.38
	Bfl_2	265–360	0.58	34.96	0.37
	Bfl_3	360–745	0.60	35.81	0.38
	Bfl_4	745–860	0.75	41.28	0.43
	BC_1	860–910	0.84	43.75	0.46
	BC_2	910–1025	0.87	44.52	0.46
	BCr	1025 +	0.92	46.39	0.48
P3	A_{pa}	0–10	1.08	48.06	0.52
	Bfl_1	10–45	1.01	47.21	0.51
	Bfl_2	45–105	0.97	46.72	0.49
	Bfl_3	105–140	1.00	47.07	0.50
	Bfl_4	140–255	0.99	47.11	0.50
	Bfl_5	255–335	0.97	46.64	0.49
	Bfl_6	335–510	0.97	46.60	0.49
	Bfl_7	510–600	0.96	46.07	0.49
	BCr	600–640	0.85	44.96	0.46
	Weathered rock		4.54	72.37	0.85

[1]Ruxton ratio (Ruxton, 1968); [2]Silica and Titanium index (Jayawardena and Izawa, 1994); [3]A index proposed by Kronberg and Nesbitt (1981).